UNIVERSITÉ DU LUXEMBOURG

PhD-FSTM-2022-090
The Faculty of Science, Technology and Medicine

DISSERTATION

Defence held on 13/07/2022 in Esch-sur-Alzette, Luxembourg

to obtain the degree of

DOCTEUR DE L'UNIVERSITÉ DU LUXEMBOURG

EN BIOLOGIE

by

Françoise Anne KEMP
Born on 24 April 1991 in Luxembourg (Luxembourg)

MODELLING COMPLEX SYSTEMS IN THE CONTEXT OF THE COVID-19 PANDEMICS

Dissertation defence committee

Dr Alexander Skupin, dissertation supervisor
Professor, Université du Luxembourg

Dr Thorsten Lehr
Professor, University of Saarbrücken

Dr Stéphane Bordas, Chairman
Professor, Université du Luxembourg

Dr Viola Priesemann
Professor, Max Planck Institute for dynamics and self-organization

Dr Jorge Goncalves, Vice-Chairman
Professor, Université du Luxembourg

Doctoral School membership

Dissertation Defence Committee:

Committee members:	Prof. Dr. Alexander Skupin (University of Luxembourg)
	Prof. Dr. Stéphane Bordas (University of Luxembourg)
	Prof. Dr. Thorsten Lehr (University of Saarbrücken)
	Prof. Dr. Jorge Goncalves (University of Luxembourg)
	Prof. Dr. Viola Priesemann (Max Planck Institute for dynamics and self-organization)
External Expert:	Prof. Dr. Thomas Carraro (University of Federal Armed Forces Hamburg)

Affidavit

I hereby confirm that the PhD thesis entitled "Modelling complex systems in the context of the COVID-19 pandemics" has been written independently and without any other sources than cited.

Luxembourg, _____ _____

Date Name

Acknowledgements

First of all, I would like thank my supervisor Prof. Dr. Alexander Skupin. He supported me, guided me and helped me through my research journey. Furthermore, I would like to thank him for our fruitful scientific meetings and our discussions around various scientific topics. Within the COVID-19 Task Force, he gave me the chance to grow as a researcher and improve my skills.

Apart from my supervisor, I would like to thank Prof. Dr. Jorge Goncalves for his valuable feedback, as a member of my CET committee as well as our discussions within the COVID-19 Task Force. Moreover, I would like to say thanks to Prof. Dr. Thomas Carraro for his guidance along my research journey from master thesis on and his valuable feedback, as a member of my CET committee.

I would like to pay my special regards to my thesis defense committee members, Prof. Dr. Alexander Skupin, Prof. Dr. Stéphane Bordas, Prof. Dr. Thomas Carraro, Prof. Dr. Jorge Goncalves, Prof. Dr. Thorsten Lehr and Prof. Dr. Viola Priesemann.

Furthermore, I thank Dr. Stefano Magni for the stimulating discussions and for the sleepless nights during which we were working together. As well as for all the fun we had.

My sincere thanks goes to Daniele Proverbio for super fruitful discussions and the amazing projects we accomplished together. As well as for all the coffees we had drunk together.

I wish to show my gratitude to Dr. Atte Aalto for his guidance, for all the scientific meetings and teaching that we had together.

I wish to express my deepest gratitude to my doctoral training unit PARK-QC. PARK-QC that gave me the opportunity to participate at interesting training courses and encouraged the social interaction between PARK-QC PhD candidates.

Additionally, I would like to express gratitude to my ICS family, Alice, Aymeric, Corrado, Cristina, David, Dimitri, Elle, Gabriela, Kamil, Lupe, Marina, Melanie, Michela, Olga, Silvia, Sofia, Sonja, Stefano and Thais that make LCSB a nice place to work and for the fun time, we spent together.

Thanks to Dr. Cristina Donato for proofreading the thesis.

I would also like to extend my deepest gratitude to Prof. Dr. Christophe Ley. He has been helpful in providing advices many times and from whom I had the chance to learn a lot. Moreover, I very

much appreciate his unconditional help and valuable advices. Furthermore, I would like to thank Clemens Werner Ostrowicz for our nice coffee breaks and fruitful discussions. Furthermore, I would like to thank Dr. Andreas Husch for our nice lunches, coffee breaks and fruitful discussions. As well, I want to thank those who accompany me on my way and will accompany me on my way. I am extremely grateful to Annick, Carmen, Charel, Cristina, Joëlle, Melissa, Michelle, Patricia, Sonja and Thais for incredible time, we spent together in the last years, their timely encouragement and endless patience. Last but not the least, I would like to thank my parents, my sister, my family and my friends for supporting me during my PhD journey as well as my life in general.

To my loved parents Annette and Carlo, my loved sister Martine, all my family and friends.

ABSTRACT

Systems biology is an interdisciplinary approach investigating complex biological systems at different levels by combining experimental and modelling approaches to understand underlying mechanisms of health and disease. Complex systems including biological systems are affected by a plethora of interactions and dynamic processes often with the aim to ensure robustness to emergent system properties. The need for interdisciplinary approaches became very evident in the recent COVID-19 pandemic spreading around the globe since the end of 2019. This pandemic came with a bundle of urgent epidemiological open questions including the infection and transmission mechanisms of the virus, its pathogenicity and the relation to clinical symptoms. During the pandemic, mathematical modelling became an essential tool to integrate biological and healthcare data into mechanistic frameworks for projections of future developments and the assessment of different mitigation strategies. In this regard, systems biology with its interdisciplinary approach was a widely applied framework to support society in the COVID-19 crisis.

In my thesis, I applied different mathematical modelling approaches as a tool to identify underlying mechanisms of the complex dynamics of the COVID-19 pandemic with a specific focus on the situation in Luxembourg. For this purpose, I analysed the COVID-19 pandemic at its different phases and from various perspectives by investigating mitigation strategies, consequences in the healthcare and economical system, and pandemic preparedness in terms of early-warning signals for re-emergence of new COVID-19 outbreaks by extended and adapted epidemiological Susceptible-Exposed-Infectious-Recovered (SEIR) models.

For the early phase of the pandemic when no pharmaceutical interventions were available, I invest-

igated synergies of non-pharmaceutical interventions to control epidemic outbreaks by an SEIR model extended by contact tracing of positive cases and subsequent quarantine. Interestingly, the findings showed that a rapid and strong lockdown attained a similar mitigation as a combination of social distancing and efficient contact tracing.

With the advancement of the pandemic and development of vaccines, the question on herd immunity as a mechanism to stop the pandemic became of general interest. For a quantitative assessment, I assessed the potential way to herd immunity by vaccination and infections by a SEIR model extended with a detailed disease progression module considering hospitalizations and deaths. With the appropriate parameterization of the model based on data from Luxembourg, Austria and Sweden, the results could disentangle the interplay between vaccination and active infections for herd immunity in dependence on social interactions. For this purpose, a new method to calculate the reproduction number R_{eff} from the systems equation was developed to provides an estimation of the minimal size of the immunized sub-population required to reach herd immunity.

To investigate the interplay between the epidemiological dynamics and economical consequences of COVID-19 crisis in Luxembourg, I co-developed an epidemionomic model that allows to compare the effect of health-related sickness leaves and lockdown on the Luxembourg economy in a sector specific manner. The analysis showed that due to the economic structure of Luxembourg, the loss in gross domestic product was be smaller than 0.4% also because only less than 2% of the population were infected at the same time.

Finally, I investigated the applicability of early warning signals (EWS) from the theory of complex systems as a tool for pandemic preparedness. EWS aim is to detect impending critical transitions of complex systems and represent therefore a promising tool to indicate potential future COVID-19 infection waves. Applying different EWS approaches to data of COVID-19 infection waves in various countries showed the potential of these indicators to inform public health administrations and the public on the risk of an epidemic wave early on.

Overall, this thesis applies extended epidemiological modelling in a systems biology manner to investigate quantitatively different aspects of the COVID-19 pandemic and provides new insights into tools for pandemic preparedness.

TABLE OF CONTENT

LIST OF FIGURES

LIST OF TABLES

LIST OF ABBREVIATION

Abbreviation	Full name	Abbreviation	Full name
MCMC	Markov Chain Monte Carlo	MH	Metropolis-Hasting
ODE	Ordinary Differential Equations	EWS	Early-warning signals
WHO	World Health Organization	ICU	Intensive care unit
RNA	Ribonucleic Acid	GDP	Gross domestic product
SARS-CoV-2	Severe Acute Respiratory Syndrome Coronavirus 2	SIR	Susceptible, Infectious, Recovered
SEIR	Susceptible, Exposed, Infectious, Recovered	E-protein	Envelope small membrane protein
M-protein	Membrane Protein	N-protein	Nucleoprotein
VOI	Variant Of Interest	VOC	Variant Of Concern
DFE	Disease-Free-Equilibrium	PCR	Polymerase Chain Reaction
GDP	Gross Domestic Product	LST	Large-Scale Testing
ROC	Receiver Operating Characteristic	AUC	Area Under The Curve
rRT-PCR	Real-Time Reverse-Transcriptase Polymerase-Chain-Reaction	SARS	Severe Acute Respiratory Syndrome
MERS	Middle East Respiratory Syndrome Coronavirus	ACF	Autocorrelation Function
CT	Cycle Threshold	NPI	Non-Pharmaceutical Interventions
RNA	Ribonucleic Acid	DNA	Deoxyribonucleic Acid
PDE	Partial Differential Equations	LISER	Luxembourg Institute Of Socio-Economic Research

LIST OF THESIS RELATED PUBLICATIONS

The results presented in my thesis have led to the following five articles:

[1] Françoise Kemp, Daniele Proverbio, Atte Aalto, Laurent Mombaerts, Aymeric Fouquier dHérouël, Andreas Husch, Christophe Ley, Jorge Gonçalves, Alexander Skupin, Stefano-Magni. Modelling COVID-19 dynamics and potential for herd immunity by vaccination in Austria, Luxembourg and Sweden. Published in: Journal of Theoretical Biology (2021).

[2] Daniele Proverbio, Françoise Kemp, Stefano Magni, Andreas Husch, Atte Aalto, Laurent Mombaerts, Alexander Skupin, Jorge Gonçalves, Jose Ameijeiras-Alonso, Christophe Ley. Dynamical SPQEIR model assesses the effectiveness of non-pharmaceutical interventions against COVID-19 epidemic outbreaks. Published in: PLOS ONE, 16 (2021).

[3] Daniele Proverbio, Françoise Kemp, Stefano Magni, Jorge Gonçalves. Performance of early warning signals for disease emergence: a case study on COVID-19 data. Published in: PLOS Computational Biology (2022).

[4] Micha Burzyski, Joël Machado,Atte Aalto, Michel Beine, Jorge Goncalves, Tom Haas, Françoise Kemp, Stefano Magni, Laurent Mombaerts, Pierre Picard, Daniele Proverbio, Alexander Skupin, Frédéric Docquier. COVID-19 Crisis Management in Luxembourg: Insights from an Epidemionomic Approach. Published in: Economics and Human Biology (2021).

[5] Daniele Proverbio,Françoise Kemp, Stefano Magni, Leslie Ogorzaly, Henry-Michel Cauchie, Jorge Gonçalves, Alexander Skupin, Atte Aalto. Model-based assessment of COVID-19 epidemic dynamics by wastewater analysis. Published in: Science of the total environment (2022).

CHAPTER 1

INTRODUCTION

> *"All models are wrong, but some of them are useful."*
>
> George E. P. Box, *1976*

As for many of us within the scientific community, the unexpected arrival of COVID-19 has not left unaffected my research work. Particularly, the focus of my studies drastically shifted from breast cancer research towards COVID-19. This thesis has evolved within the period of the COVID-19 pandemic which challenged societies world-wide at different levels including socio-economic and healthcare aspects. In December 2019, the outbreak of a new, highly contagious disease: COVID-19. A respiratory disease caused by the RNA-based virus SARS-CoV-2 that was first found in Wuhan, China. On 11 March 2020, the World Health Organization (WHO) officially declared its outbreak as a pandemic. The main focus of this thesis, however, lies on the spread of COVID-19 in Luxembourg. The first case in Luxembourg was detected on 24 February 2020 and a fast subsequent increase in daily cases led to a general lockdown in Luxembourg on 18 March 2020. Half of humanity in 90 countries were in lockdown in April 2020 [1]. In Luxembourg, implementing a general lockdown meant: a general stay-at-home order, the closure of all non-essential shops, home-schooling for pupils and students, and home-office for the working population wherever

possible.

Coming from the field of applied mathematics, I decided to bring my modelling skills to the COVID-19 Task Force. The COVID-19 Task Force provides the national political decision-makers with scientific counsel and expertise for making their decisions on mitigation measures against this, until then, rather unknown disease. This task force was set up across different research institutes and ministries to bring together trans-institutional and trans-disciplinary expertise [2]. Within the task force, one stream focusses on statistical projections based on Luxembourgish data provided by several Ministries. Since March 2020, I have been part of this very stream. My contributions helped me learn quickly how to apply my previously acquired modelling knowledge to the pandemic behaviour. It has been an intense, yet unique, challenging and exciting experience.

One of the first tasks of the COVID-19 Task Force was the general epidemic assessment in terms of determining the effective reproduction number, producing projections for hospitalization rates, and investigate asymptomatic cases. The effective reproduction number represents the number of new infections an infectious individual causes [3]. An increasing number of people were getting sick and some of them severe, needing hospital care. The goal of the projection for hospitalization rates is to simulate ICU- and hospital bed needs in the upcoming weeks and help hospitals to anticipate future capacity needs and prepare accordingly. Asymptomatic cases are people who are infected with the virus without developing symptoms. The investigation of asymptomatic cases is important, as they still can pass on the virus, mainly undetected. This was one of the reasons why Luxembourg implemented the Large-Scale testing or mass screening, besides of accompanying the reopening phase after the lockdown [4, 5].

The assessment of the, in the beginning rather unknown, impact of COVID-19 on the society and particularly on the healthcare system required an interdisciplinary approach combining domain knowledge from molecular biology, virology, computational modelling, mathematics as well as from economics and humanities. In this respect, systems biology, with its general aim to decipher the complexity of the biological system and understand mechanistically the dynamics at every organizational level by models [6], became an important interdisciplinary approach during the COVID-19 pandemics. Biological phenomena are often complex processes [7]. In complex systems, the behaviour cannot be understood without the consideration of the individual parts and their

interactions [8]. Complex systems develop by self-organization [9]. The complexity of these systems can make the establishment of a model a challenge [10] but if successful, modelling is an essential tool to advance the knowledge of the system and provide a framework to generate and hypotheses and testify these [6]. George Box, a British statistician said the famous lines "All models are wrong, but some of them are useful". The idea of the quote is that a model cannot completely represent reality, but is just an approximation of a real world object. Models simplify the real world in order to understand the fundamental characteristics of a system. A model just takes into account a selection of specific aspects of a system. Models can be of experimental or mathematical nature. Experimental modelling in biology has as goal to gain new information on biological processes and lead to biological hypotheses [7, 11, 12]. Mathematical modelling is used to describe, understand and predict systems [13]. Mathematical models are representations of basic aspects based on prior knowledge, such as physical laws and are less costly than experiments. There are different kind of mathematical models such as dynamical systems, statistical models, differential equations, or game theoretic models [13]. Since self-organisation is strongly linked to the temporal domain in which an entity is emerging, dynamics is an essential tool to reveal underlying mechanisms of complex systems. Dynamical models describing the change of system properties in time can focus on the qualitative or quantitative behavior of the solutions [14] and are often described by ordinary differential equations (ODE) [14].

In the general framework of the epidemiology of infectious diseases, mathematical modelling is a tool of great versatility. The main goal of epidemiological modelling is to gain insights into the underlying mechanisms and system properties that determine the spread of the disease. In this respect, epidemiological modelling is able to advise control and mitigation strategies. The beginning of epidemiological modelling was marked by the work of Daniel Bernoulli in the early 18th century as a response to smallpox [15] in which he analyzed the mortality of the disease in a systematic manner [16, 17]. The first model able to describe the temporal behaviour of an epidemics is the basic compartment model, introduced in 1927 by Kermack and McKendrick [18]. The Kermack and McKendrick describes the spread of infectious diseases by rates of flow between the different compartments by ODEs. Reformulation of so called SIR or SEIR compartment models (see Section 3.3 for detailed introduction) were used for the modelling of different disease outbreaks

such as severe acute respiratory syndrome coronavirus (SARS), influenza A virus subtype H5N1 in 2005 [19], influenza A virus subtype H1N1 in 2009 [20] and Ebola in 2014 [21]. Also in the recent COVID-19 pandemic, compartment models were also widely used for analyses and projections and adapted to the specificities of the virus and different societies. Extended SEIR model or SIR model for COVID-19 were developed in order to take into account for hospitalization and death [22–25]. Additionally, I want to emphasize the COVID Simulator is a mathematical model for the trend of the COVID-19 pandemic in federal states of Germany based on an extended SEIR model and applies Non-Linear Mixed Effects (NLME) approach [26]. A work to highlight is the analysis of the effect of non-pharmaceutical interventions (NPI) on the spread of COVID-19 with a combined SIR model and a Bayesian parameter inference [27]. Stochastic age-structured transmission model was used to investigate NPI in UK [28]. The impact of NPI scenarios were also analysed with an agent-based models [29].

1.1 Framework of the thesis

Also the presented thesis has extended epidemiological compartment models for the analysis of the COVID-19 pandemic with a focus on Luxembourg in a systems biology manner. For this purpose, the general scope of systems biology and its approaches are introduced in Chapter 1. Chapter 2 presents the objectives and the aims of the presented thesis. The main scientific background of the thesis such as an introduction to modelling in general as well as epidemiological modelling in particular and its different stages is given in Chapter 3. Additionally, it gives a brief overview on epidemiological modelling and the methods used for parameter estimation and for detecting early warning signals. Based on this background, the thesis investigates the effects and different stages of COVID-19 pandemic from various aspects such as mitigation strategies, health, economical and early-warning signals as re-emergence of new COVID-19 outbreaks. The first arising question of COVID-19 Task Force was to investigate possible mitigation strategies, that are highlighted in Chapter 4 focusing on the effectiveness of non-pharmaceutical interventions and analysing the effect of synergies of different mitigation strategies.

As the healthcare system was under pressure, I created a model to predict the upcoming needs of

hospital and ICU beds. Furthermore, my model is not just applicable to Luxembourg, but as well parameterized for Sweden and Austria. In December 2020, as vaccines became available, a new question gain in interest. The question arose when herd immunity is reached. These upcoming questions are tackled in Chapter 5.

The lockdown in Luxembourg became effective on 18 March 2020 and the first reopening happened on 20 April. The first sector reopened after lockdown was the construction sector. A consequence of a lockdown is obviously loss of Gross domestic product (GDP), which is part of the investigations in Chapter 6.

In Chapter 7, the performance of early warning signals (EWS) in disease re-emergence is analysed. EWS are used to detect critical transitions in the data in the framework of new COVID-19 outbreaks.

The Fig. 1.1 summarizes the different challenges faced and investigated during the on-going pandemic in Luxembourg which are tackled in the main part of this thesis.

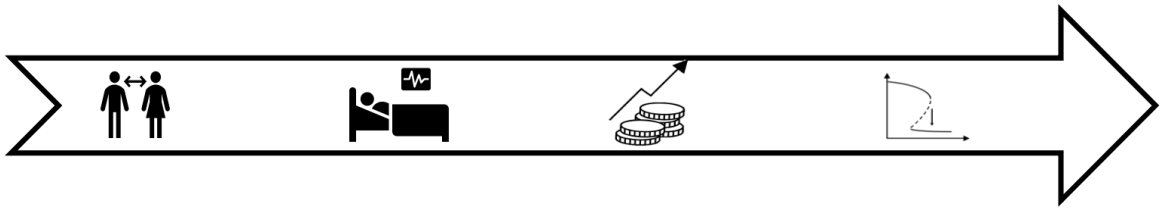

Figure 1.1: The different challenges investigated during the pandemic in Luxembourg. The images are taken from PowerPoint stock images Version 16.59

Apart from the different questions investigated in the main part of the thesis (Chapter 4-7), the additional investigations and analyses in the framework of COVID-19 Task Force provided for the Ministries are presented in Chapter 8.1. Finally, the results of the thesis are summarized in Chapter 8.2.

1.2 Systems biology and interdisciplinary research

The field of systems biology is part of life sciences and has been lately instituted. Its goal is to understand the system of living matter as a whole [30], by connecting molecular biology with complementary approaches from cell biology and physiology [31, 32]. Moreover, it is defined as an

integration of various fields such as computational and experimental research in order to decipher the mechanism underlying the complex biological processes [30] using a holistic approach [33]. Historically, the basis of systems engineering was established 60 years ago, even if Ludwig von Bertalanffy came up with the concept of systems theory in biology during 1940s. Nobert Weiner introduced the topic of system-level understanding into the field of biology by establishing the field of cybernetics [30, 34].

Furthermore, systems biology wants to understand the "broader picture" at different scales of living matter as well as complex interactions within biological systems [30]. However, new technologies allowing to explore additional dimensions of the data space are missing [35].

To tackle biological dynamics and systems biology two different approaches can be used: bottom-up and top-down. Both concepts aim at collecting information from different layers in order to gain new insights.

1.2.1 Bottom-up

The bottom-up concept is based on the assimilation of prior knowledge on the dynamics of the most important components of the system [30]. The idea of the approach is to associate pathway models leading to a predictive model for the complete system [36]. This approach is appropriated in the case the organism is well known, as it brings together organism-specific knowledge into an entire genome-scale model with the aim to gain insights into interactions arising in a system [37] and anticipate system behaviour [36]. Bottom-up systems biology are mechanism-based [36]. It is indeed based on experimental data of a subsystem which gives information on molecular properties (such as enzyme kinetics) and on a subset of the system in relation to perturbation, leading to the construction of a predictive model [36]. The models used in this approach are mostly in silico.

1.2.2 Top-down

A top-down approach aims at gaining insights into cells (such as molecular mechanisms), modules and patterns of functional behaviour by working with system-wide data [36]. The concept starts with genome-wide large experimental data sets which are then analysed and integrated. It became

a dominant approach with the establishment of the 'omics' methodology [38] and is mainly phenomenological [36]. This approach allows to better understand molecular mechanisms from data, instead of deducing them from prior knowledge and it is build on induction [36].

1.3 COVID-19 as complex system: from biology to society

Complex systems science was a key-changer for the way of thinking about science [39]. Complex systems look at the system as a whole with its many factors that cooperate. A famous quote often cited in that context, comes from Aristotle who claimed: "The whole is more than the sum of its parts". Complex systems are considered to be dynamic, nonlinear, multidimensional and adaptive [40]. The information at different scales is unified into the system by networks of relationships which lead to the "emergence" behaviors [35, 39].

The three fundamental concepts important to understand complex biological systems are robustness, emergence and modularity [41]. Robustness which is an inherent property, means that biological systems keep their phenotypic stability even in situations of perturbations [41]. Emergence in the context of complex systems is linked to emergence properties. Emergence properties are properties of individual parts which are insufficient to understand the entire system behaviour [42]. Modularity is an important characteristic that assists the system in preventing the spread of damage during the process of evolution [43].

Complexity in the context of COVID-19 pandemic can be observed as it results from multilevel and multiscale interactions between, for example, pathogen, host and external factors [44]. COVID-19 pandemic had a wide-range impact on society. The pandemic showed the vulnerability of the globalized society. There has never been such a potential for infectious disease to spread than right now with urban migration, increased global travel and population growth. All this factors led to the rapid transmission of COVID-19 across the world. In some cases, superspreader events occurred where one infected person caused a large outbreak among the guests. In order to reduce the spreading, governments implemented non-pharmaceutical interventions such as for example lockdown, masks and social distancing.

COVID-19 had not only an impact on health, but non-pharmaceutical interventions such as lock-

down had a repercussion on society and economy. For example, in the case that people could not earn money during the period of lockdown. Furthermore, COVID-19 revealed the limits of the capacities of the healthcare system. Medical stuff rushed to figure out how to treat the new disease and isolate COVID-19 patients adequately. Companies redirected their productions towards health related materials. Moreover, society resilience relies on the participation of the population. Social distancing puts individual resilience to the test.

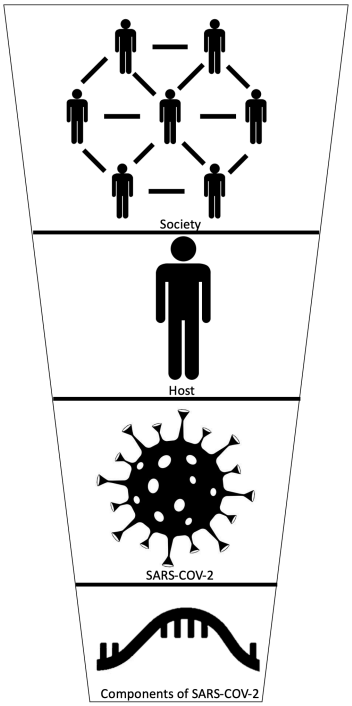

Figure 1.2: Complexity from a top-down approach

The four layers investigated in Fig. 1.2 are the components of SARS-CoV-2, SARS-CoV-2, the host and the society.

1.3.1 Components of SARS-CoV-2

Coronavirus is a membraninfold ribonucleic acid (RNA)-virus. Coronavirus creates virions with a diameter of around 80-140 nm. It consists of the following structure proteins: spike glycoprotein, envelope small membrane protein (E-protein), membrane protein (M-protein) and nucleoprotein (N-protein). On the surface of the virions is located the spike glycoprotein. The spike glycopro-

tein's task is to enter the host cell by binding to the cellular entry receptor [45]. The binding is the beginning of the infection.

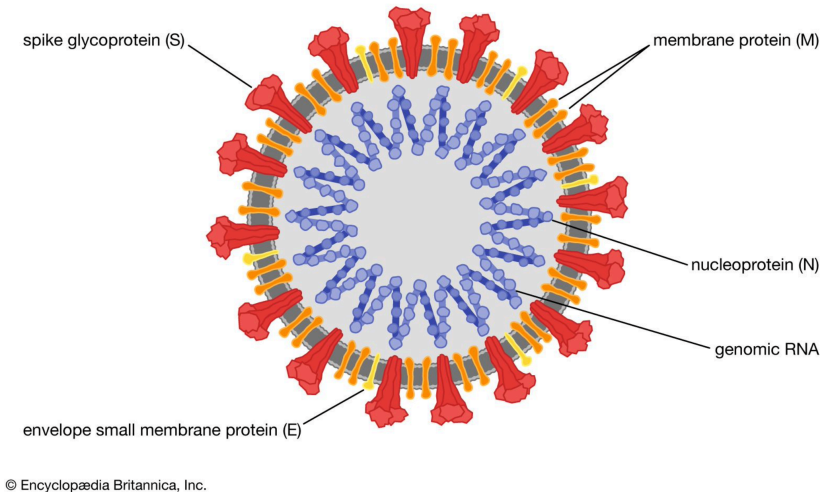

Figure 1.3: Structure of SARS-CoV-2 from [46]

1.3.2 SARS-CoV-2

Coronaviruses are a broad family of RNA viruses and pathogens for human and vertebrates [47, 48]. Furthermore, the name coronaviruses is due to the crown-like spines on their surface [49]. In the 1960s, the first coronavirus was discovered [48]. There are seven human coronaviruses 229E (alpha coronavirus), NL63 (alpha coronavirus), OC43 (beta coronavirus), HKU1 (beta coronavirus), MERS-CoV (MERS, beta coronavirus), SARS-CoV (SARS, beta coronavirus) and SARS-CoV-2 (COVID-19) and are categorized into alpha and beta species [49, 50]. Middle East respiratory syndrome coronavirus (MERS-CoV) is a zoonotic virus transferred to humans from infected dromedaries. MERS spread to 27 countries around the world in 2012 and first reported in Saudi Arabia. Worldwide, 8098 were infected and 858 died of MERS. The symptoms of MERS are fever, cough and shortness of breath [51].

SARS is a zoonotic virus transferred to humans from infected bats. SARS first appeared in Asia in 2003 and spread to 28 countries around the world. Worldwide, 8098 were infected and 774 died of SARS and the symptoms of SARS starts with high fever and other symptoms are headache, feeling of discomfort, body aches and dry cough after 2 to 7 days [52]. Most people suffering

from SARS develop pneumonia.

In December 2019, a new infectious disease first identified in Wuhan (China) caused by severe acute respiratory syndrome coronavirus 2 (SARS-CoV-2). SARS-CoV-2 is a new coronavirus widespread in mammalians, humans and avian species [53]. On 11 March 2020, world health organization (WHO) declared COVID-19 a pandemic. Until 24 May 2022, 52,6102,346 people were infected worldwide and 6278785 people had died of COVID-19 [54]. The characteristics of the infection are diverse: we can have asymptomatic, mild to severe outcome. Most common symptoms of this illness are fever, cough, tiredness and loss of taste or smell [55]. By nature, all RNA-viruses including SARS-CoV-2 change their characteristics over time. The variant can change in a way that the virus spreads easier or that the disease gets less severe.

WHO distinguishes between variants of interest and variants of concern due to the emergence of variants that put danger on the global public health [56]. A variant of interest (VOI) has specific marker linked to changes of phenotype for example in the receptor binding. Actually, WHO classified no SARS-COV-2 variant as VOI. A variant of concern (VOC) has changes in the pathogen features responsible for example for a higher transmissibility. WHO classifies the following once as VOC: alpha, beta, gamma, delta and omicron.

1.3.3 Host

Individuals can transmit the disease via close contact with an infectious person. COVID-19 is mainly transmitted by droplets which are small liquid particles of different sizes [57]. The transmission of SARS-CoV-2 can happen in three ways. First by short-range airborne which is the inhalation of infectious droplets at short reach. Second by infectious droplets having immediate contact with eyes, mouth or nose [58]. Third by, touching eyes, mouth or nose with COVID-19 contaminated hands [59]. In order to better understand the spreading of COVID-19, further research is needed.

The following basic precautions can reduce the risk of getting COVID-19. The buzzwords for reduction of the risk are keep social distance, wear a mask, disinfect and wash your hands regularly, get vaccinated and aerate spaces [60].

1.3.4 Society

The pandemic not only has an effect on health, but as well on the economy and society. COVID-19 has changed our day-to-day lives. The work mainly shifted towards remote working, and home-schooling was introduced. Other facets impacted, were traveling restrictions, disrupted supply chains, reduced social gatherings, isolation of elderly people and restriction of leisure activities [61]. COVID-19 affected all segments of the population. Poor people are more impacted by health and economic issues linked to COVID-19 [62]. Elderly people are mainly at risk to suffer badly from an infection with COVID-19, notably the once suffering from cardiovascular disease, hypertension and diabetes. Furthermore, elderly people also suffered a lot from social isolation. Not to mention the pain, people go through when they lost their most loved ones due to COVID-19. COVID-19 not only can cause death, but a range from 10 percent to more than 50 percent of all confirmed cases suffer from Long-COVID [63].

Test yourself regularly in order to avoid spreading the disease to others. Two different kinds of tests are differentiated: Polymerase chain reaction(PCR)-test and rapid antigen test.

A PCR test has as goal to detect genetic material from SARS-CoV-2 in a sample. As of 2021, for the detection of COVID-19, a modified version of PCR is used: real-time reverse transcription polymerase chain reaction (rRT-PCR) [64]. rRT-PCR test has high specificity and relatively high sensitivity [48]. rRT-PCR test is a method that allows to figure out the copy number of RNA templates and its result is noticeable directly [65]. As for the PCR test, the first step of rRT-PCR test is the collection of nasal swab. Then, the conversion from single-stranded RNA to double-stranded DNA is undertaken [66], that is called reverse transcription. This process is done as just DNA can be amplified [67]. The fragments of DNA connect to target spot of viral DNA which leads to on the one side to DNA strands and on the other side to DNA strands with marker labels [67]. In the RT-PCR machine, the composition of the step before is put in and then a chemical reaction leads to the creation of identical copies of the target spot of viral DNA [67]. The computer of RT-PCR machine measures the fluorescent dye in sample after each cycle. Additionally, the number of cycles are counted until the threshold of fluorescence is exceeded, which gives a hint about the severity of the infection. In the case of a low number of cycles, the

viral infection is severe. A high cycle threshold (CT) means a low risk of infectivity.

A positive PCR-test implies the presence of SARS-CoV-2 while, a negative result signifies either the sample does not contain SARS-CoV-2 or that the viral load is insufficient [66].

Antigen tests give information about the presence of a viral surface antigens and are point-of-care tests [68]. Furthermore, antigen test are simple and cheap [69]. The first step of the test is the nasal swab or saliva. The sample is added to chemicals which is then added to cartridge. In the case that, on the cartridge the lines C (Control) and T (Test) are coloured, the test is positive.

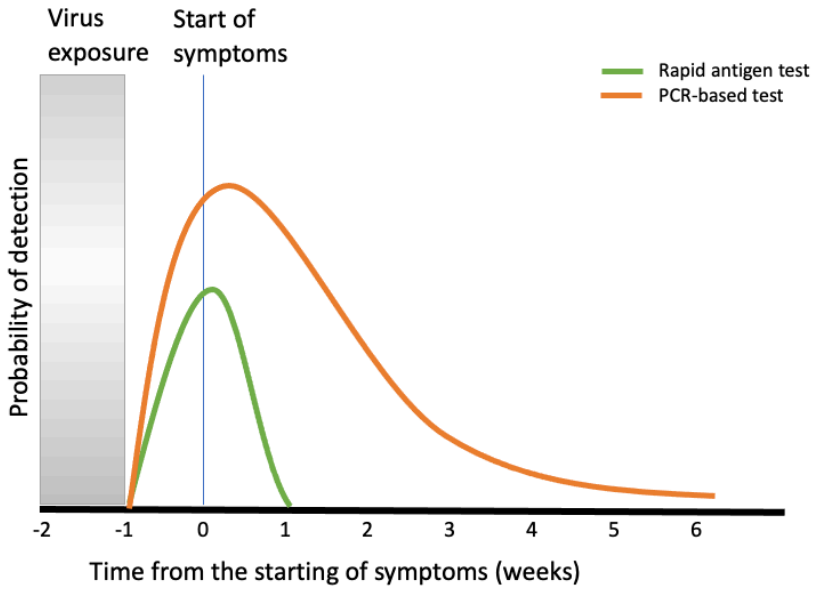

Figure 1.4: The two main types of COVID-19 tests are PCR-based tests and rapid antigen tests. The probabilities for a positive outcome depends on the moment of testing. Figure is based on [70]

Patients with high viral load can be caught by a rapid antigen test during the phase of symptom onset. In contrast to PCR-based test, which are able to detect small amounts of viral load, therefore can be a positive for a long period. PCR tests require a few hours in comparison to antigen test which need around 10 to 15 minutes to present a result. However, antigen tests are less sensitive than rRT-PCR tests [68].

Based on these specific challenges of COVID-19, the thesis applies mathematical modelling for epidemiological projections and analyses specified in the following Chapter 2 with targeted methods introduced in Chapter 3. The specific results are presented in Chapters 5-7 and are summarized

and discussed in Chapter 8.

CHAPTER 2

OBJECTIVES AND AIMS OF THE THESIS

This cumulative thesis addresses various aspects of the COVID-19 pandemics by mathematical modelling and is organized in 8 chapters. Coronavirus has changed our everyday lives and confronted society with novel challenges during the different waves. COVID-19 had a considerable effect on public health systems. In order to reduce the spread of COVID-19, non-pharmaceutical interventions (NPI) were implemented. NPI not just have an impact on the spread of the disease, but as well on the economic. To analyse these questions, research and new development was needed. I constructed a Susceptible-Exposed-Infectious-Recovered (SEIR)-based model to evaluate the effect of NPI and the economical impact. Mathematical models of epidemic are useful tools for estimating the situation and providing guidance to decision-makers. During the pandemic, adequate nowcasting and forecasting are crucial for public health planning, that is the reason for the setting up the SEIR-ICU model described in aim 2.

2.1 Specific aims of the thesis

In the following section, I briefly highlight the four main aims of this thesis which are further analysed in the corresponding result chapters. The individual aims are directly related to the different upcoming questions or phases during the on-going COVID-19 pandemic which were tackled by mathematical tools. The individual aims are then addressed in the corresponding result

chapters based on different publications where each chapter details my individual contribution to the individual manuscripts.

2.1.1 Aim 1: Mathematical modelling of suppression strategies against epidemic outbreaks

In the first phase of the pandemics, NPI such as physical distancing, stay at home measures or wear face masks were the only measure to mitigate the disease spreading [71]. To investigate most effective encroachment of NPI, I quantified the effect of them by an extended SEIR model. Firstly, the mitigation effect are investigated on a conceptual basis and in a second step data of various countries is reproduced and interpreted. SPQEIR model which is used in order to quantify the effect of NPI, has two additional compartments describing the protected (P) and quarantined (Q) proportion of the population. The model and its results are presented in Chapter 4.

2.1.2 Aim 2: COVID-19 potential path towards herd immunity in Austria, Luxembourg and Sweden

In the next phase of the pandemics, the question on herd immunity and the potential contribution of vaccination arose. In Chapter 5, I extended the SEIR model in order to incorporate hospitalization, ICU, death, social interaction and vaccination. These extended compartments represent the different stages of COVID-19. I investigated the path towards herd immunity by vaccination and infection for Austria, Luxembourg and Sweden based on data until 15 December 2020. For this purpose, I derived a method to calculate the reproduction number from the dynamics of the SEIR model as it allows the estimation of the minimum immunized population needed in order to reach herd immunity.

2.1.3 Aim 3: COVID-19 Crisis Management in Luxembourg: Insights from an Epidemionomic Approach

Another urgent question during the pandemics has been the impact on the economics. To address this challenge, a mathematical model has been developed in collaboration with Luxembourg Institute of Socio-Economic Research (LISER) that investigates the health and economic responses

to COVID-19 in Luxembourg. In Chapter 6, the model is presented which is a combination of Input-Output economic block with a multi-sector SIR of 78 socio-demographic groups (19 industries of 4 countries, students and retirees). The model allows to assess the risk of a new infection wave and investigates adequate non-pharmaceutical interventions.

2.1.4 Aim 4: Performance of early warning signals for disease re-emergence

During the further development of the pandemics, we had to observe several re-emergence of epidemic waves sometimes driven by new virus variants or changes in social interactions. An effective tool to give an early warning for the development of an epidemic wave would allow for efficient mitigation. Early warning signals are a part of complex systems theory with the aim to detect impending critical transitions. Chapter 7 aims to analyse potential early warning signals in the context of COVID-19 to detect critical transitions from empirical COVID-19 data. Furthermore, I investigate the potential of EWS to assess monitoring of the epidemic.

2.2 Structure of the thesis

Based on these specific aims, Chapter 3 gives the main scientific background on dynamical modelling and an introduction to epidemiological modelling by Susceptible-Infectious-Recovered (SIR) and Susceptible-Exposed-Infectious-Recovered (SEIR) models. Subsequently, the results are represented by my four core publications in Chapters 4-7 where in each chapter my individual contribution is clarified. These results are then summarized and put in prospective in the Discussion and Conclusion (Chapter 8.2). Along the pandemic, vaccines have been developed. However, the vaccine- and infection-induced immunity give only a short time protection [72]. As well as new variants manage to do immune escape. Additionally, wastewater is used to monitor the epidemic status and reconstruct the detected cases curves. Chapter 8 highlights these additional challenges faced later in the epidemic and analysed in the context of COVID-19 Task Force.

CHAPTER 3

BACKGROUND ON THE SCIENTIFIC APPROACH

This chapter gives the scientific background on the topics discussed in the thesis. In the first part, I introduce the situation of COVID-19 in Luxembourg and then I review the specificity of modelling with a focus on epidemiological modelling. Additionally, I give an overview on compartmental models and in particular on Susceptible-Infectious-Recovered (SIR) and Susceptible-Exposed-Infectious-Recovered (SEIR) models. Furthermore, a brief introduction to parameter estimation and early warning signals is given.

3.1 COVID-19 in Luxembourg

The outbreak of COVID-19 was first detected in Wuhan (China). The WHO declared the outbreak as a pandemic on 11 March 2020. As the thesis focuses mainly on the COVID-19 pandemic in Luxembourg, a short description on the COVID-19 development in Luxembourg is given. On 24 February, the first case was detected in Luxembourg. The lockdown for Luxembourg was declared on 18 March 2020 with a stay-at-home order, curfews and quarantines. The exit from the lockdown started with the construction sector and the reopening of do-it-yourself and gardening shops on 20 April 2020. All shops except hotels, restaurants and bars reopened on 11 May 2020. Furthermore, people were allowed to meet 6 people at home and 20 people outside again from that date on,. The measures for hotels, restaurants and bars were lifted on 24 June 2020. Accommodation

restriction were relaxed to 10 people at home on 24 July 2020. On 29 October 2020, a curfew between 11pm to 6am was introduced as well as the closing of bars at 10 pm as a response to again increasing case numbers. Gatherings of 10 to 100 people were only allowed under the condition of wearing masks and had to be held by seating. On 25 November 2020, the bars, restaurants, sports complexes, cinema and culture locations had to close again and introduction of a limitation to accommodate two people from the same household were implemented. The curfew starting at 9pm and closure of non-essential shops was introduced on 24 December 2020. On 28 December 2020, the first group of people which could get a vaccination, were healthcare workers, residents from retirement and nursing homes and people with disabilities living in facilities. The healthcare workers were among the first once that had the chance to get a dose. On December 28, 29, and 30, approximately 430 healthcare worker were invited to be get vaccinated each day [73]. On 12 March 2021, pupils in secondary school education did home schooling until 3 April 2021. Under strict rules of 2 April 2021 onward, terraces could open from 6am to 6pm and 2 people at one table were allowed. Due to the law from 14 May 2021, the curfew was postponed to 12pm and accommodation of 4 people were permitted at home. Inside of bars and restaurants, a negative test was requested. Four people at one table in bars and restaurants and gatherings with 150 people were permitted. The CovidCheck regime was introduced by a law of 12 June 2021 allowing the entry to public locations exclusively for people who can show a certificate of vaccination, recovery or a negative COVID-19 test. The CovidCheck 3G became also mandatory at workplace from 15 January 2022 until 28 February 2022 in response to the Omicron wave and required a valid certificate proofing the status of being fully vaccinated against SARS-CoV-2, recovery from a COVID-19 infection not longer than 180 days or a certified negative rapid test result (valid for 24 hours), or a negative PCR test (valid for 48 hours). The course of daily new cases, hospitalization and ICU occupation until 24 May 2022 is displayed in Fig. 3.1.

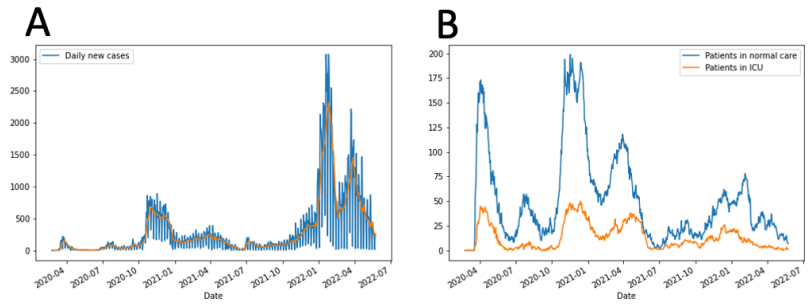

Figure 3.1: COVID-19 situation in Luxembourg until 24 May 2022. Reported are the daily new cases and 7-days moving average of daily new cases (**A**), hospital occupation (**B**) and ICU occupation (**B**).

Until 24 May 2022, 1077 people died from or with COVID-19 in Luxembourg and 247,257 cases were detected. Luxembourg was hit by 7 waves and the maximum of daily new cases was on 19 January 2022 with 3073 cases. The peak in the hospitals was reached on 17 November 2020 with 199 beds and in ICU on 16 November 2020 with 48 beds occupied. The vaccination strategy of Luxembourg is described in Section 8.2.3.

On 4 January 2021, the first case in Luxembourg of the Alpha variant was detected and 75% of the cases were caused by this variant in the week 13 of 2021 [74, 75]. The Alpha variant remained dominant until week 22 of 2021. followed by the Delta variant which was temporarily overruled by Gamma variant as the dominant variant in the weeks 26/27 of 2021 due to party activities on the National Day in Luxembourg [76]. Subsequently, the Delta variant was dominating the infection dynamics in Luxembourg [76] until week 51 of 2021 [77] when the first Omicron variant BA.1 cases appeared [78]. Since 18 March 2022, the Omicron BA.2 variant is the dominant variant in Luxembourg [79].

For quantitative analyses of this complex epidemic dynamics and corresponding projections about future developments, computational modelling became an essential tool to inform the public and political decisions makers. To support these mitigation strategies, I contributed by the different modelling approaches presented in this thesis.

3.2 General overview about modelling

According to Collins dictionary, a model is a theoretical description that allows to understand the functionalities of the system [80]. Models are employed to anticipate the behaviour of a systems and are approximations [81]. A model has different meanings to mathematicians, engineers and biologists [82]. For example, biological models can refer to experimental systems which rebuild a biological entity [83]. Experimental modelling in biology has the goal to gain new information on biological processes and lead to biological hypotheses [7, 11, 12]. In mathematics, the model is a mathematical simplified description of the essential functionalities based on knowledge which illustrate characteristics of the process [7]. However, even if the model is a simplification of the real world, the system behaviour should be maintained. The objectives of mathematical modelling are getting scientific understanding, testing various strategies and guiding decision making [84]. Mathematical modelling can be done by difference equations, in which the new value is given as a scalar of the old value and by a constant [85]. modelling often includes optimization with the goal to identify the solution fitting best to some empirical data [85]. Thus, models can be empirical meaning that the model is constructed based on the deduction of the relationships between variables of the data [86]. Empirical models are also often called data-driven models [86].

Mathematical modelling is useful to comprehend the dynamics of complex systems. The models are dynamic if they explain the evolution of the system in time [87]. They can be described by ordinary differential equations (ODEs), partial differential equations (PDEs) in continuous time or iterated maps on a low-dimensional state-space in discrete time [14]. Dynamical models allow to analyse relationships which are impossible or only hardly accessible by experimental methods [87]. Mathematical modelling is a keystone in systems biology where models are typically representations of fundamental aspects based on prior knowledge such as physical laws. The simplification gives us the possibility to understand the main characteristics of a complex system [88]. Therefore, modelling can be seen as a process of selection and subjectivity [7] since a model can just take into account a selection of system aspects.

3.2.1 Stages of modelling

The process of modelling can be divided into four stages: real world problem, mathematical model, solution and real world meaning of the result. The different stages of modelling are illustrated in Fig. 3.2.

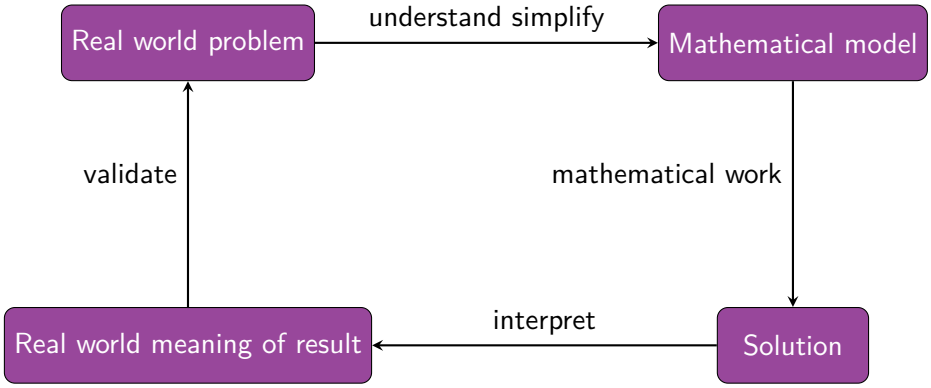

Figure 3.2: Stages of modelling. The figure is adopted according to [89, 90]

In order to build a mathematical model, the real world problem is simplified, assumptions are made and the key elements are identified. After these steps, the real world problem is translated into the language of mathematics. The interpretation of the solution of the model leads to predictive results which can then be validated in the scope of the real world problem. The model classification is done according to a set of criteria and based on that, we distinguish six different types of models: qualitative, quantitative, deterministic, stochastic, continuous and discrete models [7].

In a qualitative model, association among model components is established in contrast to a quantitative model in which to each interaction and element, a value is allocated. A deterministic model is based on the idea that the next development can be approximated from the current condition of the system in contrast to a stochastic model which yields a probabilistic distribution for the further development. In a continuous model, states and time are considered as continuous in contrast to discrete models in which time and states are discrete. A dynamic model is mechanistic and constructed in a way to represent our understanding of the system. Since self-organisation is strongly linked to the temporal domain in which an entity is emerging, dynamics is an essential tool to reveal underlying mechanisms of complex systems.

3.2.2 Dynamical systems and ODEs

A dynamical system describes the evolution of states in time to understand the qualitative behavior of the solutions [82, 87]. Dynamic models allow to make forecasts without extrapolating from data since they rely on mechanistic and potentially first principles [87]. The trajectory of a system corresponds to the dynamics of states which is followed over time from the starting point, also called the initial condition [82]. The system dynamics in continuous time and no spatial dimension is modelled by ODE where the first-order ODE has the form:

$$x_t = f(x)$$

with $x(t) \in \mathbb{R}^d$ being a vector of dependent variables, x_t denotes the time-derivative and $f : \mathbb{R}^d \to \mathbb{R}^d$ is a vector field [14].

A system biological approach is also required for approaching epidemiological studies of complex diseases based on the interplay of different layers such as gene, protein, metabolite expression, epigenomics and microbiomes [91]. The present thesis is addressing the current challenges of the COVID-19 pandemic in systems biology manner with a focus on epidemiological modelling with various aspects. The modelling of COVID-19 specific dynamics is often implemented by compartment models based on SEIR models as described in the next section.

3.3 Epidemiological modelling and infectious diseases

The term epidemiology has its roots in Greek and stands for the study of elements affecting people's health [92]. Moreover, epidemiology can be seen as the study of disease occurrence [93]. De Villalba, a Spanish physician used the term in the study of "Epidemiologia Espanola" for the first time in 1802. Today, epidemiology is an established branch of medical science and is often seen as the basic science of public health which considers the population health [92] by a data-driven and quantitative manner. A major task of epidemiology is the identification of determinants as factors which lead to a shift of the population health condition [92]. Epidemiologists originally focused on infectious disease or communicable disease which represent illnesses

caused by pathogenic microbial agents that can be divided into five groups: viruses, bacteria, fungi, parasites and prions [15].
The transmission happens when an agent exits its reservoir and the pathogen enters a susceptible host. The transmission happens as well as when a pathogen leaves its localized site in the host in the environment and to another host [94]. In this respect, reservoir corresponds to the territory of agent's life that can refer to humans, animals and the environment. In the context of COVID-19, it is important to highlight that zoonosis is a disease caused by pathogens which jumped from vertebrates to humans [95]. Prominent zoonoses of the last 200 years amongst others were the Ebola virus, SARS-CoV-2 and salmonellosis [95].

The transmission mechanisms are understood for most infectious diseases, but specific details are still often under investigation. The six different modes of transmission are: direct, droplet spread, airborne, vector-borne, environmental transmission and vertical [15, 94]. Direct transmission is given when the infectious agent called pathogen is transferred from one person to another. Droplet spread is a form of direct transmission and the spread happens in form of aerosols occurring during for example sneezing and coughing [94]. Thereby the pathogen stays in the air in small droplets which are aerosolized and inhaled by people and refers to the airborne transmission [96]. Vector-transmission is the transmission of a pathogen from a vector to a human [15]. The environmental transmission is characterized by the pathogen entering the host from the environment [15]. Vertical transmission describes an infection by the transmission of a pathogen from the mother to a child at birth [15].

Epidemiology distinguishes different levels of disease progression: epidemic, pandemic and endemic.

- Epidemics are characterized by an abrupt outbreak of a disease above the normal number of cases in a precise area [97]. Examples of epidemics are yellow fever, smallpox, measles, and polio.
- Pandemics are epidemics that spread over several countries or continents and affects a lots

of people. A recent example for a pandemic is the COVID-19 disease.

- Endemics are defined as a constant presence of a disease in a specific area. In different regions of the World, malaria is seen as an endemic. [98]

During the SARS epidemic (SARS-CoV) in 2002/2003, mathematical modelling of infectious diseases gained a huge interest as it allows to forecast further progression of the epidemic as well as the impact of different non-pharmaceutical interventions [99]. Furthermore, it allows for insights into the quantitative understanding of the dynamics of the disease including the estimate of changing transmissibility for different virus variants [100].
Compartment models are often used in epidemiological modelling where every individual is in a compartment at a given moment and can advance from one compartment to another. The population is divided into mutually exclusive groups also called compartments describing the infection status of individuals [100] as detailed below.

3.3.1 Susceptible-Infectious-Recovered (SIR) model

Kermack and McKendrick embossed the field of mathematical epidemiology with their SIR-model in 1927 [18]. The SIR-model describes the spread of an infectious disease with a coupled system of three deterministic ordinary differential equations. For this kind of model, we do not consider births or natural deaths but a 'closed' population. The population is divided into three groups according to their infectious state: susceptible (S), infectious (I) and recovered (R). The class of susceptible people considers the people who are healthy but can be infected by the pathogen. The infectious individuals are infected with the pathogen and can transmit it to other susceptible individuals. The recovered or removed individuals are immune and do not have any impact on the transmission dynamics. An underlying assumption for this kind of model is that recovering from the disease leads to lifetime immunity.

Figure 3.3: Compartmental diagram of SIR model.

$$\frac{\partial S}{\partial t} = -\beta SI$$
$$\frac{\partial I}{\partial t} = \beta SI - \gamma I$$
$$\frac{\partial R}{\partial t} = \gamma I$$

The model assumes a constant population size S+I+R=N. The transmission rate of the disease is β and the recovery rate is given by γ. The average amount of time a person stays in the infectious compartment is given by $\frac{1}{\gamma}$ [100]. A typical dynamics of an SIR model is shown in Fig. 3.4.

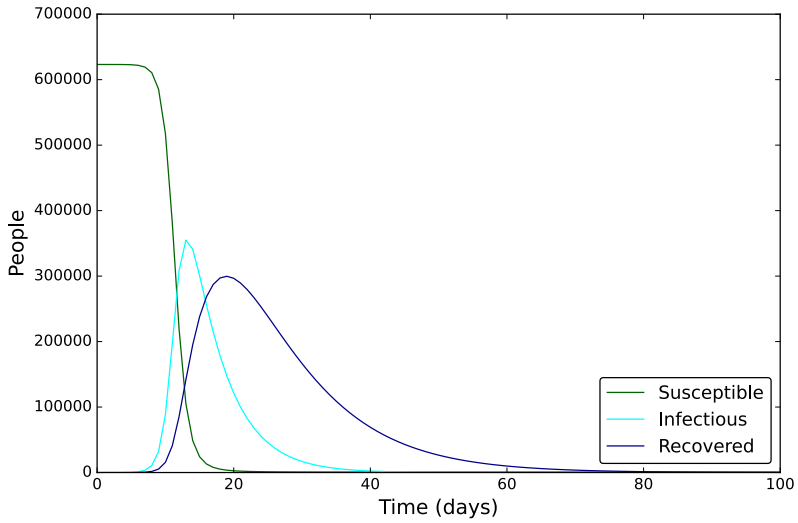

Figure 3.4: SIR model dynamics

3.3.2 Susceptible-Exposed-infectious-Recovered (SEIR) model

The SEIR-model represents and extension of the SIR model and analogously describes the spread of infectious disease by ordinary differential equations. In the SEIR model, the population is divided into four groups: susceptible (S), exposed (E), infectious (I) and recovered (R) as depicted in Fig. 3.5. With this extension, this model is more accurate compared to a SIR model because a delay between infection and becoming infectious is observed for most diseases such as Ebola and influenza. Like in SIR models, the SEIR models do not consider death and birth process leading

to a constant population size of N=S+E+I+R (Fig. 3.5). A typical dynamic of the SEIR model is shown in Fig. 3.6. The corresponding dynamics are governed by the generic equations

Figure 3.5: Compartmental diagram of SEIR model.

$$\frac{\partial S}{\partial t} = -\beta SI \tag{3.1}$$
$$\frac{\partial E}{\partial t} = \beta SI - \alpha E \tag{3.2}$$
$$\frac{\partial I}{\partial t} = \alpha E - \gamma I \tag{3.3}$$
$$\frac{\partial R}{\partial t} = \gamma I \tag{3.4}$$
$$\tag{3.5}$$

with the transition rates β, α and γ between the compartments. All the models that are part of

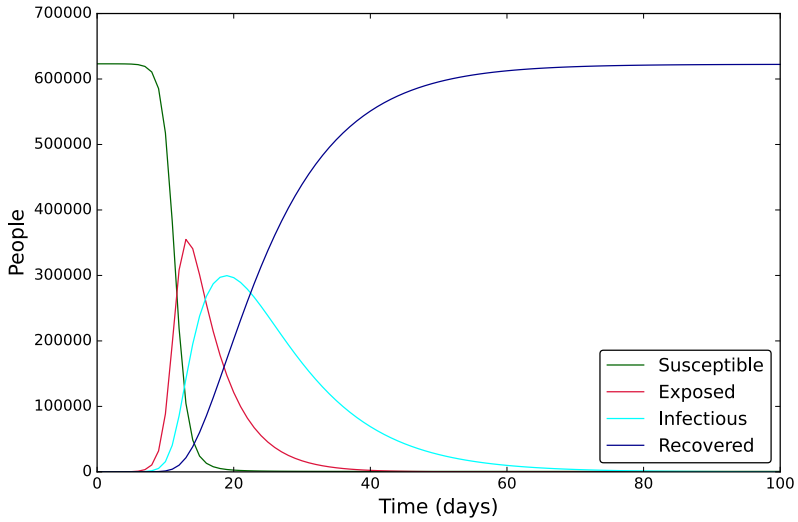

Figure 3.6: SEIR model dynamics

this thesis are based on the SEIR or SIR models. Additional compartments were added in order to answer specific scientific questions about the epidemic impact.

3.3.3 Basic reproduction number

The basic reproduction, denoted by R_0, is an important epidemiological concept and represents the average number of cases an infectious individual generates in a population. In other words, the reproduction number represents the number of secondary cases an infectious individual causes and characterizes the contagiousness of the disease [101, 102]. In the case, $R_0>1$, the spread of the disease continues and decreases if $R_0<1$. From the SEIR model, the basic reproduction number can be inferred by

$$R_0 = \frac{\beta}{\gamma}$$

where β and γ correspond to the corresponding rates.

3.3.4 Next generation matrix method

A commonly used method to compute R_0 is the next generation matrix method which requires the disease-free-equilibrium (DFE). Epidemiological models present two equilibria: the disease-free-equilibrium (DFE) and the endemic equilibrium [100]. In the case of DFE, no infected person remains in the population opposed to endemic equilibrium in which infected individuals are persistently present [100]. Following the calculation of DFE, a sub-model is set up which only deals with the disease compartments. In the case of SEIR models, the disease compartments for the creation of the sub-model are given by the exposed (E) and infectious (I) subpopulation. The sub-model takes then the following form:

$$\frac{\partial \overrightarrow{x}}{\partial t} = F(\overrightarrow{x}) - V(\overrightarrow{x})$$

with

$$V(\overrightarrow{x}) = V^{-}(\overrightarrow{x}) - V^{+}(\overrightarrow{x})$$

where $\overrightarrow{x}$ is a vector of the disease compartments, $F(\overrightarrow{x})$ incorporates the new infections and $V(\overrightarrow{x})$ consists of all other input and outputs [100]. The vectors for the SEIR model are given by

$$\begin{aligned}\frac{\partial \overrightarrow{x}}{\partial t} &= F(\overrightarrow{x}) - V(\overrightarrow{x}) \\ &= \begin{bmatrix} \beta SI \\ 0 \end{bmatrix} - \left(\begin{bmatrix} \alpha E \\ \gamma I \end{bmatrix} - \begin{bmatrix} 0 \\ \alpha E \end{bmatrix} \right) \\ &= \begin{bmatrix} \beta SI \\ 0 \end{bmatrix} - \begin{bmatrix} \alpha E \\ \gamma I - \alpha E \, . \end{bmatrix}\end{aligned}$$

The next step is the linearization around the DFE by using the Jacobian Matrix where the star denotes the equilibrium solution.

$$\begin{aligned}J(S^*, E^*, I^*, R^*) &= \begin{bmatrix} \frac{\partial E}{\partial E} & \frac{\partial E}{\partial I} \\ \frac{\partial I}{\partial E} & \frac{\partial I}{\partial I} \end{bmatrix} \Big|_{1,0,0,0} \\ &= \begin{bmatrix} -\alpha & \beta S \\ \alpha & -\gamma \end{bmatrix} \Big|_{1,0,0,0} \\ &= \begin{bmatrix} -\alpha & \beta \\ \alpha & -\gamma \, . \end{bmatrix}\end{aligned}$$

By outfactorization of the vector $\overrightarrow{x} = \begin{bmatrix} E \\ I \end{bmatrix}$ this leads to

$$\begin{bmatrix} \frac{\partial E}{\partial t} \\ \frac{\partial I}{\partial t} \end{bmatrix} = \left(\begin{bmatrix} 0 & \beta \\ 0 & 0 \end{bmatrix} - \begin{bmatrix} \alpha & 0 \\ -\alpha & \gamma \end{bmatrix} \right) \begin{bmatrix} E \\ I \end{bmatrix} \, .$$

The next generation matrix is then given by

$$FV^{-1} = \begin{bmatrix} \frac{\beta}{\gamma} & \frac{\beta}{\gamma} \\ 0 & 0 \end{bmatrix} .$$

The eigenvalues of the matrix above are $\frac{\beta}{\gamma}$ and 0 and therefore R_0 is given by

$$R_0 = \frac{\beta}{\gamma}$$

3.3.5 Effective reproduction number

During the pandemics, the transmissibility is better assessed by the effective reproduction number denoted by R_{eff} than by the basic reproduction number [103]. Furthermore, R_{eff} allows to identify changes in disease transmission over time [3]. It reports the number of secondary cases an infectious person causes on average at a given point in time depending on the immunity of the population. In order to investigate the effectiveness of interventions, the effective reproductive number is taken into consideration by [3]

$$R_t = R_0 \frac{S}{N}$$

and thereby scaling the R_0 value with the relative pool size of the S compartment. Thus, allows to estimate the effective social interactions in a population. The generation matrix method is used to determine R_{eff} of my SEIR model in Chapter 5.

3.4 Parameter estimation

A challenging problem in modelling of dynamical systems is the parameter estimation because the parameter values determine the model's behaviour [104]. In general terms, the parameter values are estimated by fitting a model to a set of data which can come for example from an experimental setup [7]. Calibrating a model to closely fit the data is a procedure in which least-squares optimization is often used. However, such methods like least-squares optimization

do not take the underlying uncertainty into account [105]. Therefore, the Bayesian framework which allows for the integration of uncertainties is typically a more powerful approach for model calibration.

3.4.1 Levenberg-Marquardt algorithm

The Levenberg-Marquardt algorithm is used to solve non-linear least-square problems. It was introduced around 1960 [106]. The goal of Levenberg-Marquardt algorithm is to find parameter values of a model by minimizing an objective function. The objective function is determined as the sum of squares of the errors between the model simulation and data. Levenberg-Marquardt algorithm is a combination of two algorithms namely the gradient descent and the Gauss-Newton method [107] that tries to solve

$$[J^T W J + \lambda diag(J^T W J) h_{lm}] = J^T W (y - \hat{y}) \ ,$$

where λ is a damping parameter, J the Jacobian matrix, h the perturbation and W denotes the inverse of the measurement error covariance matrix. The weighting matrix W is diagonal with $W_{ii} = \frac{1}{\sigma_{yi}^2}$ which corresponds to the error of $y(t_i)$ [107]. In the case, the damping parameter is large, the algorithm acts as gradient descent update. In the opposite case, the algorithm behaves like a Gauss-Newton update. The first update results to be in a steepest-descent direction. If an iteration results in a worse approximation $\chi^2(p + h_{lm}) > \chi^2(p)$ then λ is increased where χ^2 denotes the error criterion measures for the quality of the fit between the model simulation and the data. The error criterion is given by

$$\chi^2 = \frac{1}{m - n + 1} \sum_{i=1}^{m} [\frac{y(t_i) - \hat{y}(t_i, p)}{\sigma_{yi}}]^2$$

with σ_{yi} being the standard deviation, the model simulation $\hat{y}(t_i, p)$ of an independent variable t and a vector of n parameters p, and y_i corresponds to the data. In the case the quality of the fit is low, $\chi^2 > n$ holds , otherwise the quality of the fit is good with $\chi \approx n$. The model is overfitted if $\chi < n$. The Levenberg-Marquardt algorithm is used in Chapter 4 of the thesis for the parameter calibration of our model.

3.4.2 Markov Chain Monte Carlo

The Markov Chain Monte Carlo (MCMC) approach is widely used to fit complex models and it is a combination of Monte-Carlo and Markov chains. The characteristic of Monte-Carlo is the property of randomly sampling a probability distribution. A Markov chain is a stochastic process generating random samples by a sequential process [108]. MCMC was introduced soon after the Monte-Carlo method at Los Alamos. MCMC has the goal to generate a sequence of random samples $(\theta_1, \cdots, \theta_N)$ which reaches the posterior distribution with increasing N. It is based on Bayesian inference which employs the data information of a parameter and has revolutionised Bayesian data analyses [108].

The Bayes' formula is given by

$$\pi(\theta|Y) = \frac{\mathcal{L}(Y|\theta)\pi_0(\theta)}{\int_{\mathbb{R}^p} \mathcal{L}(Y|\theta)\pi_0(\theta)d\theta}$$

with $\mathcal{L}(Y|\theta)$ being the likelihood of the observations Y given a parameter set θ [109]. The aim is the determination of posterior density $\pi(\theta|Y)$ which is the probability density for a parameter value θ given the observation Y. Parameter information such as the constraints is stored in the prior distribution $\pi_0(\theta)$ [86]. The denominator corresponds to the normalization constant and ensures that the posterior integrates to one [109].

3.4.3 Metropolis algorithm

A commonly used MCMC algorithm is the Metropolis algorithm introduced by Nicholas Metropolis in 1953 with the underlying assumption of a symmetric proposal distribution [86]. For the Metropolis algorithm a possible parameter value from a proposal distribution $q(.|\theta_n)$ is generated and subsequently a transition probability is calculated. The Metropolis algorithm has three steps. The first step is to choose a starting point θ_1 and the second step is to choose a new candidate $\hat{\theta}$ from the distribution $q(., \theta_n)$. The last step is to accept the candidate with the transition probability given by

$$a(\theta_n, \hat{\theta}) = min(1, \frac{\pi(\hat{\theta})}{\pi(\theta_n)}).$$

For this purpose, a uniform random number $u \in [0,1]$ is generated. In a subsequent evaluation, the candidate parameter value is accepted if $u \leq a(\theta_n, \hat{\theta})$. Otherwise, i.e. if $u > a(\theta_n, \hat{\theta})$, the candidate parameter value is rejected and a new possible parameter value is generated [86, 110].

3.4.4 Adaptive Metropolis

A challenge in MCMC is the accurate choice of the proposal distribution [86]. The random walk Metropolis algorithm of 1953 is the basis for the adaptive Metropolis (AM) [111]. The proposal covariance matrix is determined by the whole history of states. The proposal distribution $q(.|\theta_0, \cdots, \theta_{n-1})$ has to be Gaussian and the new candidate is evaluated by applying $C_n = s_d Cov(\theta_0, \cdots, \theta_{n-1}) + \epsilon I_d$ where ϵ is a small constant and s_d a scaling factor [86]. At the beginning, an arbitrary strictly positive definite initial covariance C_0 is selected based on prior knowledge. The index $n_0 > 0$ determines the length of the initial period called burn-in period. The burn-in represents the beginning of a chain which is often removed as the sample mean of this part changes considerably. The beginning of a chain is affected by the starting point and for adaptive methods the initial choice of the parameters can be crucial [112], which holds in particular for finite chain lengths.

The covariance C_t is determined by

$$C_t = \begin{cases} C_0 & n \leq n_0 \\ s_d Cov(\theta_0, \cdots, \theta_{n-1}) + s_d \epsilon I_d & n > n_0 \end{cases}.$$

The empirical covariance matrix is defined as

$$Cov(\theta_0, \cdots, \theta_k) = \frac{1}{k}(\sum_{i=0}^{k} \theta_i \theta_i^T - (k+1)\overline{\theta}_k \overline{\theta}_k^T)$$

where $\overline{\theta_k} = \frac{1}{k+1}\sum_{i=0}^{k}\theta_i$ and θ_i are column vectors. The recursive formula for the covariance without high computational cost is given by

$$C_{n+1} = \frac{n-1}{n}C_N + \frac{s_d}{n}(n\overline{\theta}_{n-1}\overline{\theta}_{n-1}^T - (n+1)\overline{\theta}_n\overline{\theta}_n^T + \theta_n\theta_n^T + \epsilon I_d)$$

where $\overline{\theta_n}$ is the mean.

3.4.5 Metropolis-Hastings algorithm

The Metropolis-Hastings (MH) algorithm invented by Wilfred Keith Hasting in 1970 is a simple and powerful algorithm. The idea of Metropolis-Hastings algorithm is characterized by non-symmetric proposal distributions [86]. For the rest, the Metropolis-Hasting is similar to the Metropolis algorithm except the probability for the acceptance which is given by

$$a(\theta_n, \hat{\theta}) = min(1, \frac{\pi(\hat{\theta})q(\theta_n|\hat{\theta})}{\pi(\theta_n)q(\hat{\theta}|\theta_n)})$$

with $q(\theta_n|\hat{\theta})$ being the density for proposing a move from the present candidate to the next one.

3.4.6 Delayed Rejection

Delayed Rejection (DR) is based on standard Metropolis-Hastings algorithm with the goal to increase its efficiency [113]. DR allows to save CPU time as it takes the hierarchy between kernels under consideration. In DR, there can be a dependence between on the rejected values at earlier stages and the proposal of the next stage [114]. The probability of accepting the move from θ_n to $\hat{\theta}$ is given by

$$a_1(\theta_n, \hat{\theta}) = min(1, \frac{\pi(\hat{\theta})q_1(\hat{\theta}|\theta_n)}{\pi(\theta_n)q_1(\theta_n|\hat{\theta})}) \ .$$

In the case of rejection, a second stage move $\hat{\theta}^{(2)}$ is introduced from a different proposal distribution q_2 and evaluated according to the acceptance probability:

$$a_2(\theta_n, \hat{\theta}, \hat{\theta}^{(2)}) = min(1, \frac{\pi(\hat{\theta}^{(2)})q_1(\theta^{(2)}|\hat{\theta})q_2(\theta^{(2)}\hat{\theta}, |\theta_n)[1 - a_1(\hat{\theta}^{(2)}, \hat{\theta})]}{\pi(\theta_n)q_1(\theta_n, \hat{\theta})q_2(\theta_n, \hat{\theta}|\hat{\theta}^{(2)})[1 - a_1(\theta_n, \hat{\theta})])} \ .$$

In the case, the second stage proposal is accepted then an ergodic chain is created [113]. In most cases, a two-stage proposal is used. The first stage proposal is an up-scaled version of the second-stage proposal. The goal of the rejection is to test a new candidate value closer to the current point [113].

3.4.7 Delayed Rejection Adaptive Metropolis algorithm

The Delayed Rejection Adaptive Metropolis (DRAM) algorithm introduced in 2006 is a direct way of combining adaptive Metropolis (AM) and delayed rejection (DR). The idea of DRAM is to diminish the in-chain auto-correlation [112]. M-stages of DR algorithm works like the following. Like in AM, the proposal at the first stage of DR is modified [113]. From the chain points, the covariance C_n^1 is determined regardless of the stage of acceptance of the DR. At i-th stage, the covariance C_n^i is given by a scaled version of the proposal $C_n^i = \eta_i C_n^1$ with η_i being a fixed scaling factor [86, 113]. The DRAM algorithm is applied in the thesis in Chapter 4 and Chapter 5 for the parameter calibration of our model and to quantify their uncertainties.

3.4.8 Convergence

The goal of a convergence procedure is to estimate how long the chain must run to get close to the stationary distribution. Different approaches were developed for this purpose.

Gelman-Rubin approach

The method of Gelman and Rubin, established in 1992, gives insights about how close the process is to convergence and the amount of improvement that can be expected for further simulation steps [115]. The beginning of the method independently simulates $m > 2$ sequences of length $2n$. The starting point of a sequence is over-dispersed with respect to the stationary distribution [116]. The first n samples of each chain are discarded and is considered as the burn-in. The remaining part is divided into two chains to estimate if the stationary distribution is attained by each chain. In order to check if the samples are from the desired stationary distribution [116], the between-chain variance is compared to the within-chain variance. With θ_{ij} denoting the samples after discarding burn-in and the splitting into two chains, the between-sequence variance B is

defined as

$$B = \frac{n}{m-1} \sum_{j=1}^{m} (\overline{\theta_{.j}} - \overline{\theta_{..}})^2 \ .$$

The within-sequence variance is defined by

$$W = \frac{1}{m} \sum_{j=1}^{m} s_j^2$$

with

$$s_j^2 = \frac{1}{n-1} \sum_{i=1}^{n} (\theta_{ij} - \overline{\theta_{.j}})^2$$

and $\overline{\theta_{.j}} = \frac{1}{n} \sum_{i=1}^{n} \theta_{ij}$, $\theta_{..} = \frac{1}{m}$. The weighted average Var of between-sequence variance B and within-sequence variance W can be estimated by

$$\hat{Var}^{+}(\theta|Y) = \frac{n-1}{n} W + \frac{1}{n} B \ .$$

with $\hat{Var}^{+}$ being the overestimation of the maginal posterior variance. In 1992, Gelman and Rubin proposed the potential scale reduction factor $\hat{R}_c$ which is used for diagnosing convergence as

$$\hat{R}_c = \sqrt{\frac{\hat{Var}^{+}(\theta|Y)}{W}} \ .$$

If $\hat{R}_c$ is close to 1, the sequences are close to the target distribution [115].

Geweke approach

Geweke built a convergence diagnostics based on spectral density estimation in order to ensure the stationarity of the chains. The approach tests for equality of the means of the first 10% and the last 50% of a Markov chain. Geweke convergence diagnostics takes into account the autocorrelation in the calculation of the error [117]. Some functional is given by $\theta(Y)$ and $\theta^t = \theta(Y^{t+n_0})$ corresponds to a sequence with n_0 the start iteration [118]. Y corresponds to the observations. With

$$\overline{\theta}_A = \frac{1}{n_A} \sum_{t \in A} \theta^t$$

and

$$\overline{\theta}_B = \frac{1}{n - n^* + 1} \sum_{t \in B} \theta^t$$

defining means for two different iteration periods with $1 < n_A < n^* < n$ and $\frac{n_A + n_B}{n} < 1$, the sequence θ^t is stationary for $n \to \infty$

$$Z_n = \frac{\overline{\theta}_A - \overline{\theta}_B}{\sqrt{\frac{\hat{S_\theta^A}(0)}{n_A} + \frac{\hat{S_\theta^B}(0)}{n - n^* + 1}}} \to N(0,1) \; .$$

with $S_\theta(0)$ is the spectral density and $\frac{\hat{S_\theta^A}(0)}{n_A}$ and $\frac{\hat{S_\theta^B}(0)}{n - n^* + 1}$ are the asymptotic variances of θ_A and θ_B [118]. Geweke's approach has an asymptotically standard normal distribution [118]. The result of Z_n is used to test the null hypothesis of equal location of the chains at different iteration time periods. If $|Z_n|$ is large meaning that the chain has not converged by time n_0, the null hypothesis is rejected [118]. Based on this criterion, the Geweke diagnostics tackles the verification of a necessary, however not sufficient condition for convergence.

3.5 Early warning signals

All the various aspects of this section are applied in Chapter 7 in the context of COVID-19 and the related challenge to predict epidemic re-emergence. Sudden transition of complex systems from one state to another are recently addressed from the perspective of critical transitions [119, 120]. Such critical transitions needs to be understood in order to prevent or predict upcoming phenomena like stock market crashes, earthquakes, climate change or epileptic seizures. Even if these examples of phenomena seems to be of very different nature, the prevenient critical transition of such phenomena can share common descriptions. One attribute shared is that in the underlying dynamical system exhibits a sudden and rapid shift. Close to the transition, the system traverses a threshold between the two alternative states which are typically separated by a large distance [121]. A lot of efforts were made in order to predict critical transitions before they occur where early warning signals are proposed to predict critical transitions based on statistical time series signals [122]. A regime shift or critical transition is often preceded by a phenomenon called

critical slowing-down. During this period, the system requires more time to restore from small perturbations [122]. Critical slowing-down is a general feature of local bifurcations [123, 124] and occurs in each continuous model reaching a fold bifurcation [119]. The three main different kinds of critical transitions are bifurcation induced tipping (B-tipping), noise-induced tipping (N-tipping) and rate-induced tipping (R-tipping). The bifurcation induced tipping is characterized by one or more parameters reaching a critical value and leading to a bifurcation from one state to a new stable state [125]. The noise-induced tipping happens due to perturbation which leads to the switch from one state to another in a multi-stable system. For the existence of the rate-induced tipping, stable state needs to coexist consistently [125] and the change of a control parameter, i.e. the rate, is too fast for the system to remain in its local basin of attraction and switches to an alternative state as described by Wieczorek [126].
Such transitions are typically accompanied by changes in the variance and the autocorrelation which increases close to the transition point with asymmetric fluctuations in the observable x.

- Variance

  The variance is commonly used for the identification of critical slowing down. The increase of the variance close to the transition happens due to the increased time needed to restore from perturbations [125]. The variance is given by

  $$\sigma^2 = \frac{1}{N-1}\sum_{i=1}^{N}(x_i - \mu)^2$$

  with μ is the mean of the observable x_t.

- Skewness and Kurtosis

  Skewness is the measure for the asymmetry of a distribution and the third standarized moment of the distribution. It can take the values zero, negative, positive or undefined. A skewness of 0 means a symmetrical distribution. Negative skewness stands for a longer or fatter tail on the left side of the distribution and the mean is smaller than the median. Positive skewness stands for a longer or fatter tail on the right side of the distribution and the mean is greater than the median. The formula for skewness is defined for univariate

data $x_1, x_2, \cdots, x_N$ as

$$S = \frac{\sum_{i=1}^{N} \frac{(x_i-\mu)^3}{N}}{\sigma^3}$$

with μ being the mean, σ the standard deviation and N the number of data points [127]. Kurtosis is heavy-tailed or light-tailed relative to a normal distribution and represents the fourth standarized moment of a distribution. There are three types of kurtosis: mesokurtic, leptokurtic and platykurtic. If the kurtosis is equal to 3, then the distribution is mesokurtic. Kurtosis smaller than 3 means that the distribution is platykurtic. Platykurtic distributions are flat and have a thin tail. Kurtosis bigger than 3 means that the distribution is leptokurtic. Leptokurtic distributions are peaked and have a heavy tail. The formula for the kurtosis is given for univariate data $x_1, x_2, \cdots, x_N$ by

$$\kappa = \frac{\sum_{i=1}^{N} \frac{(x_i-\mu)^4}{N}}{\sigma^4}$$

with μ being the mean, σ the standard deviation and N the number of data points [127].

- Autocorrelation

  The critical slowing down leads to an increase in the correlation of the system [125]. The coefficient describing the correlation between two values in a time series is the autocorrelation function (ACF) [128]. ACF(1) is the lag 1 autocorrelation which is the correlation between values of one time step apart [128]. $ACF(\tau)$ is determined by

$$A(\tau) = \frac{1}{N} \sum_{i=1}^{N} \frac{(x_i - \mu)(x_{i+\tau} - \mu)}{(x_i - \mu)^2}$$

3.6 Detrending

In order to detect EWS, detrending is an important preprocessing step. Detrending reduces effects of trends from time series such as the seasonality and other irregularities. Time series consists of different components: trend, seasonal and noise. During the detrending phase, deterministic and stochastic trends are removed. The goal of detrending methods is to achieve stationarity of

the time course data. The detrending methods applied later in the thesis are ARIMA, moving average and Gaussian filtering.

3.6.1 Moving average

The moving average is used to smooth short-term fluctuations and is the basis of the decomposition methods given by

$$\hat{T}_t = \frac{1}{m} \sum_{j=-k}^{k} y_{t+j}$$

for smoothing order m with $m = 2k + 1$ and y_{t+j} is the time course data vector. The trend-cycle is calculated by averaging values of the time series within k periods of t [129].

3.6.2 Gaussian kernel

Smoothing means the proceeding through time series by a point by point manner and for each point a new value is calculated in relation to the neighboring points. The word 'kernel' for smoothing refers to the shape used to take the average of the neighboring points. The Gaussian kernel was introduced by the German mathematician Carl Friedrich Gauß. The 1-D Gaussian kernel is given by

$$G(x) = \frac{1}{\sqrt{2\pi}\sigma e^{\frac{-x^2}{2\sigma^2}}} .$$

Gaussian smoothing (or Gaussian kernel smoothing) computes a weighted average of the points, where the weights correspond to a Gaussian distribution with the standard deviation specified as the smoothing parameter.

3.6.3 Autoregressive integrated moving average

Autoregressive integrated moving average (ARIMA) is a statistic model for analyzing and predicting the data of time series. It intends to characterize the data auto-correlation and represents a form of regression analysis. The goal of ARIMA is to predict future data points based on previous data points [130].

In a non-seasonal ARIMA(p,d,q), the autoregressive terms p correspond to the lags of the station-

ary series, the moving average q is the lags of the forecast errors. The lagged moving average is used to smooth the data. d is the differenced order of the raw data transferring non-stationary time series into stationary time series [131]. The formula of an ARIMA is given as

$$y_t^{'} = c + \alpha_1 y_{t-1}^{'} + \cdots + \alpha_p y_{t-p}^{'} + e_t + \zeta_1 e_{t-1} + \cdots + \zeta_q e_{t-q}$$

with e_i is an error term of data point i and c is a constant. ARIMA has a lagged p for the autoregressive part and the lagged q for the moving average part [131]. Special cases of ARIMA are:

- ARIMA(0,1,0) given by $y_t = y_{t-1} + e$ corresponds to random walk
- ARIMA(0,0,0) given $y_t = e$ corresponds to white noise
- ARIMA(p,0,0) is an autoregressive model

3.7 Kendall-τ score

In 1938, Maurice Kendall introduced the Kendall-τ score. The Kendall-tau score, which is a statistic measure, gives information about rank correlation between two variables. For (x_i, y_i) and (x_j, y_j) as a pairs in the time series, $x_i < x_j$ and $y_i < y_j$ describes a concordant pair. If $x_i < x_j$ and $y_i > y_j$, then the pair is discordant. If $y_i = y_j$ then the pair is neither concordant neither discordant [132]. This property is determined by

$$\tau = \frac{\#\text{concordant pairs} - \#\text{discordant pairs}}{M(M-1)/2}$$

wit M corresponding to the number of points.

3.8 Receiver-operating characteristic curves

Receiver-operating characteristic curve (ROC) shows the trade-off between the true positives against the false positives rate [133]. It was first introduced in the domain of signal-processing and

nowadays used a lot in the field of machine learning. The performance of a binary classification test is represented by ROC [134]. In the framework of EWS, ROC is used to compare their performance by a graphical plot which analyses the statistical indicators according to their ability to correctly differentiate between a Kendall-τ scores describing a null simulation and a Kendall-τ scores describing an undergoing transition [135, 136]. ROC is a compromise between accuracy and sensitivity of EWS indicators [137]. It analyses the performance of EWS indicators as the detected sensitivity is different for stable systems to those close to a critical transition [137].
The area under the ROC curve (AUC) is the area below the ROC curve and varies between 0 and 1. Thus, AUC gives information about the predictive power between different indicators [132]. AUC close to 1 means a good performance, and AUC close to 0 indicates a bad performance. For critical transitions, an AUC close to 0.5 indicates that the statistical indicator used is not better than random in identifying the critical transition whereas an AUC close to 1 indicates a good statistical indicator with high sensitivity in identifying critical transitions [138].
The here detailed introduced methods are used in the following result chapters to address the specific aims for the analysis of the COVID-19 pandemics given in Chapter 2.

CHAPTER 4

MATHEMATICAL MODELING OF SUPPRESSION STRATEGIES AGAINST EPIDEMIC OUTBREAKS

This chapter is based on

Daniele Proverbio, Françoise Kemp, Stefano Magni, Andreas Husch, Atte Aalto, Laurent Mombaerts, Alexander Skupin, Jorge Goncalves, Jose Ameijeiras-Alonso, Christophe Ley. Dynamical SPQEIR model assesses the effectiveness of non-pharmaceutical interventions against COVID-19 epidemic outbreaks. PLOS ONE 16(5): e0252019. https://doi.org/10.1371/journal.pone.0252019

Introduction 1

In this chapter, I quantify non-pharmaceutical strategies (NPI) by an extended SEIR model. NPI are measures like physical distancing, staing at home measures, wearing face masks with the aim to slow down the spread of the virus [71]. Moreover, in most countries around the world, governments introduced a lockdown in March 2020 with socio-economic consequences. Besides vaccination, NPI are the most effective encroachments. Since an estimation of the impact of such interventions is hard to quantify, we firstly investigated the mitigation effect on a conceptual basis and in a second step, we reproduced and explained data of various countries. This investigation performed by an extended SEIR model provides information on the best synergies of NPI. The extended SEIR model consists of the classical SEIR module and two additional compartments representing protected (P) and quarantined (Q) people.

I contributed to the project by performing different analyses. Particularly, I took care of the parameter estimation by Markov Chain Monte Carlo for the various countries. Furthermore, I wrote the original draft of the paper, reviewed and edited the manuscript during the publishing process.

Abstract

Against the current COVID-19 pandemic, governments worldwide have devised a variety of non-pharmaceutical interventions to mitigate it. However, it is generally difficult to estimate the joint impact of different control strategies. In this paper, we tackle this question with an extended epidemic SEIR model, informed by a socio-political classification of different interventions. First, we inquire the conceptual effect of mitigation parameters on the infection curve. Then, we illustrate the potential of our model to reproduce and explain empirical data from a number of countries, to perform cross-country comparisons. This gives information on the best synergies of interventions to control epidemic outbreaks while minimising impact on socio-economic needs. For instance, our results suggest that, while rapid and strong lockdown is an effective pandemic mitigation measure, a combination of social distancing and early contact tracing can achieve similar mitigation synergistically, while keeping lower isolation rates. This quantitative understanding can support the establishment of mid- and long-term interventions, to prepare containment strategies against further outbreaks. This paper also provides an online tool that allows researchers and decision makers to interactively simulate diverse scenarios with our model.

Keywords

COVID-19, Cross-country comparison, Risk assessment, Epidemiological modelling, Non-pharmaceutical interventions, Public health.

4.1 Introduction

The current global COVID-19 epidemic has led to significant impairments of public life world-wide. To mitigate the spread of the virus and to prevent dramatic situations in the healthcare systems, many countries have implemented a combination of rigorous measures like lockdown, isolation of symptomatic cases and the tracing, testing, and quarantine of their contacts. In order to obtain information about the efficacy of such measures, a quantitative understanding of their impact is necessary. This can be based on statistical methods [139] and on epidemiological models [140]. Epidemiological modeling in particular can provide detailed mechanisms for the epidemic dynamics

and allow investigating how epidemics will develop under different assumptions.

Preliminary efforts have been made to quantify the contribution of different policy interventions [141], but these rely on complex models based on a number of assumptions. Instead, we base our study on a classical SEIR-like epidemiological model. SEIR models are minimal mechanistic models that consider individuals transitioning through Susceptible → Exposed → Infectious → Removed state during the epidemics [142]. The essential control parameter is the basic reproduction number R_0 [143], that worldwide non-pharmaceutical mitigation strategies aim at reducing below the threshold value 1. Several literature studies consider the effect of single interventions in SEIR-like models [144–146]. We aim at considering the added value of early interventions, namely those that target Susceptible and Exposed people, and the effect of different combinations of control strategies on the infection curve. To do so, we incorporate additional compartments reflecting different categories of control strategies, identified by socio-political studies [147]. In particular, the model focuses on four main mitigation programs: social distancing (lowering the rate of social contacts), active protection (decreasing the number of susceptible people), active removal of latent asymptomatic carriers [148], and active removal of infectious carriers. This study investigates how these programs achieve mitigation both individually and combined, first conceptually and then by cross-country comparison. By our modelling choice, we consider how and how much preventive interventions can supplement the quarantining of contagious individuals. We ultimately show that analogous containment levels of the infectious curve can be achieved by alternative synergies of non-pharmaceutical interventions. This information can supply Government decisions, helping to avoid overloading the healthcare system and to minimise stressing the economic system (due to prolonged lockdown). We expect our model, together with its interactive online tool, to contribute to crucial tasks of decision making and to prepare containment strategies against further outbreaks.

4.2 Methods

This study links policy measures to epidemiological modelling, focusing on how the dynamics of the infectious curve is controlled by several interventions. Initially, we perform a conceptual analysis, like in other works [149, 150]. Then, we investigate how well the considered control

synergies reproduce and explain the evolution of empirical data from the first COVID-19 wave in six different countries. By doing so, we hope to contribute to discussions about the relevance of such conceptual strategies in real-world conditions. In this section, we illustrate the modelling choices and the use of data.

4.2.1 The classical SEIR model

SEIR models are continuous-time, mass conservative compartment-based models of infectious diseases [18, 142]. They assume a homogeneously mixing population (or fully connected graphs) and focus on the evolution of mean properties of the closed system. All of these models are classical and widely used tools to investigate the principal mechanisms governing the spread of infections and their dynamics. There is a broad range of such models, from more conceptual to more realistic versions, e.g. SEIR with delay [151], spatial coupling [152, 153], extended compartments [154], or those that consider progression of treatments and age distribution [24].
Main compartments of SEIR models (see Fig. 4.1, framed) are: susceptible S (the pool of individuals socially active and at risk of infection), exposed E (corresponding to latent carriers of the infection), infectious I (individuals having developed the disease and being contagious) and removed R (those that have processed the disease, being either recovered or dead). The model's default parameters are the average contact rate β, the inverse of mean incubation period α and the inverse of mean contagious period γ. When focusing on infection dynamics rather than patients' fate, the latter combines recovery and death rate [155]. From these parameters, epidemiologists calculate the "basic reproduction number" $R_0 = \beta/\gamma$ [156] at the epidemic beginning. During the epidemic progression, isolation after diagnosis, vaccination campaigns and active mitigation measures are in action. Hence, we speak of "effective reproduction number" $\hat{R}(T)$ [157].

4.2.2 Data and analyzed countries

When investigating the ability of our conceptual model to explain mitigation, we compared it with empirical data. To do this, we considered the main non-pharmaceutical interventions applied by several countries, by integrating multi-disciplinary information. In fact, governments worldwide have issued a number of social measures, including those for public health safeguard, economic

support, movement restriction and non-pharmaceutical interventions to hamper disease spreading. Scholars from political sciences and sociology have recorded and classified such measures [158, 159]. Among the resources listed on the World Health Organization "Tracking Public Health and Policy Measures" [147], we used information from the ACAPS database [160] that contains a curated categorization of policy measures. ACAPS is an independent, non-profit information provider helping humanitarian actors to respond more effectively to disasters. The ACAPS analysis team has aggregated and classified interventions from different sources (media, governments and international organizations), for all countries and in time. Mitigation measures against the epidemic are classified under "Movement restrictions", "Lockdown", "Social Distancing" and "Monitoring and Surveillance". Our modelling choice is based on these categories, which are reflected by additional compartments to the classical SEIR model (see next section).

Epidemiological data for all selected countries and regions were obtained from the COVID-19 Data Repository by the Center for Systems Science and Engineering (CSSE) at Johns Hopkins University [161]. The data are from 22 Jan 2020 to 08 July 2020. Lombardy data were obtained from the Protezione Civile Italiana data repository "Dati COVID-19 Italia" [162], from 22 Feb 2020 to 08 July 2020. We acknowledge that the quality of data of early detection of COVID-19 cases is often associated with limited testing capabilities, which could bias subsequent analysis. However, across the analysed countries, the share of positive tests was similar (see e.g. [163]), and no significant deviation from expected dynamics was observed by studies applying Benford's law [164, 165], possibly indicating that these data still capture to a reasonable extent the dynamics of the epidemic wave. In addition, the analysed countries were selected based on the fact that they sufficiently met the other model assumptions, e.g. low spatial heterogeneity and large amount of cases to fulfill the mean field assumption.

This study analyses the effect of mitigation measures in flattening the curve. Despite having a precise starting date, such measures take some days to be fully effective. We estimate an average delay using the Google Mobility Reports [163, 166] for the selected countries. Google provides changes in mobility with respect to a monthly baseline, w.r.t. 6 locations: Retail & Recreation, Grocery & Pharmacy, Transit stations, Workplaces, Residential, Parks. We average the decrease in mobility at the first four locations (corresponding to those where social mixing happens more

Country	Measures	Param. involved	Starting Date	Population (rounded)
Austria (AT)	Partial lockdown	μ, ρ	16 Mar	9,000,000
	Social distancing	ρ, μ	16 Mar	
	Contact tracing	χ	16 Mar	
	Phase-out		Around 14 April	
Denmark (DK)	Social distancing	ρ, μ	13 Mar	6,000,000
	Mild surveillance	η	13 Mar	
	Phase-out		14 Apr	
Ireland (IR)	Partial lockdown	μ, ρ	28 Mar	5,000,000
	Social distancing	ρ, μ	13 Mar	
	Phase-out		18 May	
Israel (IL)	Partial lockdown	μ, ρ	15 Mar	9,000,000
	Social distancing	ρ, μ	15 Mar	
	Contact tracing	χ	15 Mar	
	Phase-out		19 April	
Lombardy (LO)	Lockdown	μ, ρ	13 Mar (Italian)	10,000,000
	Social distancing	ρ, μ	13 Mar	
	Phase-out		Around 15 Apr	
Switzerland (CH)	Lockdown	μ, ρ	16 Mar	8,500,000
	Social distancing	ρ, μ	16 Mar	
	Phase-out		27 Apr	

Table 4.1: Test countries, with corresponding implemented measures (following the ACAPS database [160]), parameters in our SPQEIR model and starting date. For Lombardy, we used the Italian official date for lockdown. Differently from other countries, Ireland issued measures on two different dates; we use this case to compare social distancing and lockdown effect in a single country. We also report the (rounded) population of each country. We assume by default that all countries worked to isolate contagious individuals; hence, the parameter η is associated to all.

frequently [167]) to get a proxy of the time needed for hard lockdown to be fully effective (cf. Fig. 4.4c).

4.2.3 The extended SPQEIR model to reflect mitigation strategies

SEIR models reproduce the typical bell-shaped epidemic curves for the number of infected people. The dynamics of this curve is of high importance for practical policy making. Not only it relates to the main stressors for the health system [24, 154, 167], but it also has an impact on the economic system [168–170], e.g. because it takes some time ($\mathbb{T}$) to mitigate the curve, until the

number of new infections is below an accepted threshold. Commonly, mitigation measures against epidemics aim at flattening the curve of new infections [148]. However, the classical SEIR model is not granular enough to investigate mitigation measures when they need to be considered or should be sequentially reduced if already in place. Therefore, we extend the classical SEIR model as in Fig. 4.1 (red insertions) into the SPQEIR model, to reflect the intervention categories described above. We particularly focus on the control of Susceptible and Exposed people, given by preventive isolation, contact tracing or social distancing measures, but we also include the control of infectious people by isolation. The model can be summarized as follows:

- The classical blocks S, E, I, R are maintained;
- A social distancing parameter ρ is included to tune the contact rate β;
- Two new compartments are introduced where:
  - Protected P includes individuals that are removed from the susceptible pool and are thus protected from the virus. This can happen through full isolation as in China in early 2020 [171] or by different vaccination strategies which reduce the susceptible pool;
  - Quarantined Q describes latent carriers that are identified and quarantined after monitoring and tracing of contacts.

We do not explicitly introduce a second quarantined state for isolation of confirmed cases after the Infectious state [154, 172] but consider this together with the Removed state, by tuning the removal rate with an extra parameter (see [173] and references therein). Quarantining infected symptomatic patients is a necessary first step in every epidemic [174]. An additional link from Q to R, even though realistic, is neglected as both compartments are already outside the "contagion system" and would therefore be redundant from the perspective of evolution of the infection. In general, protected individuals can get back to the pool of susceptible after a while, but here we neglect this transition, to focus on simulating mitigation programs alone at their early stage. Long-term predictions could be modelled even more realistically by considering such link, that would lead to an additional parameter to be estimated and is beyond the scope of the present

paper.

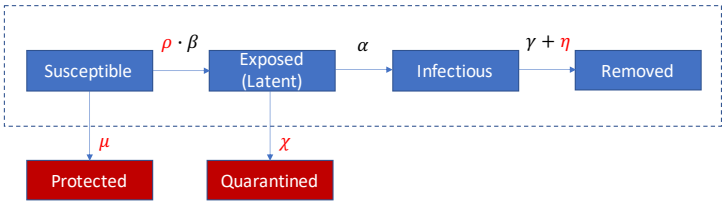

Figure 4.1: Scheme of the SPQEIR model. The basic SEIR model (framed blue blocks) is extended by the red blocks to the SPQEIR model. Parameters that are linked to mitigation strategies are shown in red. Interpretation and values of parameters are given in Table 4.2.

The model has in total 7 parameters. Three of them (β, α, γ introduced in Fig. 4.1) are based on the classical SEIR model. The new parameters ρ, μ, χ, η account for alternative mitigation programs to control the infectious curve (see Table 4.2 for details). Commonly, social distancing is modelled by the parameter ρ. In a closed-system setting where all individuals belong to the susceptible pool, but interact less intensively with each other, ρ tunes the contact rate parameter β, resulting in the effective reproduction number $\hat{R} = \rho \cdot \beta\gamma^{-1}$. The parameter μ stably decreases the susceptible population by introducing an active protection rate. This accounts for improvements of public health, e.g. stricter lockdown of communities, or reduction of the pool of susceptible people after reduced commuters' activity, or vaccination. The parameter χ introduces an active removal rate of latent carriers. Intensive early contact tracing and improved methods to detect asymptomatic latent carriers may enhance the removal of exposed subjects from the infectious network. Following earlier works [175, 176] and adjusting the current parameters, $\hat{R}$ can be then expressed as $\hat{R} = \beta\gamma^{-1}\alpha\,(\alpha + \chi)^{-1}$. Finally, η models the isolation of contagious individuals by handling the removal rate. This would correspond to identifying infectious individuals before they recover or die, and prevent them from infecting other susceptibles. Consequently, for this parameter alone $\hat{R} = \beta(\gamma + \eta)^{-1}$. Parameter values that are not related to mitigation strategies are set from COVID-19 epidemic literature [173, 177], as the main focus of the present model lies on sensitivity analysis of mitigation parameters. Our model can be further extended by time dependent parameters [174]. Default values for mitigation parameters are $\{\rho, \mu, \chi, \eta\} = \{1, 0, 0, 0\}$, corresponding to the classical SEIR model.

The dynamics of our SPQEIR model is described by the following system of differential equations:

$$\begin{aligned}
\dot{\mathsf{S}} &= -\frac{\rho\beta\mathsf{SI}}{N} - \mu\mathsf{S} \ , \\
\dot{\mathsf{E}} &= \frac{\rho\beta\mathsf{SI}}{N} - (\chi+\alpha)\,\mathsf{E} \ , \\
\dot{\mathsf{I}} &= \alpha\mathsf{E} \ - (\gamma+\eta)\mathsf{I} \ , \\
\dot{\mathsf{R}} &= (\gamma+\eta)\mathsf{I} \ , \\
\dot{\mathsf{P}} &= \mu\mathsf{S} \ , \\
\dot{\mathsf{Q}} &= \chi\mathsf{E} \ ,
\end{aligned}$$

Here, $\dot{\mathsf{N}} = 0$ with $\mathsf{N} = \mathsf{S} + \mathsf{E} + \mathsf{I} + \mathsf{R} + \mathsf{P} + \mathsf{Q}$, implying the conservation of the total number of individuals. As value for the qualitative study, we used $\mathsf{N} = 10{,}000$. For the cross-country assessment, N is adjusted to true population values for each country. Overall, the effective reproductive number becomes

$$\hat{R} = \frac{\rho\beta}{\gamma+\eta}\frac{\alpha}{\alpha+\chi}\frac{S}{N}, \tag{4.1}$$

Mitigation measures are initiated several days after the first infection case. Hence, we activate non-default parameter values after a delay τ. For data fitting, we fit and compare τ to the official date when measures are initialized (cf. Table 4.1). To integrate the model numerically, we use the *odeint* function from *scipy.integrate* Python library.

Fixed parameters	**Mitigation parameters**
β = (average contact rate in the population) = 0.85 d^{-1}	μ = (rate of active protection) [d^{-1}]
α = (mean incubation period)$^{-1}$ = 0.2 d^{-1}	ρ = (social distancing tuning)
γ = (mean infectious period)$^{-1}$ = 0.34 d^{-1}	χ = (active removal rate) [d^{-1}]
R_0 = 2.5	η = (rate of contagious isolation)[d^{-1}]

Table 4.2: SPQEIR model parameters with their standard values for the COVID-19 pandemic from literature [173, 178]. Here "d" denotes days.

4.2.4 Model fitting

To show how our conceptual analysis is able to reproduce and explain empirical data, we fit the model to the official number of currently infected (active) cases of the first epidemic wave (winter-spring 2020), for each considered country. The choice is corroborated by the fact that all considered countries applied rapid, population-wide measures [160]. Model fitting to the infectious curves is performed in two steps, using the parameters known to be active (cf. Table 4.1). First, we estimate the "model consistent" date of first infection, so that the simulated curve matches the reported data of active infections. This initial step corresponds to setting the time initial conditions of the SEIR model [154]. The fitting is performed with default parameter values, on a subset of data corresponding to the first outbreak, from first case until when measures are implemented (cf. Table 4.1). We use a grid search method for least squares, sufficient to fit a single parameter:

$$t_0 = \left\{ t' \mid RMS = \min_{t'} \sqrt{\frac{\sum_{i=t'}^{t_m} (x(i) - \hat{x}(i))^2}{n}} \right\} \tag{4.2}$$

where t_0 is the "model consistent" estimated date of first infection, t_m refers to the date measures are implemented, $\hat{x}$ and x are respectively reported and model-predicted data, and n is the number of points between t and t_m.

The second step estimates a reasonable set of the mitigation parameters that yield the best fitting of the simulated SPQEIR curve on reported data, during the first phase with implemented measures. This period is identified between the starting date t_m (also included in the fitting) and the phase-out date t_p, cf. Table 4.1. Holding the epidemic parameters to literature values to achieve cross-country comparison on intervention parameters alone, the fitting is performed for a set of mitigation parameters relative to each country, as reported by policy databases (cf. Table 4.1). The fit is performed with the widely used *lmfit* Python library. In S1 Text, we discuss such fitted parameters set and alternative ones.

We also perform a comparative quantitative analysis between our extended model and the simplest SEIR that lumps parameters under a single "social distancing" ρ. This allows comparing the estim-

ate reproduction number $\hat{R}$ and shows the similarity or divergence of different control strategies in explaining the data. To assess how well they allow to fit the data, we employ the classical reduced χ^2 statistics to evaluate the goodness-of-fit for each of the two models, considering the degrees of freedom [179]:

$$\chi^2_{red} = \frac{1}{n' - 1 - k} \sum_{j=1}^{n'} \frac{(y_j - \hat{y_j})^2}{\hat{y_j}} \tag{4.3}$$

where n' is the number of data points until phase-out, k is the number of parameters in the model, y_j are estimated values (from data) and $\hat{y_j}$ the expected ones (from model simulations).

4.3 Results

First, we focus on the conceptual analysis of the effect of preventive mitigation interventions, initially for single measures (social distancing, active protection and active quarantining) and subsequently for a number of synergistic approaches. Additionally, we compare them to the effect of isolating contagious individuals. In particular, we study how crucial quantities, namely $\hat{R}$, the infectious peak height and time to zero infectious $\mathbb{T}$, depend on mitigation parameters. We define $\mathbb{T}$ as the time when there are less than 0.5 individuals in the I compartment, because ODE models approximate discrete quantities with continuous variables. Finally, we perform model fitting and intervention assessment over a set of countries. This provides quantitative outputs about the effectiveness of control measures, informing about the synergies applied and enabling cross-comparison.

4.3.1 Simulations of single mitigation measures

Only social distancing

The parameter ρ captures social distancing effects, taking values in the interval $[0, 1]$, where 0 indicates no contacts among individuals while 1 is equivalent to no action taken. To perform the current simulations, we assume a delay τ in implementing the measures of 10 days. Such value does not modify the qualitative behavior of the epidemic dynamics but influences the quantitative estimations of peak height and mitigation timing. We refer to S1 Text for further discussion.

Overall, Fig. 4.2 reports simulation results about the effects of ρ. The curve of infectious is progressively flattened by social distancing (4.2a) and its peak mitigated (4.2b). However, the time to mitigation gets delayed for decreasing ρ, until a threshold yielding a disease-free equilibrium rapidly (4.2c). In this case, the critical value for ρ is 0.4, leading to $\hat{R} < 1$. Fig. 4.2c reveals that the dependence of $\mathbb{T}$ on ρ is not monotonous. With the current settings, values of $\rho \leq 0.3$ are best effective to minimise the mitigation timing. In general, the optimal ρ value that minimises mitigation timing depends on τ, as discussed in supporting S1 Text. In fact, longer delays in issuing interventions are not only associated with higher peaks in the infection curves, but also in more stringent parameter values that are necessary to obtain minimal $\mathbb{T}$. This fact further stresses the importance of prompt interventions to control the quantitative aspects of epidemic mitigation.

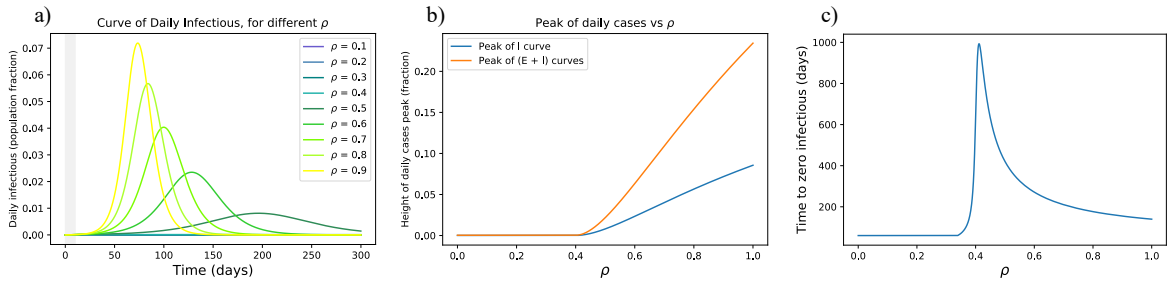

Figure 4.2: (a) Effects of social distancing on the epidemic curve. The grey area indicates when measures are not yet in place. (b) The peak is progressively flattened until a mitigation is reached for sufficiently small ρ. For these settings, the critical value for ρ is 0.4 (it pushes $\hat{R}$ below 1). (c) Unless ρ is small enough, stronger measures of this kind might delay the mitigation time $\mathbb{T}$ of the epidemic.

Only active protection

As discussed above and in S1 Text, our simulations take into account 10 days delay from the first infection to the initiation of active protection. Small values can reflect continuous improvement of protection measures (as people learnt better how to deal with the virus) or different vaccination strategies (thus going beyond non-pharmaceutical strategies). Higher values are considered to model certain effects of a step-wise hard lockdown (see following paragraph). The results are reported in Fig. 4.3. We see that small precautions can make an initial difference (Fig. 4.3a,b). The time to zero infectious is decreased with higher values of active protection (Fig. 4.3a,b). In

particular, $\mu = 0.01\, d^{-1}$ mitigates the epidemics in about 6 months by protecting 70% of the population. Higher values of μ achieve mitigation faster, while protecting almost 100% of the population. It is probably not fully realistic to consider that these protection rates are obtained only by isolation. Instead, they could represent improved hygiene routines or vaccination strategies and are thus worthy to consider.

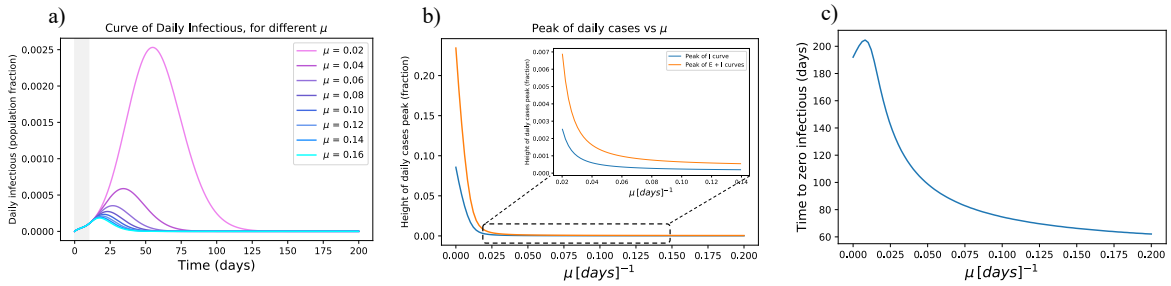

Figure 4.3: (a) Effects of active protection on the infectious curve. The grey area indicates when measures are not yet in place. μ is expressed in d^{-1}. (b) Dependency of peak height on μ: the peak is rapidly flattened for increasing μ, then it is smoothly reduced for higher parameter values. (c) High μ values are effective in anticipating the mitigation of the epidemic, but require protecting more than 90% of the population.

In addition to what analysed above, we also consider strategies which isolate many people at once [180]. This corresponds to reducing S to a relatively small fraction rapidly. Since μ is a rate, we mimic what could happen during a step-wise hard lockdown: large values of μ, but whose effect only lasts for a short period of time (Fig. 4.4b). We thus use the notation μ_{ld}. In the figure, an example shows how to rapidly protect about 68% of the population with a step-wise μ_{ld} function. In particular, we use an average four-days long step-wise μ_{ld} function (Fig. 4.4b) to mimic the rapid, but not abrupt, change in mobility observed in many countries by Google Mobility Reports [166] (Fig. 4.4c). The effects of strong, rapid protection are reported in Fig. 4.4a, showing that such strategy is effective in mitigating the epidemic curve and in reducing the time to mitigation.

Only active quarantining

Controlling latent carriers before symptom onset is an important strategy to limit transmission. We here consider how mitigation is achieved by targeted interventions, e.g. by contact tracing, and we quantify the interplay between precision and delay in tracing, thus expanding [181]. As

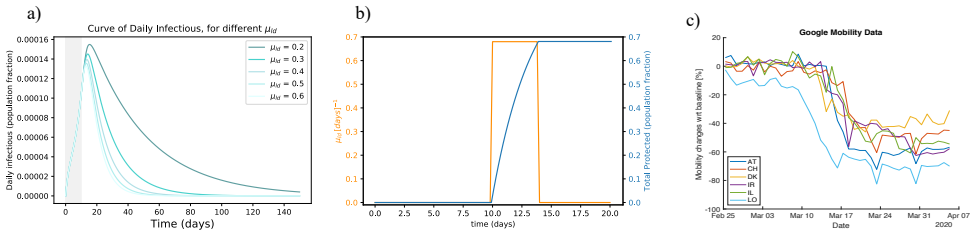

Figure 4.4: (a) Flattening the infectious curve by hard lockdown. Rapidly isolating a large population fraction is effective in mitigating the epidemic spreading. (b) Modeling hard lockdown: high μ_{ld} (orange) is active for four days to isolate and protect a large population fraction rapidly (blue). As an example, we show $\mu_{ld} = 0.28 \quad d^{-1}$ if $t \in [10, 14]$. It results in protecting about 68% of the population in two days. Higher values, e.g. $\mu_{ld} = 0.65$ d^{-1} would protect 93% of the population at once. (c) Google Mobility Report visualization [166] for analysed countries, around the date of measures setting. Each line reports the mean in mobility change across Retail & Recreation, Grocery & Pharmacy, Transit stations, and Workplaces, around the date of implementation of the measures. A minimum of four days (from top to bottom of steep decrease) is required for measures to be fully effective. Abbreviations explanation: AT = Austria, CH = Switzerland, DK = Denmark, IL = Israel, IR = Ireland, LO = Lombardy.

above, not only we consider the impact on $\hat{R}$ but on the whole infectious curve, its height and its time evolution.

The simulations in this part are based on realistic assumptions: testing a person is effective only after a few days that that person has been exposed (to have a viral charge that is detectable). This induces a maximal quarantining rate θ, which we set $\theta = 0.33 \quad d^{-1}$ as testing is often considered effective after about three days from contagion [182]. Therefore, we get the active quarantining rate $\chi = \chi' \cdot \theta$, where χ' is a tuning parameter associated e.g. to contact tracing. As θ is fixed, we focus our analysis on χ'. As above, we also assume that testing starts after the epidemic is seen in the population, i.e. some infectious are identified with 10 days delay in the activation of measures.

The corresponding results are reported in Fig. 4.5. The curve is progressively flattened by latent carriers quarantining and its peak mitigated, but the time to mitigation gets delayed for increasing χ'. This happens until a threshold value of $\chi'_{thr} = 0.9$ that pushes $\hat{R}$ below 1. This value holds if we accept a strategy based on testing, with $\theta = 0.33$. If preventive quarantine of suspected cases does not need testing (for instance, when it is achieved by contact tracing apps), the critical χ' value could be drastically lower. In particular, $\chi'_{thr} = 0.3\, d^{-1}$ if $\theta = 1\, d^{-1}$, i.e. latent carriers are quarantined the day after a contact.

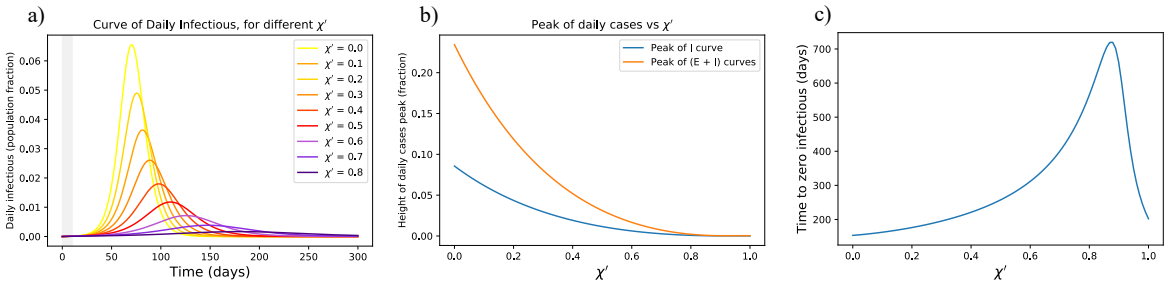

Figure 4.5: (a) Effects of active latent carriers quarantining on the epidemic curve. The grey area indicates when measures are not yet in place. (b) The peak is progressively flattened until a disease-free equilibrium is reached for sufficiently large χ'. (c) Unless χ' is large enough, stronger measures of this kind might delay the mitigation of the epidemic. Note that the critical χ' can be lowered for higher θ, e.g. if preventive quarantine does not wait for a positive test.

The parameter χ' tunes the rate of removing latent carriers. Hence, it combines tracing and testing capacities, i.e. probability of finding latent carriers (P_{find}) and probability that their tests are positive (P_+). The latter depends on the false negative rate δ_- as

$$P_+ = (1 - \delta_-)\,. \tag{4.4}$$

So, $\chi' = P_{find} \cdot P_+$. Hence, mitigating the peak of infectious requires an adequate balance of accurate tests and good tracing success as reported in Fig. 4.6. Further quantifying the latter would drastically improve our understanding of the current capabilities and of bottlenecks, towards a more comprehensive feasibility analysis.

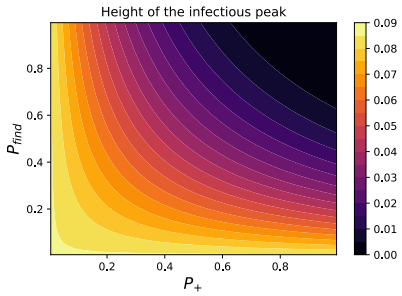

Figure 4.6: Assessing the impact of P_{find} and P_+ on the peak of infectious separately. This way, we separate the contribution of those factors to look at resources needed from different fields, e.g. network engineering or wet lab biology. Solutions to boost the testing capacity like [183] could impact both terms.

Only isolation of infectious

Isolating contagious individuals is a first step to contrast the pandemic, on top of preventive measures. In this section, we consider its effect alone, to be compared with that of other single parameters shown above. As discussed above, we here consider simulations that include a delay of 10 days from the first infection to the initiation of the measures. Quantitative changes associated with different τ are discussed in the supporting S1 Text. The results are reported in Fig. 4.7. Targeting the infectious population means that fewer people can spread the contagion. The curve of infections is progressively flattened, the more rapidly contagious people are identified and isolated, until a threshold value $\eta = 0.51$ (for our initial parameters). In turn, the mitigation time gets longer if η is increased, but has not yet crossed the threshold value. These findings point to the importance of complementing the control of contagious individuals with additional preventive measures such as the ones presented above. We acknowledge that these results are valid on average, but that breaking the infectious chain at specific links can have additional benefits in heterogeneous social networks.

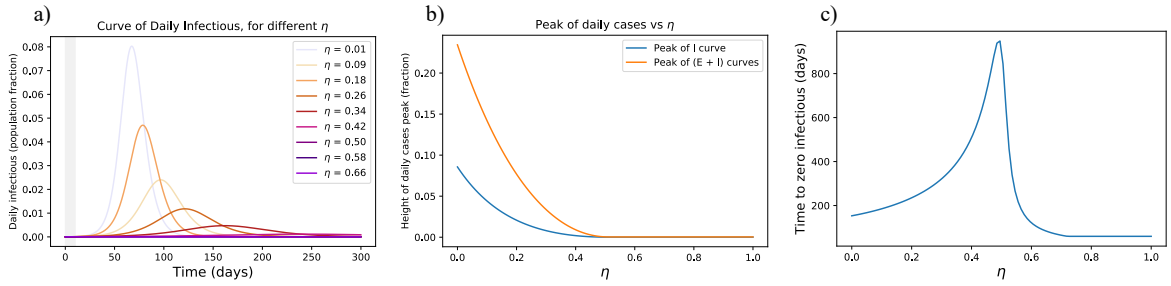

Figure 4.7: (a) Effects of isolation of contagious individuals on the epidemic curve. The grey area indicates when measures are not yet in place. (b) The peak is progressively flattened until a disease-free equilibrium is reached for sufficiently large η. (c) Unless η is large enough, stronger measures of this kind might delay the mitigation of the epidemic. Note that the critical η can be higher if there is delay in intervening, i.e. if infectious individuals are isolated after several days and can thus spread the infection.

4.3.2 Synergistic scenarios

Fully enhanced active quarantining and active protection might not be always feasible, e.g. because of limited resources, technological limitations or welfare restrictions. On the other hand, the isolation of a limited portion of contagious individuals could not be sufficient. Therefore a

synergistic approach is very attractive as it can flatten the curve with combinations of interventions that target different population groups and require distinct resources. This section shows a number of possible synergies, concentrating as before on abstract scenarios to investigate how combining different mitigation programs impact the control parameter $\hat{R}$ (*cf.* Eq. D.2), the infection curves and the mitigation timing.

As case studies, we consider the 6 synergistic scenarios listed below. Parameters are set without being specific to real measures taken: their value is so far conceptual and meaningful when compared across scenarios. Just like above, we consider a 10 days delay from the first infection to issuing measures; as suggested in other studies [184], delaying action could worsen the situation. To differentiate between a rapid isolation and a constant protection, we use μ_{ld} (associated to "hard lockdown strategies", see Section 4.3.1) separated from μ. To get $\hat{R}$ when measures are initiated, we follow Eq. D.2, considering $\chi = \chi' \cdot \theta$ as in Section 4.3.1. Our scenarios are the following:

1. During the first COVID-19 wave, many European countries opted for a lockdown strategy. A quite large fraction of the population was isolated, individuals were recommended to self-quarantine in case of suspected positiveness, social distancing got mandatory but was sometimes not fully followed, masks and sprays were suggested for protection. So, we set an initial "rapid protection" $\mu_{ld} = 0.12$ to protect around 38% of the population quickly. Then we chose $\rho = 0.7$, $\chi' = 0.12$, $\eta = 0.12$ and $\mu = 0$. This yields $\hat{R} = 0.65$.

2. In case that isolation of contagious individuals fails, an alternative procedure is to rapidly protect only the population fraction at high risk ($\mu_{ld} = 0.06$, driving 15% of initial S to P). Social distancing and latent carrier quarantine should then be enforced ($\rho = 0.65$, $\chi' = 0.55$). This gives $\hat{R} = 0.67$.

3. In case both preventive quarantine of latent carriers and isolation of contagious are not greatly effective ($\chi' = 0.03$, $\eta = 0.07$), and in case of low protection rate and scarce isolation ($\mu = 0$, $\mu_{ld} = 0.08$), we rise social distancing for all individuals doing business as usual ($\rho = 0.45$). In this case, $\hat{R} = 0.64$.

4. If there are no safety devices that provide an adequate protection ($\mu = 0$) and no isolation is foreseen ($\mu_{ld} = 0$), we set $\rho = 0.6, \chi' = 0.2, \eta = 0.25$ to get $\hat{R} = 0.65$.

5. This case has higher $\hat{R}$ than the previous ones, namely $\hat{R} = 0.84$. The corresponding parameters are $\mu_{ld} = 0.1$, $\mu = 0.002$, $\rho = 0.7$, $\eta = 0.1$. This shows that even low enforcement of single interventions can achieve $\hat{R} < 1$, even thought the corresponding mitigation is slower.

6. Finally, we consider "draconian" [185] measures such that $\hat{R} = 0.32$ only through isolation and massive screening, that targets Exposed and Infectious individuals. So, $\mu_{ld} = 0.3$, $\chi' = 0.1$, $\eta = 0.2$ while $\rho = 1$ and $\mu = 0$. This points to the importance of tracing capacities to minimise the total isolation period.

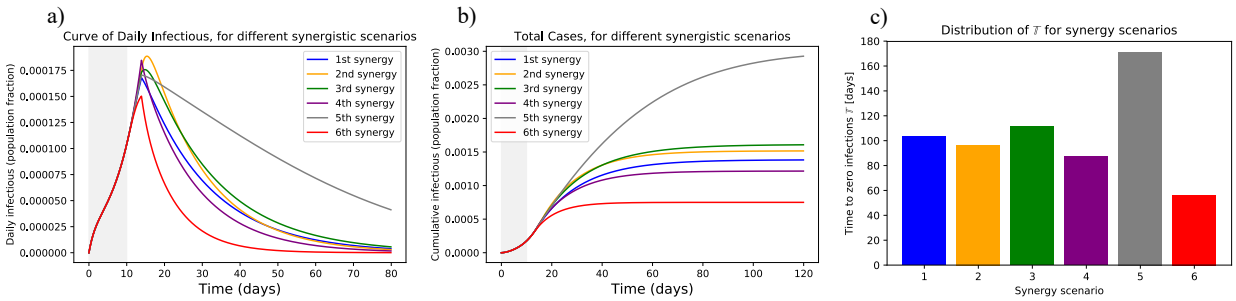

Figure 4.8: Simulations of the 6 synergistic scenarios. (a) Curves of infectious Individuals, (b) Cumulative cases. The grey area indicates when measures are not yet in place. It is evident that scenarios leading to similar $\hat{R}$ could show different patterns and mitigation timing. (c) Distribution of times to zero infections $\mathbb{T}$ for different scenarios.

Simulation results in Fig. 4.8 show that different synergies can lead to different timing, even though the peak is contained similarly (Fig. 4.8a). This has an impact on the cumulative number of cases (Fig. 4.8b) that will be reflected on the death toll. This holds even when the $\hat{R}$ values are very close, as in scenarios 1 to 4: even though $\hat{R}$ is the main driver of the epidemic, the contribution of finer-grained parameters is relevant for the fine-tuning of interventions. Focusing on scenarios 2 and 3, we notice that prevention measures and latent quarantine accelerate the mitigation, even when isolating only vulnerable people. This achieves similar effects as strong social distancing. In addition, active protective measures with relatively low values further concur in mitigating the peak. This finding asks for rapid assessment of masks and sanitising routines.

Overall, the strength of mitigation measures influences how and how fast the epidemic is flattened. μ_{ld} mostly governs the peak height after measures are implemented, ρ mainly tunes the curve steepness together with μ, while χ shifts the decaying slope up and down. Overall, a $\hat{R} < 1$ suffices to avoid breakdown of the health system, but its effects could be too slow. Decreasing its value with additional synergistic interventions could speed up epidemic mitigation. A careful assessment of measures' strength is thus recommended for cross-country comparison.

4.3.3 Model fitting and interventions assessment

In this section, we test our results on several datasets, to estimate the likely impact of different strategies and to show which combination could have yield a similar $\hat{R}$.. This way, we show how countries could achieve mitigation through a synergy of control measures with similar impact on the epidemic but different management and possibly socio-economic impact.

Model fitting

As described in the Methods section, we first estimate the "model consistent" date of first infection t_0, *i.e.* the temporal initial condition for the SPQEIR model. Comparing this date with the starting date for intervention measures (Table 4.1) corresponds to estimating τ for each country. We do not claim this to be the true date of first infection in a country; it is the starting date of infections in case of homogeneous transmission, under the assumption of no superspreading events [186], and with the hypothesis of coherent R_0 (cf. Table 4.2). During the second fitting step, we also estimate the date at which mitigation measures start having effect on the infectious curve, t_m. Comparing t_m with official intervention dates from Table 4.1, we notice that about 8 days are necessary to register lockdown effects. This is consistent to early findings on lockdown effectiveness [187]. Estimated dates are reported in Table 4.3.

Then, we fit mitigation parameters to data of active cases, from the estimated starting date of control measures t_m to phase-out t_p (*cf.* Table 4.1). The active parameters for the fit are reported in the same table. For the protection parameter, we used μ_{ld} acting on 4 days (as introduced in Fig. 4.4) since it better reflects the rapid population-wide protection that happened during the first COVID-19 wave. Since $S \sim N$, its quantitative impact is anyway greater on the S

Country	AT	DK	IR	IL	LO	CH
1^{st} **official detection**	24 Feb	04 Mar	29 Feb	21 Feb	21 Feb	25 Feb
$\mathbf{t_0}$	22 Jan	22 Jan	29 Jan	24 Jan	05 Jan	14 Jan
$\mathbf{t_m}$	26 Mar	21 Mar	06 Apr	30 Mar	19 Mar	21 Mar

Table 4.3: Dates of official detection of first COVID-19 case [161], estimated dates for first infection t_0 (according to Eq. 4.2) and date at which measures start being effective t_m, per country.

compartment. The results of the model fitting are reported in Fig. 4.9. The SPQEIR model, with appropriate parameters for each country (cf. Table 4.1), is fitted to reported infection curves and, overall, model fitting have good agreement with data. This supports the model structure as very simple yet realistic enough to capture the main dynamical behaviour of the infection curves in multiple countries. In addition, it allows for each country to obtain multiple sets of parameters representing different strategies. We notice that the effect of social distancing (ρ) is predominant as it homogeneously prevents the big pool of Susceptible individuals to stream into the Exposed compartment. However, also tracing and isolation can have a considerable effect in complementing population-wide interventions. The values associated to the fitted parameters correspond to non-negligible numbers of individuals affected by the interventions. Such values are discussed in S1 Text. This is informative about how synergistic approaches can realistically explain the mitigation of the infectious curve, and highlight the potential advantages associated with modifying the combination of strategies in subsequent epidemic waves. Finally, it allows a comparison between different countries through the corresponding best fit parameters. For Ireland, although initial social distancing advises were issued on 13th March (cf. Table 4.1), fitting the complete curve was only possible when considering the lockdown date (28th March) as the major driver of the mitigation.

Model fitting is slightly hindered by data quality. For instance, Ireland reported intermittent data, while Lombardy is not perfectly represented, probably because of some data reporting issues and larger heterogeneity in its spacial patterns.

Finally, the reduced χ^2 metric (Eq. 4.3) reports that the complete SPQEIR model and the simple social distancing one attain similar goodness of fit, although values for the SPQEIR are slightly

lower in all cases. Country-specific extra parameters (*cf.* Table 4.1) are thus useful to fine-tune the reproduction of epidemic curves, as noticed in the conceptual analysis Sec. 4.3.2. This shows that synergistic measures are able to provide a similar mitigation of the curve of infections, and an analogous $\hat{R}$, as the pure social distancing scenario. In turn, synergistic approaches allow lower social distancing values, possibly having less severe social and psychological impacts on the population. This in turn supports the use of several interventions to control the epidemic curve in an effective and timely manner, while balancing social benefits. In addition, the SPQEIR is confirmed to be informative, on top of being fully interpretable and linked to recognised social policy categories.

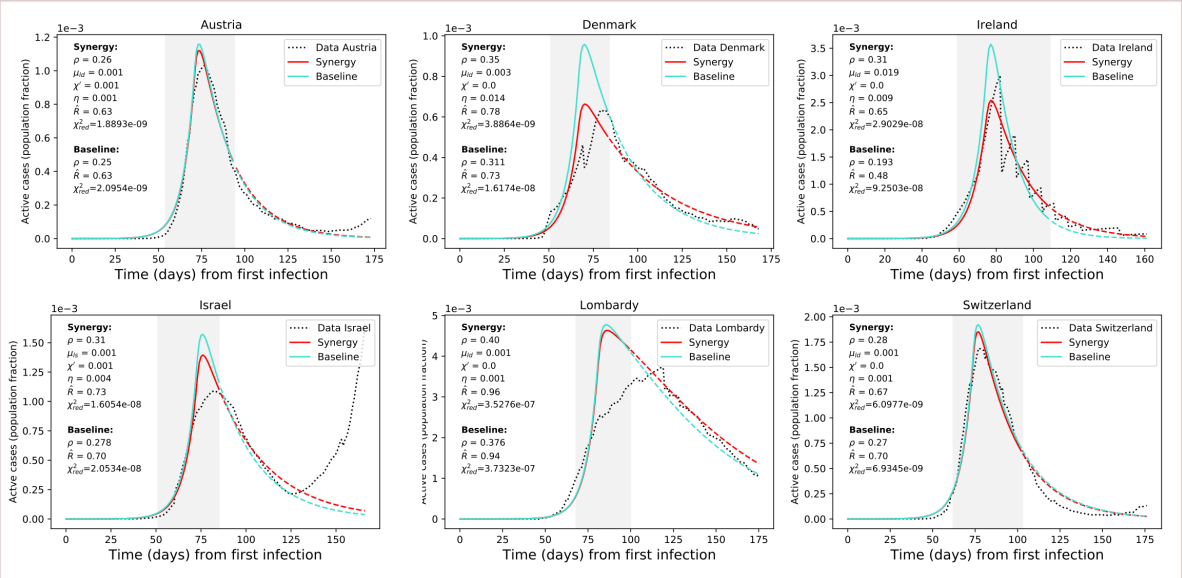

Figure 4.9: Results of model fitting. Infection curves for the considered countries (dotted) are fitted with the SPQEIR model with appropriate parameters (red curves). We also show a comparison with the fitted curve obtained from the "basic" SEIR model with only social distancing (turquoise curves). Parameter values are reported for each country, as well as the corresponding $\hat{R}$ (for the grey area, following Eq. D.2) and χ^2_{red}. The period of measures enforcement, from t_m to t_p, is highlighted by the grey region. Time progresses from the estimated day of first infection t_0 (cf. Table 4.3). Population fraction refers to country-specific populations (cf. Table 4.1). After phase-out, we prolong the fitted curve (parameter values unchanged) to compare observed data with what could have been if measures had not been lifted (dashed lines). From the data, we can observe a resurgence of cases that points to possible "second outbreaks" (particularly in Israel).

Cross-country interventions assessment

Fitting a number of countries with the same model containing the same epidemiological parameters allows to perform a comparison on the efficacy of their interventions, to inform future decision making. In Fig. 4.9, parameter values providing the best fit of model to data are reported, together with the simulation results (mean values) calculated by the *lmfit* algorithm [188]. Different synergies yield similar values for $\hat{R}$, but the curve is different in its evolution as already observed in the previous sections. As expected from the model analysis above, the lower $\hat{R}$ is (below 1), the faster the mitigation of the epidemic. In addition, different parameter combinations generate curves that differ in amplitude and time evolution. This might well explain differences in reported total cases and deaths between various countries. Comparing Austria, Denmark and Lombardy, we observe that contact tracing and monitoring contribute to speeding up the curve decay, despite the fact that population-wide interventions played so far a major role. In general, combined isolation and tracing strategies would reduce transmission in addition to social distancing or self-isolation alone. In general, a strong, rapid lockdown that combines protection and social distancing seems the best option, as also suggested by the conceptual analysis. However, intervening with additional synergies is a viable option to mitigate the epidemic faster and with lower social values.
Finally, we observe the value of timely interventions: we see that intervening earlier with respect to the date of first infection helps reducing the daily curves by almost a factor of 10. For instance, we can compare Denmark and Lombardy in Fig. 4.9: the first one got a peak corresponding to about 0.08% of the whole population, while the second region registered a number of active cases of about 0.5% of the whole population. This translates in more than 3800 infectious on the Danish peak, and on more than 37000 on Lombardy's.

4.4 Discussion

The SPQEIR model assesses and compares the effectiveness of several control measures to mitigate the COVID-19 epidemic curve. It integrates previous literature and considers synergy strategies often considered alone. In particular, we focus on preventive measures, i.e. those that target people that are not yet fully infectious. Initially, we perform conceptual simulations to investigate

the effect of single and combined measures not only on $\hat{R}$, but also on the complete time evolution of the infectious curve. Then, we compare them with the isolation of contagious individuals. The possibility of choosing among several strategies is of practical importance for decision makers: a comparison of Figs. 4.2, 4.3, 4.5 and 4.7 reveals that increasing social distancing delays and decrease the height of the peak of infections, increasing active protection as well decreases the height of the peak of infections, but anticipates the occurrence of such peak, increasing active quarantining also delays and decrease the height of the peak of infections like social distancing, but the same peak mitigation by active quarantining is associated with shorter delays than with social distancing.

Moreover, the model is fitted to several countries, to estimate the plausible impact of synergistic strategies. The fit is performed until phase-out dates for the first epidemic wave (winter-spring 2020), when measures are progressively lifted and therefore the model assumptions do not hold anymore. We remark that the current set of parameters may not be unique, as there is high correlation among parameters. This is a common identifiability issue of SIR parameters, particularly when several of them contribute to the same control parameter $\hat{R}$ [189]. For instance, the *lmfit* diagnostic reports 0.9 correlation between ρ and μ_{ld} and 0.99 between ρ and χ, for Austria. This means that they can equally well explain the evolution of the curve, so they could be alternatively chosen for epidemic control, while targeting different population groups. This is in line with our above analysis, as we aim at showing how different combinations of interventions can tune the mitigation of infection curves. We remark that, due to this degeneracy of parameters (*i.e.* several combination can yield to same $\hat{R}$), the ones reported in Fig. 4.9 constitute a reasonable set obtained by an automatic least-square algorithm, but estimating their true values (inverse problem) needs to be complemented with alternative, targeted approaches.

In Fig. 4.9 we extrapolate the model, with same parameter values, after phase-out (dashed lines), to compare observed data to the most optimistic scenario, where measures would not have been lifted. We observe that, up to July 8th, the infection curves mostly maintained an inertial decreasing trend: despite some fluctuations that make them generally higher than the best scenario, they kept on following a downward trend similar to that of the model. We speculate that this phenomenon is linked to changed behaviors, face masks [190] and improved sanitising practices

that maintained social distancing values, as well as contact tracing practices issued by many countries along with the phase-out. However, some countries (Israel in particular, but also Austria) already showed a worrisome upward trend, eventually associated to a second outbreak [163]. As this is not a low probability event, we stress the usefulness of our analysis to prepare for future developments in pandemic progression.
It has been asked whether the peak of infections was reached because of herd immunity or because of interventions [191]. An added value of this study is to confirm that the peak of infection, for the considered countries, was not reached because of herd immunity. On the contrary, it is the effect of a number of mitigation measures that reduced the number of cases artificially. This should warn about the high numbers of people that are still susceptible.

We acknowledge the limitations of our analysis. Due to its structure and the use of ordinary differential equations, the model only accounts for average trends. However, it cannot reproduce fluctuations in the data, being them intrinsic in the epidemic, or from testing and reporting protocols that might differ among countries. The model focuses on initialization of measures that last for short-medium periods, as it does not include out-fluxes from the "safeguarded" compartments P and Q. This assumption is not completely realistic and we are aware that household infections concurred to a significant number of contagions. Like other studies [192], our simulations thus underestimate the disease burden coming from this source. However, the synergy with other parameters can retain the modulation of the dynamics posed by different behaviors. Overall, our model is used to assess the validity of control measures rather than to predict the complete evolution of the epidemic. Similarly, in order to concentrate on the generic control of infectious curves, we did not include further compartments about hospitalization, as they are already upstream with respect to the I compartment, nor we considered asymptomatic patients, that would not impact the main findings about synergistic mitigation. In addition, the constant nature of parameters used in this analysis allows good agreement between model and data when countries implemented rapid and strong measures point-wise in time, with little follow-ups. Further studies, with time varying parameters, could obtain more precise values. In the same way, transferring models from country to country requires fulfilling the same assumptions on model structure and basic

hypothesis. This is shown by the different fitting performances, that suggest that a transfer is not always possible. The same fitting performance is often impacted by the data quality, related to monitoring, testing and reporting; despite our carefulness in selecting countries that had similar positive rates, there could be additional uncertainties to the parameter values that we estimated. Finally, we remark that the retrospective dates in Table 4.3 should be interpreted under the model assumptions: they could suggest that the first infection happened several weeks before the official detection, but they could as well be associated to the inherent identifiability limits of SIR-like parameters [193, 194].

In general, this study is not intended to make a ranking of country responses, nor to suggest that different strategies could have led to better outcomes. Contrariwise, it should be used as a methodological step towards quantitatively inquiring the effect of different intervention categories and of their combinations. It examines possible abstract scenarios and compares quantitative, model-based outputs, but it is not intended to fully represent specific countries nor to reproduce the epidemic complexity within societies. In fact, the model does not provide fine-grained quantification of specific interventions, e.g. how effective masks are in protecting people, how much proximity tracing apps increase P_{find}, how changes in behavior are associated with epidemic decline [195] and so on. We acknowledge that the new compartments cannot perfectly match policy measures, but are a reasonable approximation. Some real measures might also affect multiple parameters at once, e.g. safety devices and lockdown could impact both μ and ρ. Comparing results of this macro-scale model with those of complex, micro-scale ones [141] could inform researchers and policy makers about the epidemic dynamics and effective synergies to hamper it. Any conclusion should be carefully interpreted by experts, and the feasibility of tested scenarios should be discussed before reaching consensus.

4.5 Conclusion

We have developed a minimal model to link intervention categories against epidemic spread to epidemiological model compartments. This allows quantitative assessment of non-pharmaceutical mitigation strategies on top of social distancing, for a number of countries. Strategies have differ-

ent effects on epidemic evolution in terms of curve flattening and timing to mitigation. As with previous studies [167, 196], we have observed the need to enforce containment measures (i.e., detect and isolate cases, identify and quarantine contacts and at risk neighborhoods) along with mitigation (i.e., slow down viral spread in the community with social distancing).
By extending the classic SEIR model into the SPQEIR model, we distinguished the impact of different control programs in flattening the peak and anticipating the mitigation of the epidemic. Depending on their strength and synergy, non-pharmaceutical interventions can hamper the disease from spreading in a population. First, we performed a complete sensitivity analysis of their effects, both alone and in synergy scenarios. Then, we moved from idealised representations to fitting realistic contexts, allowing preliminary mapping of intervention categories to abstract programs. We verified that the model is informative in interpolating the infection curves for a number of countries, and performed cross-country comparison. We could then obtain model-based outputs on the strength of interventions, for a number of countries that respected the model assumptions. This provides better, quantitative insights on the effect of mitigation measures and their timing, and allows improved comparison.

Overall, this work could contribute to quantitative assessments of epidemic mitigation strategies. To tackle current epidemic waves, and against possible resurgence of contagion [197] (also cf. Fig 4.9), better understanding the effect of different non-pharmaceutical interventions could help planning mid- and long-term measures and to prepare preventive plans while allowing a relaxation of social distancing measures. In fact, this synergistic approach still remains of high importance in this second lockdown times, where countries still need to balance different non-pharmaceutical interventions to keep the infection at bay while complementing vaccination strategies and containing the impacts on other aspects of society.

4.6 Shinyapp

A user-friendly online shinyapp to interactively simulate different scenarios with the SPQEIR model is available on: https://jose-ameijeiras.shinyapps.io/SPQEIR_model/. It allows

to reproduce the present outputs and to perform sensitivity analysis.

Ethics

The application of anonymized data for the purpose of epidemic modelling has been endorsed by the accessed databases.

Data accessibility

Databases of social measures can be accessed at https://www.who.int/emergencies/diseases/novel-coronavirus-2019/phsm [147].
ACAPS database is at https://www.acaps.org/covid19-government-measures-dataset [160].
Worldwide epidemiological data collection from John Hopkins University is at https://github.com/CSSEGISandData/COVID-19 [161].
Lombardy data were retrived from https://github.com/pcm-dpc/COVID-19 [162].
Google mobility data [166] were accessed through https://ourworldindata.org/covid-mobility-trends [163].
The code for analysis can be found at https://github.com/daniele-proverbio/assessing_strategies.

Authors' Contributions

DP, AH designed the study. DP, FK, SM developed the model. DP, FK, JAA implemented the model. DP, FK, SM, AH, AA, LM, AS, JG, CL analyzed and interpreted the results. SM, AH, AS, JG, CL supervised and coordinated the project. DP, FK, SM, CL wrote the first draft. All authors contributed to the final draft. All authors gave their final approval for publication.

Competing interest

The authors declare no competing interests.

Funding

Fundings: DP and SM's work is supported by the FNR PRIDE DTU CriTiCS, ref 10907093. FK's work is supported by the Luxembourg National Research Fund PRIDE17/12244779/PARK-QC. A.H. work was partially supported by the Fondation Cancer Luxembourg. JG is partly supported by the 111 Project on Computational Intelligence and Intelligent Control, ref B18024. AA is supported by the Luxembourg National Research Fund (FNR) (Project code: 13684479). JAA is supported by the FWO research project G.0826.15N (Flemish Science Foundation), GOA/12/014 project (Research Fund KU Leuven), Project MTM2016-76969-P from the Spanish State Research Agency (AEI) co–funded by the European Regional Development Fund (ERDF) and the Competitive Reference Groups 2017–2020 (ED431C 2017/38) from the Xunta de Galicia through the ERDF. LM and AA are partly supported by FNR COVID-19 Fast-Track (project PREVID 14863306).

Acknowledgments

The authors thank the Research Luxembourg - COVID-19 Taskforce for mutual collaborations. They also thank two anonymous reviewers for helpful comments and suggestions that led to an improvement of this paper.

Conclusion 1

The developed SPQEIR model allows a model-based output for a quantitative estimate and comparison of the effect of NPI in various countries. The investigation allows to deal with the possible resurgence of contagion [197] and the actual epidemic waves. Furthermore, it gives a better understanding of the effects of the different NPI. My analyses show that a rapid and strong lockdown leads to similar mitigation than a combination of social distancing, lower isolation rates and early contact tracing. In the model of Chapter 5, NPI plays a crucial role as the parameter for social interaction ρ takes into account exactly for that. The social interaction parameter is time-dependent in order to characterize the different phases of COVID-19 such as lockdown and reopening. Additionally, the extended model has the elements of hospitalization, death, vaccination, undetected, ICU and recovered.

CHAPTER 5

COVID-19 POTENTIAL PATH TOWARDS HERD IMMUNITY IN AUSTRIA, LUXEMBOURG AND SWEDEN

This chapter is based on

Françoise Kemp, Daniele Proverbio, Atte Aalto, Laurent Mombaerts, Aymeric Fouquier dHérouël, Andreas Husch, Christophe Ley, Jorge Gonçalves, Alexander Skupin, Stefano Magni. Modelling COVID-19 dynamics and potential for herd immunity by vaccination in Austria, Luxembourg and Sweden. Journal of Theoretical Biology. Volume 530,2021,110874, ISSN 0022-5193, https://doi.org/10.1016/j.jtbi.2021.110874.

Introduction 2

In this publication, I extended the SEIR model introduced in Chapter 3.3.2 by compartments for hospitalization, ICU, undetected cases, vaccination and death in order to simulate the spreading of COVID-19 and its specific implications. COVID-19 is a novel coronavirus, detected in December 2019 in Wuhan (China). The extended SEIR model is calibrated for three countries: Austria, Luxembourg and Sweden until 15 December 2020. Additionally, I developed a method to calculate the reproduction number as it allows the estimation of the minimum size of the immunized population needed to reach herd immunity. In particular, I estimated the vaccination rates which are needed to reach herd immunity by 2021 in relation to the social interactions and active infections.

For the project I designed the study, developed, implemented the model and performed all simulations. Furthermore, I analyzed, interpreted the results and wrote the first draft.

Abstract

Against the COVID-19 pandemic, non-pharmaceutical interventions have been widely applied and vaccinations have taken off. The upcoming question is how the interplay between vaccinations and social measures will shape infections and hospitalizations. Hence, we extend the Susceptible-Exposed-Infectious-Removed (SEIR) model including these elements. We calibrate it to data of Luxembourg, Austria and Sweden until 15 December 2020. Sweden results having the highest fraction of undetected, Luxembourg of infected and all three being far from herd immunity in December. We quantify the level of social interaction, showing that a level around 1/3 of before the pandemic was still required in December to keep the effective reproduction number below 1, for all three countries. Aiming to vaccinate the whole population within 1 year at constant rate would require on average 1,700 fully vaccinated people/day in Luxembourg, 24,000 in Austria and 28,000 in Sweden, and could lead to herd immunity only by mid summer. Herd immunity might not be reached in 2021 if too slow vaccines roll-out speeds are employed. The model thus estimates which vaccination rates are too low to allow reaching herd immunity in 2021, depending on social interactions. Vaccination will considerably, but not immediately, help to curb the infection; thus limiting social interactions remains crucial for the months to come.

5.1 Introduction

In December 2019, a novel strain of coronavirus SARS-CoV-2 (severe acute respiratory syndrome coronavirus 2) was first reported in Wuhan, China. In severe cases, it causes an acute respiratory distress syndrome (ARDS), which can lead to respiratory failure, septic shock, multi-organ failure and death [198]. By mid December 2020, worldwide 72 million confirmed cases and 1,6 million dead people had been identified to be infected with SARS-CoV-2.

To help mitigating the coronavirus disease 2019 (COVID-19) pandemic, mathematical modelling has become a major tool in understanding its spreading [140]. As COVID-19 is currently widely spread across the globe, short- and medium-term modelling forecasts assess the need for containment strategies. For these purposes, one of the most employed models is the Susceptible-Exposed-Infectious-Removed (SEIR) model, for which numerous extensions have been developed

recently. Extensions including compartments for hospitals and deaths have been developed among others for Italian regions [25] and Sweden [24]. An extension to investigate the crucial role of asymptomatic cases was developed in [199]. One approach including a time-varying transmission rate was presented in [200] for France and Ireland. A network-based version of the SEIR model focused on Italian regions [201] showed that the effects of the employed measures have been decisive in preventing much worst outcomes. An extension including asymptomatic cases showed that the timing of social distancing is crucial [202]. Various synergies of different mitigation strategies can lead to similar suppression of the infection, with different consequences [203]. Different models were developed to investigate the effectiveness of specific non-pharmaceutical interventions employed as lockdown-like measures and universal masking [204] or social distancing and travel restrictions [205]. Different measures have different economical consequences, and the epidemiological and economical aspects of the pandemic strongly influence each others [206].

In this study, we extend the SEIR model including a social interaction parameter, the presence of undetected cases, vaccination and the disease progression through hospitals, ICU, recovery and death. The aim is to understand the different phases of the pandemic which occurred in countries employing different policies, and to investigate how the interplay between vaccination strategies and social interactions might lead towards herd immunity throughout 2021. We focus on the epidemic dynamics of three countries: Luxembourg, having the highest fraction of detected COVID-19 cases per 100,000 inhabitants in Europe in December 2020; Sweden, following different intervention strategies, not imposing a full lockdown and considered having attempted to reach herd immunity early on; Austria, showing dynamics comparable to Luxembourg. We calibrate the model separately to publicly available data of each country, and employ it to compare the epidemic dynamics during infection waves within and between countries.

The model is further used to investigate dynamical trends associated with vaccination. As several vaccines became available at the end of 2020, systematic vaccination campaigns have taken off in a number of countries in the first months of 2021. They are of extreme interest, not only to protect the most vulnerable people, but also to contribute to eradicate the virus in the population through herd immunity [207]. Herd immunity is achieved when a certain fraction of the total population is immune to the infectious disease (through natural infection or vaccination), so that

the infectious agent can no longer generate large outbreaks [208]. Much remains to be learned about immunity to SARS-CoV-2 [209], and there exist additional challenges to mass vaccination, associated to supplying of vaccines and the logistic of their deployment. A key question in the current COVID-19 pandemic is thus how and when herd immunity could be achieved [208].

To tackle this question, we use our model to investigate the potential impact of various vaccination strategies and their synergy with social measures for the considered countries. We investigate when herd immunity might be reached depending on vaccines rollout speed in plausible scenarios. The desirable objective would be to achieve herd immunity primarily by mass vaccination, while avoiding the saturation of healthcare systems and having as few cases and deaths as possible. In fact, the alternative to achieve herd immunity primary by infection has been shown to pose severe risks of overwhelming the health care system and to lead to high numbers of deaths [210].

With our study, we are aligned to a long standing tradition of using mathematical models in the design of mass immunization programs [211]. Recently, some works presented results based on simple models and conceptual scenarios [212–215]. Attainability of herd immunity by vaccination in the UK is investigated in [216]. Instead, the presented model is calibrated on data from multiple countries and includes compartments for disease progression and undetected cases and has the scope to systematically investigate the interplay of vaccination strategies and plausible social interaction scenarios in the pursuit of herd immunity. This model was also employed during the ongoing pandemic to investigate the impact of reductions of social interaction and to generate projections to inform policy-making.

5.2 Methods

5.2.1 Mathematical model

We develop a mathematical model of the transmission of COVID-19 within a country's population, extending the standard Susceptible-Exposed-Infectious-Removed (SEIR) model [217] to include 1) undetected cases; 2) varying social interaction; 3) the progression of severe cases through hospitalization, intensive care and eventually death or recovery and 4) vaccination. The model, Fig. 5.1, is implemented through a set of ordinary differential equations (Eqs. B.2 in Appendix).

The total population N of the considered country is streamed at time t into 16 compartmental variables, Tab. B.1. An important fraction of infected people is usually not detected [218], so we introduce a separation between detected and undetected cases. One branch (detected cases) can lead to quarantine and possibly to hospital and/or ICU. The other (undetected cases, either because they are asymptomatic [199] or simply due to lack of testing) continues spreading the infection until recovery or death. The probability of an infected individual to be detected is indicated as p_1 and assumes different values for each country and wave of infections, Tab. B.2 and Tab. B.6.

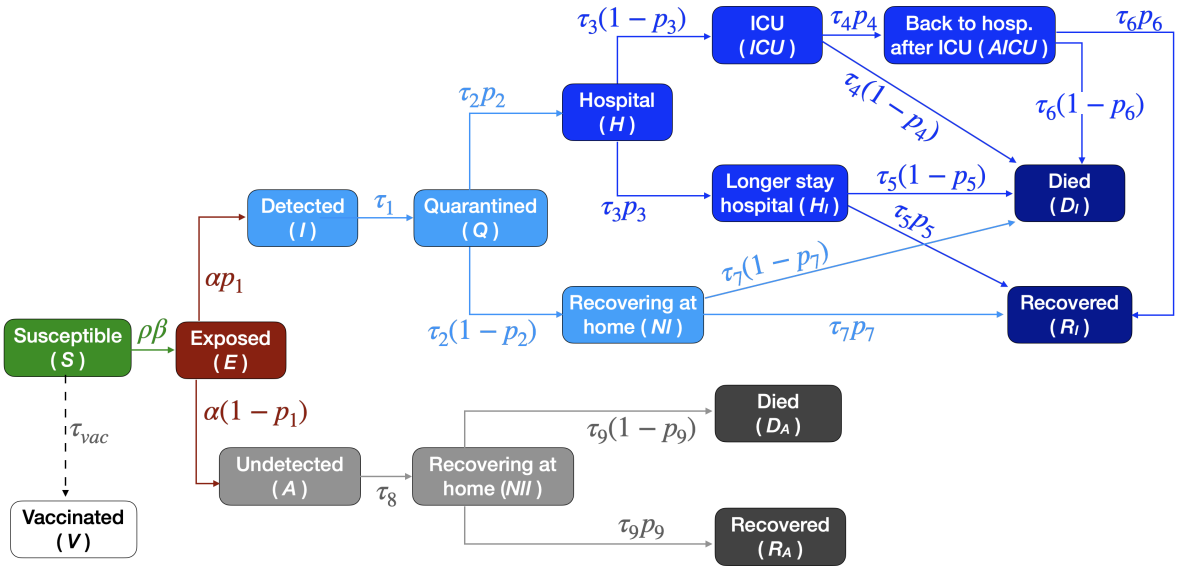

Figure 5.1: Scheme of the mathematical model with the model construction is described in Sec. 5.2.1. Each compartment is associated to a variable, see Appendix Tab. B.1 and Eqs. B.2. Each variable represents the fraction of individuals in that state at a given time. Arrows represent flow of individuals between states, with associated probabilities and rates reported in Tab. B.2. Their values for each country and wave are summarized in Tab. B.6. Vaccination is assumed to occur at a constant rate, to have 100% efficacy and to be administered to susceptible individuals only. These assumptions lead to the projections involving vaccination to be optimistic, see Sec. 5.2.1 and Sec. 5.4.

Most model parameters represent either probabilities p_i of going to one compartment or another, or rates τ_i describing how fast individuals flow through compartments (i is an index over parameters, their values are listed in Tab. B.2). Probability parameters determine which fraction of population goes to one branch, which to the other. Rates, representing the inverse of the average length of stay in a compartment, capture how fast (on average) individuals flow from one pool to the next.

The only parameter not representing a rate or probability is the social interaction parameter $\rho(t)$, which tunes the average contact rate β. It represents the fraction of social interactions taking place at any given time, with respect to the one pre-pandemic. Thus, a value of $\rho(t) = 1$ means the same level of social interaction as in the beginning of 2020. This parameter incorporates non-pharmaceutical interventions and changes in population behaviour similarly affecting the dynamics. It changes whenever new measures or major updates in social interactions take place (lockdown, schools opening/closure, summer vacation, etc.).

Mathematical models are necessarily simplifications of reality. They balance complexity, including the factors crucial to answer the investigated questions and to learn useful real-world lessons, with simplicity, as they need to be simple enough to be numerically and/or computationally tractable. Hence, the present model relies on a number of assumptions.

As other SEIR models, the present model is deterministic and mean-field, so it does not describe the stochastic aspects of the epidemic, e.g. super-spreading events, but concentrates instead on its average evolution. Alternative approaches to ODE-based models have been developed, e.g. agent-based models [219], recently applied e.g. in Luxembourg [220], Switzerland [221] or Australia [222]. Deviations from mean-field effects are expected to play an important role in periods of low infections numbers, where e.g. one or few super-spreading events can make the difference between starting or not a wave of infections [223]. However, with high case numbers we expect a deterministic description to be sufficiently accurate, especially when it comes to the progression of infected individuals into more severe stages as hospitalisation, ICU and death.

The model does not include age structure. As COVID-19 case fatality rate, hospitalization and ICU admission rates vary with age, the values of our parameters represent an average over age groups. Instead of capturing the age-dependent risk of disease progression, the present model fits and simulates aggregated hospitals and ICUs occupations and deaths. This allows to compare simulated scenarios for the evolution of aggregated quantities under different assumptions, for which age structure is not crucial. Moreover, not considering explicitly the age structure reduces the number of parameters to fit, thus improving calibration and reducing fitting uncertainties. In addition, while in principle the effective reproduction number $R_{eff}(\mathbf{t})$ can be derived analytically in age-structured SEIR-like models [224–226], the absence of age structure here contributes to

make its derivation much more tractable in practice. Nonetheless, the current assumption could lead our estimates to represent a pessimistic case, since previous computational studies have shown that including age-dependent contacts in an agent based model can reduce the threshold for reaching herd immunity [227].

The other factor contributing to make $R_{eff}(\mathbf{t})$ analytically tractable is the way we implement vaccination. Vaccination is also modelled in a simplified manner, namely as individuals flowing at a constant rate out of the susceptible compartment (see also B). This implies four assumptions. First, we assume that vaccination proceeds at a constant rate. In reality, the rate depends among other factors on vaccines availability; hence, the vaccination rate in the model is intended as an average, reference value. Second, we use the terms vaccination and "vaccinated people" referring to individuals who have been fully vaccinated (not those with half coverage from two-doses vaccines). This should be considered when comparing real numbers to the vaccination rollout speeds employed in this paper. Third, we assume 100% vaccine efficacy in preventing an individual from getting infected, developing symptoms and infecting others. This is an optimistic approximation. Fourth, we assume that only susceptible individuals are vaccinated, while in reality also recovered individuals are. While the number of recovered individuals is in the countries and scenarios investigated here considerably lower than the number of susceptible, to some extent supporting this approximation, removing this assumption would somewhat increase the vaccination rates needed to obtain the same results with respect to our estimates. Overall, these assumptions make our vaccination simulations an optimistic limit. However, the absence of age-structure makes our estimates of the herd immunity threshold a pessimistic limit, so the two effects might compensate to some extent, which is difficult to quantify. The impact of the assumptions mentioned here is discussed in more detail in Sec. 5.4.

5.2.2 Model calibration and fit to public data

The model is fitted to available public time-series data (from February to 15th December 2020), independently for each wave and country. Detailed methodology, data and dates are discussed in Appendix. These data are displayed in Fig. 5.2 for total detected cases (**A**, **B**, **C**) and corresponding daily new cases (**D**, **E**, **F**), hospital occupation (**G**, **H**, **I**), ICU occupation (**J**, **K**, **L**)

and deaths (**M**, **N**, **O**). Subsequent waves of infections have occurred; we refer to them as 1st and 2nd wave for Austria and Sweden, respectively for those starting in February and September. Luxembourg had an additional wave during July (see Fig. 5.2 **D**). So, we refer to it as 2nd wave, and to the rise in September as 3rd wave.

For each country and epidemic wave, we initially manually calibrate a set of parameters that allow the simulations to fit the data while incorporating literature knowledge (see B). In the rest of the paper, we will refer to this parameter set as "manual fit" or "manual calibration". In particular, these parameters are obtained from non-country-specific literature as [173, 178, 228], or from country-specific literature or data as [229–232], or from assumptions. Details are provided in B: rates and probabilities used are listed in Tab. B.6; social interaction parameter values and their changes over time are displayed in Fig. 5.3 (main text) and listed in Appendix Tab. B.3 (Luxembourg), Tab. B.4 (Austria) and Tab. B.5 (Sweden). Values of the social interaction parameter employed for a given time-period (between two changes in measures) are obtained by best fitting the simulation of new cases to the moving average of the corresponding data. This method already returns good agreement between simulations and data from several time-series data (*cf.* Fig. 5.2), thus supporting our choice of parameters.

We further cross-validate the calibration of our model by Bayesian inference and Markov Chain Monte Carlo (MCMC) methods (*cf.* B). Such methods have been widely applied in the framework of the pandemic to infer epidemiological parameters from SEIR-based or other models, e.g. for Spain [233], Germany [234] and in a comparison of 11 countries, including Austria and Sweden [235]. Most of these studies did not include hospitalisations, ICU, deaths and undetected cases and all of them focus on one country, except [235] which focuses on the basic reproduction number. The set of MCMC simulations is performed to obtain an estimate of the parameters and to quantify their uncertainties. The choice of prior probability distributions for the parameters is specified in B; chains are verified to converge in B. The values of the manual fit are usually included within the Bayesian credible intervals and are thus consistent (*cf.* Fig. B.3). We observe high degeneracy between parameters, with combinations (e.g. ratios) of parameters being often better constrained than individual ones (*cf.* Appendix, Figs. B.4 — B.10 and corresponding sections). The MCMC is extremely useful to estimate the uncertainty that affects our estimate of parameters and their

potential ranges of values, but it does not provide a unique parameter set due to poor identifiability, common to SEIR models [189]. In fact, the two parameter sets obtained respectively from the maxima of the posteriors (maximum a posteriori estimate) and from the means of the posteriors are rather different from each other due to asymmetric posteriors. Moreover, certain parameters are poorly constrained by the data, resulting in rather flat posterior probability distributions. For the simulations, we thus employ the manually calibrated parameter set, which is unique, consistent with the results of the MCMC, and incorporates domain knowledge from literature as explained in B.

5.3 Results

5.3.1 The model accounts for undetected cases and projects potential scenarios

The model (Fig. 5.1) is developed and calibrated so that it fits available time-series data from considered countries (*cf.* Sec. 5.2.1). To improve the identification of the model parameters, we cross-validate the manual calibration, used in model simulations, with a Bayesian fit (*cf.* B, B, B and Fig. B.3). Data evolution and model simulations are reported in Fig. 5.2.

The model also accounts for undetected cases, through a dedicated compartment flow. In particular, the probability p_1 of being detected is estimated for each country and wave from available prevalence data, see Appendix Tab. B.6. These undetected cases are reported in panels **A**, **B** and **C** of Fig. 5.2 as cumulative numbers. Over time, this number (violet dashed curve) is approximately between one and two times the number of detected cases for Luxembourg and Austria, while it is up to three to four times for Sweden. The percentage of undetected is in all three countries higher than that of detected, which is in line with estimates like [236]. Nevertheless, for Austria and Sweden the sum of detected cases and the estimated number of undetected cases until December remains more than an order of magnitude smaller than the population of the country, while for Luxembourg it is higher. In fact, our model shows that until the 15th December, the percentage of population having been infected by SARS-CoV-2 in Luxembourg is about 18.3% (7.2% detected and 11.1% undetected); in Austria 9% (3.7% detected and 5.3% undetected) and in Sweden 14.5% (3.5% detected and 11% undetected). For all three countries, this made herd

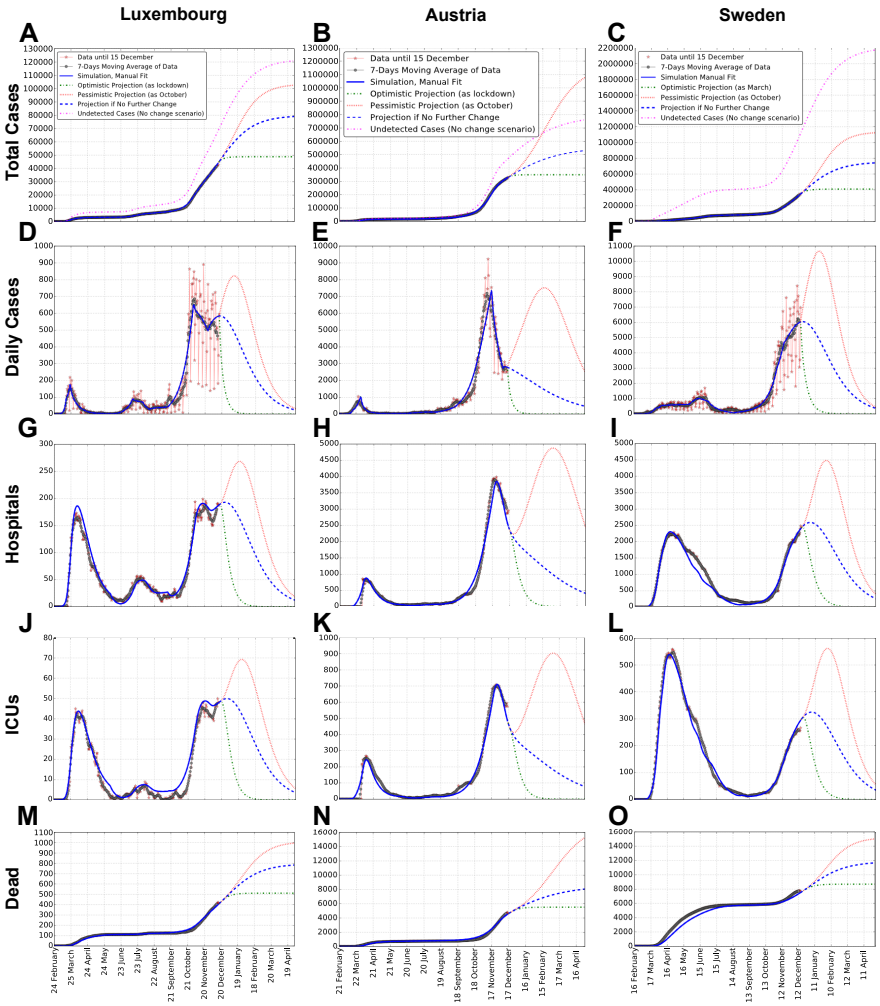

Figure 5.2: Data, model simulations and projections of total cases, daily cases, hospital and ICU occupation and dead, for each country. Reported are: total cases (**A**, **B**, **C**), daily new cases (**D**, **E**, **F**), hospital occupation (**G**, **H**, **I**), ICU occupation (**J**, **K**, **L**) and deaths (**M**, **N**, **O**). Such values are respectively estimated from Appendix Eqs. B.8–B.12, for each country (see columns). In addition to model simulation, raw data are shown (red stars), together with their weekly moving average (gray dots). Panels **A**, **B**, **C** also report (in violet) the cumulative number of estimated undetected cases, obtained as the sum of undetected cases being either infectious, recovering, recovered or dead, see Appendix. Entries of panel **A**'s legend hold for each panel, except the one for undetected cases, displayed only in panels **A**, **B** and **C**. Projections for several months after the last data point illustrate the potential simulated scenarios explained in the main text.

immunity still far from being reached in December 2020.

On top of reproducing the historical development, the model is employed to simulate potential future scenarios of the epidemic in each country. In Fig. 5.2 (dashed lines), we simulate the possible progression of the epidemic in the early months of 2021 until spring. Three scenarios are

considered: one corresponds to no change in social interaction w.r.t. mid December; an optimistic scenario where social interaction becomes as low as during the lockdown in March; a pessimistic scenario where it becomes as high as in October. These three scenarios are meant to represent an average outcome and two extreme, but plausible cases. While instructive, projections might be accurate for few weeks, but less so on longer time periods as small changes in e.g. social interaction and corresponding parameter can lead to large changes in the simulated outcome. Consequently, their goal is mainly to investigate potential scenarios that might unfold from the current situation [233] and compare them between each other.

5.3.2 Social interaction drives epidemic dynamics

The parameter $\rho\,(t)$ tunes social interactions, and changes when new measures or major behavioural changes occur. It is thus implemented as a piece-wise constant function of time. Its value changes at specific dates t_n when modifications in non-pharmaceutical measures took place. A mean constant value ρ_n is estimated from fitting model simulations to data, and assumed over the subsequent period of time. The evolution of ρ_n is reported in Fig. 5.3 for Luxembourg, Austria and Sweden, respectively in panels **A**, **C** and **E**. Measures, dates and ρ_n values are summarized in Appendix Tab. B.3 (Luxembourg), Tab. B.4 (Austria) and Tab. B.5 (Sweden). When interpreting the results for $\rho(t)$, it should be recalled that it lumps both population-wide non-pharmaceutical interventions and targeted ones. This choice contributes to make the calculation of $R_{\mathit{eff}}\,(t)$ analytically tractable, dramatically reduces the number of free parameters, reduces their estimated uncertainties and does not require additional data stratified over population groups. In turn, this description does not capture the effects of heterogeneous measures across population groups (e.g. working sector, etc.). This aspect was instead investigated for Luxembourg in [206]. As a result, $\rho(t)$ corresponds to an estimate of the average social interaction across all groups of the population.

Panels in Fig. 5.3 show values of ρ_n from both manual calibration and Bayesian inference, which are both proportional to daily cases number. Manually calibrated social interaction values are consistent with the Bayesian estimates, falling within the 50% or 90% credible intervals (respectively, dark green or light green bands). This supports the validity of manually calibrated $\rho(t)$ values,

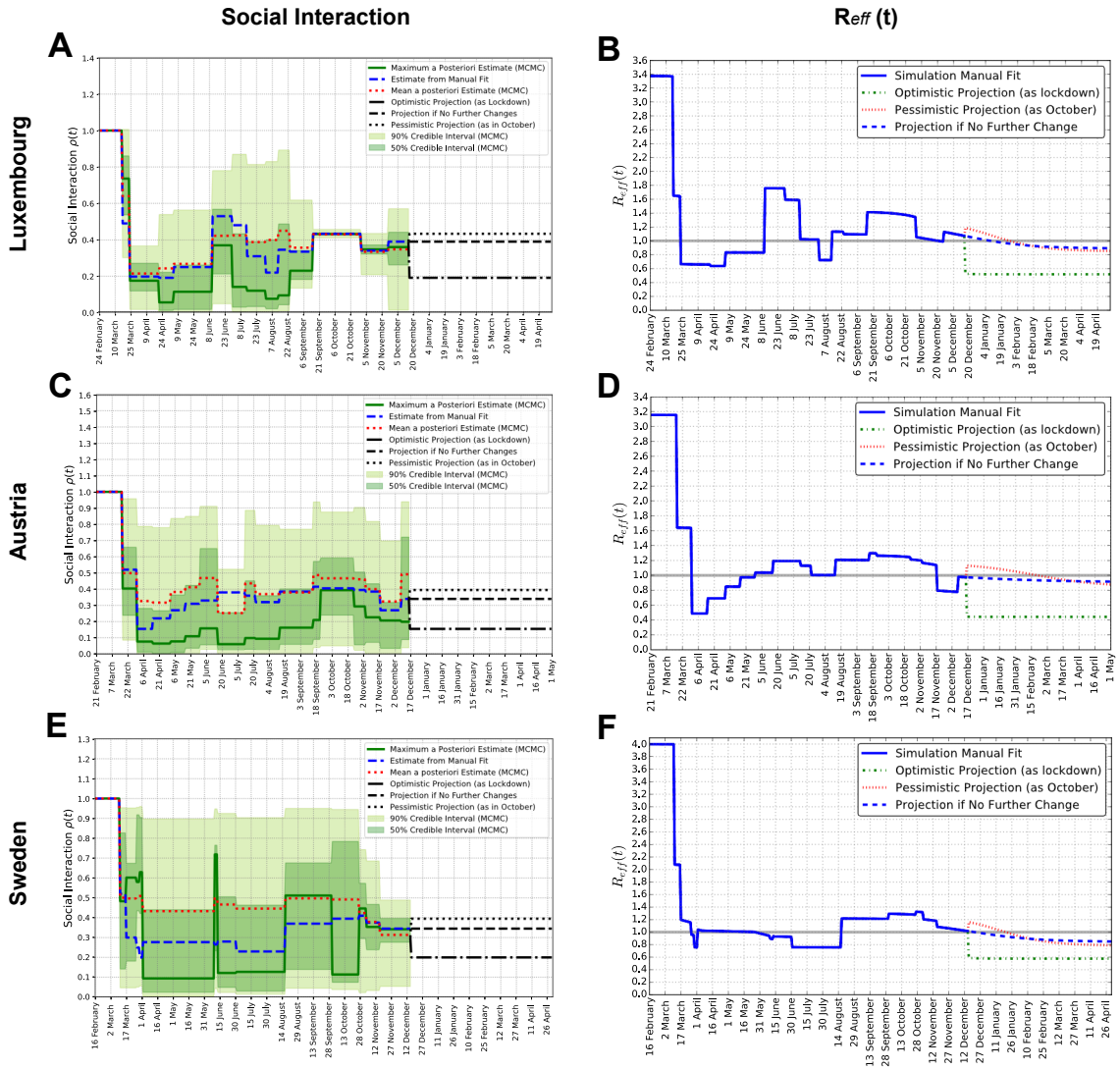

Figure 5.3: Social interaction parameter $\rho\,(\mathbf{t})$ and effective reproduction number $R_{eff}\,(\mathbf{t})$ for each country where panels **A**, **C**, **E**: social interaction parameter $\rho\,(t)$, manual and Bayesian estimates for Luxembourg, Austria and Sweden. Dates of change and parameter values are reported in Appendix Tab. B.3 for Luxembourg, Tab. B.4 for Austria and Tab. B.5 for Sweden. Panels **B**, **D**, **F**: effective reproduction number $R_{eff}\,(t)$, computed from Appendix Eq. B.4, corresponding to the values of the social interaction parameter for Luxembourg, Austria and Sweden, from their manually calibrated parameter sets.

which yield very good model fit to data of detected cases, see Fig. 5.2, panels **A**, **B**, **C**. This identifies social interaction as an essential model parameter, in turn underlying the importance of social interaction management for epidemic control.

Directly proportional to $\rho(t)$ and to the susceptible population fraction is the effective reproduction

number $R_{eff}(t)$. Its time evolution (analytical derivation in Appendix, see Eq. B.4) for each country is displayed in Fig. 5.3, panels **B**, **D** and **F**. Step-wise changes in $R_{eff}(t)$ arise from changes of $\rho(t)$, while gradual changes are instead due to depletion of the pool of susceptible individuals. The value of $R_{eff}(t)$ at the pandemic beginning provides the basic reproduction number $R_0 \doteq R_{eff}(t=0)$. We estimate $R_0^{\mathsf{LUX}} \approx 3.38$ for Luxembourg, $R_0^{\mathsf{AUT}} \approx 3.16$ for Austria and $R_0^{\mathsf{SWE}} \approx 4.00$ for Sweden. Such values are consistent with those of independent studies. In general, estimates of R_0 from Western Europe vary between 2 ad 6 [237–239], depending on country, study, method and associated uncertainties. [235] estimates $R_0 = 3.11$ for Austria and 2.89 for Sweden, with posterior probability distributions extending from 2 to 4 (see Fig. 2 therein). In Luxembourg, [220] provides a value of $R_0 = 2.45$ with its baseline SEIR model. Our full estimates of $R_{eff}^{\mathsf{LUX}}(t)$ is also consistent with that reported in the official Luxembourg government website (https:275//covid19.public.lu/fr/graph.html, last accessed on 26/07/2021), estimated with independent methods. There, R_0 is estimated to be around 3.3.

From Fig. 5.3, we can evince the value of R_{eff} at the last data-point, namely 15th of December, which is 1.07 for Luxembourg, 0.97 for Austria and 1.01 for Sweden, all very close to $R_{eff} \approx 1$. The percentage of social interaction (w.r.t. before the pandemic and corresponding measures) needed at that date to have $R_{eff}(t) \approx 1$ was similar across countries: 36% in Luxembourg and 34% in both Austria and Sweden.

5.3.3 Parameter fitting reveals probability of hospitalization decreases between waves

The social interaction parameter $\rho(t)$ changes a limited number of times to represent changes in non-pharmaceutical interventions or population behaviour. To fit the first waves of Luxembourg and Austria, all other parameters are constant (though slightly different between the two countries), as the time evolution of daily new cases, hospital and ICU occupation are alike, although scaled and delayed. However, the same parameters from the first wave overestimate the hospital progression during the second wave.

Fig. 5.4 reports the parameter fold-changes (FCs) between one wave and the subsequent. There, we display the changes observed by different fitting methods, to discuss how stable such results

are. In the manually calibrated parameter sets (green circles) the probability of being hospitalized when detected positive, p_2, needs to be decreased between each wave and the subsequent, both in Luxembourg and Austria (among other parameter changes). The same trend in the parameter p_2, which decreases considerably, is also observed in the maximum a posteriori estimate (blue dots) from the Bayesian estimate both between the 2nd and 3rd waves of Luxembourg (panel **B**), and between the 1st and 2nd waves of Austria (panel **C**). Only from the 1st to 2nd wave of Luxembourg the Bayesian estimate shows a slight decrease for the maximum of the p_2 estimate, but conversely a slight increase in the mean (red squares). Notice that different parameters appear on the horizontal axes of different panels. For Sweden, instead of a step-wise change, we assume a continuous decrease in $p_2\,(t)$ from 0.9 in March to 0.1 from June onward. This is based on data of new daily cases and hospital admissions; further analysis is reported in B and Fig. B.2 (panel **D**). These findings underline that, overall, the probability of being hospitalized when detected (p_2) decreased for subsequent waves of each investigated country. This likely reflects the improvement and up-scaling of testing strategies over time, leading to an increased capacity to detect asymptomatic or non-severe cases. In fact, p_2 represents the probability of being hospitalized if tested positive. So, more effective or widespread testing combined with similar severity of the disease would result in a decrease of p_2. Supporting this interpretation is the fact that in Luxembourg and Sweden we estimated p_1, the probability of being detected positive if infected, to be higher (or constant at most) at subsequent times (see Appendix Tab. B.6 and corresponding sections).

The MCMC estimates do not fully reflect the changes in some parameters that we performed between one wave and the next in the manually calibrated parameter set (see Fig. 5.4 and Appendix Tab. B.6). These discrepancies could indicate that, due to the large uncertainty in parameter identification in our Bayesian inference, multiple parameter sets could provide equally good fit between model and data (see Appendix for further discussion about system identifiability). Supposedly, means provide more robust information than maxima, which are representative of the posterior distribution only when the posterior has a clear peak and is not almost flat. This results in some of the FCs obtained from the maxima (large blue dots) having extreme values, in particular those associated with τ_4, τ_5, τ_6 and τ_7, i.e. the rates involved in the patient progression

through hospital and ICU.

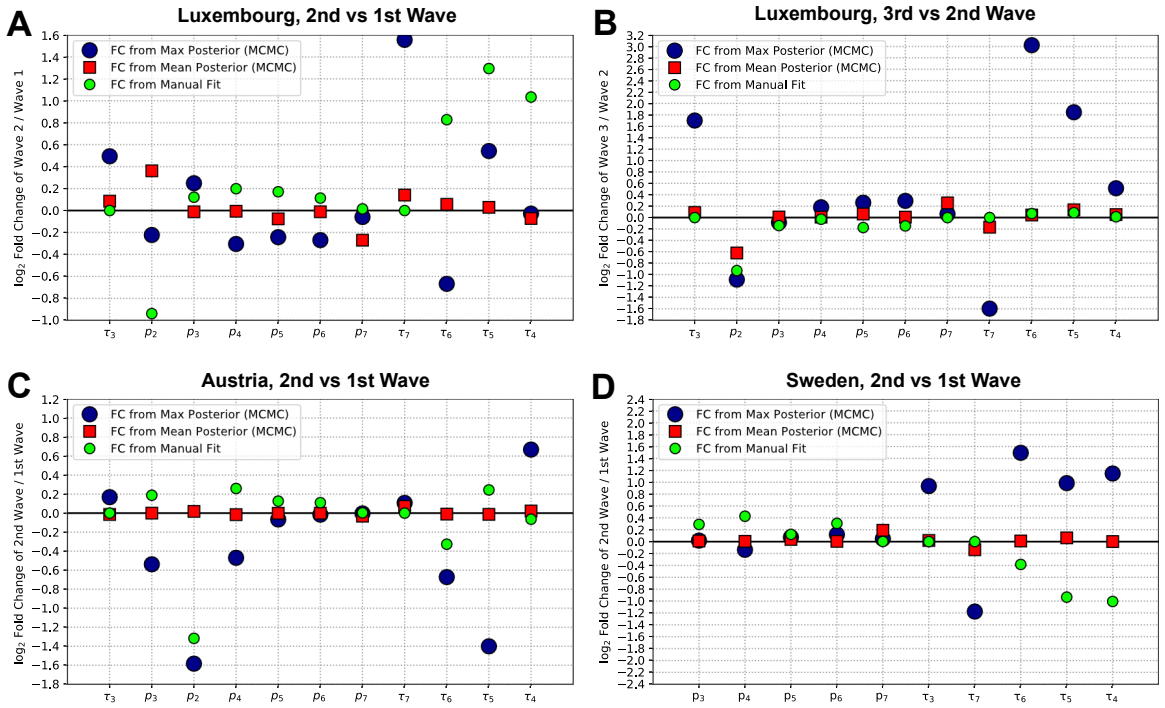

Figure 5.4: Fold-changes (FC) of the estimates of each parameter, between a wave and the subsequent, for each country. **A**: 2nd wave versus 1st wave, Luxembourg. **B**: 3rd wave versus 2nd wave, Luxembourg. **C**: 2nd wave versus 1st wave, Austria. **D**: 2nd wave versus 1st wave, Sweden. The values for the parameters employed are displayed in Appendix Fig. B.3 for both manual and Bayesian fit, and summarized in Tab. B.6 for the manually calibrated parameter set. The vertical axes indicate $\log_2(FC)$, with $FC \doteq \tau_{2^{\text{nd}}\text{Wave}}/\tau_{1^{\text{st}}\text{Wave}}$ for each parameter, generically indicated as τ. A value of 0 corresponds to no change, 1 to doubling from the previous wave to the next, -1 to halving from the previous wave to the next, and so on. The green small dots depict the fold changes for the manually calibrated parameter sets. Errors on the means were computed by the standard error of the mean, but are too small to be noticeable in the figure.

5.3.4 Social interactions strongly impact infection in early 2021, along with vaccination

The model includes fully protective vaccination and investigates the interplay between its dynamics and social interaction Three potential vaccination strategies (corresponding to three vaccines rollout speeds) are simulated, starting from 1st January 2021: vaccinating all the country population within the first 6 months of 2021, within 1 year, or within 1.5 years. These would correspond to fast, average and slow rollout, respectively, and represent potential timelines that countries

might attempt to implement.

For comparison, we consider the baseline case where no vaccination is performed. The results are displayed in Fig. 5.5. Panels **A**, **B**, **C** report people fully vaccinated over time for various scenarios, panels **D**, **E**, **F** display $R_{eff}\,(t)$, panels **G**, **H**, **I** the number of total detected cases and panels **J**, **K** and **L** show the number of new daily detected cases. Dashed curves represent the four different vaccines rollout strategies. To investigate the interplay between social measures and vaccination strategies, we simulate combinations of the two. We consider two alternative values of social interactions: a value corresponding to the pessimistic scenario of Fig. 5.2 (going back to the levels of October 2020, shown in red), and a value corresponding to the average scenario (no change in social interaction w.r.t. December 2020, shown in blue). The optimistic scenario for social interaction is not included, because it corresponds to full lockdown, unlikely to happen for several months consecutively.

Panels **A**, **B** and **C** in Fig. 5.5 shows that, for high social interaction levels, a smaller number of people will need vaccination, since more people already got infected naturally. Slower vaccination strategies will also result in less people to be vaccinated as more people will by then have acquired immunity naturally. These observations are consistent across considered countries.

Panels **D**, **E** and **F** report the simultaneous effects of social interaction and shrinking of the pool of susceptible, due to both infection and vaccination, on $R_{eff}\,(t)$. In each country, for any vaccination strategy as well as for no vaccination, the pessimistic scenario (red) starts with a higher $R_{eff}\,(t)$ than the "no change" scenario (blue). However, the situation is eventually inverted due to larger shrinking of the susceptible pool associated with higher social interactions. This suggests that the interplay between social interaction and vaccination is non-trivial; it is deeper investigated in the next section.

Panels **G**, **H** and **I** illustrate the changes in dynamics of total detected cases for the same scenarios and strategies. We observe that the faster the vaccines rollout, the fewer total detected cases are reached asymptotically. Any vaccination strategy considered leads to considerable reduction of the detected cases number w.r.t. no vaccination. This discrepancy is larger than the difference in cases between the three strategies. For all three countries, the number of total cases is impacted more, or with similar magnitude, by the different social interaction scenarios (compare red and blue

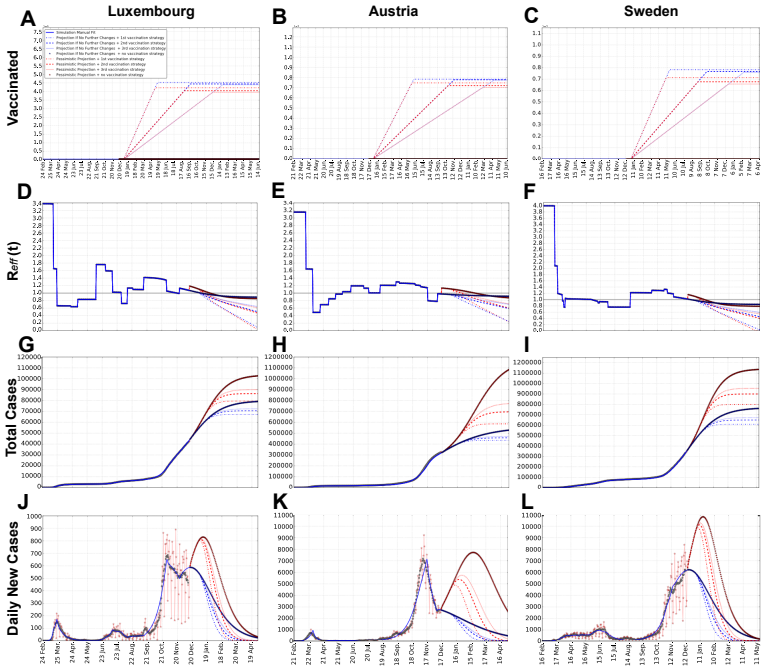

Figure 5.5: Simulations of different vaccination strategies: projections of number of fully vaccinated people, $R_{eff}\,(t)$ and total detected cases for each country where panels **A**, **B** and **C** show the number of fully vaccinated people as a function of time. Panels **D**, **E** and **F** show $R_{eff}\,(t)$. Panels **G**, **H** and **I** show the number of total detected cases. Panels **J**, **K** and **L** show the number of new daily detected cases. Luxembourg (**A**, **D**, **G**, **J**), Austria (**B**, **E**, **H**, **K**) and Sweden (**C**, **F**, **I**, **L**) are reported. Projections for several months after the last data point illustrate potential simulated scenarios, for three alternative vaccination strategies and for no vaccination, both in the case of the "pessimistic" scenario (red, corresponding to social interaction as high as in October) and the "no change" scenario (blue, corresponding to no change in the social interaction) from Fig. 5.2 and Fig. 5.3. For each social interaction scenario, we show the curves for no vaccination and for three alternative vaccination strategies (each corresponding to a different vaccines rollout speed), which correspond to vaccinating all the population of a country in, respectively, 6 months, 1 year or 1.5 years, starting from January 1st, 2021. Scientific notation is used in some panels, where 1e7 stands for ten millions. Assumptions of vaccination are summarised and discussed in Sec. 5.2.1 and Sec. 5.4

.

groups) than by vaccination (different dashed curves for the same group color). The corresponding new daily cases plots are displayed in panels **J**, **K** and **L**.

Thus, we can conclude based on this analysis that, at least until spring 2021, social interaction measures are expected to still play an important, dominant role.

5.3.5 Vaccinating whole population in a year, herd immunity not before mid summer

Expanding what considered above, we tackle the following question: when might herd immunity be reached, depending on combinations of social interaction and vaccination strategies? In mean field SEIR-like models with homogeneous mixing of the individuals, the population fraction needing to be immune, in order to reach herd immunity in the absence of measures is estimated as $p_c = 1 - 1/R_0$ [208]. To answer the above question, we compute this quantity for the three countries. Using the values of R_0 previously estimated, we obtain: $p_{c,Lux} = 1 - 1/3.38 \approx 0.70 = 70\%$ for Luxembourg, $p_{c,Aus} = 1 - 1/3.16 \approx 0.68 = 68\%$ for Austria and $p_{c,Swe} = 1 - 1/4.00 \approx 0.75 = 75\%$ for Sweden, with the pool of susceptible left given by the remaining population. When additional complexities are included in the model, the formula above might not perfectly hold. Hence, we confirmed its results by numerically analysing the model outputs, as described in B. Briefly, the procedure involves finding the fraction of susceptible, in the measures-free model, that corresponds to the maximum of the Infectious curve, which corresponds to herd immunity by definition. The herd immunity thresholds estimated computationally in our model are $p_{c,Lux} \approx p_{c,Aus} \approx 73\%$ for Luxembourg and for Austria, $p_{c,Swe} \approx 76\%$ for Sweden. These values are similar to the ones obtained analytically and potentially more representative; so, they will be employed in the remaining of the analysis. As reference, Manaus (Brazil) registered a 76% of infected population and a catastrophic losses of lives, before the epidemic naturally slowed down, without relevant interventions (from antibody tests performed in October 2020 [240]). Hence, similar values for the herd immunity threshold might occur in reality, and there is consensus [208, 241] in aiming for herd immunity primarily by vaccination, instead of natural infection, as the latter could yield symptoms of various severity, occupation of health care facilities and, in a fraction of cases, death. Nevertheless, Manaus also witnessed a major surge in cases in early 2021 [242], leaving open the question if herd immunity against COVID-19 can be reached in real settings.

Fig. 5.6 addresses specifically how we could aim at herd immunity primarily by vaccination, displaying the time at which herd immunity might be reached for all possible social interaction values and vaccines rollout speed. Average social interaction values are assumed to apply from December

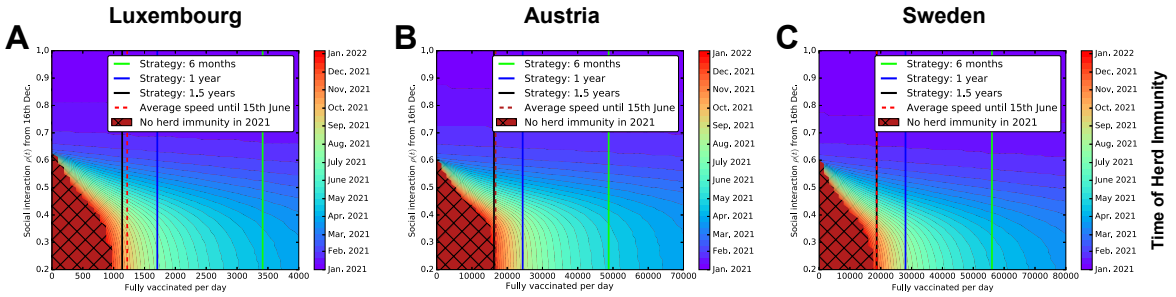

Figure 5.6: Systematic investigation of the interplay between vaccination strategies and social interaction scenarios, to estimate the time by which herd immunity might be reached for Luxembourg (**A**), Austria (**B**) and Sweden (**C**). Panels **A**, **B** and **C**: indicative dates at which herd immunity might be reached, depending on combinations of social interaction parameter and number of fully vaccinations/day. The black grid indicates the combinations of social interaction and vaccination speed that would not allow to achieve herd immunity until 2022. In all panels, vertical lines indicate the three alternative vaccination strategies described in the main text. Depending on measures and population behaviour, estimated levels of social interaction since the beginning of the pandemic have been mostly between 0.15 and 0.5 (i.e. 15% to 50% w.r.t. before the pandemic). Assumptions of vaccination, like 100% efficacy, are summarised and discussed in Sec. 5.2.1 and Sec. 5.4. The red dashed line represents an estimate of the number of fully vaccinated people per day for each country, averaged over time from December 27th, 2020 to July 15th, 2021.

16th onward; the constant number of fully vaccinated people per day is assumed to apply from 1st January, and it should be intended as an average value over time. By requiring the percentage of people still susceptible to be less or equal than p_c, we identify when herd immunity would be reached for each combination of parameters. Herd immunity can be either reached purely by natural infection (by moving along the vertical axis), or purely by vaccination (by moving along the horizontal axes), or by a combination of the two. The three vertical lines in the panels of Fig. 5.6 show the number of full vaccinations/day required to vaccinate the country's whole population respectively within 6 months, 1 year or 1.5 years. The corresponding vaccination rates are derived in B. A vaccines rollout strategy aiming to full vaccinate the whole country's population in a year would require approximately 1,700 full vaccinations/day in Luxembourg, 24,000 in Austria and 28,000 in Sweden, and could potentially lead to achieve herd immunity during July in Luxembourg and during August in Austria and Sweden. In all three countries, herd immunity cannot be achieved within 2021 with the typical levels of social interactions that were observed so far, without vaccination nor with too low vaccination rates.

For Luxembourg, all three vaccination strategies considered in this study might well obtain herd immunity within 2021, for Austria and Sweden the 1.5 years strategy is only borderline sufficient

to reach herd immunity by the end of 2021, while the other two are enough for each country. It remains to be seen if the actual availability of vaccines will make possible any of these example strategies; in the end of this section and in the discussion we compare them with real vaccines rollout speeds recorded until July 2021. If herd immunity had to be reached purely by vaccination (or at low levels of social interaction), the 6 months strategy would take approximately until April for Luxembourg, and May for Austria and Sweden, and the 1 year strategy until July for Luxembourg and August for Austria and Sweden. Higher values of social interactions might anticipate it, but with undesired consequences on the healthcare. Several factors not included in the model might influence these estimates, making herd immunity more difficult or easier to achieve, e.g. reinfections and age structure of the population, discussed at the end of the paper. As COVID-19 is an ongoing situation, we further estimate the vaccine rollout speeds taking place in reality and which can be compared with the three reference strategies of Fig. 5.6. Based on the model's assumptions, we hence consider the number of individuals fully vaccinated, averaged over time. In Luxembourg, 248995 people have been fully vaccinated in 200 days, from 27 December 2020 until 15th July 2021; in Austria 3937701 and in Sweden 3716260. In Luxembourg, this corresponds to around 42% of the total resident population being fully vaccinated, in Austria 44% and in Sweden 36.3%. These numbers would correspond to an average of 1245 fully vaccinated people/day in Luxembourg, 19689 people/day in Austria and 18581 people/day in Sweden. We display these estimates in each panel of Fig. 5.6 as a dashed red vertical line.

5.4 Discussion

This work consists of two main analysis. First, we calibrated our model to fit time series data of quantities of epidemiological interest, for three countries. By doing so, we tackled the problem of identifiability of complex model parameters, we demonstrated the valuable use of mean field models to describe epidemiological trends in different countries and we obtained a reliable baseline model. Next, we used the knowledge about the epidemiological situation to infer the impact of vaccination campaigns in the pursuit of herd immunity. This provides data-based estimations of the interplay between social measures and vaccination rollouts.

To obtain a reliable dynamical model, we estimated its parameters. Complex epidemiological models might suffer from poor identifiability of their parameters [189] often associated with data quality, quantity and fitting methods. To address this and provide consistent estimates, the parameter set was initially manually calibrated and then cross-validated by Bayesian inference, which elucidates parameters uncertainties. Out of such analysis, three remarks are particularly relevant. First: the uncertainties associated to each parameter are non-negligible, and sometimes rather large (e.g. Fig. B.3) , possibly due to large number of parameters. Second: several parameter combinations are better constrained than the corresponding individual parameters (e.g. Fig. B.4 and subsequent). Third: the manual calibration is compatible with the Bayesian estimate (Fig. B.3) , but its set of parameters correspond to one possible choice and shouldn't be considered fully exhaustive. These characteristics are common to any epidemiological model. Here, we carefully investigate them, and where possible we incorporate domain knowledge from literature. The main parameter controlling the model behaviour is the social interactions parameter $\rho(t)$, which represents both measures applied by policy-makers and population behaviour. This confirms the well-established fact (e.g. [243]) that social interactions are a major driver of epidemic dynamics and of the reproduction number $R_{eff}(t)$. Changes in $R_{eff}(t)$ are also driven by the depletion of the pool of susceptible that only starts having noticeable effects in fall 2020. So far the effect of $S(t)$ on $R_{eff}(t)$ is more pronounced for Luxembourg, where a larger fraction of total population has been infected, than for Austria and Sweden. However, its impact is predicted to become visibly more relevant with subsequent months across 2021 as more people get infected. This is evident from the stronger gradual bending of the curves in winter and spring 2021, especially for the pessimistic scenario, in Fig. 5.3.

For the model to fit the data, other parameters can be kept constant within single waves in Luxembourg and Austria. However, their value change between waves. This aspect can be explained by reduced probabilities of being hospitalized, as we tested with the manually calibrated parameter set. For Luxembourg (see Fig. 5.4 and Appendix Tab. B.6), p_2 decreases from 15.3% in 1st wave to 8.0% in 2nd to 4.2% in 3rd. For Austria, from 16.2% in 1st to 6.5% in 2nd. These changes where also supported by similar changes in the maxima of the Bayesian estimates for 3rd versus 2nd wave in Luxembourg and 2nd versus 1st wave in Austria. This is most likely driven

by testing strategies which improved over time, and it might also reflect changes in treatment capacities, in the influenced age categories, and in other factors. For Sweden, considering a different set of parameter values is not enough to fit its data with the same model structure. Instead, time-dependent probabilities of being detected and hospitalized when tested positive, dramatically decreasing from March to June 2020, need to be introduced within each wave. This does not reflect a rise in infections, but rather a major change in testing strategy and a better prognosis linked to younger patients [244, 245].

The model also allows to estimate the fraction of undetected cases from prevalence data. Luxembourg and Austria display (see Fig. 5.2) similar fractions of undetected, while Sweden has more, accumulated mostly during the first wave. Until 15th December, in Luxembourg about 18.3% (7.2% detected and 11.1% undetected) of the population had SARS-CoV-2; in Austria 9% (3.7% detected and 5.3% undetected) while in Sweden 14.5% (3.5% detected and 11% undetected). Despite the different policies, Sweden is actually not only far from herd immunity, but also further than Luxembourg as of December 2020.

Once calibrated, the model allows to inspect future scenarios to inform data-driven decisions. The epidemic time evolution is simulated in three alternative scenarios for each country (Fig. 5.2): no change in social interaction w.r.t. mid December 2020; social interaction as low as during lockdown/March 2020 (optimistic); social interaction as high as in October (pessimistic). Infection curves for the three scenarios are well separated from each other, indicating that they could be further reduced by decreases of social interactions (by measures or changes in population behaviour) to values close to those during the first lockdown. In Luxembourg and Austria, the level of social interactions of December 2020 seems to be sufficient to maintain a sub-linear growth of number of total cases in the subsequent months. However, for any of the three countries, an increase of the social interaction parameter to the levels of October would likely trigger a considerable rebound of the infection curve. This would be associated with a rebound in hospital and ICU occupations, thus calling for the maximum caution by population and policymakers alike. In addition, the number of deaths is proportional to the area under the daily infections curve. Thus, keeping daily cases contained to avoid hospitals and ICU saturation does not fully prevent a steady growth of the cumulative number of dead, in particular in the pessimistic scenario.

After calibration, we extended the model with a vaccination compartment and we quantified how long it would take to reach herd immunity. First, we considered the same scenarios as above (*cf.* Fig. 5.5). The difference between the detected cases curves of the two considered social interaction scenarios is larger than the difference between the different vaccination strategies. This indicates that during the vaccination process, reduced social interactions are still going to be crucial to keep the number of cases under control, to avoid saturation of hospitals and ICUs and to reduce the number of deaths.

Considering herd immunity by vaccination only (Fig. 5.6) the strategy of vaccinating everyone in 6 months, alone, would provide herd immunity by April for Luxembourg and May for Austria and Sweden. Slower strategies will lead to herd immunity later on, depending on social interaction values. With an average value of social interactions compared to March-December, aiming to vaccinate the whole population within 1 year at a constant rate could lead to herd immunity by mid summer, in particular by July in Luxembourg and August in Austria and Sweden. Vaccines rollout slower than approximately 1,000 full vaccinations/day in Luxembourg, 16,000 in Austria and 18,000 in Sweden would not allow to reach herd immunity within 2021 in the country, except with high levels of social interaction, which would come with their undesired consequences.

We also compared the simulated strategies to an estimate of the average number of fully vaccinated people per day recorded until July the 15th (*cf.* Sec. 5.3.5). So far and for all three countries, the estimated average vaccine rollout speed has been very close to the simulated scenario labelled Strategy: 1.5 years, which was the slowest of the three considered and aimed at vaccinating all of the countrys population within 1.5 years (Fig. 5.6). This estimate overlaps with the 1.5 years strategy for Sweden, and it is slightly faster for Austria and Luxembourg. Simulations indicate that, if vaccination would continue with this same average value in the coming months, and for moderate values of social interaction (below or around 0.4), Luxembourg would still not obtain herd immunity until beginning of the autumn, Austria and Sweden not until end of the year. We can thus conclude that, despite the current advancement status of the vaccination campaign in these three countries, herd immunity has not been reached so far as of 15th July 2021 and thus keeping social interaction contained within a reasonable extent is still crucial until a larger fraction of the population will be fully vaccinated.

What just discussed depends on the interplay with the social interaction ρ. Having $\rho \leq 0.4$ would be roughly consistent with the estimates for most of 2020 and possibly until spring 2021. Nevertheless, with the widespread relaxation of measures starting from end of spring and beginning of summer 2021, higher values of ρ might occur. Moreover, variants with increased infectiousness such as Alpha (B.1.1.7) and Delta (B.1.617) have become widespread. The increased infectiousness of such variants can be modeled as an additional factor v (greater than 1) multiplying $v \cdot \rho \cdot \beta$, thus the increased infectiousness of the variants would have a similar effect as a higher ρ. Together with actual vaccine efficacy and its variability w.r.t. different virus variants, these factors modify the potential to reach herd immunity. Additional research would be needed to further investigate this. Moreover, it still remain to be seen if herd immunity against COVID-19 will be eventually obtained because the disease might anyway become endemic, depending on circulation within groups of not vaccinated people or due to fading immunity, insufficient vaccine efficacy or insufficient overall number of people getting vaccinated. Overall, while vaccination is helpful in protecting the vulnerable, limiting social interactions will still play a major role until the vaccination effects become dominant by far.

As any modelling effort, the current model comes with limitations. To begin with, it does not include an age structure. Age distribution can influence hospital admission rates and fatality rates, and has been suggested to play a role in lowering the herd immunity fraction potentially down to 30-50% [220, 227, 246]. The age distribution should be considered when designing vaccination campaigns, as literature studies agree that vaccinating the elderly first would reduce the hospital burden and death toll [247–249]. As a consequence, our model was primarily used to investigate the aggregated dynamics and to project reasonable scenarios with homogeneous interventions in pursuit of overall herd immunity, but it does not cover the design of age-dependent measures.

As for standard SEIR-like models, we assumed that recovered people are immune and cannot be reinfected. It has been shown that individuals who were infected with SARS-CoV-2 develop some level of immunity to the disease for a certain time [209], but the duration is not yet clear. Cases of reinfection by SARS-CoV-2 have been reported but there is still low statistics and consensus [208, 250–252]. On our considered time scale (up to end 2021), reinfection is likely to play a negligible role, but might become relevant over years, potentially challenging herd immunity. The model

simulations are to be considered reasonable for time periods that do not exceed considerably the duration of the acquired immunity.

Similarly, the quality and duration of immunity by vaccination is still unclear. Despite their higher or lower efficacy, none of the available vaccine protect at 100% [253, 254] and it is not yet assessed to what extent current vaccines prevent individuals not only from developing the disease, but also to be infectious (as assumed in the model). Moreover, evolving variant strains of the virus might present increased resistance to vaccines [255]. These effects could contribute to challenge herd immunity [212], contrasting the effect of age distribution. Conceptual models [214] have been developed to investigate the interplay between naturally achieved individual immunity, immunity by vaccination and waning immunity, but much still need to be done with more supporting data. Finally, the evolving impact of new variants — e.g. escaping antibodies [256] or causing longer infections [257] — is not fully clear and thus not considered in the model. However, it can be easily incorporated after changing the appropriate parameters once additional evidence is collected. Finally the case of Manaus, Brazil, which was though to have obtained herd immunity by October 2020 [240], but witnessed a major surge in cases in early 2021 [242] leave open the question if it will be possible to reach herd immunity against COVID-19 in reality.

5.5 Conclusions

Our comprehensive model describes the past epidemic dynamics and make reasonable projections. Despite some modelling assumptions, its basic structure allows to control the calibration uncertainties and to investigate and compare different scenarios. In particular, we estimated that herd immunity could be within reach in 2021, but rather towards the second half of the year (beginning of fall for Luxembourg and end of the year for Austria and Sweden) or longer, depending on how fast countries continue to vaccinate their population. As discussed above, the current projections for herd immunity are to be considered optimistic. Hence, the challenge over this year will be for governments and populations to obtain and use COVID-19 vaccines efficiently, while still containing social interaction. Limiting social interactions will still be a major driver to control the pandemic in the incoming months, until vaccination effects become strongly dominant in curbing

the pandemic.

Data availability

This study employs publicly available data-sets, provided by sources external to the authors. Each data-set employed is referenced and extensively described in B, B and B. To foster reproducibility, a copy of the time-series data employed for model fitting is provided along with the code, both are made publicly available on GitHub at https://github.com/StefanoMagni/Model_COVID19_Dynamics_Luxembourg_Austria_Sweden.

Code availability

The code implementing model, analysis and simulations is publicly available on GitHub at https://github.com/StefanoMagni/Model_COVID19_Dynamics_Luxembourg_Austria_Sweden.

Competing interests

The authors declare no competing interest.

Funding

FK's is supported by the Luxembourg National Research Fund (FNR) PRIDE DTU PARK-QC [grant number: PRIDE17/12244779/PARK-QC]. DP's and SM's work are supported by the FNR PRIDE DTU CriTiCS [grant reference: 10907093]. A.H.'s work is partially supported by the Foundation Cancer Luxembourg. JG is partly supported by the 111 Project on Computational Intelligence and Intelligent Control [reference: B18024]. AA is supported by the FNR [project code: 13684479]. AS is supported by the FNR [project: C14/BM/7975668/CaSCAD] and by the National Biomedical Computation Resource (NBCR) [grant number: NIH P41 GM103426] from the National Institutes of Health.

Authors' contributions

Françoise Kemp, Stefano Magni and Daniele Proverbio: Conceptualization, Methodology. Françoise Kemp, Stefano Magni: Software. Françoise Kemp, Stefano Magni, Daniele Proverbio, Andreas Husch, Atte Aalto, Aymeric Fouquier d'Hérouël, Laurent Mombaerts, Alexander Skupin, Jorge Goncalves, Christophe Ley: formal analysis. Stefano Magni, Andreas Husch, Alexander Skupin, Jorge Goncalves, Christophe Ley: Supervision, Project administration. Françoise Kemp, Stefano Magni, Daniele Proverbio, Jorge Goncalves, Christophe Ley, Alexander Skupin: Writing - Original Draft. All authors: Writing - Review and Editing.

Acknowledgments

The authors thank the Research Luxembourg - COVID-19 Task Force for mutual collaborations. The findings in this paper do not necessarily represent the views of the Task Force. Any errors or omissions are the authors' responsibility. The authors are also grateful to Matías Nicolás Bossa for useful discussions and to the editors and the anonymous reviewers for the precious feedback.

Conclusion 2

The extended SEIR model is not just a reasonable fit to the epidemic dynamics, but allows to make reasonable projections. Additionally, I investigated the problem of model parameters identifiability by cross-validating the manual calibration with Bayesian inference. Various NPI such as the reduction of social interaction were made into place at different moments of the pandemic with the goal to reduce the spread of the pandemic. Social interaction is the key driver of the pandemic. Therefore, the social interaction is a piece-wise constant function which changes when new implementations of non-pharmaceutical measures took place. Until 15th December, 18.3% (7.2% detected and 11.1% undetected (model estimation)) of the population in Luxembourg had SARS-CoV-2; in Austria 9% (3.7% detected and 5.3% undetected (model estimation)) and 14.5% (3.5% detected and 11% undetected (model estimation)) in Sweden. Apart from the investigation of the dark number of infections, the reproduction number was set up as it gives the estimation of the minimum immunized population needed in order to reach herd immunity. Herd immunity in Luxembourg can be reached beginning of autumn 2021 in the case of continuation of the vaccination speed of the period between December and 15 June 2021 and for moderate values of social interaction (below or around 0.4). Austria and Sweden will reach herd immunity end of the year under the condition of continuation of then vaccination speed of the period between December and 15 June 2021 and for moderate values of social interaction (below or around 0.4). The pandemic has not just an impact on health care system, but as well on economy. Therefore, the Chapter 6 looks into the impact of COVID-19 crisis not just from an epidemiological, but as well from an economical point of view.

CHAPTER 6

COVID-19 CRISIS MANAGEMENT IN LUXEMBOURG: INSIGHTS FROM AN EPIDEMIONOMIC APPROACH

This chapter is based on

Michal Burzynski, Joël Machado, Atte Aalto, Michel Beine, Jorge Goncalves, Tom Haas, Françoise Kemp, Stefano Magni, Laurent Mombaerts, Pierre Picard, Daniele Proverbio, Alexander Skupin, Frédéric Docquier.COVID-19 crisis management in Luxembourg: Insights from an epidemionomic approach, Economics & Human Biology, Volume 43, 2021, 101051, ISSN 1570-677X, https://doi.org/10.1016/j.ehb.2021.101051.

Introduction 3

In this Chapter 6, I co-developed a mathematical model that takes into account health and economic responses to COVID-19 to analyse economic effects of the pandemic. The model is a combination of an Input-Output economic block with a multi-sector SIR of 78 socio-demographic groups (19 industries of 4 countries, students and retirees). The model analyses the risk of a new infection wave and investigates adequate NPI. Furthermore, it considers in the Input/Output model as cornerstones teleworking, parental leaves, testing and quarantining policies. The Input/Output model investigates demand-side and supply-side behaviour as the intersectoral linkages of the 19 industries in Luxembourg. The epidemiological part of the model covers the infection chains inside and outside the workplace including cross-border workers.

My specific contribution of this work consisted in the development of the multi-sector SIR model. Furthermore, I participated in the process of writing, reviewing and editing the manuscript.

Abstract

We develop an *epidemionomic* model that jointly analyzes the health and economic responses to the COVID-19 crisis and to the related containment and public health policy measures implemented in Luxembourg. The model has been used to produce nowcasts and forecasts at various stages of the crisis. We focus here on two key moments in time, namely the deconfinement period following the first lockdown, and the onset of the second wave. In May 2020, we predicted a high risk of a second wave that was mainly explained by the resumption of social life, low participation in large-scale testing, and reduction in teleworking practices. Simulations conducted 5 months later reveal that managing the second wave with moderately coercive measures has been epidemiologically and economically effective. Assuming a massive third (or fourth) wave will not materialize in 2021, the real GDP loss due to the second wave will be smaller than 0.4 percentage points in 2020 and 2021.

Keywords: Growth, Productivity, Coronavirus, Lockdown, public health.

6.1 Introduction

The COVID-19 pandemic has affected people's health and economic indicators all around the globe. Focusing on Luxembourg's economy and workers from neighboring regions (representing about one half of Luxembourg's labor force), we develop an *epidemionomic* model that combines an extended Input-Output economic block with a multi-sector SIR epidemiological block, and use it to analyze the public health and economic effects of the COVID-19 crisis week after week throughout the years 2020 and 2021. The Input-Output structure allows us to account for the cascading responses to *non-pharmaceutical* interventions, due to inter-industry and inter-country linkages.[1] The SIR epidemiological block accounts for interactions between transmission rates on the job in each industry (influenced by employment rates), and transmission rates outside the labor market (at school and in social life, in Luxembourg and in its contiguous regions).

[1] [258] argued: "this virus is as economically contagious as it is medically contagious. As the production of basic and intermediate goods in some countries is put on hold, the production of more advanced goods is also paralyzed. These disruptions induce shortages, especially, but not exclusively, in the healthcare sector, and result in surges in prices and competition between consumers and between countries.

Our model is the product of a collaborative effort involving economists and epidemiologists from various institutions based in Luxembourg. It has provided nowcasts and forecasts to assist decision makers at various stages of the crisis.

In particular, our paper focuses on two key moments in time. The first one is the deconfinement period following the first lockdown (May 2020). As virus transmission rates had reached very low levels in Luxembourg, this seemed an ideal time for lifting containment measures. The model was used to highlight the risk of a rebound in the infection curve and to identify appropriate accompanying measures. The second moment brings us back to October 2020, when the COVID-19 second wave was hitting much of Europe. It is thus with a weary sense of *déjà vu* that Luxembourg's citizens were impacted by new packages of restrictions implemented to contain the virus. The specter of a re-confinement hanged over the economy. Our model was used to compare the implications of moderately and highly coercive sanitary measures, and to assess the macroeconomic impact of the second wave.

The key principle of our model is that it treats economic and epidemiological trends as interdependent, which is justified for several reasons. Firstly, it has been abundantly documented that *non-pharmaceutical* measures implemented at various stages of the crisis have affected public health and economic indicators jointly. In particular, lockdown and social distancing measures were necessary to flatten the infection curve and avoid a collapse of the health care system, at the cost of generating sizeable cuts in economic output.[2] Secondly, after several phases of generalized or partial lockdown, policymakers implemented gradual measures to restart the economy. Lifting containment measures induces changes in employment which in turn, revive on-the-job interactions between workers as well as between workers and customers. Depending on PCR testing policies, contact tracing, social distancing, hygiene and prevention measures at the workplace and in social activities, these interactions impacted the propagation of the virus within the country as well as in the cross-border regions. In turn, changes in infection rates in the neighboring regions

[2]Some authors have seen lockdown measures as resulting from a tradeoff between public health and economic objectives [259, 260]. This tradeoff is much more ambiguous than it is apparent as the recession could have been deeper without the lockdown, as evidenced from the 1918 Spanish flu [261]. It is hard to identify whether the measures implemented to curb the infection curves contributed to increase or decrease confidence in the economic system. A severe public health crisis alone could have generated panic and (potentially drastic) changes in individual behaviors. Many economic crises were associated with panics from depositors or from the banking sector.

affect the number of workers available for the labor market and potential employment levels. Uncertainty around the scale of these interactions and around the effectiveness of lockdown and deconfinement plans remains substantial. We use our epidemionomic model to produce nowcasts and forecasts of the effects of the crisis and related containment policies, refining the estimates provided by [262] and [263] and producing results by period of one week throughout the years 2020 and 2021. Our main findings are the following. During the first deconfinement period, we were relatively optimistic that the restarting of lockdown industries *per se* would not generate a relapse of the pandemic if teleworking practices could be maintained. By contrast, we argued that bringing teleworkers back to the workplace and, perhaps more importantly, the resumption of social life were likely to generate a rebound in the infection curve. Five months later, almost at the onset of the second wave, we were relatively optimistic about the effectiveness of moderately coercive sanitary measures implemented in 2020Q4 and 2021Q1. We estimate that the management of the second wave translates into a GDP loss that is smaller than 0.4 percentage point in the years 2020 and 2021. Our scenario is still valid today and compatible with the vaccination campaign. If Luxembourg can escape a massive third and/or fourth wave – a threat linked to the propagation of new variants of the virus – in the post-Summer period, real GDP growth should be around 3.7% in 2021, a level that is slightly inferior to the long-run trend.

We contribute to a recent and fast-growing literature linking public health and economic responses to the COVID-19 crisis. Part of the literature focuses on the dynamics of the disease, including the role of social-distancing [264] and the quantification of the work that can be done from home in order to slow down the spread of the virus [see e.g., 265–267]. An increasing number of papers adds epidemiological blocks to macro-economic models to evaluate the cost of the lockdown and different restarting strategies [268–271]. For example, [272] extend the canonical epidemiological model to study how endogenous consumption and labor supply decisions of utility-maximizing agents affect contagion. The competitive equilibrium of their model is not socially optimal because infected individuals do not internalize how their actions amplify the spread of the virus. More similar to us, [273] use an input-output model calibrated on Germany to evaluate the impact of work-from-home (henceforth referred to as teleworking) on infection risk and output at the regional level. Simulating a confinement where production is done exclusively by workers

who can work-from-home, they find that confinement reduces labor supply by 58% and implies a weekly GDP loss equivalent to 1.6% of the annual GDP. [274] calibrate a standard network model using French input-output linkages. These two papers are similar in spirit to our strategy but our model also accounts for other important ingredients such as teleworking, parental leaves, testing and quarantining polices, etc. Moreover, our epidemiological block accounts for the spread of the virus outside the workplace in addition to differential infection rates of cross-border workers, a specificity of the Luxembourgish labor market.

The remainder of this paper is organized as following. Section 6.2 describes the epidemionomic model and its parameterization. Health and economic effects of the COVID-19 crisis and lockdown measures and restarting scenarios are investigated in Section 6.3. Section 6.4 concludes.

6.2 An Epidemionomic Model for Luxembourg

We develop a model that links the economic and epidemiological aspects of the COVID-19 crisis. Individuals and firms behaviors are not micro-founded, but embedded in scenarios. We parameterize it on Luxembourgs economy and population – accounting for cross-border labor movements between Luxembourg and its contiguous regions – and use it to nowcast/forecast the public health and economic effects of the pandemic and related containment measures at different key stages of the crisis. The model has a weekly structure, and assumes that one week corresponds to the time of delivery of intermediate inputs from one industry to another.

6.2.1 Economic Structure

The COVID-19 crisis has required total or partial lockdown measures implemented in several industries (accommodation and food services; arts, entertainment and recreation services; construction; wholesale, retail trade and repair services; and to a lesser extent in the manufacturing industry; transportation and storage services; real estate services). Given intersectoral linkages, these lockdown measures have gradually “contaminated" the other sectors of the economy, leading to cascading effects. Similarly, lifting economic containment measures induces ripple effects on the rest of the economy. Large benefits from deconfinement arise in industries exhibiting the

greater linkages with lockdown sectors, while simultaneously not suffering from disrupted global supply chains.

To account for intersectoral linkages, we develop here an extended Input-Output (I/O) model that accounts for both demand-side and supply-side mechanisms. This extended I/O framework is intended to characterize the functioning of the economy with fixed prices, fixed capital stocks, fixed technology and fixed workforce size by industry (i.e., no intersectoral mobility). Industries are denoted by $i = 1, ..., I$. Our model distinguishes between nineteen industries. Before adding the time dimension, we first focus on the (stationary) equilibrium of the model.

Standard I/O model. – The standard I/O model ignores supply-side constraints and assumes that each sector's output is determined by total demand – demand of intermediate inputs by other sectors, and demand for final goods by domestic and foreign actors. Typically, the total sales of industry i (X_i^d) are given by:

$$X_i^d = \sum_j X_{ij} + D_i + E_i, \tag{6.1}$$

where $X_{i,j}$ is the demand for intermediate inputs by industry j, D_i is the domestic (Luxembourgish) demand for final goods, and E_i is the demand for exports.

The demand for intermediate inputs by industry j is assumed to be proportional to the total sales of that industry. We thus have $X_{ij} = a_{ij} X_j^d$, where the a_{ij}'s represent constant technological coefficients. Eq. (6.1) can be rewritten as:

$$X_i^d = \sum_j a_{ij} X_j^d + D_i + E_i, \tag{6.2}$$

which links the total sales of industry i to the toal sales of all other industries.

Using matrix notations and denoting the matrix of technological coefficients by A, this gives $X^d = AX^d + D + E$ which represents a system of I equations. The well-known solution of the standard I/O model is given by $X^d = (1 - A)^{-1}(D + E)$. In this framework, a positive demand shock in industry i generates a direct increase in output. This increases the demand for intermediate inputs addressed to the other sectors, which in turn increase their own demand for intermediate inputs and thereby generate indirect effects on the economy. The exact opposite

mechanism arises when the economy is subject to a negative demand shock. The larger the linkages with the other sectors (i.e., the larger the a_{ij}'s), the larger the total effect on the economy.

Non-binding supply-side. – The underlying supply side of the standard I/O model is governed by the following relationship:[3]

$$X_i^d = \sum_j X_{ji} + Y_i + M_i, \tag{6.3}$$

where X_i^d is the amount produced in industry i. On the right-hand side, the first term of the sum represents the value of domestic intermediate inputs (such that $X_{ji} = a_{ji}X_i^s$), Y_i is the value added in industry i, whose production requires using K_i units of physical capital and L_i workers (i.e., $Y_i = F(K_i, L_i)$),[4] and M_i is the demand for foreign inputs (i.e., imports). As local intermediate inputs, imports are proportional to total sales ($M_i = m_i X_i^d$). Hence, Eq. (6.2) determines the equilibrium level of sales in all industries (X_i^d), and Eq. (6.3) determines how sales revenue is distributed among domestic and foreign suppliers of intermediate inputs, workers and capital owners.

For a given stock of physical capital (K_i) and a given supply of labor (L_i^s) in each industry i, the maximal value added can be expressed as $Y_i^s = F(K_i, L_i^s)$. The full-employment condition in industry i is given by:

$$X_i^s = \left[\sum_j a_{ji} + m_i\right] X_i^s + Y_i^s = \frac{Y_i^s}{1 - \sum_j a_{ji} - m_i}, \tag{6.4}$$

which implies that total sales and value added in each industry i are linked by a relation of proportionality (whether the full-employment condition holds or not).

The implicit assumption of the standard I/O model is that $X_i^d < X_i^s$ in all sectors, or equivalently, $Y_i^d < Y_i^s$ and $L_i^d < L_i^s$.[5] Hence, firms can respond to the rising demand from the other sectors

[3] Eq. (6.3) corresponds to a column of the I/O matrix, whereas Eq. (6.2) corresponds to a row.

[4] In the Cobb-Douglas case, we have $Y_i = B_i K_i^{1-\alpha_i} L_i^{\alpha_i}$ where α_i is the labor income share in industry i, and B_i denotes total factor productivity.

[5] Another implicit assumption is that L_i^s is smaller than the optimal level of employment L_i^* (corresponding to a value added of $Y_i^* = F(K_i, L_i^*)$ and a level of total sales of X_i^*). The latter level is determined by profit maximization.

and from final consumers by producing more. As K_i is fixed, the only variable of adjustment that firms can use is L_i, the level of employment. When supply follows demand, firms adjust the level of employment to meet total demand for their product. Hence, $L_i^d = F^{-1}\left[X_i^d\left(1 - \sum_j a_{ji} - m_i\right)\right]$. When demand increases, firms in industry i increase their value added (Y_i^d) and their imports (M_i) without constraints to meet demand for their goods. The supply-side plays no role, except that it determines how revenues are distributed between capital owners, workers, domestic and foreign suppliers of intermediate goods.

Binding supply-side constraints. – When modeling the effect of the COVID-19 crisis and of lockdown measures, we need to enrich the standard model with binding supply-side constraints. First, containment measures reduce the permitted level of employment in lockdown industries. Second, some workers are infected by COVID-19 and cannot supply labor. Third, in addition to infection, school closures imply that many workers are forced to take parental leave. Fourth, disrupted global value chains can be such that the required amount of imported intermediate goods ($m_i X_i^d$) is not available on the market. In Luxembourg, firms did not report shortages of foreign intermediate inputs during the COVID-19 crisis. However, lockdown and sanitary measures have drastically reduced the maximal level of employment during the lockdown (L_i^s), and this has affected the maximal levels of value added Y_i^s and of sales. We will explain how the level of L_i^s is linked to lockdown and epidemiological conditions in the next section.

Starting from the pre-crisis stationary equilibrium, our economic block can be used to simulate the economic effect of the crisis and resulting lockdown measures (i.e., constraints on $L_{i,t}^s$ and $Y_{i,t}^s$) on activity. Two important ingredients govern our simulated trends. First, we assume that each iteration of the I/O matrix takes one week of time. Final demand is met instantaneously when supply constraints allow for it, while supplying intermediate inputs involve a delivery delay of one week. We thus include a time subscript t into the notations. Second, at each iteration, we combine demand and supply constraints, allowing the condition $X_{i,t}^d < X_{i,t}^s$ to be violated in some industries.

The dynamics of the extended I/O model with supply-side constraints are now characterized by:

$$X_{i,t} = \min \left[X^s_{i,t}, \sum_j a_{ij} \min \left(X^d_{j,t-1}, X^s_{j,t-1} \right) + D_{i,t} + E_{i,t} \right]. \tag{6.5}$$

Given the parameters of the Luxembourg I/O table and the economic/health shocks induced by COVID-19, the simulated solution of this model determines the endogenous production regime of each industry (excess supply or constrained supply capacity) as well as industry-specific multiplier effects. For industries in excess supply capacity, demand determines the total level of sales which, in turn, determines the level of employment and value added. For industries in constrained supply capacity, the maximal level of employment determines the value added which in turn, determines the total amount of sales. As stated above, the existence of supply constraints induces a disciplined and sizeable cut in output. Binding supply constraints also limit the magnitude of the I/O multiplier. This slows down the recovery when some confined sectors are restarted or when final demand increases.

6.2.2 Epidemiological Structure

The epidemiological block consists of a multi-sector SIR compartmental model governing the shares of susceptible, infected and recovered people from 78 socio-demographic groups. These include Luxembourguish students and retirees (2 groups of inactive nationals), as well as workers from 4 countries of residence who can be employed in 19 industries (76 groups of workers). In sum, we have:

- Six age/origin groups (denoted by superscript a): students (with $a = y$ for for young), workers (with superscript $a \in o$, denoting the country of residence of workers) and retirees people (with $a = r$). For workers, we distinguish four countries: $o = (L, F, G, B)$ for Luxembourg, France, Germany and Belgium. Students and retirees are all living in Luxembourg. We thus have six age/origin groups, $a = (y, L, F, G, B, r)$.

- Twenty-one sectors of the society (denoted by $i = 0, 1, ..., I, I + 1$) in which within-group interactions take place: schools are denoted by sector $i = 0$ and relate to group y only,

nineteen industries are denoted by sectors $i = 1, ..., I$ (in line with the notations of the previous section) and relate to groups $o = (L, F, G, B)$ only, and the old-age sector is denoted by $i = I + 1 (= 20)$ and relates to group r only (it includes retirement homes and social activities for retirees).

The total population of each socio-demographic group is denoted by N_i^a and is assumed to be constant over time. Our SIR model thus ignores deaths.[6] At time t, the population of each group is divided into $S_{i,t}^a$ susceptible, $I_{i,t}^a$ infected, and $R_{i,t}^a$ recovered. The group of infected includes $A_{i,t}^a \equiv \theta I_{i,t}^a$ infected and asymptomatic people ($\theta < 1$). Combining all possible categories, we obtain 312 groups (78 socio-demographic groups times 4 possible health status).

Virus transmission rates in sector i (i.e., on the job for workers, at school for students, and in the old-age sector for retirees) and in the place of residence are endogenous. The contamination process depends on the quantity of within-group interactions (influenced by the fraction of time spent in one's own sector, $e_{i,t}$) and between-group interactions (determined by $1 - e_{i,t}$). As explained below, we refer to the extensive margin mechanism when discussing the role of time allocation. The contamination process also depends on the sector-specific transmission rates, which are influenced by sanitary policies as well as by the number of people interacting, as explained later. We refer to the intensive margin mechanism when discussing the latter effect. The population dynamics in the 312 groups are governed by:

$$\begin{cases} S_{i,t+1}^a = S_{i,t}^a - e_{i,t}^a b_{i,t} \dfrac{S_{i,t}^a \sum_a I_{i,t}^a}{\sum_a N_i^a} - (1 - e_{i,t}^a) \beta_t^a S_{i,t}^a \bar{i}_t^a \\ I_{i,t+1}^a = I_{i,t}^a + e_{i,t}^a b_{i,t} \dfrac{S_{i,t}^a \sum_a I_{i,t}^a}{\sum_a N_i^a} + (1 - e_{i,t}^a) \beta_t^a S_{i,t}^a \bar{i}_t^a - G_{i,t}^a \\ A_{i,t+1}^a = \theta I_{i,t+1}^a, \\ R_{i,t+1}^a = R_{i,t}^a + G_{i,t}^a, \end{cases} \tag{6.6}$$

where $b_{i,t}$ is the within-sector virus transmission rate in sector i in Luxembourg, β_t^a is the virus transmission rate outside the sector (in family life, leisure, etc.) in the country of residence of

[6] Assuming deaths are proportional to the number of infected retirees would not change significantly the results. As of July 1st 2021, the country has recorded 818 deaths due to COVID-19, representing 0.14% of its population only.

group a, $\bar{i}_t^a$ is the country-wide average proportion of infected people in the population of the country of residence, and $G_{i,t}^a$ is the flow of recovered in group a and in week t. These parameters are defined over a period of one week in our model. Before the vaccine is available, we assume that immunity is obtained after having been infected and is permanent.[7]

In the case of COVID-19, most infected people recover after 10 days on average. In a model with a daily structure, we would define the number of recovered as the number of new contagious cases nine days before. Here, the weekly structure of our model implies that the flow of recovered during week t is a weighted sum of the flow of contagious cases in weeks $t-1$ and $t-2$. Following analytical developments in Appendix A of [275], the weekly flows of recovered group a and industry i during period t can be approximated by a weighted sum of the flows of new infections at time $t-2$ and $t-1$:[8]

$$G_{i,t}^a = \frac{2}{7}\left[e_{i,t-2}^a b_{i,t-2}\frac{S_{i,t-2}^a \sum_a I_{i,t-2}^a}{\sum_a N_i^a} + (1-e_{i,t-2}^a)\beta_{t-2}^a S_{i,t-2}^a \bar{i}_{t-2}^a\right] + \frac{5}{7}\left[e_{i,t-1}^a b_{i,t-1}\frac{S_{i,t-1}^a \sum_a I_{i,t-1}^a}{\sum_a N_i^a} + (1-e_{i,t-1}^a)\beta_{t-1}^a S_{i,t-1}^a \bar{i}_{t-1}^a\right]. \quad (6.7)$$

Turning our attention to transmission rates, they depend on the frequency of contacts between infected and susceptible people within each sector of the society. We assume that sick and symptomatic workers/students/retirees self-isolate as soon as they feel the symptoms. This is a reasonable assumption in Luxembourg as medical doctors received the means to quarantine potentially infected people and to provide PCR tests throughout the pandemic (even at the very early stage). As symptoms are felt a few days after becoming infectious (say 2.5 to 3 days), a fraction $\mu_{i,t}$ of symptomatic people maintain within-sector interactions while being contagious if PCR testing is not performed on a daily basis. Some individuals are asymptomatic during the whole cycle of the disease and never self-isolate. A (greater) fraction $\overline{\mu}_{i,t}^a$ of asymptomatic indi-

[7] The duration of immunity from COVID-19, if any, is not determined yet. The model predictions are thus valid for time periods that do not exceed the duration of the acquired immunity.

[8] We numerically show in Appendix A of [275] that predicting the weekly flow of recovered using Eq. (6.7) improves the predictive power of the model in comparison with a probabilistic model relying on a constant recovery rate (i.e., $G_{i,t}^a = g \times L_{i,t}^{OI}$). The reason is that, contrary to the flow of new infections within the week, the total stock of contagious people ($I_{i,t}^a$) has no reason to be distributed uniformly over the 10 daily contagious cohorts: this stock increases fast during the first phase of the pandemic (i.e., when the number of COVID-19 cases increases rapidly), and decreases fast after the peak of the infection curve has been reached.

viduals maintain within-sector interactions. The fractions $(\mu_{i,t}, \overline{\mu}^a_{i,t})$ depend on the efficiency and frequency of PCR testing as well as contact tracing. Within-sector and out-of-sector transmission rates can be expressed as:

$$\begin{cases} b^a_{i,t} = \overline{b}_i \overline{\rho}_{i,t} e^{\chi_i}_{i,t} \left[(1-\theta)\mu_{i,t} + \theta \overline{\mu}^a_{i,t} \right] \\ \beta^a_t = \overline{\beta}^a \rho^a_t, \end{cases} \tag{6.8}$$

which allows to highlight the main determinants of virus propagation:

- Within-sector transmission rates depend on the average number of contacts per person and per unit of time, and on the probability that infected people have contacts with susceptible subjects. Infected people's probability to have contacts with susceptible subjects depends on the probability of a contagious individual to maintain interactions with his peers, which is given by $\left[(1-\theta)\mu_{i,t} + \theta \overline{\mu}^a_{i,t} \right]$ in Eq. (6.8). This probability depends on the share of asymptomatic cases (θ) as well as on testing and tracing measures implemented to isolate infected workers $(\mu_{i,t}, \overline{\mu}_{i,t})$.

- The number of contacts per unit of time within sector i is expressed as the product of $\overline{b}_i$, a sector-specific parameter that reflects working conditions in normal times (i.e., physical proximity, exposure to disease, age group, etc.), by $\rho_{i,t}$, a variable that can be normalized to unity at the beginning of the pandemic, and that captures prevention and physical distancing measures implemented in the sector. In addition, physical distancing might partly depend on the density of people in the sector (influenced by $e_{i,t}$), a mechanism that is referred to as the intensive-margin effect of employment on transmission rates. A potential specification is $\rho_{i,t} = \overline{\rho}_{i,t} e^{\chi_i}_{i,t}$, where χ_i is the elasticity of physical distancing to the within-sector density of people in sector i. The other variable $\overline{\rho}_{i,t}$ captures the effect of sanitary measures.

- Similarly, in all regions of residence, the number of contacts per unit of time spent outside the sector can be expressed as the product of $\overline{\beta}^a$ by ρ^a_t. Hence, two regions or countries sharing different economic and socio-demographic characteristics exhibit different levels of $\overline{\beta}^a$, while ρ^a_t is governed by nation-wide or local social distancing and prevention measures.

To close the epidemiological block, we consider that the trajectories of $\bar{i}_t^a$ are exogenous outside Luxembourg (i.e., for $o = (G, F, B)$), whereas the trajectory of $\bar{i}_t^L$ is endogenous and given by the average of all groups of Luxembourgish population:

$$\bar{i}_t^L = \frac{\sum_i \sum_{a=(y,L,r)} I_{i,t}^a}{\sum_i \sum_{a=(y,L,r)} N_i^a}. \tag{6.9}$$

6.2.3 Epidemionomic interdependencies

We now highlight interdependencies between the economic and epidemiological blocks. First, sanitary policy measures and the evolution of the number of infected workers influence the number of workers available in industry $i = 1, ..., I$ in Luxembourg. Labor supply in COVID-19 times can be expressed as:

$$L_{i,t}^s = \sum\nolimits_a \phi_{i,t}(1 - \lambda_{i,t}^a) \left(S_{i,t}^a + R_{i,t}^a + \mu_{i,t}(1-\theta) I_{i,t}^a + \overline{\mu}_{i,t} \theta I_{i,t}^a \right), \tag{6.10}$$

where $\phi_{i,t}$ is the lockdown constraint on employment ($\phi_{i,t} < 1$ in lockdown industries and $\phi_{i,t} = 1$ in the others), $\lambda_{i,t}^a$ is the share of workers on parental leave, equal to the share of parents with young children when schools are closed in sector a, and zero if schools fully re-open. A total lockdown would imply that $\phi_{i,t} = 0$. In practice, a minimal level of post-lockdown activity is observed in all sectors, either because the lockdown applies to a sub-sector only, or because entrepreneurs find ways to maintain a certain level of output by re-orienting their activity (e.g., restaurants providing catering services with delivery at home). As $\mu_{i,t} \leq 1$, Eq. (6.10) clearly shows that a rise in the number of infected workers decreases the supply of labor and potentially influences the level of economic activity. In the same vein, PCR testing and quarantine measures allow identifying asymptomatic cases and reducing $\overline{\mu}_{i,t}$.

Reciprocally, the evolution of employment in each industry governs the time allocation of each type of individual and influences transmission rates through the extensive and intensive margins. Within each sector of the society, the rate of presence (at the workplace, at school or in the

old-age sector) can be expressed as:

$$e_{0,t} = \epsilon \mathbf{1}_t^{School} e_{i,t} = \epsilon \left(1 - \tau_{i,t}^a\right) \frac{\min\left(L_{i,t}^d, L_{i,t}^s\right)}{\sum_a N_{i,t}^a} \text{ for all i=1,...,I} e_{I+1,t} = \frac{\epsilon}{2} \tag{6.11}$$

where $\epsilon \leq 1$ is a constant capturing the fact that employed workers and students do not spend one hundred percent of their time at the workplace or at school.[9] For students, $\mathbf{1}_t^{School}$ is a dummy equal to one when schools are open, and zero otherwise. In the productive sectors $(i = 1, ..., I)$, the second term, $\min\left(L_{i,t}^d, L_{i,t}^s\right) / \sum_a N_{i,t}^a$ is the employment rate of group a in industry i. When the employment rate is smaller than unity, we assume that employees present at the workplace are randomly drawn from the industry-specific labor force, which means that employment rates are identical across countries of residence for active workers. In addition, $\tau_{i,t}^a$ denotes the share of employees in situation of teleworking in sector i. In the old-age sector, we assume that retirees spend half of their time interacting with retirees, and half of their time interacting with other groups.

In our setting, lifting economic containment measures in industry i implies an increase in the rate of presence at the workplace ($\Delta e_{i,t}$) and a resulting rise in the weekly flow of infected workers that is governed by:

$$\frac{dI_{i,t+1}^a}{de_{i,t}} = \underbrace{\left[b_{i,t} \frac{S_{i,t}^a \sum_a I_{i,t}^a}{N_{i,t}^a} - \beta_t^a S_{i,t}^a \bar{i}_t^a\right]}_{\text{Extensive margin}} + \underbrace{\chi_i b_{i,t} \frac{S_{i,t}^a \sum_a I_{i,t}^a}{N_{i,t}^a}}_{\text{Intensive margin}}. \tag{6.12}$$

Eq. (6.12) shows that shocks in employment rates and teleworking practices influence the infection curve through two mechanisms. Changes in workers' presence rate mechanically influence the flow of new infections through the **extensive margin** – changes in time spent on the job, where exposition to the disease differs from that prevailing in the place of residence – and through the **intensive margin** – changes in physical distancing and transmission rates on the job due to the higher density of employees. If $\chi_i = 0$, changes in employment rates have no effect on transmission rates (at the intensive margin), although they affect the weight given to $b_{i,t}$ relatively to β_t^a in

[9] When workers are fully employed, the daily amount of time spent interacting with other workers is shared between a fraction ϵ on-the-job, and a fraction $(1 - \epsilon)$ in the place of residence.

Eq. (6.6); this is the first term of the derivative above. In such a setting, the lockdown-driven decrease in $b_{i,t}$ can be considered as permanent. In contrast, if $\chi_i > 0$, part of that decrease in transmission rate is lost when workers get back to their workplace; this is the second term of the derivative.

6.2.4 Parameterization

Our epidemionomic model is an evolving tool that aims to promptly deliver initial results at first, and then increasingly more refined results and predictions as the set of available data on socioeconomic variables and leading indicators increases. Hence, our inputs and parameters have been frequently updated throughout the course of the crisis. Our quantitative analysis below focuses on two key moments in time, the end of the first lockdown (starting in April 2020), and the onset of the second wave (October 2020). We explain here how the model has been (re-)parameterized at these two key stages of the crisis.

Parameterization of the economic block. – Our economic block includes a set of parameters that have not been updated during the crisis. It is calibrated to match the I/O table of 2017, which defines the matrix of technical coefficients (a_{ij}) and provides initial values for the industry-specific levels of sales $(X_{i,0})$, value added $(Y_{i,0})$, employment $(L_{i,0})$, stock of physical capital $(K_{i,0})$, imports $(M_{i,0})$, exports $(E_{i,0})$ and domestic demand $(D_{i,0})$. Social security (IGSS) and SILC data allow to identify workers originating from Luxembourg, Germany, France and Belgium. The production side of the model relies on the assumption that the production technology is Cobb-Douglas in each sector, the parameters of which are calibrated to match the capital income shares and the levels of value added.

Placing ourselves back in April 2020, the problems were to nowcast the cost of the lockdown and forecast the consequences of a gradual deconfinement. We calibrated the economic block of the model to match the lockdown data available at the beginning of April. Our hypotheses are reported in Cols. 1 to 6 of Table C.1 for all industries.[10] They are based on the following sources:

- The share of workers in parental leave after school closing (λ^a_{it}) is taken from STATEC, and split across industries and origin countries using the proportion of workers with children

[10] A more detailed description is provided in [275].

aged 6-15 from SILC.

- The share of people in partial unemployment ("chô partiel") due to lockdown measures (u^a_{it}) is obtained from ADEM, being aware that data on "chô partiel" refer to applications and might overestimate the real extent of the employment effect. Unemployment and parental leave data are combined to proxy the post-lockdown levels of employment by sector ($L_{i,t} \equiv \text{Min}(L^d_{i,t}, L^s_{i,t})$).

- For the lockdown industries (i.e., manufacturing products; construction; wholesale and retail trade, repair services; transportation and storage services; accommodation and food services; real etate; arts, entertainment and recreation services; other services), we assume that the observed levels of employment correspond to the maximal labor supply ($\text{Min}(L^d_{i,t}, L^s_{i,t}) = L^s_{i,t}$) and calibrate $\phi_{i,t}$ as a residual from Eq. (6.10).

- In the other industries, we assume that $\text{Min}(L^d_{i,t}, L^s_{i,t}) = L^d_{i,t}$. Observed employment levels are used to predict the value added and sales using Eq. (6.4). Assuming that non-lockdown industries are not supply-constrained, final demand ($D_{i,t} + E_{i,t}$) is made compatible with these output levels. More precisely, we use export forecasts of the ifo institute and calibrate $D_{i,t}$ as a residual from Eq. (6.5). It will appear later that these forecasts were too pessimistic, at least in the financial sector which represents a share of Luxembourg GDP that is close to 30%.

- By contrast, lockdown industries are supply-constrained. Final demand cannot be observed. We assume a 20% decrease compared to normal times in industries producing essential goods, and a 40% decrease in industries producing non-essential goods, in line with the forecasts of the ifo institute.

- Finally, data on the share of workers in teleworking ($\tau^a_{i,t}$) are taken from the survey of the Chamber of Commerce.

To put things in the context of October 2020, we update the hypotheses above using observed macroeconomic data for the first three quarters of 2020 from STATEC. The quarterly growth rates for 2020Q1, Q2 and Q3 are equal to -1.4%, -7.2% and +4.8%, respectively. We recalibrated

changes in final demand to match these numbers. In the absence of data by industry, we assumed proportional adjustments across sectors that are not subject to lockdown measures. We also updated data on teleworking and "chô partiel" using data from STATEC and from ADEM. Parental leaves went back to their pre-lockdown levels after the reopening of schools. More details on the re-parameterization will be provided in Section 6.3.2.

Table 6.1: Macroeconomic shocks by industry (as of April 1st, 2020)

	(1) $\lambda^a_{i,t}$	(2) $\phi_{i,t}$	(3) $u^a_{i,t}$	(4) $\tau^a_{i,t}$	(5) $\frac{\Delta E_{i,t}}{E_{i,t}}$	(6) $\frac{\Delta D_{i,t}}{D_{i,t}}$
Agric., forestry, fishing	-0.068	0.000	-0.159	-0.194	-0.491	-0.400
Mining, quarrying	0.068	1.000	0.089	0.372	-0.200	-0.200
Manufactured products	0.068	1.000	0.367	0.313	-0.200	-0.200
Electricity, gas, steam	0.068	1.000	0.350	0.543	-0.991	-0.400
Water, sewerage, waste	0.068	1.000	0.184	0.322	-0.498	-0.400
Construction	0.089	0.053	0.224	0.060	-0.200	-0.200
Wholesale, retail, repair	0.066	0.535	0.388	0.060	-0.200	-0.200
Transport, storage	0.079	1.000	0.263	0.285	-0.200	-0.200
Accommodation, food	0.075	0.235	0.679	0.103	-0.200	-0.400
Information, comm.	0.093	1.000	0.105	0.856	-0.482	-0.400
Financial, insurance	0.082	1.000	0.000	0.700	-0.167	-0.400
Real estate	0.087	0.803	0.084	0.586	-0.200	-0.400
Prof, scient, techn	0.087	1.000	0.080	0.798	-0.129	-0.400
Adminis, support	0.087	1.000	0.214	0.363	-0.200	-0.200
Public administration	0.085	1.000	0.000	0.416	-0.307	-0.200
Education	0.100	1.000	0.018	0.900	-0.400	-0.200
Health, social work	0.084	1.000	0.019	0.134	-0.200	-0.079
Arts, entertainment	0.061	0.742	0.172	0.525	-0.200	-0.400
Other services	0.061	0.604	0.327	0.143	-0.200	-0.200

Notes: Col. (1) workers in parental leave from STATEC disaggregated by industry using IGSS data on workers aged 30 and less and workers with young children. Cols. (2): authors' computations. Col. (3): data on "chômage partiel" from IGSS. Col. (4): data on teleworking from the survey conducted by Chamber of Commerce in April. Col. (5): authors' computations based on the I/O matrix; Cols (6): authors' hypotheses based on the survey conducted by Chamber of Commerce in April.

Parameterization of the epidemiological block. – In our SIR compartmental model, transmission rates are calibrated to match data on the cumulative number of detected COVID-19 cases in the inactive population (students and retirees) and in the active population by sector. Daily data on COVID-19 cases by sector and by region of residence are available from the IGSS database

from the beginning of March until October 19, 2021.[11] We aggregate COVID-19 cases per week, creating a database of 34 weeks times 21 sectors of the society (714 observations) corresponding to $I^a_{i,t}$ in Eq. (6.6).

Over the same period, we also use data on the region-wide shares of infected cases ($\bar{i}^a_{i,t}$ for $a = (G, F, B)$) in the neighboring regions (Rhineland-Palatinate and Saarland for Germany, Grand Est for France, and Wallonia for Belgium). We calibrate time-varying transmission rates ($\beta^a_{i,t}$ for $a = (G, F, B)$) in each of the three contiguous regions to match the evolution of the share of infected people, using a simplified and independent SIR model by region. We consider the trajectory of transmission rates in these regions as independent of the sanitary conditions in Luxembourg.

Transmission rates in Luxembourg are sector-specific. The philosophy of our parameterization is to rely on a limited number of parameters and fitting assumptions. Many epidemiological models rely on complex polynomial functions to fit many daily data points. Obviously, the higher the number of parameters, the better the fit. This does not mean that the predictive power of such complex models is satisfactory – at least over sufficiently long periods of time – and that these models can predict the effects of out-of-trend shocks such as a deconfinement or the implementation of a new public health policy measures. A more structural approach such as ours is worth investigating. Taking as given the parameters of the neighboring regions, we fit the 21 infection curves by estimating 3 parameters per sector (i.e. 21 times 3 parameters) and 2 parameters governing transmission rates outside the sector.

In Eq. (6.8), we compute proxies for $(\mu_{i,t}, \overline{\mu}_{i,t})$ as explained at the end of this section, and combine them with data on employment and school attendance to proxy $e_{i,t}$. To compute $e_{i,t}$, we need to specify the share of weekly social interactions that occur in each sector of the society, ϵ. Fully employed workers spend about 55 hours at the workplace and in transportation, and of a weekly total of 75 hours of interactions with family members, friends and other contacts. Assuming professional interactions involve three times more contacts than private contacts, we obtain a

[11] As our model does not include working-age individuals who are not registered to IGSS (i.e., inactive and dependent individuals), we re-scale the number of infected individuals by sector so that the total number of infected people living in Luxembourg exactly matches the total number of COVID-19 cases in the Luxembourg population. We apply the same rescaling factors to cross-border workers.

fraction $\epsilon = 0.7$ on-the-job, and a fraction $1 - \epsilon = 0.3$ in the place of residence. These fractions have little influence on the results as they determine the scale of the transmission parameters.

Within-sector transmission rates are thus influenced by three sector-specific parameters, $(\overline{b}_i, \overline{\rho}_i, \chi_i)$. First, the scale parameter $\overline{b}_i$ determines the pre-lockdown transmission rates (before March 17th, 2020). Second, we allow $\overline{\rho}_i$ to be smaller than one in the weeks during which the sector is constrained by sanitary measures, and set it equal to unity otherwise. Third, we estimate χ_i using variations in transmission rates and presence rates in the sector. Similarly, transmission rates outside their main sector of activity (i.e., industry, school, retirees' sector) are influenced by two parameters, $(\overline{\beta}^L, \rho^L)$. The scale parameter $\overline{\beta}^L$ determines the pre-lockdown transmission rates outside the sector. We allow ρ^L to be smaller than one in the weeks during which social and family activities are constrained, and set it equal to unity otherwise.

The calibration of the parameter set $\Gamma = \left(\overline{b}_i, \overline{\rho}_i, \chi_i, \overline{\beta}^L, \rho^L\right)$ relies on the *Simulated Method of Moments*, which identifies the vector of transmission rates to make simulated model moments $(\hat{I}^a_{i,t}(\Gamma))$ match data moments $(I^a_{i,t})$:

$$\underset{\Gamma}{\text{Min}}\Lambda = \sum_t \sum_i \sum_a \left(\hat{I}^a_{i,t}(\Gamma) - I^a_{i,t}\right)^2. \tag{6.13}$$

Figure 6.1 compares our estimated infection curves (dashed black curves) with data on COVID-19 cases by sector (gray curves). Our fit is very good in most sectors of the society and excellent when focusing on the aggregate number of cases. As illustrated on the bottom-right graph, our model almost perfectly matches the evolution of the aggregate number of detected COVID-19 cases in the Luxembourgish workforce. In the pre-lockdown period, the correlation between $\overline{b}_i$ and indices of exposure to risk by industry – reflecting heterogeneity in workers' exposure to disease and physical distance at work – is around 0.6, suggesting that our method is meaningful. In the post-lockdown period, the correlation is small (around 0.1), suggesting that lockdown measures were effective in reducing physical distance and exposure to disease.[12]

Once transmission rates are known, we identify its components in line with Eq. (6.8). The third component, $\left[(1-\theta)\mu_{i,t} + \theta\overline{\mu}_{i,t}\right]$, depends on the share of asymptomatic subjects among conta-

[12] Results are presented in the Appendix of [275].

Figure 6.1: Calibration of the SIR model by sector

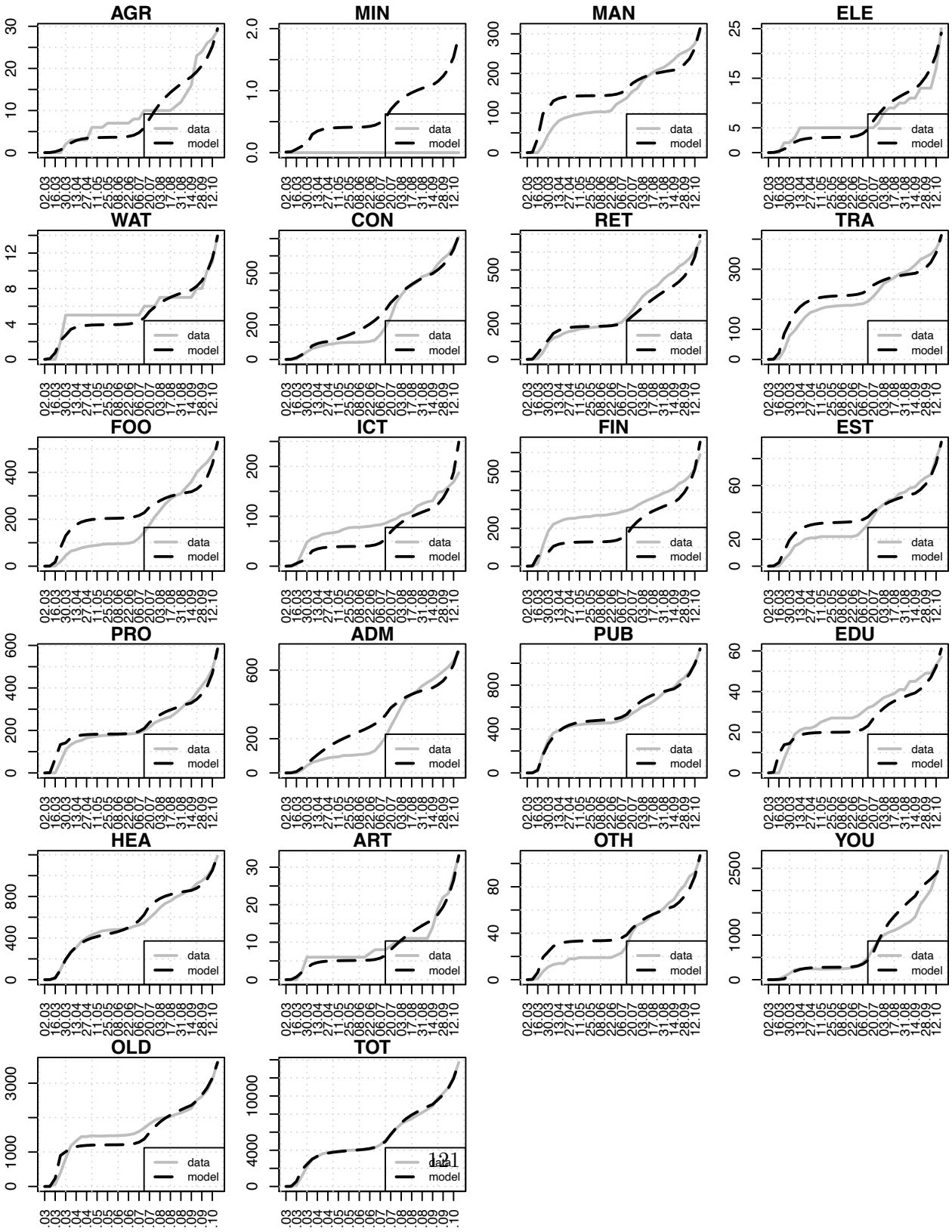

Note: Data on COVID-19 cases by sector (gray curve) are obtained from IGSS and aggregated by week. Estimation of SIR model are represented by the dashed black curve.

gious individuals and on the fractions of infected workers who are still active on the labor market. Regarding the share of asymptomatic (θ), the recent *CON-VINCE Study* [229] conducted on 1,862 Luxembourgish individuals identifies 35 cases with antibodies. These include 11 individuals who self-report to have been tested positive in the past months. This means that 1.3% of individuals (24 out of 1862) were undetected. Applying this percentage to the whole population gives a stock of asymptomatic of around 8,000, which is twice as large as the total stock of detected cases. Given the small number of people in the sample, the accuracy of these numbers is low. Our calibration assumes that $\theta = 0.5$.[13]

The fractions of infected people who are still active within each sector of the society ($\mu_{i,t}, \overline{\mu}_{i,t}$) depend on the efficiency and frequency of PCR testing. In the absence of testing, we assume that infected workers self-isolate when they show some symptoms. Asymptomatic people never self-isolate. Calculations presented in the Appendix of [275] allow approximating the fraction of working days supplied by symptomatic and asymptomatic infected workers under several testing scenarios:

- In the absence of testing, we obtain $\mu_{i,t} = 0.20$ and $\overline{\mu}_{i,t} = 1.0$ for all t.
- If a *weekly test* is performed, we have $\mu_{i,t} = 0.15$ and $\overline{\mu}_{i,t} = 0.25$ for all t.
- If a *daily test* is performed, we have $\mu^v_{i,t} = \overline{\mu}_{i,t} = 0$ for all t.
- If a *one-shot test* is performed at time T, we have $\mu_{i,T} = \overline{\mu}_{i,t} = 0$, and we get back to $\mu_{i,t} = 0.20$ and $\overline{\mu}_{i,t} = 1.0$ thereafter (i.e., for all $t > T$).

As massive testing was not implemented at the beginning of the lockdown, we can hypothesize that $\left[(1-\theta)\mu_{i,0} + \theta\overline{\mu}_{i,1}\right] = 0.6$ at the beginning of the crisis. When simulating deconfinement plans, we consider several testing scenarios.

[13] [276] cover 21 studies based on various contexts. The range of estimates of this proportion varies from 5% to 80%. In the case of the Diamond Princess cruise in which all individuals were tested, about 18% were found to be asymptomatic. More recently, [277] conduct a survey in a French high school involving pupils, teachers and non-teaching staff in the Oise region which was one of the first affected places of the epidemics in France. They find a rate of asymptomatic people of 17% only, but argue that this is likely to underestimate the rate in the general population.

6.3 Results

The calibrated model is used to produce two sets of experiments. We first use it to simulate the trajectory of public health and economic indicators during the first deconfinement period, from April to June 2020. This first part summarizes the results presented in the initial version of this paper [275]. Next, we use our model to quantify the epidemiological and economic effects of the second wave of COVID-19 and related containment policies, extending the time horizon to cover the year 2021.

6.3.1 Back to May 2020: Managing the First Deconfinement

Lockdown measures were implemented on 20 March 2020. Without taking stance on the potential trade-off concerning human lives versus material goods and/or social losses, lockdown measures induce opposite economic and epidemiological consequences. On the one hand, they generate a decline in activity driven by a disciplined cut in lockdown industries, a decrease in final demand, and cascading effects in the other industries. Using industry-specific parameters from Table C.1, our model predicts that each week of lockdown during the first wave translated into an output loss of about 28% compared to the pre-crisis level, as illustrated in Figure 6.2b. The most adversely affected industries were 'Construction' (-66%), 'Accommodation and Food' (-62%), Mining and Quarrying (-43%), and 'Wholesale/retail trade and repair services' (-42%). The least impacted industries are 'Health and social work' (-3%) and 'Finance' (-6%), 'Education' and 'Public administration' showed limited responses of around 10%. On the other hand, the lockdown reversed the trend of rising infections.

As shown in Figure 6.2a, the peak of the infection curves was observed during the first week of April with around 1,850 detected COVID-19 cases (we exclude asymptomatic people who were not detected as positive). The number of infected people gets smaller than 50 by mid-June, implying a number of recovered people converging towards 4,400 individuals (i.e., 0.7% of Luxembourg's population). The lockdown has drastically limited the propagation of the virus, which implies that there was still a majority of susceptible workers in the Luxembourg labor force after the first wave. Any economically meaningful strategy of deconfinement required that non-infected and

non-immune workers were gradually brought back to work, which induced a risk of a relapse.

Deconfinement scenario. – In Figure 6.2, we simulate the economic and health implications of the deconfinement measures implemented between April and June 2020 in Luxembourg. The deconfinement policy was gradual:

- The first *restarting stage* started on April 20 and mainly involved the reopening of construction sites.
- Secondly, schools gradually reopened after May 4. Reopening started with graduating classes in the secondary education, practical exercise classes and internships at University and for the Advanced Technician Certificates. Secondary schools reopened on May 11. Primary schools and public childcare services reopened on May 25. This reduced the number of workers in parental leave.
- Other measures were implemented on May 11. These consisted of removing constraints in all other sectors of the economy, with the exceptions of HORESCA as well as Arts, Entertainment and Recreative Services.
- We also consider a resumption of social activities from the beginning of June. We allow transmission rates at the place of residence to partly return to their initial level once social life restarts. This might be due to restarting meals and parties with a limited number of friends and/or with family members, sport in small groups, more intensive use of public transportation, more contacts in shopping areas, mass departures during the holiday season or at weekends, etc.
- To be consistent, we combine the deconfinement with the optimistic trade scenario involving a gradual recovery of exports from the beginning of June. We consider for the time being that teleworkers continue to work from home in the non-lockdown industries.

Epidemiomonic results. – The public health effects of these measures are presented in Figures 6.2a and 6.2b, in which we consider that testing policies are not implemented. As a benchmark, we

consider a best-case scenario in which transmission rates within sectors and in the total population are kept at their post-lockdown levels.

In the other scenarios, we assume that employment constraints are relaxed in all sectors (i.e., $\phi_{i,t} = 1$) except HORESCA and Arts, Entertainment and Recreative Services. This increases the level of employment in all sectors, due to cascading economic effects. We analyze the effects of this deconfinement policy considering a set of sanitary scenarios. As a result from physical distancing, hygiene and prevention measures, transmission rates decreased drastically in Luxembourg and in the Greater Region after the lockdown. Part of the changes in transmission rates can be considered as permanent. In an optimistic scenario, depicted by the dashed black curve, we assume that (i) masks, distancing and hygiene measures are maintained and allow to keep transmission rates ($\overline{\rho}_i$) at 50% of their pre-lockdown levels in all industries, (ii) post-lockdown teleworking practices remain in force in all sectors, and (iii) the resumption of social life has no effect on transmission rates outside the labor market and schools ($\overline{\rho}^L$ is kept at the post-lockdown level). Due to intensive margin effects, this optimistic deconfinement scenario translates into a second (flatter) wave that reaches its peak in the course of 2021.

To illustrate the fragility of the health situation, we then consider that the resumption of social life influences transmission rates outside individuals' sector of activity, with $\overline{\rho}^L$ becoming equal to 50% of the pre-lockdown levels. We allow changes in $\overline{\rho}^L$ to materialize in Luxembourg only (dashed red curve) or in the regions of origin of cross-border workers only, i.e., in Wallonia in Belgium, Grand-Est in France, Saarland and Rhineland-Palatinate in Germany (dashed green curve). In both cases, the infection curves shifts upwards and the second wave is more severe. Finally, the blue curves show that bringing teleworkers back to their workplace (all workers in blue, or cross-border workers only in dashed blue) reinforces the intensive-margin effects and generates a rapid and drastic increase in the infection curve.

The economic effects are depicted in Figure 6.2b. In the best-case scenario, weekly GDP slowly goes back to its pre-crisis level before the end of the year. Remember that this scenario assumes a gradual recovery of final demand after June 2020. Considering the worst-case epidemiological scenario (with changes in $\overline{\rho}_i$ and $\overline{\rho}^L$) has limited economic effects as the number of infected peaks at around 15,000 persons, including 10,000 workers (2% of the workforce) who can be

partially replaced by those in partial unemployment. Hence, the effect of changes in the flow of new infections on the economy are rather small, contrary to the huge effects induced by generalized or partial lockdown measures. Overall, the annual GDP decreases by 8% compared to a no-crisis scenario. By contrast, assuming that changes in exports are permanent would lead to a long-lasting drop in GDP and an annual input loss of 15%. Hence, in an open-economy context such as in Luxembourg, economic prospects for 2020 were highly sensitive to international economic conditions. For illustrative purpose, we also simulated a scenario in which all cross-border workers and teleworkers are unemployed, the loss of GDP would have exceeded 30%. The role of teleworking has been instrumental to limiting the economic output loss and the propagation of the virus.

Testing policies. – The results above indicate that the deconfinement policy implemented between April and June 2020 was likely to generate a second wave if it was not accompanied by appropriate testing and tracing measures. In Figure 6.2c, we start from a scenario combining intensive margin effects with changes in $\overline{\rho}_i$ and $\overline{\rho}^L$ (a mix of dashed black and dashed red curves in Figure 6.2a). The continuous black curve clearly indicates that a second wave occurs in the absence of testing. Starting from the same transmission rates, we simulate the effect of bi-monthly and monthly tests, as well as monthly tests for domestic workers only (i.e., excluding cross-border workers).

We find that testing all workers and residents once per month (dashed black) is sufficient to avoid the second wave. By contrast, testing domestic workers only (blue dashed curve) generates a slow and gradual relapse of the pandemic, and testing all workers every two months generates a quick and drastic rebound. Obviously, stricter testing policies are needed if one considers a more pessimistic scenario where teleworkers are brought back to work or if transmission rates cannot be kept below 50% of their pre-lockdown levels.

Figure 6.2: Epidemionomic analysis of the first deconfinement

(a) Fragility of the sanitary situation

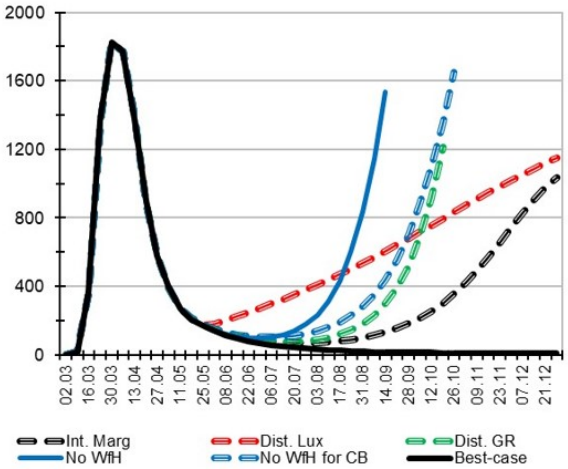

(b) Economic scenarios for 2020

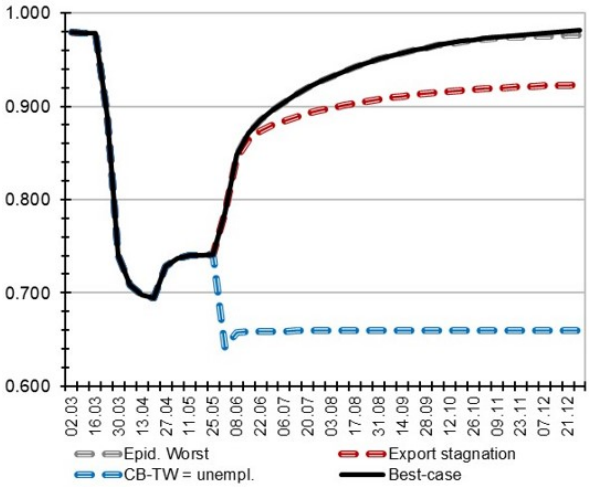

(c) Effectiveness of testing policies

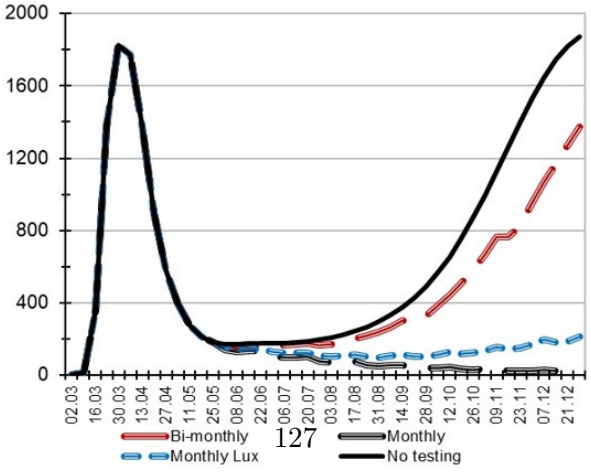

Although April-May-June 2020 was a good time for lifting containment measures, our model was helpful to highlight the fragility of the sanitary situation. In particular, epidemiological predictions were highly sensitive to the evolution of teleworking practices, transmission rates outside the labor market, and testing policies. Three precautionary measures were drawn from our initial analysis [275]:

- Maintaining *teleworking practices* is vital. All of our simulation results indicated that a cessation of teleworking practices would induce large epidemiological damages, even if drastic mitigation policies were implemented.
- Maintaining hygiene measures and high levels of physical distancing in social life has an important impact on the number of COVID-19 cases. Our results also indicated that the evolution of the number of COVID-19 cases is highly sensitive to transmission rates outside the labor market.
- Monthly PCR testing of domestic and cross-border workers were necessary (but perhaps not sufficient) to prevent a rebound in the infection curve.
- Combining testing with contact tracing would reduce transmission rates further. [278] show that tracing pre/a-symptomatic people with a phone app and quarantining contacts of new detected cases would reduce the transmission rate by up to 50%.
- Preventing HORESCA activities to exceed half of their full capacity was also recommended.

Ex-post evaluation. – Four months after our studies, available statistics allowed to assess the relevance of our nowcasts, forecasts and recommendations. A rebound in the infection curve appeared in late July, followed by a drastic second wave which started to materialize in September. In line with our model predictions, this second wave can be essentially explained by a decrease in the share of teleworkers and, more importantly, by the changes in transmission rates outside the labor market (in schools and in social life) and by the coverage of the testing policy. Although the government invited its residents and cross-border workers to be tested on a monthly basis, the participation rate had been around 25%, which is almost equivalent to testing everyone every

four months only. Hence, the Luxembourg testing agency operated way under its capacity levels, and was able to deliver testing results within a few hours only. The model predicted that the second wave was inevitable under these circumstances.

Economically speaking, the model correctly predicted that the direct impact of changes in the infection curve on the economy proved to be relatively small. This is because the stock of infected people never exceeded 2% of the population, and workers in sick leave could easily be replaced by workers in partial unemployment. By contrast, containment measures induced large economic costs. Data reveals that GDP decreased drastically during the lockdown months, although our economic forecasts proved to be too pessimistic. The economy has been more resilient than expected, which is mostly due to the fact that the domestic and international demand for financial services did not decrease as strongly as assumed in Table C.1. Overall, the economic loss amounted to 1.4% and 7.2% in the first and second quarters of 2020, while our model predicted twice these amounts. The model assumptions were thus revised in October 2020 to predict the epidemiological and economic consequences of the second wave, as explained in the next section.

6.3.2 Back to October 2020: Managing the Second Wave

The outlook for the global economy was highly uncertain after the summer 2020. In October 2020, we relied on scenarios developed by [279] to delineate best-case and worst-case macroeconomic scenarios for Luxembourgs GDP over the quarters of 2020 and 2021.[14] We adjusted our sanitary and final demand hypotheses to be compatible with these extreme scenarios, defined an intermediate and more relevant scenario relying on the moderately coercive measures implemented in the country, and predicted its epidemiological and economic effects for 2020 and 2021.

Second-wave scenarios. – The best-case scenario (labeled as **NoSW**) assumes the absence of a second wave and a quick recovery of the international environment. It predicts that scientific advances will be such that restrictions can be completely lifted from 2020Q4. The effects of fear and uncertainty on final demand gradually disappear during 2020Q4 and 2021Q1. Using observed

[14] The latter were elaborated with the help of STATEC, building on their flagship macroeconomic model Modux.

macroeconomic data for the first three quarters of 2020, STATEC estimates that this **NoSW** scenario translates into annual GDP growth rates of -3.5% in 2020 and +4.0% in 2021, which basically means a fast recovery towards the no-COVID trend. The underlying epidemiological trajectory assumes that virus transmission rates decrease monotonically towards zero between September 2020 and May 2021, and that medical advances (including a large-scale vaccination campaign) make it possible for social distancing to fully relax without implying a rebound in the infection curve.

By contrast, the worst-case scenario (labeled as **SWLO**) predicts a second wave requiring generalized lockdowns throughout Europe. In the case of Luxembourg, STATEC assumes a new confinement of longer duration (covering 6 months during 2020Q4 to 2021Q1) in the same industries as in March-April (i.e., construction, sales in non-essential businesses, services to households, food and accommodation) as well as in leisure, family and social life. This will be accompanied by a long-lasting decrease in final demand due to lockdowns abroad and to a degradation of the confidence of local and foreign actors. STATEC estimates that this SWLO translates into annual GDP growth rates of -4.5% in 2020 and -0.5% in 2021, implying two years of negative real growth. The underlying epidemionomic trajectory suggests that GDP will be 15 to 17% below the No-COVID hypothetical trend during the lockdown weeks and will slowly recover afterwards. The reality is somewhere in the middle. After a dip in new cases in July and August, Luxembourg reported a higher number of cases than during the first peak. Hence, the second wave materialized and the question was: how bad will it be? Luxembourg avoided to strongly re-confine its economy in late October 2020. Besides testing, tracing and quarantining tools, the government decided to prohibit movements of people between 11PM and 6AM (i.e., a curfew), to reinforce social distancing measures in restaurants, bars and cafés, to limit private gatherings and presence in shops, to promote medical teleconsultation, to forbid sports activities involving more than four people, etc. The effectiveness of these sanitary measures and their economic implications are highly uncertain as they strongly depend on the degree of adhesion of the population as well as on external factors such as the evolution of preventive measures and epidemionomic conditions in the neighboring regions. In addition, after November 26, the government re-implemented a partial lockdown, which consisted of limiting family contacts and closing cafés and restaurants,

cinemas, theaters, swimming pools and sport centers.

We relied on an optimistic parametric interpretation of these sanitary measures, that we refer to as the **SWNL** scenario (for 'second wave with no generalized lockdown'). More precisely, compared to early October and starting in November 2020, we assume a 50% decrease in contamination rates outside the labor market in the neighboring regions, and an increase in teleworking (up to 50% of the April level). We also assume a trajectory of final demand that is less optimistic than under **NoSW** (-20% in 2020Q4 and 2021Q1, followed by a gradual recovery) due to consumers fears and uncertainty. We also considered a new lockdown in HORESCA and in the "Arts, Entertainment and Recreative Services" from November 26 to the end of 2020.[15]

A spectrum of epidemionomic prospects. – Figure 6.3 depicts the aggregate results of our model, and Table 6.2 summarizes estimates of quarterly growth rates for the years 2020 and 2021. Under the **NoSW**, the spread of the virus remains rampant until June 2021 with low intensity from January. Under the **SWLO** scenario, a new generalized lockdown starting in September 2020 would have prevented the infection curve to skyrocket.

The most likely scenario (**SWNL**) generates intermediate results. Our parametric interpretation of sanitary measures has been chosen to generate a decrease in the infection curve that is comparable to that of the lockdown scenario, which has been confirmed by the observed trajectory of the infection curve. The model predicts that the number of symptomatic active COVID cases will peak at 14,500 by mid-December 2020 (one month later compared with **SWLO**) and then fall until May 2021. Interestingly, the number of active cases was already greater than 10,000 on November 10. By the end of 2021, the cumulative share of people who have ever been infected will be around 25% (i.e., 120 000 individuals). The major difference with **SWLO** relates to the macroeconomic implications of the containment measures. We estimate that this **SWNL** scenario translates into annual growth rates of -3.9% in 2020 and +3.7% in 2021, which is quite close to the **NoSW** scenario (-3.5% and +4.0%, respectively).[16] Hence, managing the second wave with

[15] Note that the average occupancy rate in hotels was already low, in the range of 15 to 25% of their pre-lockdown levels, according to recent newspaper article.

[16] Simulations in line with the robustness checks below suggest that about 3/4 of the growth differential with **NoSW** in 2020Q4 is due to epidemiological effects: the labor force decreases by about 30,000 persons in December (14,500 infected and approximately the same number of quarantined people). By contrast, the stock of active cases will be much smaller in 2021 and 4/5 of the growth differential in 2021Q1 is due to the deterioration of final

moderately coercive measures has limited the cost of the second wave to 0.3 and 0.4 percentage point of GDP in 2020 and 2021, respectively.

Figure 6.3: Weekly path of epidemionomic outcomes under three scenarios

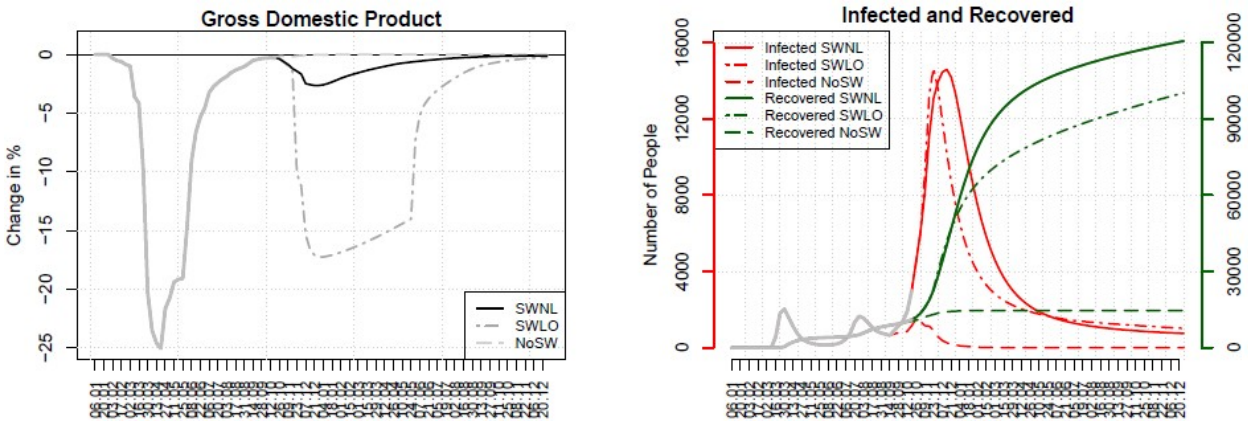

Note: The left panel reports the percentage of deviation in weekly GDP from the hypothetical No-COVID situation. The right panel reports the number of detected COVID-19 active cases (left scale) and the total number of recovered (right scale).

Sensitivity to hypotheses. – There was considerable uncertainty on whether moderately coercive sanitary measures will prove strong enough to contain the second wave and on the concomitant evolution of the international environment. The predictions of the **SWNL** strongly depend on our parametric interpretation of existing measures. To quantify that uncertainty and to identify the key mechanisms at play, we started from the **SWNL** and considered 8 variants (one variant at a time) implying (i) more or less teleworking (100% vs. 0% of the sectoral share of March-April), (ii) higher or lower adhesion to distancing measures in leisure, social and family life (contamination rates outside the labor market equal to 25% or 75% of those observed in early October), (iii) more or less testing/tracing (50% of participation in large-scale testing and 6 quarantined people per case vs. total absence of testing/tracing), (iv) more optimistic or pessimistic trajectory for exports (no shock vs. -40% in 2020Q4 and 2021Q1). These variants are considered as independent of each other, which means that we disregard the fact that variations in the infection curve can

demand.

Table 6.2: Trajectory of Luxembourg GDP under three scenarios, 2020-2021 by quarter

	2020				2021			
	Q1	Q2	Q3	Q4	Q1	Q2	Q3	Q4
No-COVID reference (Ref)	13206	13286	13365	13445	13526	13607	13689	13771
NoSW	12947	12016	12595	12595	12658	12911	13169	13432
Cumulated index (Ref=100)	98.0	90.4	94.2	93.7	93.6	94.9	96.2	97.5
Quarterly growth rate (%)	-1.4	-7.2	+4.8	0.0	+0.5	+2.0	+2.0	+2.0
Annual GDP growth rate			-3.5				+4.0	
SWLO	12947	12016	12593	12089	11726	12195	12561	12938
Cumulated index (Ref=100)	98.0	90.4	94.2	89.9	86.7	89.6	91.8	94.0
Quarterly growth rate (%)	-1.4	-7.2	+4.8	-4.0	-3.0	+4.0	+3.0	+3.0
Annual GDP growth rate			-4.5				-0.5	
SWNL	12947	12016	12595	12388	12430	12817	13132	13415
Cumulated index (Ref=100)	98.0	90.4	94.2	92.1	91.9	94.2	95.9	97.4
Quarterly growth rate (%)	-1.4	-7.2	+4.8	-1.6	+0.3	+3.1	+2.5	+2.1
Annual GDP growth rate			-3.9				+3.7	

Note: The No-COVID reference scenario assume a 1.5% growth rate per quarter. **NoSW** stands for absence of second wave. **SWLO** stands for second wave requiring a generalized lockdown. **SWNL** stands for second wave requiring moderately coercive measures only. Numbers in bold characters are observations. Source: STATEC (2020). Note de Conjoncture of December 2020.

induce pressures on ICU admissions, panic or protest movements, which could translate into final demand responses. Figure 6.4 illustrates the epidemionomic consequences of these variants.

We first focus on adhesion to public health measures. Changes in teleworking practices have small effects on the infection curve. Within the context of our model, this is explained by the fact that highest transmission rates during the second wave were observed outside the labor market. Changes in social distancing have bigger effects, increasing the number of cases by 4,500 at the peak (low distancing) or decreasing it by 1,000 (high distancing).[17] Changes in testing/tracing practices induce moderate epidemiological effects, increasing the number of cases by 2,500 at the peak (absence of large-scale testing and tracing) or decreasing by 1,500 (higher adhesion). These sanitary variants induce negligible effects on the economy (contrary to the deep-set trend in COVID cases), while annual GDP growth rates are sensitive to the evolution of the international environment. Turning our attention to export shocks, we find opposing results. The epidemiological consequences of output and employment shocks are negligible, which again

[17] The low-distancing variant roughly translates into 140 admissions in intensive care units by the very end of the year, leading to a quasi-saturation of the ICU system.

results from the fact that transmission rates on the job were relatively well contained. By contrast, the economic trajectory for 2021 is sensitive to exports. For 2020, the effect is smaller as GDP levels for Q1 to Q3 are already given. In particular, the low-export variant translates into an annual growth rate of -3.9% in 2020 and 2.9% in 2021 (against -3.8% and +3.6% under **SWNL**). Epidemiologically speaking, moderately coercive variants show that uncertainty about the spread of the virus remained large. A lockdown-type policy would have generated much more foreseeable epidemiological effects at the cost of a much bigger recession.

Figure 6.4: Sensitivity of the SWNL scenario to epidemionomic variants

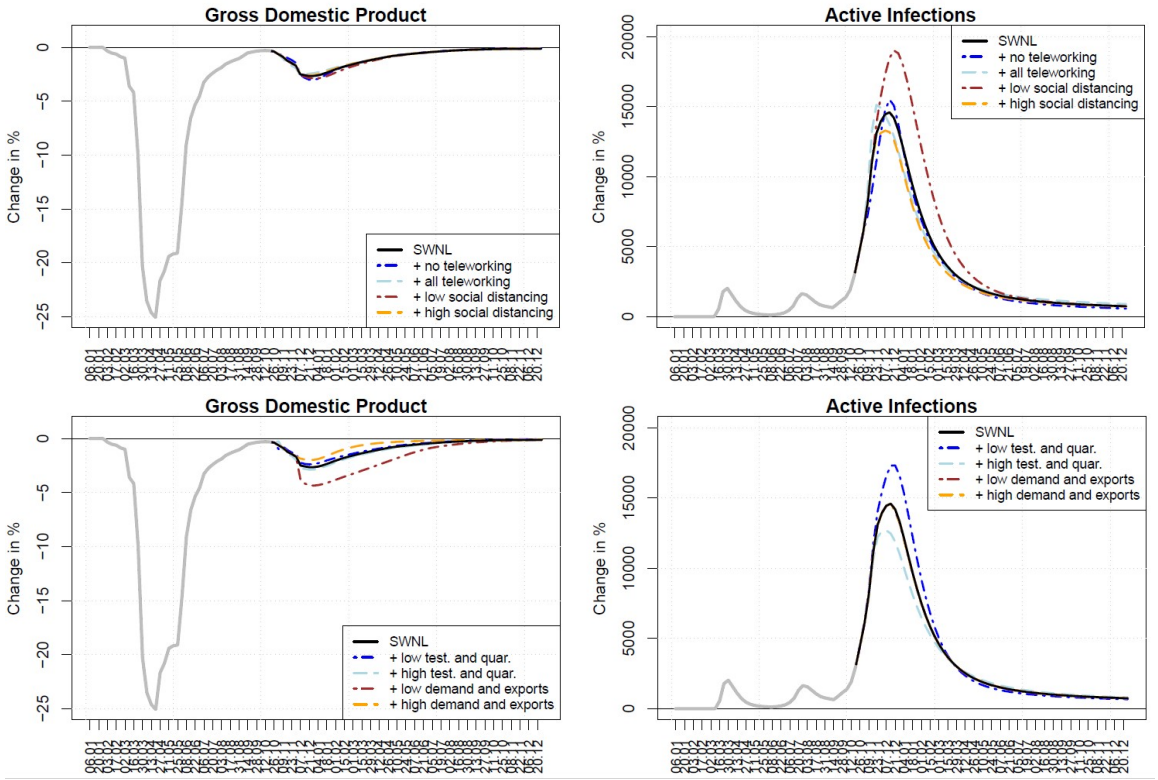

Note. The left panel reports the percentage of deviation in weekly GDP from the hypothetical No-COVID situation. The right panel reports the number of detected COVID-19 active cases.

6.4 Conclusion

Our model jointly endogenizes the health and economic responses to the COVID-19 crisis and the related containment and public health policy measures implemented in Luxembourg and in its neighboring regions. It allows us to quantify the economic and public health effects of the first and second waves of COVID-19 under various economic, epidemiological and public health scenarios. We focus here on two key moments in time. The first one is the deconfinement period following the first lockdown (May-June 2020). Our set of nowcasts and policy experiments conducted in May 2000 predicted that the restarting of lockdown industries *per se* was unlikely to induce a relapse of the pandemic if teleworking practices could be maintained. Nevertheless, we predicted that the resumption of social life and, to a lesser extent, the cessation of teleworking practices were likely to generate a rebound in the infection curve. We thus recommended to maintain teleworking practices and high levels of physical distancing in social life, as well as promoting monthly testing and quarantining measures. Available statistics revealed that we overestimated the economic costs of the first wave; this is because the financial sector has been much more resilient than initially assumed. However, the second wave materialized after the Summer 2020. In line with our predictions, this is explained by higher transmission rates outside the labor market, low participation in testing and a decrease in teleworking.

Five months later, history was repeating itself. As the COVID-19 second wave was hitting much of Europe, some countries entered a new (total or partial) lockdown allowing people to leave their home only to go to work (when teleworking was not feasible) or to buy essential goods and seek medical help, banning or limiting social gatherings, prescribing curfews, shutting non-essential activities, etc. Luxembourg followed suit by taking new measures but avoided to re-confine part of its economy. Besides testing, tracing and quarantining tools, the government decided to prohibit movements of people between 11PM and 6AM, to reinforce social distancing measures in public transport, to limit private gatherings and presence in shops, to promote medical teleconsultations, to forbid sport activities involving more than four people, and to close restaurants, bars and cafés. We re-parameterized our model to assess the effectiveness of these sanitary measures and the macroeconomic cost of the second wave. We estimate that the management of the second wave

translates into moderate GDP losses in the years 2020 and 2021. If Luxembourg can escape a massive third and/or fourth wave, real GDP growth should almost get back to its long-term level in 2021.

Conclusion 3

The model is fitted to the first and second wave of COVID-19 from an economical and health perspective and gives insights on its effects. The direct impact on Luxembourgish economy is small, because never more than 2% of the population were infected at the same time. However, the containment measures lead to higher economic costs. The developed model's forecast was too pessimistic for the GDP loss during lockdown period. "Financial and insurance service" is the biggest industry in Luxembourg which was more resistent and its decrease was not that dramatic. The first version of the model suggests that to prevent a second wave, all workers and residents needs to get tested once per month.
The first and second wave were analysed from a health and economical point of view. In order to better predict the next outbreak of COVID-19, the chapter 7 investigates the performance of early warning signals (EWS) in disease re-emergence.

CHAPTER 7

PERFORMANCE OF EARLY WARNING SIGNALS FOR DISEASE RE-EMERGENCE

This chapter is based on

Daniele Proverbio, Françoise Kemp, Stefano Magni, Jorge Gonçalves. Performance of early warning signals for disease re-emergence: a case study on COVID-19 data. PLOS Computational Biology 18(3): e1009958. https://doi.org/10.1371/journal.pcbi.1009958

Introduction 4

The following chapter is an investigation of the performance of EWS in disease re-emergence. EWS are a class of statistical time series signals [122]. They are used to predict critical transitions which needs to be understood in order to prevent or predict upcoming shifts of the system. In particular, this chapter focuses on the analyses of potential EWS in order to detect critical transitions in empirical data in the framework of COVID-19. My contribution to the following project consisted in the formal analysis of the data. I also came up with the idea and the implementation in Python of ARIMA 3.6.3 as a detrending method for the COVID-19 datasets. Furthermore, I participated in the writing process from reviewing to editing.

Abstract

Developing measures for rapid and early detection of disease re-emergence is important to perform science-based risk assessment of epidemic threats. In the past few years, several early warning signals (EWS) from complex systems theory have been introduced to detect impending critical transitions and extend the set of indicators. However, it is still debated whether they are generically applicable or potentially sensitive to some dynamical characteristics such as system noise and rates of approach to critical parameter values. Moreover, testing on empirical data has, so far, been limited. Hence, verifying EWS performance remains a challenge. In this study, we tackle this question by analyzing the performance of common EWS, such as increasing variance and autocorrelation, in detecting the emergence of COVID-19 outbreaks in various countries. Our work illustrates that these EWS might be successful in detecting disease emergence when some basic assumptions are satisfied: a slow forcing through the transitions and not-fat-tailed noise. In uncertain cases, we observe that noise properties or commensurable time scales may obscure the expected early warning signals. Overall, our results suggest that EWS can be useful for active monitoring of epidemic dynamics, but that their performance is sensitive to certain features of the underlying dynamics. Our findings thus pave a connection between theoretical and empirical studies, constituting a further step towards the application of EWS indicators for informing public health policies.

Author summary

To extend the toolkit of alerting indicators against the emergence of infectious diseases, recent studies have suggested the use of generic early warning signals (EWS) from the theory of dynamical systems. Although extensively investigated theoretically, their empirical performance has still not been fully assessed. We contribute to it by considering the emergence of subsequent waves of COVID-19 in several countries. We show that, when some basic assumptions are met, EWS could be useful against new outbreaks, but they may fail to detect rapid or noisy shifts in epidemic dynamics. Hence, we discuss the potential and limitations of such indicators, depending on country-specific dynamical characteristics and on data collection strategies.

7.1 Introduction

Epidemics such as the current COVID-19 pandemic pose important and long-lasting threats to human societies [451]. Hence, developing tools for rapid and early detection of disease emergence is important to perform science-based risk assessment [446]. In principle, detailed mechanistic understanding could help formulate predictive models. However, combinations of non-linearity, noise and a lack of curated data sets hamper the development of mechanistic models. Therefore, numerous recent studies have suggested using different methods, agnostic of detailed mechanistic models, that could detect shifts in epidemic dynamics [135, 427, 428, 438, 439]. These methods are based on the theory of critical transitions in dynamical systems [119] and require the calculation of statistical early warning signals (EWS) from observed data. However, the applicability of such early warning signals is still debated, as it might depend on the interplay of modelling predictions and empirical observed dynamics.

Critical transitions encompass a broad class of complex phenomena characterized by sudden shifts in the system dynamics. Key mechanisms for deterministic shifts are dynamical bifurcations [435], i.e. qualitative changes of equilibria due to leading eigenvalues crossing a threshold value. In epidemiology, the leading parameter is the reproduction number R, the average number of secondary infections from a single contagious case in a susceptible population [143]. When this evolves over time, e.g. reflecting the effect of pharmaceutical or non-pharmaceutical interventions, we speak of effective time-dependent reproduction number $R(t)$ [157]. Re-emergence of infectious diseases thus involves a transmission system that is pushed over the critical point $R(t) = 1$ through a transcritical bifurcation [438]. As a consequence, it may in principle be possible to apply results from the theory of critical transitions to detect impending epidemic re-emergence. In particular, proposed early warning signals (EWS) are summary statistics indicators that might change in a predictable way when approaching the critical threshold. Common EWS are increasing variance and autocorrelation, which have been suggested to be generically applicable to detect impending regime shifts in different systems [120, 443]. If this would be the case, the consequence would be the possibility to expand the set of epidemic indicators. Several theoretical and computational studies already investigated EWS performance on abstract epidemiological models [132, 135, 436,

438, 452], but so far only a few testings on empirical data have been performed. A first observation was reported in [421]; further data-driven approaches have been applied in [424]. An approach derived from bifurcation theory on networks was applied on COVID-19 data in [423]. A review can be found in [422]. Performing more tests is thus a necessary next step towards the application of EWS in routine surveillance procedures. In addition, it is essential to characterise the potential confounders that might affect the expected signals.

In this study, we aim at testing the performance of EWS in detecting the re-emergence of observed epidemics, and at interpreting the observed performances based on the correspondence of modelling assumptions and dynamic features observed in the data. Specifically, we are not screening all possible EWS on all possible empirical data as it was done in [425, 426]; on the opposite, we are testing whether some EWS work when they are expected to, what happens in other cases, and why. In fact, theoretical predictions like early warning signals should ideally be tested in controlled experiments [462], but these are often not feasible in complex phenomena like epidemics. Instead, the present work considers curated observational data from many outbreaks of the same disease, following the strategy of "natural experiments" [472]: first, constructing a data set that includes relevant time series data; second, accounting for possible confounders, i.e. dynamical characteristics that might alter the expected signals; third, evaluating the performance of EWS and interpreting it in light of previous theoretical results.

To this end, we use worldwide data from the current COVID-19 epidemic. The COVID-19 disease, caused by severe acute respiratory syndrome coronavirus 2 (SARS-CoV-2) [464], rapidly diffused in the whole world during 2020 and 2021. After a first outbreak, characterised by a sudden emergence followed by an exponential diffusion, countries worldwide managed to curb the local infection curves with combinations of non-pharmaceutical interventions. From a dynamical perspective, this corresponded to tuning the effective time-dependent reproduction number $R(t)$ to values below 1 [431]. Later during the year 2020, many countries experienced epidemic re-emergences (often called "second waves") associated to $R(t)$ re-crossing 1 from below [449, 450]. We thus concentrated on this re-emergence, in order to study signals associated with a bifurcation being crossed. The unprecedented diffusion of the virus, as well as the various degrees of intervention strengths, provide abundant epidemic data to construct the test set. Known dynamical features

associated to modelling assumptions, such as noise and rate of evolution of $R(t)$ [441], are then accounted for by analysing the time series of each country. These features allow to interpret the trends observed in empirically derived EWS and their performance in different contexts.

The paper is organised as follows. First, we recall theoretical results from literature, to allow the subsequent comparison with expected EWS behavior. Then, we describe how the test set was constructed and analysed. After that, we study the behavior and the performance of EWS from empirical data and their dependence on dynamical characteristics associated with modelling assumptions. Finally, we discuss the current findings, their limitations and their implications for future studies.

7.2 Methods and Mathematical Theory

7.2.1 Mathematical theory and derivation of EWS

The scope of this article is to test theoretical predictions in light of their assumptions. Hence, we provide a brief review of the theoretical basis of critical transitions in epidemic dynamics, as well as on the derivation and assumptions that underlie their associated early warning signals. This way, we highlight the theoretical results to be tested as well as their supporting hypothesis, which will be central for this study. Further details can be found in the supporting information material S1 as well as in the references provided.

It is often recognised that epidemics can be described as complex systems, whose macro-scale dynamics evolves out of equilibrium [120, 428, 438]. In different complex systems, sudden dynamical changes can happen when the system is pushed over a critical point through a bifurcation [124]. Critical transitions observed in complex systems are often associated with such bifurcations [410]. Recent studies have shown that the trend of certain statistical indicators may signal the approach to a critical transition in slowly forced dynamical systems [435, 454]. In general, a slowly forced system with variables $\mathbf{x}$ and control parameter q is [469]:

$$\begin{cases} \dot{\mathbf{x}} = \mathbf{f}(\mathbf{x}, q) \\ \dot{q} = \epsilon \mathrm{g}(\mathbf{x}, q) \end{cases} \tag{7.1}$$

with $0 < \epsilon \ll 1$. Typical models of epidemic dynamics, such as SIR based models [352, 431], can be expressed as a slowly forced system like Eq. 7.1 when the control parameter R slowly approaches its critical value 1.

In the presence of small random fluctuations, the approach to the critical point is often associated with predictable trends of several statistical indicators of variability, which have been proposed as early warning signals of impending transitions [453, 457]. The reason is that noise can push the system state around the deterministic trend of Eq. 7.1; at the same time, its statistical properties might change as the system approaches the transition and could be used to detect it [469]. If the noise is relatively small with respect to the deterministic trend and normally distributed, the trend of the most common summary statistics (variance, autocorrelation, skewness, coefficient of variation), computed on detrended residuals, is expected to increase next to the transition, thus providing an early warning signal [120, 442]. If this signal can be observed prior to the transition, it would constitute an early warning.

Several early warning signals from the critical transitions theory have been predicted to apply on epidemiological models. A particularly relevant theoretical result is from [438]. The authors consider an extended SIR model:

$$\begin{aligned} \dot{X} &= \mu(1-p) - \beta XY - (\eta+\mu)X \\ \dot{Y} &= \beta XY + \eta X - (\gamma+\mu)Y \\ \dot{Z} &= \mu p + \gamma Y - \mu Z \end{aligned} \tag{7.2}$$

with variable X for susceptible, Y for infectious, Z for removed. β represents the infection rate and γ the removal rate [178]; μ describes the flux of people across country boundaries; η is an influx of infected cases that could trigger a new infection; p represents a protection rate for the susceptible population, either by non-pharmaceutical interventions or by vaccination [325]. In this case, the reproduction number is [438]:

$$R = \frac{\beta}{\gamma+\mu}(1-p)\,. \tag{7.3}$$

There is a transcritical bifurcation on the (Y, p) diagram when R reaches its critical value $R = 1$ for

$p^* = 1 - (\gamma + \mu)/\beta$. The R introduced above corresponds to the empirical effective reproduction number $R(t)$ if we explicitly consider the time-dependence of p as $p(t)$. When considering the stochastic version of Eq. D.1, it is possible to analyse its fluctuations next to the transition and extrapolate the early warning signals from the associated summary statistic indicators. The kind of noise (additive or multiplicative) that is considered constitutes a modelling assumption. How the most common indicators — variance and lag-1 autocorrelation — are derived (from [438]) is reported in the supporting information, along with their predicted evolution next to the critical transition when the slow-fast assumption is satisfied, or not (Fig. S1). Their increasing trends prior to the transition provide the predicted early warning signal.

Further computational results, which also consider additional indicators, suggest that the increases in variance are the best performing indicators of re-emergence, in terms of signal-to-noise ratio and of detection performance [135, 428]. However, as noticed in follow-up studies [134, 447, 469], their performance is linked to whether their modelling assumptions are satisfied. If it is the case, such indicators perform well; but what happens in other contexts is still less clear.

We here recall the main modelling assumptions underlying the prediction of EWS, as well as their relevance for their performance. (1) critical transitions are local phenomena. Hence, EWS are not global measures, but are expected to work in the vicinity of the regime shift. (2) it should be possible to express the epidemic dynamics in terms of a fast-slow system like Eq. 7.1. When approximating R approaching to 1 as a linear trend, the modelling assumption Eq. 7.1 is satisfied if the regression coefficient (the slope of the linear trend) is small. Otherwise, literature results suggest that the expected patterns will be either distorted or will not occur [428, 438]. (3) the closer random fluctuations are to be additive noise, the more robust the performance of EWS is. If there are deviations from white noise, EWS trends can be modified or disrupted. For instance, decreasing variance was observed in case of non-white multiplicative noise [447]. (4) In case of combinations of non-white noise and of non-fast-slow description, one might observe bifurcation delays, i.e. changes of the system state (and of its indicators) that lag behind the theoretical bifurcation. This would translate in a warning signal that emerges much time later than the epidemic re-emergence. (5) If the transition is triggered by large random fluctuations — the so called noise-induced transitions [435] — no EWS is expected to be observed [411].

7.2.2 Data collection and curation

This paper studies the re-emergence of infectious diseases, with COVID-19 as a case study, in a number of observations from all over the world. Our aim is to verify whether EWS work when they are expected to based on the theory recalled above and explain why they might malfunction otherwise, rather than perform an observational study over all COVID-19 re-emergencies (for such a study, refer to [425]). Consequently, to construct the data set, we considered data from countries that faced a re-emergence of positive COVID-19 cases between beginning of March (starting of wide viral diffusion) to mid-September 2020. We did not consider further data points as many countries began issuing new social measures that rapidly impacted the epidemic trends. These would hinder the careful analysis of confounders.

When possible, we use prevalence data, i.e. active cases over the whole population of a regional area, in accordance to what is modeled by SIR-like models and to what was suggested in literature [132]. Active cases from Luxembourg are directly retrieved from the government website (COVID19.public.lu/fr/graph). They are derived from random samples over the whole population, using a Large Scale Testing strategy [396] and careful control of the hospital system. As they are not directly available for the other countries, active cases A are estimated, following [154], by the proxy:

$$A = C - D - \tilde{R} \tag{7.4}$$

where C indicates the cumulative positive cases, D the number of registered deaths and $\tilde{R}$ the number of recovered patients. Country data are obtained from public repositories of confirmed detected, deceased and recovered cases: the John Hopkins University collection [161] and the European Centre for Disease Prevention and Control database (https://www.ecdc.europa.eu/en/COVID-19/data). We also use Italian data from the Veneto region, as an example of regional data with an identifiable second wave during the considered time interval. Veneto time series for detected, deceased and recovered cases are retrieved from the Github repository of the Italian "Dipartimento della Protezione Civile - Emergenza Coronavirus" (https://github.com/pcm-dpc/COVID-19). All databases are accessed up to 15/09/2020.

To best curate the database, an initial screening on data quality is performed. We reject time series with very few active cases, as in such time-series the intrinsic stochasticity of the contagions and the measurement noise dominate over the deterministic behaviour captured by SIR-like models. We also discard time series for which the share of positive cases over performed tests is $> 5\%$ next to the transition, as WHO guidelines suggest possible undertesting (we refer to WHO reports such as https://bit.ly/3dARcy1). Information about the share of positive tests is obtained from the OurWorldInData curated dashboard [163] and is reported as a summary in supplementary table S1. As EWS from critical transitions are based on mean-field homogeneous SIR-like models, we do not consider whole countries with clear spatial heterogeneity like Italy [460], but we instead use regional data if available. Finally, we discard some public time series that behave clearly differently from the common reconstructed epidemiological curves [154] (see electronic supporting information Fig. S2).

We acknowledge that data quality, particularly about $\hat{R}$ cases, plays a major role to obtain a robust estimator for A. The selection criteria were designed to enhance data quality; hence, in the remainder of this study, we focus on prevalence data to compare the results with interpretations from various literature sources. In addition, we perform an investigation on the use of incidence data, using reported daily new cases from the same sources listed above. Incidence data might as well be influenced by testing bias (e.g. lower testing over weekends) and other factors; hence, this analysis complements the one on prevalence data by investigating EWS performance on real-world monitoring protocols. Such analysis is reported in electronic supplementary material Sec. S8.

7.2.3 Analysis of dynamical features

To identify the transition *a posteriori* and get a "ground truth" date of re-emergence, we use a data-driven estimation of the time-dependent $R(t)$. Similar to [135, 413, 414], $R(t)$ is estimated with Bayesian inference by means of a Markov Chain Monte Carlo (MCMC) method. For each day when data are available, we estimate the probability of observing a certain value of $R(t)$ by calculating the likelihood of seeing k new cases, given the candidate $R(t)$, following a Poisson transmission process. To avoid fitting spurious bumps, the data are previously smoothed with a Gaussian window of 7 days. Note that, since this is only used for a retrospective analysis, it does

not modify the non-anticipating scheme for the EWS. We update the prior at time t with the posterior at time $t-1$. A Metropolis-Hastings MCMC scheme was used to generate candidates for $R(t)$. We describe this in depth in electronic supporting information Sec. S4. As we adapted a previous implementation from [414], we also refer to it for further details.

Then, we employ the posterior probability density function obtained from the Bayesian framework: $p(R|\text{data})$. This was used to estimate the probability that the control parameter is greater than 1, $\mathcal{P}(R(t) > 1)$. This was calculated, as for any stochastic variable, by integrating over all possible probability values associated with $R(t) > 1$:

$$\mathcal{P}(R(t) > 1) = \int_1^\infty p(R|\text{data})dR \ . \tag{7.5}$$

Since $R(t) > 1$ is associated with an exponential increase of infectious cases after a transcritial bifurcation, $\mathcal{P}(R(t) > 1)$ can be interpreted as the probability of seeing an epidemic outbreak. Then, the most likely day t_{em} in which the transition happened, assumed as our ground truth, corresponds to the first time when $\mathcal{P}(R(t) > 1)$ from Eq. 7.5 reaches its maximum value of 1 (see electronic supporting information Fig. S3).

After calculating the outbreak date, we test the modelling assumptions of normally distributed fluctuations and of slow approach to the critical transition.

To test the additive noise assumption, we analyze the global distribution of stochastic fluctuations, filtered from the time series with a 7-days moving Gaussian kernel as suggested in [440, 466]. The window size reflects typical cycles of data reporting and of COVID-19 fluctuations [458]. The distribution of fluctuations over the complete time series is indicative of the average noise distribution. We computed skewness and kurtosis to measure deviations from Gaussian noise, which is characterized by skewness=0 and kurtosis=3 [179].

To test the assumption of slow approach to the transition, we measure the rate of approach of the control parameter to its critical value. For this, we compute the time-dependent $R(t)$ like above and, consistently with the fast-slow system description of Eq. 7.1, we fit a linear function:

$$R(t) = a + b \cdot t \tag{7.6}$$

in the interval $t \in [\tilde{t}, t_{em}]$. Here, t_{em} corresponds to the day associated with novel disease emergence as explained above; $\tilde{t}$ is the day associated with the minimum of $R(t)$ after the first wave. The regression coefficient $b \pm \sigma_b$ measures the ramping speed of the control parameter (along with its uncertainty). As an indication, $R(t)$ is said to be "slowly evolving" if it goes from its minimum value to 1 in a period of time that is much longer than the COVID-19 serial interval (around 4 days [461]), which is a proxy of the disease duration time scale. For the fitting, we use the *scipy* Python library. Refer to electronic supporting information Sec. S5 for details.

7.2.4 Estimation of EWS

Estimation of early warning signals from time series data is performed following standard methods from literature [441].

First, we detrend the time series to obtain a moving average, representative of the deterministic trend. The "residuals" or detrended fluctuations are obtained by subtracting the moving average from the original time series. To investigate possible effects of detrending approaches — as discussed in previous theoretical studies [120, 440, 454] — we use and compare three detrending methods: a uniform moving mean, a Gaussian kernel, and ARIMA models [412]. The ARIMA models are specifically tuned for each country, see electronic supplementary material.

Then, we compute the statistical indicators associated to each point with a backward sliding window, i.e. one where the associated time point is the rightmost one. In a similar spirit, all detrending methods are non-anticipating. This way, all estimates are agnostic of future values and reflect practices used in active monitoring: the estimation of an indicator is performed as soon as a new data point becomes available. All EWS indicators are estimated on the detrended time series. We initially calculate the variance, which is suggested to be the most robust indicator for epidemic re-emergence [132, 135, 428, 438] as:

$$\mathrm{Var}_{i,t} = \frac{1}{M-1} \sum_{s=t_0}^{t} (A_{i,s} - \hat{A}_{i,s})^2 \tag{7.7}$$

for any time point i with active cases A, over a sliding window with size $t - t_0$ including M time points. $\hat{A}$ is the moving average. We also estimate other common statistics such as lag-1

autocorrelation AC(1), coefficient of variation (CV) and skewness, which are constructed similarly to the variance over the same sliding window. The sampling frequency of COVID-19 data is not sufficient to allow estimation of the power spectrum reddening [459] or of the sample entropy [428]. All indicators are estimated with their corresponding MATLAB functions. Note that the estimation of $\mathcal{P}(R(t) > 1)$ is done a posteriori, that is, once we know the complete time series. Instead, the early warning signals are calculated a priori, without knowing in principle if a transition is approaching.

7.2.5 Quantification of EWS trends and Receiver Operator Characteristics analysis

Recent studies [132, 134, 441] suggest to quantify the expected increasing trend of EWS next to the transition with the Kendalls τ coefficient of monotonicity. The Kendall's τ score is defined as [474]:

$$\tau = \frac{\#\text{concordant pairs} - \#\text{discordant pairs}}{M(M-1)/2}.$$

M is the number of considered time points. Two generic points (t_1, x_1) and (t_2, x_2) are said to be a concordant pair if, for $t_1 < t_2$, $x_1 < x_2$, and a discordant pair otherwise. A constant trend is expected to have $\tau = 0$. We compare this value with the τ scores calculated on time series with identified transitions. To go beyond simple visual inspection, we quantify the detection power of each statistical indicator using its time-changing trend, classifying data as either belonging to the second wave or not. After calculating each indicator on a moving window (its size is discussed later in the text) for each detrended time series, we estimated the Kendall's τ score for each timepoint on windows of the same size, over an overall period $-30 < t_{em} < 5$ days around the transition, as our positive data set. $t > -30$ is chosen to avoid significant overlaps with the first epidemic wave, $t < 5$ to account for possible small bifurcation delays [120]. For the negative data set, we use τ values taken way before the transition occurs, that is on windows associated with timepoints $t < -30$.

We use Receiver Operator Characteristics (ROC) analysis to classify each time point as either

before or after re-emergence. We compare each statistical indicators ability to correctly distinguish which Kendall's τ scores belong to those from before or after re-emergence, that is, we determine whether the estimated τ is higher or lower than some threshold value at that timepoint and determine whether each time series is classified correctly by that threshold. This gives a proportion of true positives and false positives. To do so, we compare various values for $0 < \tau < 1$ to those of the positive and negative data set, for each country. We calculate the indicator for each country in a test set at the given timepoint, and then group the specificity and sensitivity results to obtain the final ROC curve. The ROC analysis returns the Receiver Operator Characteristics (ROC) curve, a parametric plot of the sensitivity and specificity of a classification method as a function of the detection threshold [135, 136]. The overall detection performance of each EWS is quantified by the area under the ROC curve (AUC). A value AUC$= 0.5$ means that the statistics detection performance is as good in classifying as randomly guessing. A good indicator should have AUC close to 1, which informs that it is possible to identify the transition by the increasing trend of the indicator. An AUC close to 0 indicates good classification, although resulting from a decreasing indicator that does not correspond to the predetermined theoretical prediction.

7.3 Results

7.3.1 Analysis of country-wise dynamical characteristics associated to the spread of COVID-19

Tab. 7.1 reports the list of countries that satisfy the curation requirements discussed in Materials and Methods and are thus included in the analysed data sets. Tab. 7.1 also reports the dates of re-emergence, identified by the analysis of $R(t)$. Fig. 8.4a shows an example of time series of active cases for Luxembourg, from March to mid-September 2020, with the date of estimated re-emergence (dashed line).

The time series of the considered countries show different dynamical features. Fig. 8.4b shows various ranges of noise distribution, measured by skewness and kurtosis. Austria, Luxembourg, Nepal, Singapore and Veneto display noise distributions that are close to Gaussian, while noise in the other countries is further away from white than in the previously mentioned ones. This could

Country	Abbr.	Date
State of Victoria (Australia)	AUS	27/06/2020
Austria	AUT	01/07/2020
Denmark	DNK	03/08/2020
Israel	ISR	01/06/2020
Japan	JPN	28/06/2020
Korea, South	KOR	13/08/2020
Luxembourg	LUX	29/06/2020
Nepal	NPL	29/07/2020
Singapore	SGP	25/07/2020
Veneto (Italy)	VEN	29/07/2020

Table 7.1: Selected countries for the dataset, abbreviations and date of second epidemic insurgence. Refer to "Data Collection and Curation" for how the date marking the second wave is obtained.

be associated to social dynamics or imperfect data reporting [465].

The rate of approach of $R(t)$ to its critical value also differs, as indicated in Fig. 8.4c by the regression coefficient of a linear fit for $R(t)$ (*cf.* Eq. 7.6). State of Victoria, Austria, Luxembourg, Singapore and Veneto display a slow approach to the critical value and can thus be better suited to be appropriately described as slow-fast systems like Eq. 7.1. Japan and South Korea show intermediate values, while other countries - Denmark, Israel and Nepal - have a faster evolution of the control parameter, which does not satisfy the assumption of slow evolution.

Following this analysis, we subdivide the considered countries into two test sets, based on whether the country satisfies or not some of the assumptions of slow approach to the transition and noise distribution close to white. These two properties can be assessed respectively from Fig. 8.4c and Fig. 8.4b. Instead of using hard thresholds, we use group clustering to make the subdivision. As discussed above, State of Victoria, Austria, Luxembourg, Singapore and Veneto are grouped together to represent the assumption of slow rate, as can be seen from Fig. 8.4c. Moreover, except for Australia, their noise distribution is close to Gaussian, as their skewness and kurtosis show in Fig. 8.4b. They thus form the test set $\mathcal{Y}$, used to further assess the performance of EWS. On the other hand, Denmark, Israel and Nepal display higher rates of approach to $R(t) = 1$ and large deviations for Gaussian noise distribution. Hence, they are grouped together in a set

$\mathcal{N}$; this is used to interpret the performance of EWS in settings that are not properly described by theoretical models and represent possible limitations of the predetermined predictions. South Korea and Japan are more ambiguous when clustering over the slope of $R(t)$, therefore we split them into $\mathcal{Y}$ and $\mathcal{N}$, respectively, based on their relative vicinity to Gaussian noise distribution. Among these countries, Luxembourg is peculiar, as it satisfies the modelling assumptions and is the closest to being a "controlled experiment" according to the criteria described in the section about deriving EWS. In fact, we know from literature and practical experience that the country is small, homogeneous population-wide interventions were in place, and a Large Scale Testing (LST) strategy was implemented to best monitor the virus diffusion in the country [396]. This country wide testing strategy reached more than 70.000 tests per week over a population of about 600.000, thus allowing extensive and frequent monitoring. Hence, we use it as an initial sample to test the theoretical predictions about the local behavior of EWS.

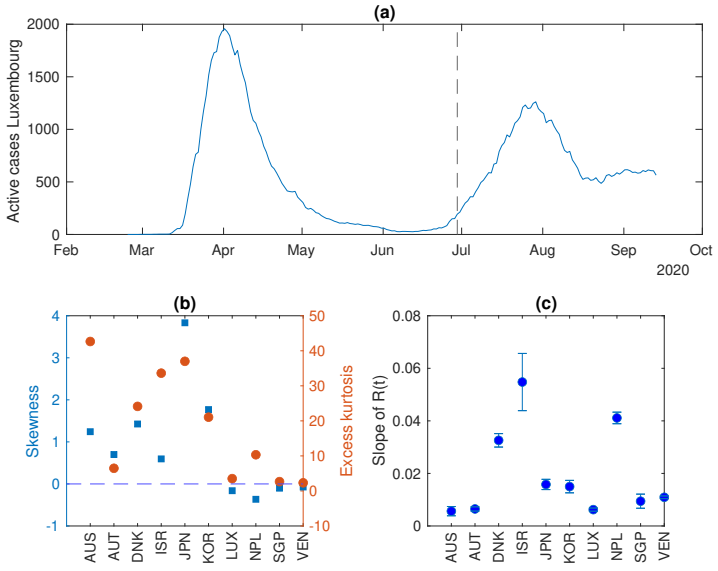

Figure 7.1: Analysis of the dynamical characteristics of the countries included in the data set. a) An example of an epidemiological curve of active cases from Luxembourg. The dashed line indicates the transition, measured by $R > 1$. The latter is objectively identified by the date at which the probability of $R(t)$ to be greater than 1 is at its first maximum (see "Analysis of dynamical features"); b) Measures of the distribution of data fluctuations. Skewness μ indicates the symmetry of the distribution, whereas kurtosis γ indicates the relevance of its peak with respect to the tails. Large deviations from $\mu = 0$ (dashed line) and $\gamma = 3$ are associated with non-normal distributions, so we display the excess of kurtosis $\gamma - 3$. c) The regression coefficient of $R(t)$ and its associated uncertainty, as obtained from the linear fit Eq. 7.6.

7.3.2 Local trends on controlled data and impact of detrending methods

We first focus on Luxembourg, that displays the best data in terms of curation of prevalence data (see Methods) and of satisfaction of theoretical assumptions (see above). Here we test the theoretical predictions about the local behavior of common EWS. Summary statistical indicators are estimated from the detrended fluctuations (residuals) around prevalence data as per standard methods [441].

We first investigate the effect of the detrending method in generating residuals. To do so, we compare the fluctuations around the deterministic trend obtained with a Gaussian kernel smoothing [440, 454], a moving average filtering [120] and an ARIMA(2,1,3) model [412]. Fig. 7.2 shows the time evolution of the residuals obtained with the three methods, as well as their mutual correlations. As quantified by the Pearson correlation coefficient, the Gaussian and moving average filtering have similar output (correlation coefficient $\rho = 0.95$). This is likely related to the Gaussian bandwidth of 7 days, used to reflect known weekly fluctuations related to testing routines. Consequently, the Gaussian kernel smoothing is used in the rest of the analysis. However, the ARIMA method returns residuals that are less correlated with the previous ones ($\rho = 0.23$), whose effect on EWS needs further investigation.

Then, we study the behavior of the variance (theoretically, the most robust EWS [135]) next to the transition point, identified as the day when the estimated $R(t)$ crosses 1 (dashed line in Fig. 7.3). The increase in variance prior to the transition, as expected from theoretical studies, is evident in Fig. 7.2, irrespective of the moving window size and on the detrending method. Although the lead time is slightly advanced for shorter window sizes, the corresponding Kendall's τ measure of monotonous increase is similar for both methods and all window sizes (*cf.* values reported in Fig. 7.3). In general, a large window size produces smaller fluctuations but a visually reduced absolute increase; in addition, too large windows might capture old decreasing trends, that we want to avoid analysing. On the contrary a small window size is associated with less smoothed curves but a larger absolute value of variance. Nonetheless, it might not include enough data points to capture the trends in more noisy estimators like AC(1) [440]. From here on, we will use a window of 14 days as a reasonable trade-off, collecting enough data to be robust without

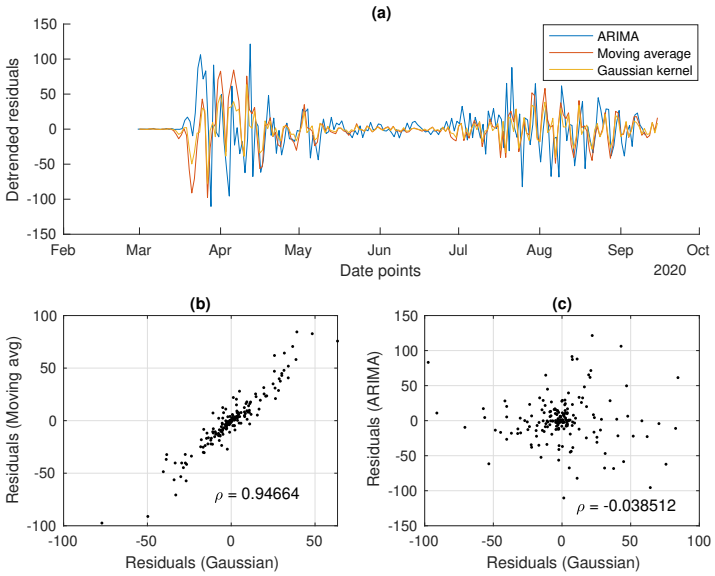

Figure 7.2: Analysis of the residuals from the detrending methods (case study from Luxembourg shown). a) The detrended fluctuations time series. b) Correlation between residuals obtained from Gaussian or moving average filtering. c) Correlation between residuals obtained from Gaussian or ARIMA filtering.

being over-dependent on past history. The ARIMA residuals produce a visually clearer increase in variance, but the Kendall's τ quantifies an analogous trend (even slightly lower). For the incoming quantitative analysis on the EWS performance, we will thus study the effect of both detrending methods.

These findings confirm that, in a controlled setting that satisfy the modelling assumptions (Luxembourg), an increasing trend of the variance in the vicinity of the transition point could serve as early warning to detect the transition to disease emergence.

7.3.3 Global trends of EWS

After confirming the local behavior of the variance in the Luxembourg highly controlled setting, we widen the analysis to the global performance of other EWS, *i.e.* far from the bifurcation, and for different countries from the pre-defined dataset, *cf.* Tab. 7.1. This way, we further test the theoretical predictions and the EWS potential use in more general contexts.

Among the indicators, we estimate lag-1 autocorrelation (AC(1)), skewness and coefficient of

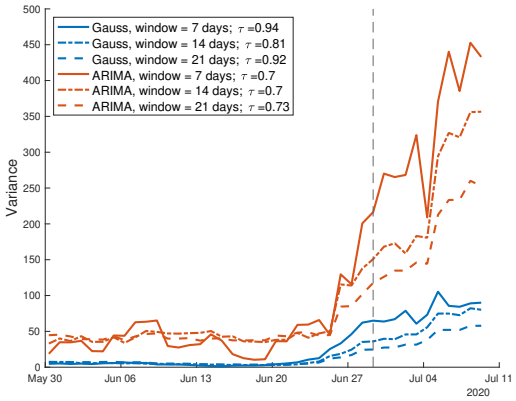

Figure 7.3: Analysis of the variance in the Luxembourg setting. Its increase is evident prior to the transition (dashed vertical line). τ, which quantifies the overall increasing trend, is little sensitive to the sliding window size, as displayed by the three curves and by τ values reported in the text. The variance is computed over the residuals from Gaussian filtering and ARIMA detrending. The increasing trend during the considered time window is quantified by the associated τ values.

variation (CV), which are often proposed as alternatives to the variance. The size of the moving window is set to 14 days as discussed above. To compare the trend of EWS with the approach to the bifurcation, the probability of $R(t)$ to be greater than one (from Eq. 7.5) is also calculated and reported.

Fig. 7.4 shows the results for Luxembourg, Austria, State of Victoria (from the test set $\mathcal{Y}$). In addition, Israel, which does not satisfy the EWS assumptions (*cf.* Fig. 8.4) is reported to inspect a deviant case. The figure focuses on EWS trends after the first wave, up to about a month after the second epidemic insurgence. The graphs for other countries from Tab. 7.1 are reported in electronic supporting information Fig. S5, along with their associated prevalence data and estimated $R(t)$. In Fig. 7.4, the left column refers to indicators estimated after Gaussian filtering, while the right column is for indicators estimated after ARIMA detrending.

Focusing first on Luxembourg and Austria, the variance follows its theoretically predicted behavior closely (*cf.*, e.g., Fig. 9b in [438] and Fig. S1), with a small but visible increase prior to the transition and a subsequent monotonous trend along the second wave. In Austria, though, it still displays some fluctuations after the relaxation of the first wave. The same happens for the coefficient of variation CV, which depends on the variance and on a stable equilibrium in infectious numbers. On the other hand, the lag-1 autocorrelation shows an increasing trend very close to

the transition point, but gives possibly spurious signals during the global time series. Finally, the skewness does not display immediately detectable relevant trends, as anticipated by computational studies [132]. This might be related to noise properties, as suggested by [473].

Variance and CV on Australian data, when processed by eye, start increasing close to the transition, but this becomes more pronounced around the 7^{th} of July. This might be related to the so-called "bifurcation delay", which is associated with deviations from Gaussian noise [120, 447], or to delays due to tests results reporting or symptoms onset.

Finally, Israel provides an interesting case study as it diverges from the theoretical assumptions, see Fig. 8.4. In fact, its transition to epidemic re-emergence is rapid, and the noise distribution is far from being Gaussian. These characteristics disrupt the EWS trends as predicted by the theory. In fact, the variance remains flat around the transition (it is even slightly decreasing), CV and skewness slightly decrease, while lag-1 autocorrelation does not display informative patterns. A delay is reported more than 20 days after the transition, but it is as abrupt as the exponential increase in infectious data (see electronic supporting information). This shows that the application of early warning signals indicators on appropriate contexts is crucial to obtain reliable signals for developing risk assessment analysis.

Similarly to what observed in Fig. 7.3, the variance trends are similar between Gaussian- and ARIMA-related indicators. We quantify their potentially different performance in the next section. The behavior of CV and AC(1) is also qualitatively rather similar. On the other hand, the skewness behaves differently. For instance in Austria, it increases when the detrending is performed with Gaussian kernel, but it decreases after ARIMA. This might be associated to the fact that the skewness is very sensitive to the noise distribution [473]: small changes in the residuals, due to the different filtering procedure, might suffice to modify its trend.

7.3.4 ROC quantitative analysis of EWS performance

For the online detection of incoming re-emergence, distinguishing between robust increases and spurious fluctuations is crucial to optimise the true positive signals and minimise the false negatives. Hence, a retrospective analysis of time data is often not sufficient and is only useful for offline detection. Thus, we provide a quantitative estimation of EWS performance in robustly detecting

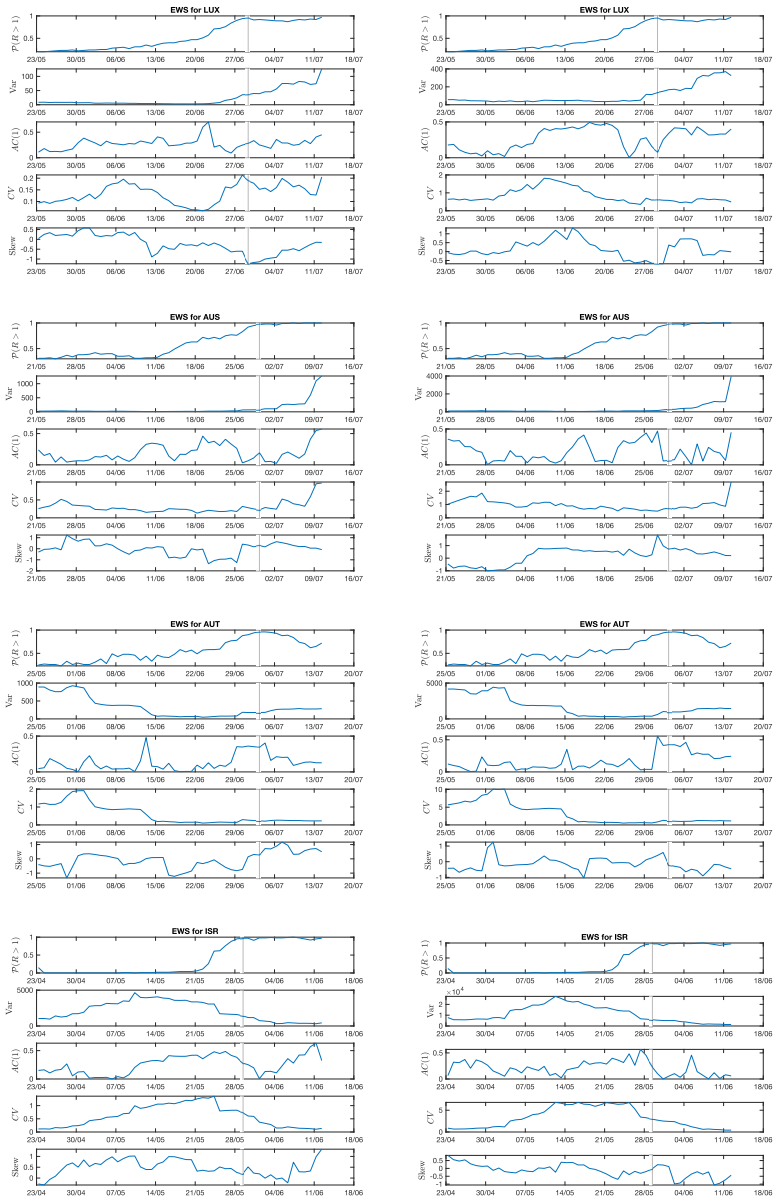

Figure 7.4: Evolution of EWS far from the transition point. Four example countries are shown: Luxembourg and Austria, with controlled features; State of Victoria (Australia), with small deviations from controlled features; and Israel that does not satisfy theoretical conditions. Considered EWS are the most common ones (variance, lag-1 autocorrelation, coefficient of variation, skewness). In addition, to mark the approach to the transition, $\mathcal{P}(R(t) > 1)$ from the Bayesian estimation (see Eq. 7.5) is displayed. The vertical line reports the transition date. Left column: detrending method employed: Gaussian filtering. Right column: detrending method employed: ARIMA. Other countries are reported in SI Appendix

the transition. The Kendall's τ score is used to evaluate if a certain indicator corresponds to an increasing or decreasing trend and compare this for different data types [132, 134]. Hence, we evaluate τ for each indicator, over the same 14 days window, and we assess which values are associated with a passage through the transition point. The increase in τ is reflected in the Receiver Operator Characteristics (ROC) curve and quantified by Area Under the Curve (AUC) scores. Fig. 7.4 shows the ROC curves for the considered indicators averaged over the countries in $\mathcal{Y}$. Panel (a) reports ROC curves calculated over data detrended with Gaussian filtering; panel (b) focuses on ARIMA detrended data. Tab. 7.2 reports the corresponding AUC values, for both methods. The variance is the only indicator that consistently performs better than a random classifier, while the lag-1 autocorrelation seldom performs slightly better than that. This is in line with aforementioned theoretical results from literature, e.g. [132, 135]. Instead, the skewness does not improve the detection performance. This is probably due to its fluctuations around the 0 value, as noticed in Fig. 7.3, which is in turn associated with noise distribution of original data. Interestingly, the coefficient of variation is overall the worst performer. We speculate that this is due to its sensitivity to data fluctuations, which are often non negligible even in countries that belong to the test set $\mathcal{Y}$ (*cf.* Fig. 8.4). We acknowledge that our findings are sensitive to the estimated time of emergence, which also complicates the estimation of the lead time. Currently, the best lead time is of 5 days for Luxembourg, a setting that is close to the analytical assumptions. For all indicators, the ARIMA detrending method yields better performances, quantified by higher AUC values. AC(1) is an exception, as both methods return similar values, close to the ones of a random classifier. That ARIMA residuals yield higher AUC is potentially linked to the ARIMA estimating trends more closely at different time scales, thus returning more accurate fluctuations; on the contrary, the Gaussian filtering might be slightly more rough in considering only average time scales and returns approximated estimates for the fluctuations. This argument might explain why the skewness performs slightly better than a random classifier over ARIMA residuals: by considering more fine-grained time scales, the ARIMA seems able to pick the slight asymmetry in residual distributions that yield to skewness-related signals [473]. This analysis thus indicates the importance of choosing the detrending method to increase the detection performance of various indicators.

The same analysis was performed over the set $\mathcal{N}$ of countries that do not satisfy the theoretical assumptions. Their AUC values are reported in Tab. 7.2. Such values clearly show that the considered indicators are not able to detect the transitions, overall performing worse than random classifiers. This supports what was already noticed for Israel in Fig. 7.3, where disrupted trends were observed, contradicting what was expected and thus returning a false negative signal. For variance and CV, an AUC value close to 0 indicates that the transition is well detected by decreasing trends. This would contradict the theoretical predictions. Investigating this issue reveals that such features are possibly linked to non-complete relaxation of the indicators after the first wave or to delays. We thus conclude that it is an instance of spurious signal, to be carefully interpreted. See also electronic supplementary material Sec. S7 and Fig. S6 for further discussion. The time series for indicators of other countries in $\mathcal{N}$ are also reported in electronic supporting information Fig. S5. Hence, if a system is not known or there is difficulty in determining the type of data, incorrect conclusions could be drawn when interpreting the time series trend.

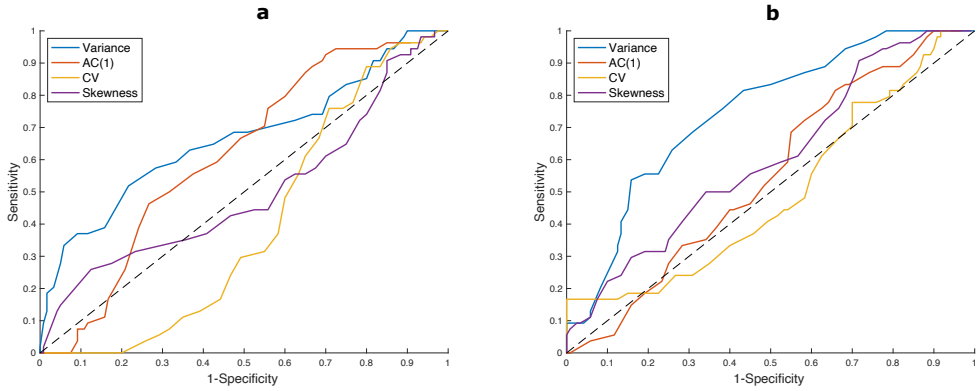

Figure 7.5: ROC curves for each considered indicator, with sensitivity and specificity calculated on each timepoint for all countries in $\mathcal{Y}$. Each point corresponds to a test value for τ, to define if the detection is positive. The diagonal line corresponds to the ROC of a random classifier. Curves above it imply better performance. a) Computed on Gaussian filtered data; b) Computed on ARIMA detrended data.

7.4 Discussion

Research on early warning signals from the theory of dynamical systems has greatly progressed in the last years, with a relevant focus on disease re-emergence. However, verifying and interpreting

	Gaussian det.		ARIMA det.	
Indicator	over $\mathcal{Y}$	over $\mathcal{N}$	over $\mathcal{Y}$	over $\mathcal{N}$
Variance	0.6671	0.1981	0.7123	0.0934
AC(1)	0.5258	0.4995	0.5182	0.2840
CV	0.3968	0.1043	0.3626	0.0368
Skewness	0.4664	0.2925	0.5482	0.4609

Table 7.2: AUC scores for different indicators, over $\mathcal{Y}$ and $\mathcal{N}$ datasets, after Gaussian or ARIMA detrending methods.

empirical analysis according to theoretical assumptions has been so far limited. In this study, we observe that some EWS from the critical transitions framework are able to detect the transition to disease re-emergence when necessary theoretical assumptions like normal distribution of data fluctuations and slow change rates are satisfied. On the contrary, we observe (along with [425]) that noise and commensurable time scales can obscure the early warning signals, which calls for caution when interpreting monitoring outputs. We suggest that dynamical-based EWS can be suitable candidates for epidemic monitoring. Theory-based indicators can provide useful evidence, particularly when scarce data and few prior information are a constraint for using large scale statistics or Machine Learning (ML) methods. However, their alternate performance on unknown dynamics asks for careful assessment of the underlying dynamics. EWS have the potential to complement the existing toolbox of indicators to improve epidemic risk assessment and deserve further investigation by scholars and decision-makers.

To support the growing corpus of theoretical studies, this study tested whether observed epidemic outbreaks behave consistently with the theory. When randomised experimental studies are not possible, observational studies provide stronger evidence if consistent patterns are seen in multiple locations and at multiple times, after checking for possible confounders. Hence, we employed world-wide available data about the ongoing COVID-19 pandemic, concentrating on the re-emergence of the disease after a first wave in spring 2020. To limit biases associated with country-specific testing and reporting capacities, we constructed a limited, but curated set of time series data. Like $R(t)$ and other indicators [455], EWS are estimates that rest on assump-

tions; hence, we screened the dataset to assess the matching of empirical features and theoretical assumptions. This pre-analysis showed that the same disease in diverse countries might have different noise distributions and evolve at different rates, which could depend on several factors including human behavior and population-wide interventions [167].

Furthermore, we tested how the best performing EWS detected the epidemic re-emergence. We carried out an extensive analysis of the effect of different detrending methods, showing that they are overall robust in highlighting the local trends of EWS. Such trends were studied both qualitatively and quantitatively, with ROC/AUC values. In particular, the ROC analysis assesses the robustness of online detection in distinguishing between real increasing trends and spurious fluctuations, which are often not studied in retrospective observations of time series data. In controlled settings, our results reconstructed the expected trends in early warning signals and the potentials of the indicator system proposed. In particular, we showed that dynamical EWS are likely to operate successfully in contexts where the approach to the transition is gradual and not subject to high fluctuations. Further studies could associate these features to social behaviours and political strategies.

We also studied the different impact of detrending methods on the performance of warning signals. We showed that detrending time series with ARIMA models, appropriately calibrated for each country, increases the AUC score. This observation supports early theoretical works [440] and informs researchers about the importance of data processing methods to improve the performance of various indicators.

Finally, we analysed the potential limitations of the indicator system in other contexts, characterised by different dynamical features such as rapid increases of $R(t)$ and strong or non-additive noise. This emphasises that, for EWS to properly work, the real system must fulfill the discussed conditions underlying the theoretical modelling. These open problems highlight that knowledge of the type of collected data is imperative to avoid misleading judgements in response to time series trends: EWS as epidemiological constructs will only remain valuable and relevant when used and interpreted correctly [456].

We acknowledge the limitations of this study, which might be overcome when new and better

curated data sets will become available. First, data quality could be a limiting factor, despite being representative of real world monitoring capacities. Reliable estimates of recovered and dead patients are necessary to guarantee the robustness of a proxy for active cases like A. Another potential data quality issue is that the official numbers of positives might still neglect undetected asymptomatic cases. The data set selection highlights the importance of monitoring and of high quality prevalence data (as already suggested in [132]). Secondly, our estimators come with uncertainties: the empirical $R(t)$ is an estimate of the true reproduction number that rests on the assumption of homogeneous dynamics, while the use of moving windows might yield odd behaviors of EWS [440] which can contribute to poor signals, in addition to rapid transition and non-white noise. Third, our definition of "ground truth" transition date is somewhat conservative, as we requested to have maximum probability of $R(t)$, the control parameter, to be greater than 1. In the real world, the appropriate detection threshold is conditional on the various costs of a late outbreak alert, and requires an assessment by public health authorities which could modify the estimated lead time. This aspect might also influence our interpretation of the "bifurcation delays": depending on the definiton of the "ground truth", they might be less severe than what discussed before. Moreover, an alternative explanation for such observed delays might involve COVID-19 latency periods and reporting delays. When extra data are available, this aspect can be further elucidated using nowcasting methods [437]. Fourth, due to statistical uncertainties, a reliable estimation of the lead time - how much in advance a re-emergence can be predicted - was not entirely possible. Future studies will likely concentrate on this aspect, as early prediction would advance the current on-time detection.

This study uses a proxy A for active cases (Eq. 7.4) to compare theoretical results from various literature sources obtained from on prevalence data. To expand the testing of EWS on epidemic data, to compare them with more recent studies on incidence data [132, 426] and to avoid the potential biases associated with the proxy A (see discussion above), we also investigated the potential use of incidence data themselves. The related results and plots are displayed in electronic supplementary material Sec. S8. We observe consistency with the results here presented on prevalence data, but also some notable differences worth discussing. Firstly, we notice different noise

distributions, diverging from Gaussian, that make the interpretation of the EWS performance more challenging. Secondly, we observe a higher correlation between residuals from ARIMA and other detrending methods, possibly linked to weekly trends being mostly driven by testing routines and being equally smoothed. Finally, we observe an improved performance for the skewness over the $\mathcal{Y}$ test set, which contrasts with the results of [132], but is more in line with what suggested in [473]. We speculate that this might be related to the interplay of the approach to the transition and the noise distribution, but we limit ourselves to report the observation and to leave additional theoretical and computational analysis to further studies. Overall, such analysis still stresses that EWS performance is sensitive to the underlying modelling assumptions and, if not assessed carefully, could hinder our capability to extend them in uncertain contexts. In addition, the fact that performances over prevalence or incidence data are slightly different underline how much the approaches relying on EWS depend on the quantities that are measured and use for EWS calculation. Hence, from a practical point of view, looking at a measure or another might make a difference for the monitoring efficacy.

In recognition that real epidemics might behave differently that what is commonly modelled, we nonetheless conclude that minimal dynamical models have the potential to predict relevant aspects of complex epidemics. While more detailed and complete multivariate models are being developed, macro-scale models based on complex systems theory can provide insights and indicators to detect epidemic re-emergence. On the one hand, our results begin supporting the theoretical literature findings and their basic assumptions; on the other, they warn against naive applications of summary statistics as EWS: if not correctly applied, they could return possibly misleading spurious signals. In addition, our findings call for future studies on forecasting techniques based on pattern recognition in different dynamical regimes. For instance, validated EWS could serve as basis for the feature selection of automated Machine Learning-based algorithms [424]. The dual synergy of theoretical predictions and empirical studies will continue to play a role in the field of epidemic control and will likely have a impact in informing public health decisions.

Author contribution

DP conceived and designed the study, collected the data, performed the analysis and interpreted the results. FK performed the analysis and interpreted the results. SM and JG supervised the project and interpreted the results. All authors wrote and approved the manuscript.

Declaration of interest

The authors declare no competing interests.

Acknowledgments

The authors thank the Research Luxembourg - COVID-19 Taskforce for mutual collaborations, and Professors P. Ashwin and A. Skupin for their useful feedback. DP's and SM's work is supported by the FNR PRIDE DTU CriTiCS, ref 10907093. FK's work is supported by the Luxembourg National Research Fund PRIDE17/12244779/PARK-QC. JG is partly supported by the 111 Project on Computational Intelligence and Intelligent Control, ref B18024.

Code availability

The analysis was performed in MATLAB and Python. They require the *Statistics Toolbox* and the *scipy* library, respectively. Code and curated data are accessible on: https://github.com/daniele-proverbio/EWS_epidemic.

Conclusion 4

EWS can detect disease re-emergence, in the case the condition of normal distribution and slow change rates are fulfilled. Minimal dynamical models are able to predict the main aspects of complex epidemics. EWS based on dynamical systems can be used to monitor the epidemic. EWS have the potential to assess the epidemic monitoring. The effect of different detrending methods which allow to emphasize the trends of EWS, are qualitatively and quantitatively investigated with ROC/AUC. In the application of summary statistics as EWS, be careful to correctly apply them otherwise the result could report misleading signals. In the case, the noise distributions is different from Gaussian, the interpretation of EWS is not clear.

CHAPTER 8

DISCUSSION AND CONCLUSION

The presented thesis has applied different mathematical concepts to open questions on the complex dynamics of the COVID-19 pandemic driven the different layers of complexity given by the properties of the SARS-CoV-2 virus, the COVID-19 disease, the host and the society behavior. In particular, Chapter 4 has focused on **(i)** *Mathematical modeling of suppression strategies against epidemic outbreaks*, Chapter 5 on **(ii)** *COVID-19 potential path towards herd immunity in Austria, Luxembourg and Sweden*, Chapter 6 has discussed **(iii)** *COVID-19 Crisis Management in Luxembourg: Insights from an Epidemionomic Approach*, Chapter 7 has discussed **(v)** *Performance of early warning signals for disease re-emergence* as a potential integrative framework.
The main conclusions can be summarized as follows:

(i) Mathematical modeling of suppression strategies against epidemic outbreaks. The SPQEIR model based on Susceptible-Exposed-Infectious-Recovered (SEIR) allows a quantification and a comparison of NPI effects' in various countries. The analyses allow to handle with the comeback of contagion and actual COVID-19 waves. The investigations prove that a rapid and strong lockdown leads to a similar mitigation effect as a combination of social distancing, lower isolation rates and early contact tracing.

(ii) COVID-19 potential path towards herd immunity in Austria, Luxembourg and Sweden. The developed extended SEIR model with the compartments hospitalization, ICU, undetected

cases, vaccination and death gives not just a reasonable fit to the epidemic dynamics, but makes consistent future projections. Besides the development of the model, the issue of model parameters identifiability is investigated. The model parameters are identified by a manual calibration and cross-validated by Bayesian inference. Various NPIs like reduction of social interaction and face masks were implemented at different stages of the pandemic with the goal to mitigate the spread of the pandemic. Social interaction is the key driver of the pandemic. The extended SEIR model leads to the estimation for the end of 2020 that 18.3% (7.2% detected and 11.1% undetected) of the population in Luxembourg had SARS-CoV-2; in Austria 9% (3.7% detected and 5.3% undetected) and 14.5% (3.5% detected and 11% undetected) in Sweden. The reproduction number of the extended model is calculated allowing for information about the threshold for reaching herd immunity. The analysis shows that if the vaccination speed of the period between December and 15 June 2021 is kept at the same level for the upcoming months and moderate values of social interaction lead to a reach of herd immunity until beginning of the autumn for Luxembourg whereas Austria and Sweden would not reach this until end of the year.

(iii) COVID-19 Crisis Management in Luxembourg: Insights from an Epidemionomic Approach. The Epidemionomic model for Luxembourg is a combination of an economical and an epidemiological model fitted to the first and second wave of COVID-19 in Luxembourg. The economical part is represented by an Input-Output model. The epidemiological part is described with a multi-sector SIR of 78 socio-demographic groups (19 industries of 4 countries, students and retirees). The economical forecast of the model for the GDP loss was too pessimistic for lockdown period and the direct impact on Luxembourg economy is small because, less than 2% of the population were infected at the same time. Higher economic costs where provoked due to the containment measures.

(iv) Performance of early warning signals for pandemic preparedness. EWS from the framework of critical transitions can detect disease re-emergence in the case the condition of normal distribution and slow change rates are fulfilled. Our results suggest a careful application of summary statistics of EWS because otherwise they may report misleading signals. Nevertheless, EWS have the potential to support epidemic monitoring and preparedness.

Overall, I analysed the different phases and aspects of the COVID-19 pandemic. Modelling analyses investigated various NPI and the effects of NPI synergies on the epidemic peak and case numbers. In order to reduce the spread of COVID-19, NPI such as lockdown and face mask measures were in place. The impact of the lockdown and of the second wave on the economy in Luxembourg was considered. COVID-19 puts a lot of pressure on the health care system. Therefore, my mathematical models with its reasonable projections support the pandemic preparedness of the society. Finally, I analysed the potential of EWS for epidemic monitoring.

8.1 Discussion

COVID-19 has been the enormous challenge in the last years around the world. In the beginning, the transmissibility mechanisms of COVID-19 was not clear. Asymptomatic cases play a crucial role in the spread of COVID-19 as they do not have symptoms, but are infectious and spread the virus to other people [285, 290]. The genetic code of SARS-CoV-2 changes over time during the replication [291]. The corresponding variants can lead to a virus that is more contagious or more/-less destructive [289]. In December 2020, vaccines became available protecting against severe outcome but unable to completely prevent infection particularity for specific virus variants [288]. In addition to newly appearing variants, waning immunity became an additional challenge during the COVID-19 pandemics [72].

Mathematical modelling represents an important tool for the analyses of COVID-19 spreading and supporting the political decision making process [140, 293]. Thereby, SEIR models and their extensions allow to simulate short- and medium-term modelling forecasts and to monitor the epidemic dynamics [292]. To monitor epidemic dynamics, SEIR models are widely used and adapted to the above mentioned specific challenges. Extensions of SEIR models with hospitalization and death compartments, are developed for various countries such as for example Italian regions [25] and Sweden [24]. Furthermore, agent-based models were developed to explore NPI scenarios [29]. Agent-based models have a large demand for computational processing and typically require large and detailed information for parametrization.

For the impact analysis of NPIs, flexible hierarchical Bayesian transmission models were used to

investigate the epidemic dynamics such as for 17 European countries [286]. The effect of NPI is analyzed with a combined SIR model and a Bayesian parameter inference [27]. Besides forecasts of the epidemiological dynamics, combinations of epidemiological models with macro-economic models were developed to analyse the costs of lockdowns and various exit strategies [268–271]. Similar to the results presented in Chapter 6, these studies show the strong interdependence of social interactions, infections and economic activity. The COVID Simulator is a mathematical model for the trend of the COVID-19 pandemic in federal states of Germany based on an extended SEIR model and applies Non-Linear Mixed Effects (NLME) approach [26] similar to the presented approach in Chapter 5. A major difference is the consideration of the age and gender structure of cases in the COVID Simulator which were only implicitly considered in my modelling approach by the corresponding adaptations of the hospitalization rates. Both approaches take into account the vaccination status, the percentage of the variants, the number of tests and positivity rates used to adjust the corresponding rate parameters defining the transitions from one compartment to the next one. Furthermore, the COVID Simulator also distinguishes between ventilated ICU and not ventilated ICU cases since this represented a potential bottleneck in Germany whereas in Luxembourg each ICU bed was equipped with a ventilation setup. A SIR based model showed that test-trace-and-isolate (TTI) can hold back the spread of COVID-19 **??**.

In Chapter 4, SPQEIR model does not have compartments for hospitalization of COVID-19 and shows just average trends. Furthermore, the simulation of the model allows only for measures in place for short-to-medium periods. Furthermore, asymptomatic cases are not considered in this model which can have a significant effect on the spreading dynamics. Nevertheless, the overarching results are in line with independent investigations [27, 286]. The SEIR-ICU model in Chapter 5 was developed in the early phase of the vaccination development and does therefore not consider reinfections or virus-variant specific changes and assumes vaccination efficacy of 100% since corresponding data were not available yet. Therefore, the model does not reflect the detailed dynamics observed later during the pandemic but, provided a more general analysis on the interplay between social interactions, vaccination rate and herd immunity. Despite the fact that the age structure has an impact on hospital admission, the age structure could not considered explicitly in the model due to some initial concerns on data security but was taken into account implicitly

by adaptation of the corresponding hospitalization rate obtained from the data. Hence, potential changes in the age-structure could be investigated by changing the overall hospitalization risks by a weighted average and compared with models considering the age structure explicitly [26].

The epidemionomic model presented in Chapter 6, does neither take hospitalization or vaccination or reinfections into account. While hospitalization would not have a direct impact on the economic analysis since positive cases are in isolation anyway and therefore unable to contribute to the economic activities, reinfections and vaccinations could have a significant impact on the overall dynamics. However, that major aim of the model was to investigate short-to-midterm effects of the initial lockdown period where reinfections would not contribute significantly. Obviously, vaccination can have a strong impact on the epidemionic dynamics but were not yet available when the model was developed and could now be incorporated by a corresponding reduction in the infection rate based on recent data. Despite these limitations, the results are in line with other studies [268–271] where the specific properties of the Luxembourg economics with the high amount of remote working capacity has led to general lower economic burden.

In Chapter 7, the potential of early warning signals (EWS) for pandemic preparedness were evaluated. The underlying idea of EWS is based on generic properties of complex systems with alternative states where changes in fluctuations of the system output can indicate a transition towards another dynamical regime [119]. While the concept of EWS is a rather appealing framework to predict arising epidemic waves, the analysis showed that the power of such predictions is limited by the data quality including the negligence of undetected cases, the resulting uncertainties and a reliable estimation of the lead time. Based on the assessment with real-world data, the analysis shows that under specific circumstances, EWS may gives an indication of a transition within a 2 weeks period. However, for other cases with noisy data, the approach can also miss upcoming epidemic waves. Hence, further analysis is needed to clarify the applicability and required data quality of EWS-based methods for pandemic preparedness.

8.2 Remaining challenges and outlook

Besides the challenges addressed in the thesis above, the COVID-19 pandemic constantly led to additional open questions at different levels. As COVID-19 is not just be transmitted by symptomatic carriers, but as well by asymptomatic carriers [285, 290], the government of the Grand-Duchy of Luxembourg implemented a large scale testing program that started on 25 May 2020 and ended on 30 September 2021 to detect such asymptomatic cases and break infection chains. This has led to the question to what extend such a mass screening platform can mitigate the pandemics. On 28 December 2020, the vaccine campaign started in Luxembourg. Importantly to mention, vaccination does not prevent SARS-CoV-2 infection, but it decreases the probability of COVID-19 severe outcomes. With the availability of vaccines, the question arose about quantification of the efficacy of the vaccines and how they can contribute to mitigation strategies. Additionally, the effect of waning immunity was observed in old people six months after vaccination [432] for the earlier virus variants and also for younger people and on shorter periods for later virus variants. Thus, recent research shows that the concept of herd immunity may not apply due to new variants coming up and related waning immunity [72]. For this purpose, I investigated the effects of the vaccines in relation to the different variants. These variants can change in a way that the virus spreads easier or that the disease gets less or more severe. Also the establishment of the CovidCheck regime was the starting-point of the discussion for the introduction of a mandatory vaccination. Therefore, I performed simulations to investigate the impact of a mandatory vaccination for 50+ people. Finally, I co-implemented a COVID-19 Wastewater Analyser method (CoWWAn) that assess epidemic dynamics and monitor the COVID-19 situation based on virus prevalence measured in wastewater which might represent a powerful tool for pandemic preparedness [314].

The open questions at the beginning of the pandemic are treated in the Chapter 4- 7. The additional challenges investigated in the context of the COVID-19 pandemic such as the second phase of large-scale testing, wastewater sampling for monitoring the epidemic status, waning immunity, vaccine efficacy and new variants are summarized in the Fig. 8.1 and briefly discussed below.

Figure 8.1: The different challenges investigated during the pandemic in Luxembourg. The images are taken from PowerPoint stock images Version 16.59

8.2.1 Large-scale testing

The peculiarity of Luxembourgish COVID-19 crisis management was the introduction of a Large-scale testing (LST). The LST is a population-wide (including cross-border workers) voluntary rRT-PCR-testing [4]. The testing was accompanied by contact tracing. In the case of a positive test result, the person was put into isolation and her/his last 48 hours contacts were traced and put into quarantine, too. The aim was to improve the removing of lockdown measures and to prevent a second wave during the opening. Moreover, the testing allowed to detect asymptomatic cases who continued spreading the virus in the population. The first phase led by the COVID-19 Task Force lasted from 25 May to 15 September 2020 and the second phase led by the Ministry of Health from 15 September 2020 to 30 September 2021. The analysis of the first phase showed that the participation rate was around 49% for residents and 22% for cross-boarder commuters. Due to mass screening, 1099 cases were detected with 850 index cases and 249 cases via contact tracing during the first phase [5].

In order to better understand the impact of second phase LST, I set up a SEIR-model, based on [352].

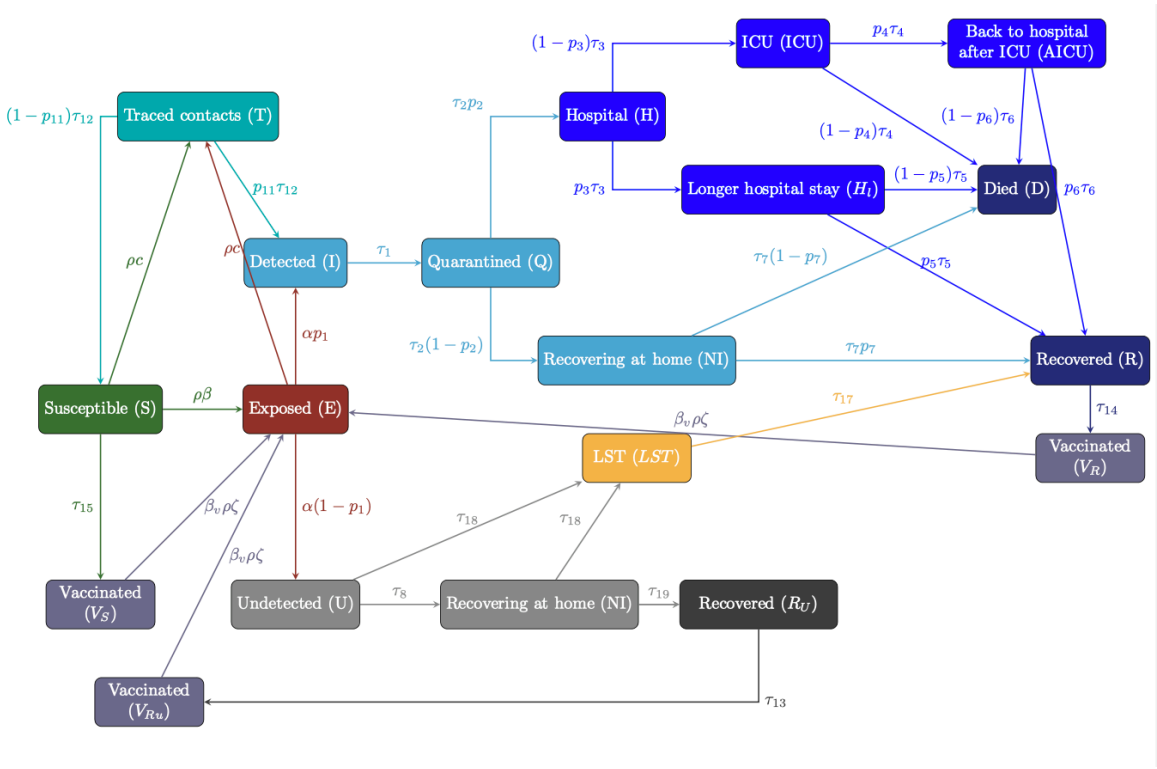

Figure 8.2: Scheme of the mathematical model for the impact analysis of Large-scale testing in Luxembourg.

The mathematical model of COVID-19 transmission is included in addition to the different possibilities to get tested like large-scale testing and tested due to contact with a positive person [352]. The traced contacts compartment takes into account all the people who were in contact with a positive case within the last 48 hours. Those people get quarantined for 5 days and then tested. The vaccination is not 100% effective in preventing a person from getting infected. The total population N of Luxembourg is at every time t in one of the 19 compartments. Like in the standard SEIR model, the common compartments are susceptible (S) and exposed (E). An exposed person can either become detected meaning entering the "infectious and detected" (I) compartment or is undetected (U). After being detected, the person needs to quarantine (Q) and then either requires hospitalization (H) or simply stay at home for recovering (NI). If the health of the person gets worse, the individual goes to "ICU" (ICU) otherwise simply "requires longer hospitalization" (H_l). In the stage of ICU, the person's health can improve which lead to entering the compartment "Back to hospital after ICU" ($AICU$) or otherwise can die (D).

From the compartment "Long hospital stay" (H_l), as well as from the compartment (NI), the individual can either recover (R) or die (D). The idea of LST is to detect asymptomatic carriers who just recover and do not need hospitalization. In order to take contact tracing into account, a compartment "traced contacts" (T) is included in the model. As of 28 December 2020, vaccines got available. Therefore, the susceptible (S), the recovered undetected (V_{RU}) and recovered detected (V_R) could get a vaccination from that day on based on the corresponding rates. The total population size N is conserved (birth is neglected):

$$N = S+E+I+Q+H+H_l+ICU+AICU+NI+D+T+R+U+LST+V_S+V_{RU}+V_R \ . \quad (8.1)$$

The parameter p_i represents a probability to go from one compartment to another. The parameter τ_i is a rate and the inverse of the average stay in a compartment. The social interaction is given by $\rho(t)$ as a step-wise function changing in time in order to take changing NPIs into account. A $\rho(t) = 1$ corresponds to the social interaction before the pandemic and changes in $\rho(t)$ are given by the Table E together with the potential explanation for it.

The model is fitted to time-series data from 24 February 2020 to 14 October 2021 by manual calibration. The time-series data is displayed in Fig. 8.3 for daily new cases (**A**), hospital occupation (**B**), ICU occupation (**C**), traced contacts (**D**), positive traced contacts (**E**) and positive large-scale tests (**F**).

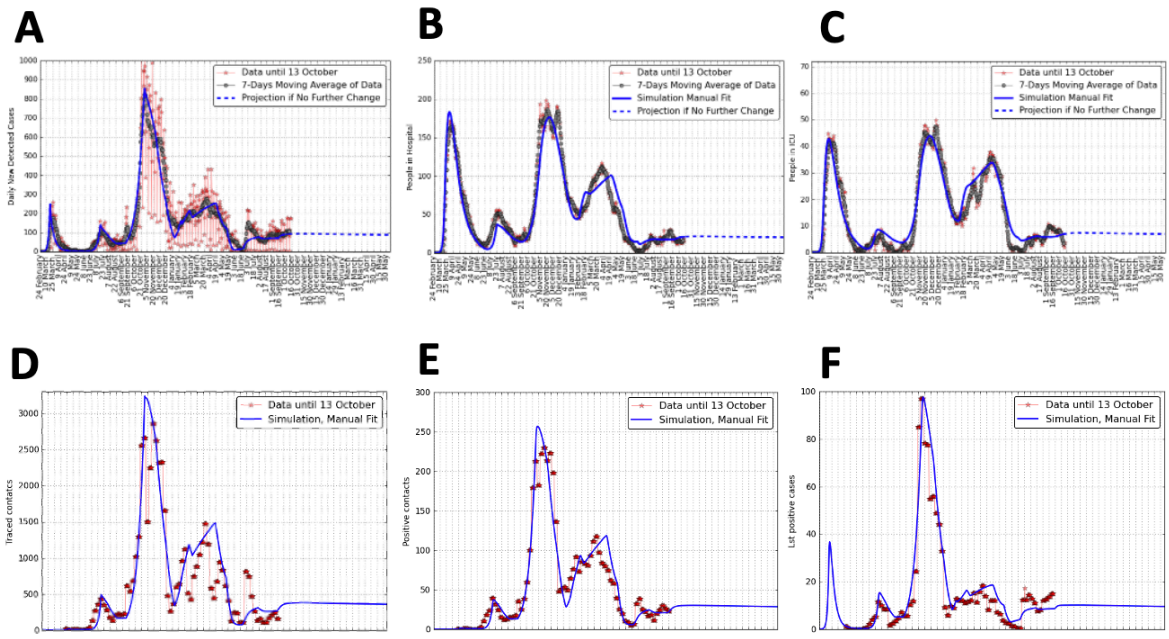

Figure 8.3: Data, model simulations and projections of daily cases (**(A)**), hospital occupation (**(B)**), ICU occupation (**(C)**), traced contacts (**(D)**), positive contacts (**(E)**) and positive LST results (**(F)**).

Due to large-scale testing, 7,610 index cases were identified during the two phases. In total 344,138 people were contact traced with 29,929 people being a secondary case from 20 April 2020 to 13 September 2021. That corresponds to 9% of the contact traced cases were positive. On average 42% of cases came from contact tracing. Therefore, a good working contact tracing is essential to mitigate the spread of infectious diseases and break infection chains.

8.2.2 COVID-19 Wastewater Analyser (CoWWAn) method used for the assessment of COVID-19 dynamics [1]

CoWWAn (COVID-19 Wastewater Analyser) is a method to estimate epidemic dynamics from cost-effective SARS-CoV-2 viral load measurements in wastewater and allows the estimation of the future epidemic dynamics. It is based on a SEIR model integrating time course data by an

[1]The section "COVID-19 Wastewater Analyser (CoWWAn) method used for the assessment of COVID-19 dynamics" is based on Daniele Proverbio, Françoise Kemp, Stefano Magni, Leslie Ogorzaly, Henry-Michel Cauchie, Jorge Gonçalves, Alexander Skupin, Atte Aalto. Model-based assessment of COVID-19 epidemic dynamics by wastewater analysis. Science of The Total Environment,2022, 154235, ISSN 0048-9697, https://doi.org/10.1016/j.scitotenv.2022.154235.

Extended Kalman filter (EKF). The SEIR-based model combines noisy wastewater data with the number of daily cases and can thereby estimate the dark number of cases if appropriate calibrated. The compartments in the model correspond again to Susceptible S(t), Exposed E(t), Infectious I(t) and Recovered R(t). The total population N is again assumed to be constant $N = S+E+I+R$. Transmission and viral sheeding is modelled by a stochastic SEIR model in which each transition between compartments is given by a random process described by

$$\begin{cases} \frac{d}{dt}S(t) = \frac{-\beta(t)S(t)I(t)}{N} - \sqrt{\frac{\beta(t)S(t)I(t)}{N}}w_1(t) \\ \frac{d}{dt}E(t) = \frac{\beta(t)S(t)I(t)}{N} - \alpha E(t) + \sqrt{\frac{\beta(t)S(t)I(t)}{N}}w_1(t) - \sqrt{\alpha E(t)}w_2(t) \\ \frac{d}{dt}I(t) = \alpha E(t) - \tau I(t) + \sqrt{\alpha E(t)}w_2(t) - \sqrt{\tau I(t)}w_3(t) \\ \frac{d}{dt}R(t) = \tau I(t) + \sqrt{\tau I(t)}w_3(t)\ , \end{cases} \tag{8.2}$$

where α^{-1} is the mean incubation and w_j is white noise process. The rate β is estimated by the Kalman filter and changes over time to take into account changes in social interactions (such as masks, lockdown, $\cdots$). The additional compartment $A(t)$ stands for viral flows into wastewater and allows to investigate the effective number of sheeding cases by

$$\frac{d}{dt}A(t) = \frac{\beta(t)S(t)I(t)}{N} - \gamma A(t) + \sqrt{\frac{\beta(t)S(t)I(t)}{N}}w_1(t) - \sqrt{\gamma A(t)}w_4(t)\,. \tag{8.3}$$

The rate γ combines the properties of the virus and information about wastewater sampling for each region. The CoWWAn method allows to calculate the effective reproduction number R_{eff} which gives information about the number of secondary cases an infectious person causes on average [157] and is given by the following extrapolated formula [352]:

$$R_{\text{eff}} = \frac{\beta(t)}{\tau}\frac{S(t)}{N}\,, \tag{8.4}$$

with $\beta(t)$ and $S(t)$ corresponds to the state estimates. For the model, the following data are needed: data of COVID-19 RNA load in wastewater, COVID-19 cases linked to the area covered by the sewage system, and possibly the estimates about the ratio of detected versus true case

numbers. The model is applicable to different data sets with various normalisation protocols for wastewater. The approach puts the measurements from real world into SEIR model via the EKF and is displayed in Fig 8.4. In every time step, from the projections of old state with SEIR model, the new state is forecasted and the predicted measurement is estimated by the measurement model of the new state estimate. The difference between the data and model-predicted measurement leads to an update of the state estimate.

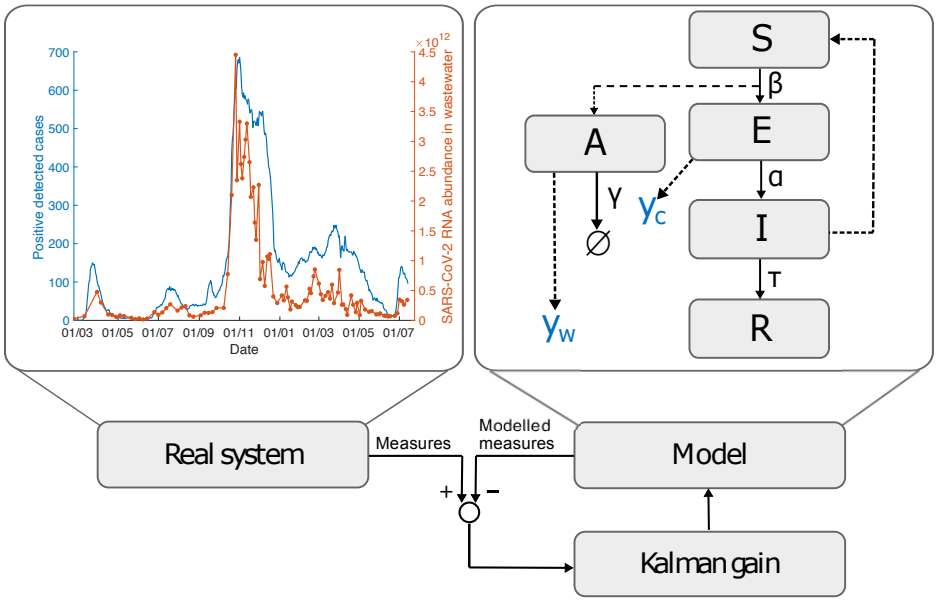

Figure 8.4: The workflow of the model according to [314]. The approach puts the measurement from real world into an SEIR model by an EKF. In blue the smoothed moving average of daily positive cases is shown , and in orange the wastewater sampled data with unit of measure of RNA copies/day/10.0,000 equivalent inhabitants (example for Luxembourg) are shown.

The model comes with a number of free parameters to be estimated by the EKF given in Table 8.1 with a short description. To assess the potential of CoWWAn for pandemic monitoring, the short term predictions of the epidemic model are investigated. In order to predict the future behaviour, model is simply simulated further based on the last state of paramterization. Fig 8.5 exhibits an example of such a short term simulation for Luxembourg. It displays detected cases in blue compared to the predicted case numbers from the wastewater data in orange or from case number data in yellow. The correlation between wastewater predictions and case projections is $\rho = 0.95$ and for real case data $\rho = 0.94$. In conclusion, the CoWWAn method has the potential to assess

Symbol	Explanation	Value
α	Rate $E \to I$	0.44 d^{-1}
τ	Rate $I \to R$	0.32 d^{-1}
$\beta(0)$	Initial infectivity	0.44 d^{-1}
Δt	Time step length	0.1 d
$q_{\beta,1}$	Variance of $\beta(t+1) - \beta(t)$ when $t \leq 30$	0.05^2 d^{-2}
$q_{\beta,2}$	Variance of $\beta(t+1) - \beta(t)$ when $t > 30$	0.005^2 d^{-2}
κ	EKF sensitivity parameter	4
N	Population size	634,730
γ	Rate $A \to \varnothing$	1.62 d^{-1}
ν	Ratio of y_w/A	$6.40 \cdot 10^4$
ε	Exponent in nonlinear mapping of WW data	0.613
U_W	Measurement error variance of wastewater data	$1.75 \cdot 10^{12}$
$E(0)$	Initial size of E-compartment	8
$I(0)$	Initial size of I-compartment	11

Table 8.1: CoWWAn model parameters with their description and values as well as references. The parameter $\beta(t)$ is adjusted after 30 days in order to take into account for sudden changes in the start of the pandemic. d denotes "days".

the epidemic status and reconstruct the detected case curves from wastewater. It is a powerful and cost-effective approach to give information of the actual evolution of the pandemic and an alternative to large scale testing routines. The method is not just applicable to Luxembourg, but was also successfully applied to 11 additional data sets from areas of Europe and North America (Barcelona,Kitchener, Kranj, Lausanne, Ljubljana, Milwaukee, Netherlands, Oshklosh, Raleigh, Riera and Zürich). During the pandemics, in more than 50 countries and 260 universities the monitoring of the wastewater has been implemented demonstrating its potential for pandemic preparedness.

8.2.3 Vaccine efficacy and immunity waning[2]

The vaccine campaign in Luxembourg started on 28 December 2020. The vaccination strategy was divided into 6 phases [296] and until 3 March 2022, four different vaccines were available: Pfizer BioNTech, Moderna, AstraZeneca Oxford and Janssen JJ. Starting from the week of 3 March

[2]The section "Vaccine efficacy and immunity waning" is based on a paper entitled "Vaccine efficacy estimation" written by Atte Aalto, Françoise Kemp, Paul Wilmes, Jorge Gonçalves and Alexander Skupin.

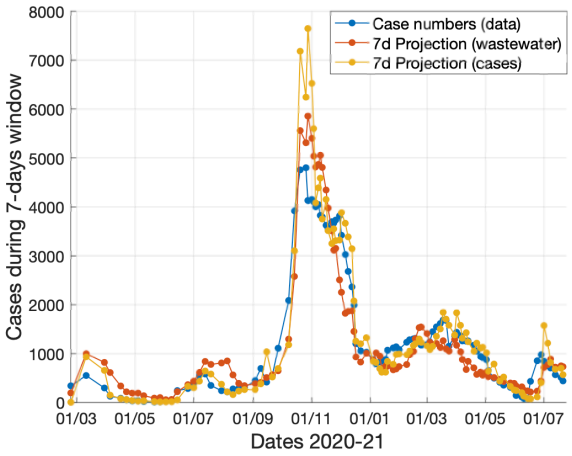

Figure 8.5: CoWWAn predictions for Luxembourg.

2022, the additional vaccine Novavax was available. The first phases started on 28 December with health care workers, residents from retirement and nursing homes and people with disabilities living in facilities. On December 28, 29, and 30, approximately 430 health care worker were invited to get vaccinated each day [73]. The second phase was the phase of the age category 75+ and highly vulnerable people. The age range from 70-74 years represented the third phase of the vaccination strategy. The fourth phase consisted of the age category from 65 to 69 years and the fifth was considering the age range from 55-64 years. The last category was the general population meaning from 16 to 54 years old. In Luxembourg, the period between the first and the second dose is 28 days.

In the following, fully vaccinated refers to two doses for Moderna, Pfizer BioNTech and AstraZeneca or one dose for Janssen JJ. In June 2021, the question about the efficiency of the vaccines was raised based on data from Luxembourg. In order to investigate that question, a Bayesian risk ratio estimate was used and allowed the calculation of age-specific and vaccination-status dependent efficacies (Fig. 8.6).

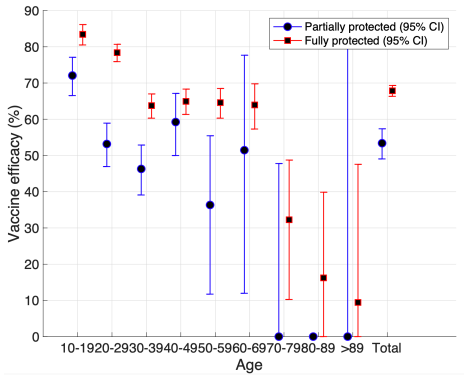

Figure 8.6: Vaccine efficiency of the period from 27 June 2021 to 17 October 2021 where the Delta variant was the dominant virus variant.

The vaccine efficacy for 2 doses is for the period from 27 June to 17 October 2021 around 68% for the total population of Luxembourg. Furthermore, the vaccine efficiency for 1 dose for the total population is around 53%. The analysis covers the period when the Delta variant was the most abundant variant.

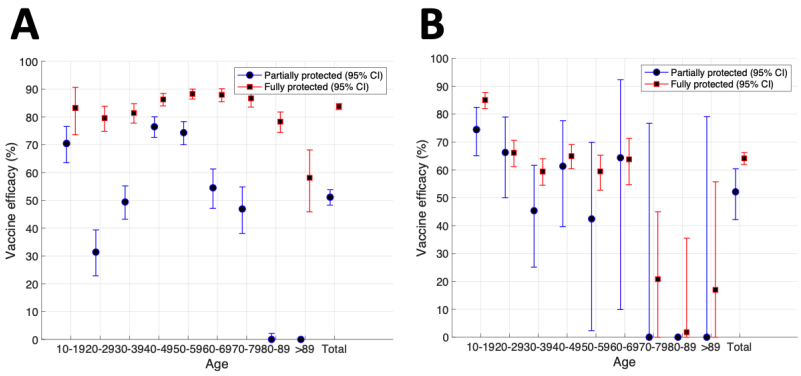

Figure 8.7: Vaccine efficiency of the period from 7 February to 15 August 2021 and from 22 August to 17 October 2021.

An additional challenge arose by the immunity waning after infection as well as after vaccination. During the period from 7 February to 15 August 2021, vaccine efficacy for the fully vaccinated population was 83.7%. The vaccine efficacy from 22 August to 17 October 2021 was 64.1% for the fully protected total population. The plots in Fig. 8.7 show that immunity against COVID-19 is waning.

An observed phenomenon is the increasing number of reinfections where only two positive tests

occurring within a period of 90 days were considered as reinfections by the Ministry of Health in Luxembourg.

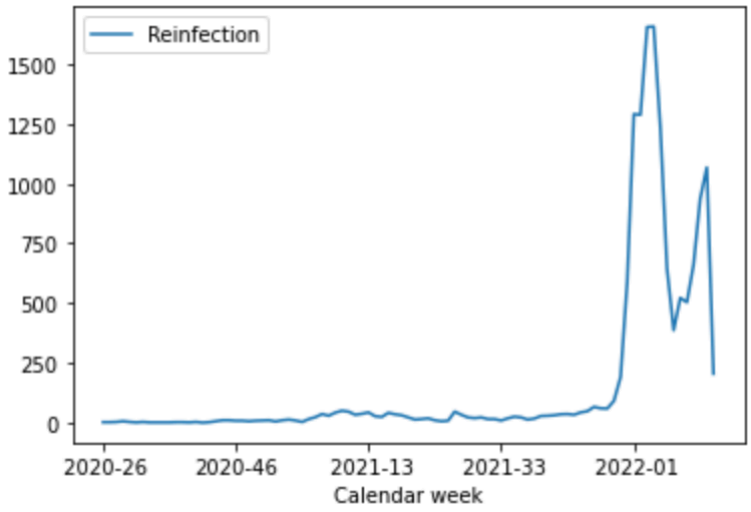

Figure 8.8: Number of reinfections from week 26 in 2020 to week 13 in 2022 (based on [315])

According to Ministry of Health in Luxembourg, 15,357 reinfections happened from week 26 in 2020 to week 13 in 2022. Overall, 114 people are known to have three episodes of infections with COVID-19 [315].

8.2.4 Simulation for mandatory vaccination in the context of potential future epidemic rebounds [3]

For the investigation of the future development of the COVID-19 epidemic in Luxembourg, the feedback of two experts in viral evolution, namely Prof. Dr. Richard Neher from the University of Basel and Prof. Dr. Tom Wenseleers from the University of Leuven, were considered. The feedback led to three potential variant scenarios discussed below. The three considered scenarios, are a variant descending from the Omicron variant, a variant descending from the Delta variant and a variant combining properties from the Delta and Omicron variants by recombination. One of

[3] The section "Simulation for mandatory vaccination in the context of potential future epidemic rebounds" is based on the report of Research Luxembourg COVID-19 Task Force of 2 March 2022 entitled "Scenarios reflecting the future development of the COVID-19 epidemic in Luxembourg" written by Françoise Kemp, Atte Aalto, Paul Wilmes, Jorge Gonçalves and Alexander Skupin.

three scenarios is likely to happen in the future, even if the probabilities cannot be well estimated. The limitations of the scenarios are the immunity status, as it depends on the vaccine efficiency, and the immunity waning. The model used for the scenarios is based on an extended SEIR model similar to the model used in Chapter 5 fitted to data from Luxembourg and taking into account the effect of vaccination and immunity waning. In the model, the population is divided into two groups, a low-risk and a vulnerable group. Given the data from Luxembourg, 73% of the population and 84% of the vulnerable group are vaccinated. Furthermore, 54% of the population and 76% of vulnerable group took a third dose until March 2022. The vaccine effectiveness is given by the following table:

	Effectiveness against transmission		Effectiveness against hospitalization	
	delta	omicron	delta	omicron
2 doses <5 month	68%	43%	87%	77%
2 doses >5 month	57%	4%	70%	65%
3 doses <5 month	86%	48%	85%	75%
3 doses >5 month	57%	4%	70%	65%

Table 8.2: Vaccine effectiveness based on [429]

Hospitalization dropped by 69% for the low-risk group and 60% for the vulnerable group for the Omicron variant versus Delta variant. Entering ICU has dropped by 85% for low-risk group and by 72% for the vulnerable group, for the Omicron variant versus the Delta variant. For the simulation of the mandatory vaccination of vulnerable people, 30,000 people needed to get vaccinated and 110,400 people needed a third dose which were given from May on for the first dose and 28 days later the second dose with a rate of 15,000 doses per week. Additionally, a scenario is simulated in which 85% of the whole population is fully vaccinated with 3 doses. The rebound has to be anticipated for autumn 2022 linked to immunity waning and increased indoor activities.
For the three different variant scenarios (Omicron descendant, Delta descendant and a Deltacron variant), the model considers immunity waning, effectiveness of the vaccine against severe outcome and infection and transmissibility of each variant based on the Luxembourg data.

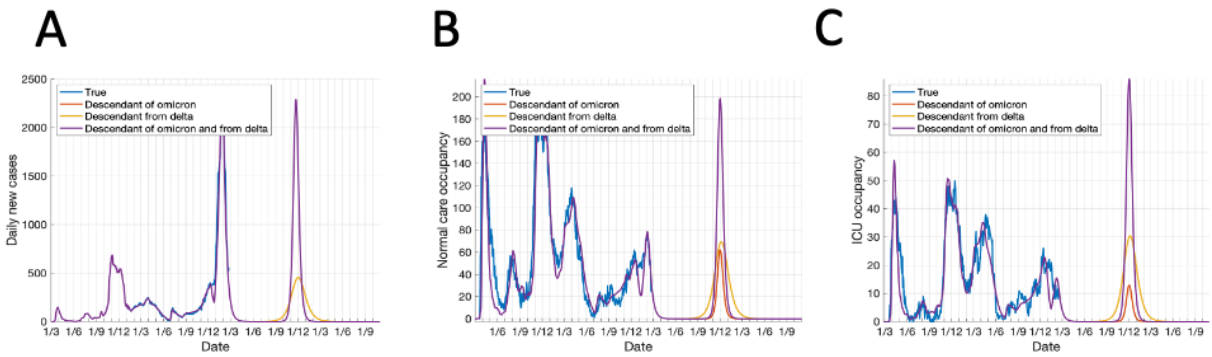

Figure 8.9: Projections for the three possible scenarios with different variants such as Omicron (orange), Delta (yellow) and Deltacron (purple). Daily cases (Panel **A**), normal care occupancy (Panel **B**) and ICU occupancy (Panel **C**) are shown.

	Cases	Hospital	ICU
Descendant of omicron (baseline)	70,960	7069	1974
Descendant from delta	37,846 (-46.7%)	10,268 (+45.3%)	3803 (+92.6%)
Recombinant of omicron and delta (Deltacron)	70,960 (0%)	11,294 (+59.8%)	4243 (+114.9%)

Table 8.3: Table for the qualitative assessment of the effect of the three potential variant scenarios.

The omicron scenario is the most optimistic one and is based on the appearance of a new sub-lineage of the actual omicron variant. Due to the reduced hospitalization risk, the impact on the healthcare system would be rather small. By contrast, the scenario for a descendant of the Delta variant exhibits a higher impact on the healthcare system.

The scenario of Fig. 8.10 has as baseline a descendant of the Delta variant. The yellow curve is the mandatory vaccination of 18+ and the projection for mandatory vaccination of 50+ is purple.

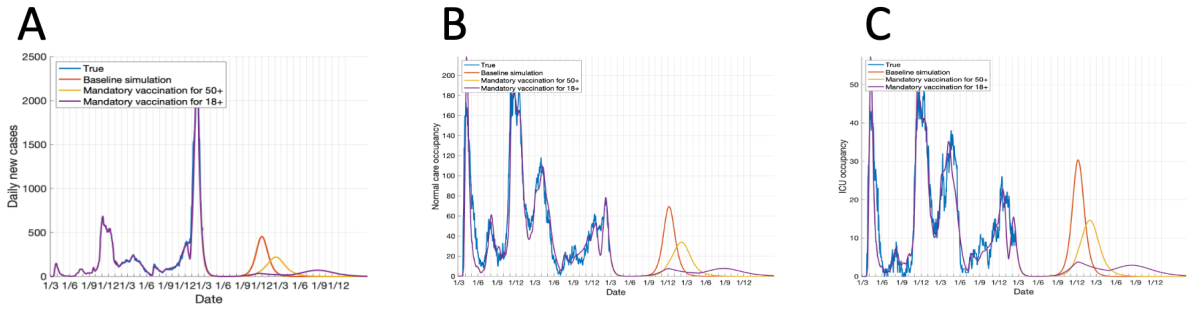

Figure 8.10: Projections for a descendant of the Delta variant (orange), projections for a descendant of the Delta variant with mandatory vaccination for 50+ (yellow) and projections for a descendant of the Delta variant with mandatory vaccination for 18+ (purple). Daily cases (Panel **A**), normal care occupancy (Panel **B**) and ICU occupancy (Panel **C**) exhibit the effect of a vaccine mandate.

	Cases	Hospital	ICU
Baseline simulation	37,846	10,268	3803
Mandatory vaccination 50+	29,809 (-21.2%)	9073 (-11.6%)	3242 (-14.7%)
Mandatory vaccination 18+	23,104 (-39%)	7839 (-23.7%)	2727 (-28.3%)

Table 8.4: Table for the quantitative assessment of the effect of mandatory vaccination for people above 50 years and a scenario for mandatory vaccination for people above 18 years for a Delta variant descendant.

The mandatory vaccination of 50+ in the case of delta descendant leads to a reduction of 21.2%in cases, 11.6% in number of hospitals, 14.7% in number of ICU in comparison to the baseline. The mandatory vaccination of 18+ in the case of delta descendant leads to a reduction of 39% in cases, 23.7% in number of hospitals, 28.3% in number of ICU in comparison to the baseline.

The scenario of Fig. 8.11 has as baseline a descendant of the omicron variant. Omicron is less severe than the Delta variant which has a small impact on the healthcare system. However, it is more virulent. The yellow curve is the mandatory vaccination of 18+ and the projection for mandatory vaccination of 50+ is purple.

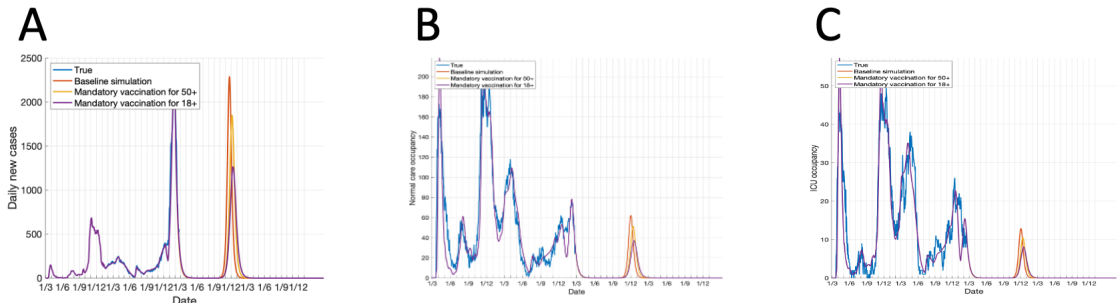

Figure 8.11: Projections for a descendant of the Omicron variant (orange), projections for a descendant of the Omicron variant with mandatory vaccination for 50+ (yellow) and projections for a descendant of the Omicron variant with mandatory vaccination for 18+ (purple). Daily cases (Panel **A**), normal care occupancy (Panel **B**) and ICU occupancy (Panel **C**) are shown.

	Cases	Hospital	ICU
Baseline simulation	70,960	7069	1974
Mandatory vaccination 50+	67,036 (-5.5%)	6947 (-1.7%)	1939 (-1.8 %)
Mandatory vaccination 18+	58,950 (-16.9%)	6735 (-4.7%)	1908 (-3.3%)

Table 8.5: Table for the quantitative assessment of the effect of mandatory vaccination for people above 50 years and a scenario for mandatory vaccination for people above 18 years for an Omicron descendant variant.

The mandatory vaccination of 50+ in the case of an Omicron descendant leads to a reduction of 5.5%in cases, 1.7% in number of hospitals, 1.8% in number of ICU in comparison to the baseline. The mandatory vaccination of 18+ in the case of Omicron descendant leads to a reduction of 16.9% in cases, 4.7% in number of hospitals, 3.3% in number of ICU in comparison to the baseline. Aside from Omicron and Delta variant, possible recombination of variants can arise and lead to a mixture of the insides shown above. Overall, these additional investigations demonstrate how specific challenges can be addressed by targeted approaches. Furthermore, the different analyses show that there are remaining and future COVID-19 challenges ahead of us which will require further interdisciplinary approaches to support mitigation strategies until we eventually reach an endemic regime. And even then, long-COVID symptoms [281–283] may have a long-term impacts on the healthcare systems the consequences of which can currently only be roughly estimated. Hence, COVID-19 is likely to stay in the scientific focus for some more time also beyond the

hopefully past emergency period.

8.3 Final remarks

To conclude, I showed that mathematical modelling can be used for pandemic preparedness and to understand the spread of COVID-19 through populations. Mathematical modelling can guide the epidemic progression and public health measures. Modelling became a key tool to monitor the epidemic dynamics and to inform decision-makers about potential various future scenarios. Epidemiological modelling is an interdisciplinary task since it implies discussions with immunologist about immune response and with virologists about the potential upcoming variants.

I am very grateful to be part of the COVID-19 Task Force which made my PhD a unique experience. During COVID-19, I saw how mathematical modelling could be used in practice to guide policymakers' decisions based on the soundest information possible. I learned so much about interdisciplinary and team-based research in quite a short amount of time due to the urgency of the pandemic.

APPENDIX A

APPENDIX OF MATHEMATICAL MODELLING OF SUPPRESSION STRATEGIES AGAINST EPIDEMIC OUTBREAKS

Effects of τ on epidemic curves properties

In the main text, we focused the conceptual analysis on the sensitivity of epidemic dynamics on mitigation parameters. However, it is well known that early adoption of interventions is also important [184]. In the SPQEIR model, the delay in applying interventions is modeled by an extra parameter τ. In this section, we analyse its impact on qualitative and quantitative properties of epidemic curves.

We observe that, for all mitigation parameters, τ does not significantly alter the qualitative properties of epidemic dynamics: their corresponding diagrams "height of peak vs param" is maintained, as well as the trend of mitigation timing. Instead, τ affects their quantitative aspects: the height of the peak before mitigation and the values of mitigation timing $\mathbb{T}$. Overall, this justifies the use of an arbitrary value for τ for the conceptual analysis (Sec. 3.1 in Main Text), whereas it was properly estimated for each country when the fit was performed (Sec. 3.3 in Main Text).

Combining τ and ρ

Different delays in issuing interventions governed by the parameter ρ display the same diagram "height of peak vs ρ", with the same critical value of the parameter $\rho = 0.4$ that yields mitigation (Fig. A.1). Instead, τ modifies the peak value that is reached before mitigation, for $\rho < 0.4$. When considering the mitigation timing, Fig. A.1 (Right) shows that its non-monotonous trend is overall not altered by τ. However, the maximum time decreases, since longer delays are associated to a higher depletion of the Susceptible pool. On the other hand, the optimal value for minimising the mitigation time becomes smaller, meaning that stronger measures are required to flatten the curve in minimal time.

This analysis implies that, while qualitative characteristics associated to the epidemic dynamics are conserved, quantitative values change under the influence of τ, that should therefore be taken into account when studying real-world scenarios.

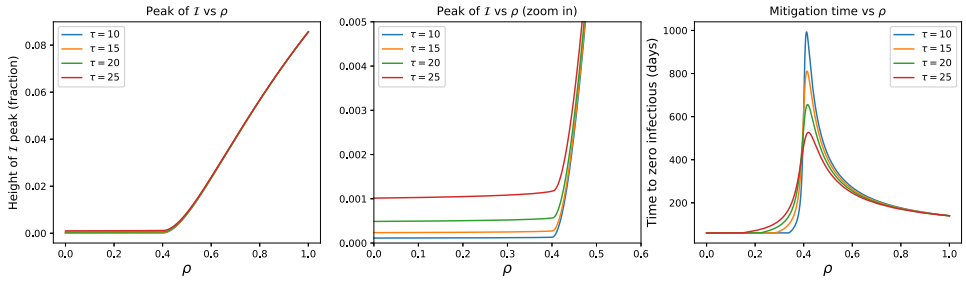

Figure A.1: (Left) Global dependence of the peak of daily cases on ρ, for different τ values. (Center) A closer look on the infectious peak, depending on ρ values associated to mitigation and on delays τ. Although the qualitative trend is maintained, the peak values change for different τ. (Right) Mitigation timing depending on ρ, for different τ. To minimise the timing, a smaller τ can be coupled with higher ρ, whereas longer delays require smaller ρ values to be as efficient.

Combining τ and μ

When mitigation is pursued after acting on those measures associated to the parameter μ, time delays are associated with higher peaks of the infectious curve (Fig. A.2 Left and Center), but the trend is conserved. The mitigation timing might be slightly reduced when small μ values are active but, for stronger protection rates, it is significantly decreased by prompt interventions (Fig. A.2 Right).

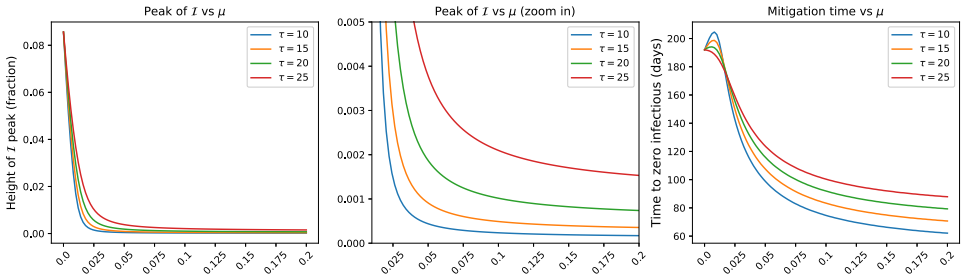

Figure A.2: (Left) Global dependence of the peak of daily cases on μ, for different τ values. (Center) A closer look on the infectious peak, depending on μ values associated to mitigation and on delays τ. The qualitative, monotonous trend is maintained, but the peak values change for different τ. (Right) Mitigation timing depending on μ, for different τ. For small μ values, a longer delay could yield faster mitigation because of the faster depletion of the Susceptible pool, but the trend is soon inverted for higher μ values.

Combining τ and χ'

This section considers the removal of E individuals from the epidemic system, for instance because of quarantining after contact tracing. In the SPQEIR model, this strategy is modelled by the parameter χ' (see Main Text for discussion). Longer delays in issuing such interventions do not alter the global features of the bifurcation diagram, but are associated with higher peak values (Fig. A.2 Left and Center). Longer delays are also associated with faster mitigation timing, due to the fact that more people have the chance to develop the infection. The trade-off is resolved when employing the most effective measures (maximum χ'), which yields minimal peak height as well as shortest mitigation timing.

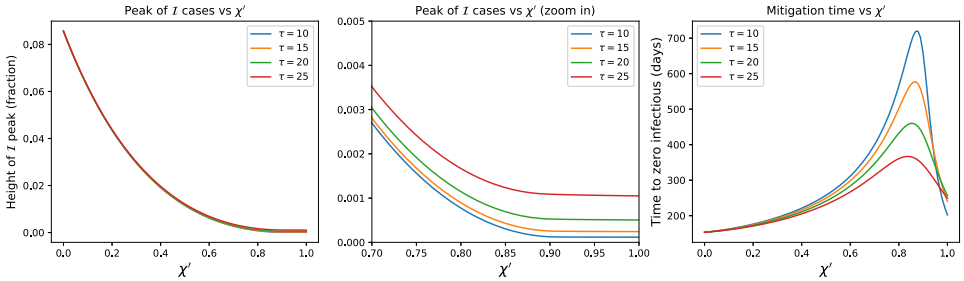

Figure A.3: (Left) Global dependence of the peak of daily cases on χ', for different χ' values. (Center) A closer look on the infectious peak, depending on χ' values associated to mitigation and on delays τ. The bifurcation diagram is maintained, but the peak values after mitigation change for different τ. (Right) Mitigation timing depending on χ', for different τ.

Combining τ and η

In the SPQEIR model, further removal of Infectious individuals (e.g. for tracking and isolation) is parameterised by η. As for other parameters, the qualitative behavior of the epidemic dynamics, when driven by η, remains unaltered by extra delays τ. As shown in Fig. A.4, the bifurcation diagram remains consistent, even though the quantitative values of mitigated peaks are higher for higher τ. However, contrariwise with what observed for other parameters, delays in issuing measures slightly change the critical η values that are necessary to achieve mitigation (Fig. A.4, Center), that are lowered for higher τ. This is a byproduct of having let the virus spreading more in the population and resulting in a higher initial peak. In addition, longer delays correspond to overall longer mitigation timing for same η (Fig. A.4, Right). This expands what discussed e.g. in [180], further stressing the importance of prompt isolation of infectious individual for epidemic management and control.

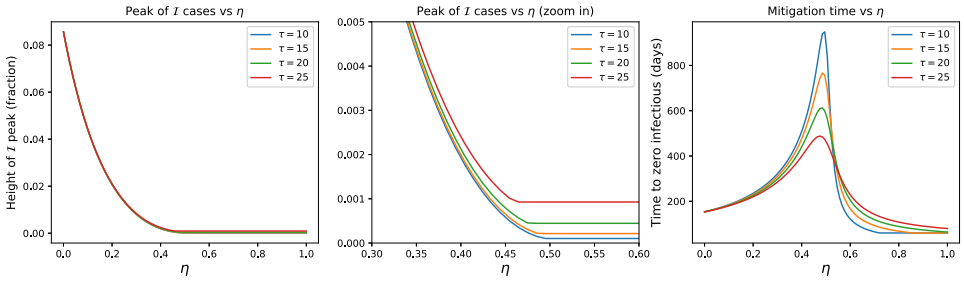

Figure A.4: (Left) Global dependence of the peak of daily cases on η, for different τ values. (Center) A closer look on the infectious peak, depending on η values associated to mitigation and on delays τ. The bifurcation diagram is maintained but the critical value is slightly shifted. Peak values after mitigation change for different τ. (Right) Mitigation timing depending on η, for different τ.

Discussion on model fitting

As discussed in the Main Text, we fitted the SPQEIR model on several countries to show that such minimal model can reproduce epidemic curves and enable further explanation of the impact of several non-pharmaceutical interventions. However, the structure of the model retains a certain level of degeneracy among its parameters, which lead to identifiability limitations that are known in SIR-like models [189]. In particular, several parameter combinations could yield to similar values of the control parameter $\hat{R}$. In this section, we further discuss the relevance of the *lmfit* fitting presented in the Main Text and we compare and support it by discussing the results of a Bayesian inference approach based on a Markov Chain Monte Carlo (MCMC) scheme for model fitting, that allows us to fully explore the parameter space and relevant combinations of the parameters. This procedure enables a detailed analysis of the identifiability of our parameters and justifies the subsequent use of a least-square methodology to estimate a single, reasonable set of parameters that could well explain the empirical data.

Discussion on least-squares fitting

As explain in the Main Text, we first fitted the SPQEIR model with a single free parameter, to get a meaningful value for $\hat{R}$ (the "only social distancing" setting). Then, we fitted the full model, with country-specific parameters (*cf.* Table 1), making sure that analogous $\hat{R}$ values were obtained. We recall that not all parameters were allowed to be free, but only some were applied, i.e. those that can be matched with a corresponding measure documented to have been applied in the real country. Although possibly not unique, the identified parameter values are the most likely after gradient descent [188] and yield to non-negligible numbers of individuals being affected by the corresponding measures. Table A.1 reports the cumulative numbers of individuals that flowed to Q and P compartments during the first intervention period, marked in grey in Fig. 9 of the main text, due to fitted parameter values (also reported in Fig. 9 of main text). These estimates are useful, as order of magnitudes, to appreciate the effect of single, targeted interventions coming from different non-pharmaceutical interventions, in addition to population-wide social distancing. Further verification and precise assessment of such values are demanded to future, complementary

studies that make use of welfare partner data.

Country	Quarantined	Protected
Austria (AT)	430	63000
Denmark (DK)	2500	120000
Ireland (IR)	4000	730000
Israel (IL)	2200	63000
Lombardy (LO)	3100	69000
Switzerland (CH)	520	59000

Table A.1: Total numbers of individuals flowing to outer compartments of the SPQEIR model, during the considered time period (grey area in Fig. 9 of main text), under the action of fitted parameters. Following the discussion about parameter identifiability, these numbers are meaningful as orders of magnitude, and are thus reported with rounding on the second significant digit.

Parameter space characterization by means of Markov Chain Monte Carlo

We next verified the constraints on model paramters and the degeneracy between them with an additional analysis, based on Bayesian inference implemented by means of a Markov Chain Monte Carlo (MCMC) approach, which allows to further identify the individual parameters values and the constraints on their combinations in the parameter space, as well as the associated uncertainties. For the current MCMC analysis, we employed as likelihood function a commonly used sum of square residuals (SSR), which measures the distance between the model simulation and the data as:

$$SSR\left(\overline{\tau}|data\right) = \sum_{i=T_0}^{T_f} \left[C^{data}\left(t_i\right) - C^{model}\left(t_i, \overline{\tau}\right)\right]^2 . \tag{A.1}$$

In Eq. B.7, $\overline{\tau}$ is the array of parameters representing measures relevant for that country, $t_i \in \{T_0, T_0+1, \ldots, T_f-1, T_f\}$ indicates the number of days from the beginning of the epidemic (assumed for that country), T_0 and T_f are respectively the first and last day under investigation, C^{data} indicates data of active infections and C^{model} to the corresponding model quantity. The SSR is related to the reduced χ^2, both being ways to measure the geometric distance between model simulation and data.

The applied sampling technique is the Delayed Rejection Adaptive Metropolis (DRAM) scheme [113], from the python package *pymcmcstat* [105]. We run 8 chains in parallel, initialized at

random initial conditions. Each chain has 50000 iterations, which ensure the convergence of the chain. For the Bayesian steps, the simplest non-informative flat priors probability distributions are assumed on each parameter. These are chosen as there is no need to incorporate additional information on the parameter values, except for the boundaries of the intervals which are allowed. Furthermore, flat priors do not introduce any further bias towards a particular parameter set. The parameter intervals to be explored are chosen to be reasonable with respect to the conceptual analysis: ρ ranges from 0.1 to 0.4, μ from 0.001 to 0.12, χ from 0.001 to 0.7 and η from 0.001 to 0.1. The chain convergence was assessed by the Gelman-Rubin diagnostic, which analyses the variance within and between each chain set. Results of the Bayesian fitting are reported below, and we repeated the procedure on several of the countries considered.

As mentioned in Main Text, we observe that several combinations of parameters lead to similar good agreement (measured by the SSR) between the model simulation and the data, and thus result in a high posterior probability (dark red color in the figures). Other combinations lead to poorer agreement between model and data, and are thus associated to low posterior probability distribution (light red, blue or dark blue regions). In order not to overload the text, we report 3 example countries with different parameter sets. Others are analogous and can be reconstructed with the shared code. The figures below (Figs. A.5 for Austria, A.6 for Ireland and A.7 for Switzerland) showcase which areas of the parameter space have a higher posterior probability, and thus indicate which combinations of parameters would be more likely to provide a good fit between model and data. The figures are reconstructed by marginalising the full distribution from MCMC chains over couples of parameters at a time. In fact, some parameter pairs are correlated, and a certain degree of degeneracy exists between parameters, in the sense that often simultaneous changes in two parameters would equally well allow the model to fit the data. This highlights the identifiability issues discussed in the Main Text, namely that multiple sets of parameter values could be employed resulting in similar fit of the model to the data. Eventually, to provide one plausible choice, we reported in the Main Text the best gradient descent fit obtained with *lmfit* scheme.

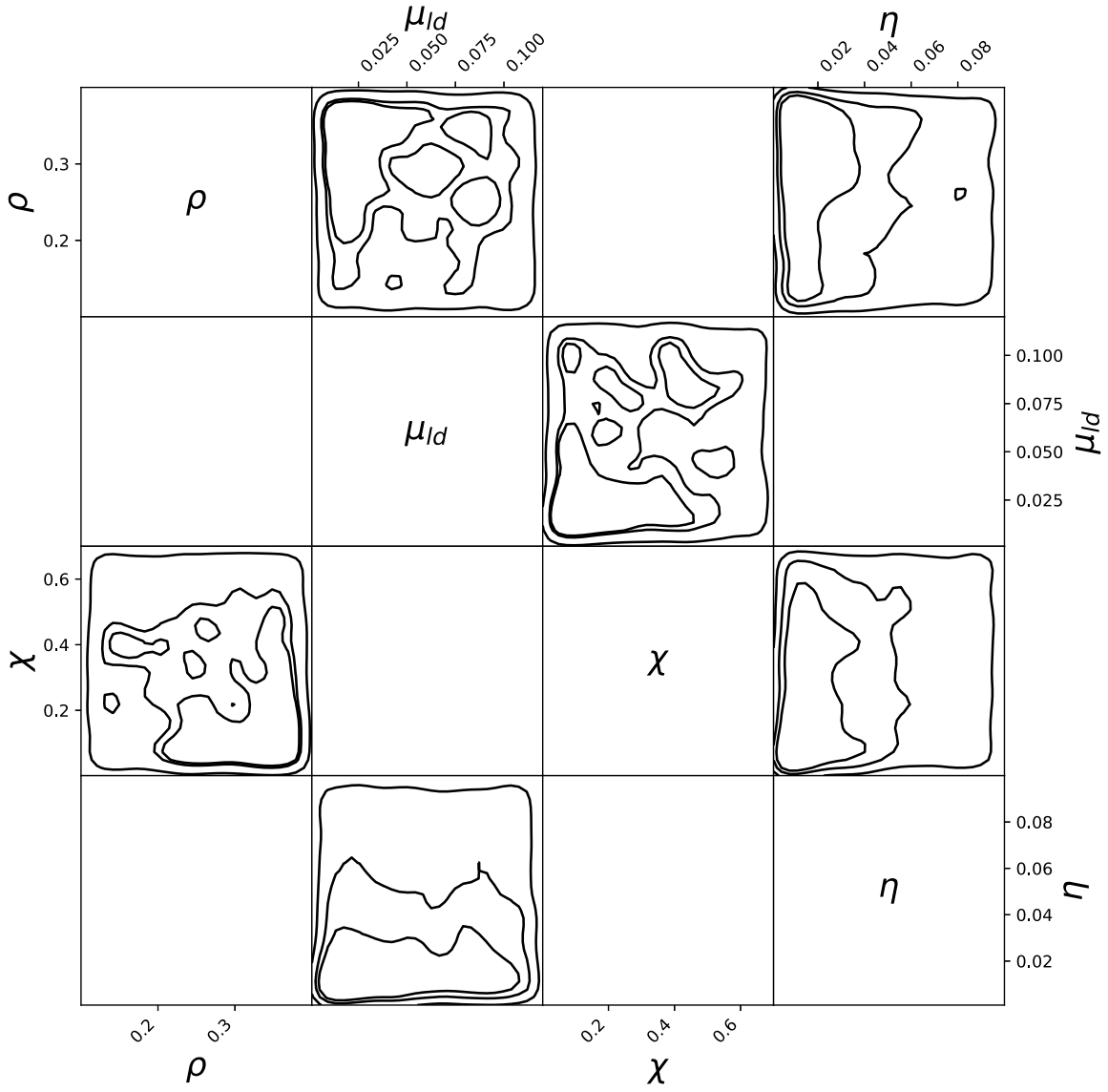

Figure A.5: Estimated posterior probability distribution from Markov Chain Monte Carlo projected over each couple of parameters, for Austria. Each square shows 2D projection of the posterior over two parameters. The parameter names are reported at the margins and on the diagonals. Each 2D projection is reported only once once as they are symmetric, thus the white squares. The posterior probability is represented by the nuances of red towards blue, with red being high probability and blue being low (probability close to 0). The three black contours correspond to 25%, 50% and 90% Bayesian credible regions.

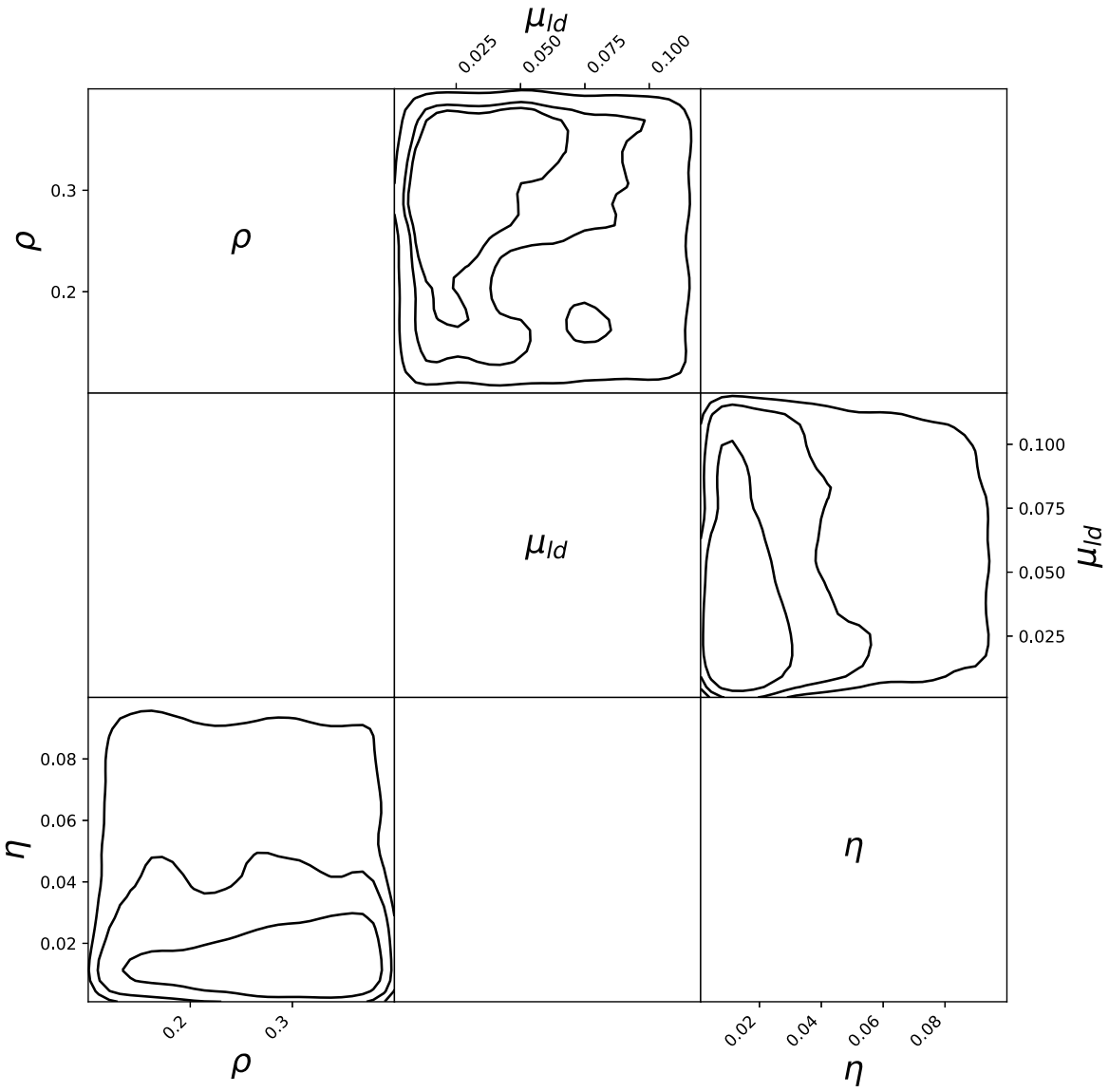

Figure A.6: Estimated posterior probability distribution from Markov Chain Monte Carlo projected over each couple of parameters, for Ireland. Each square shows 2D projection of the posterior over two parameters. The parameter names are reported at the margins and on the diagonals. Each 2D projection is reported only once once as they are symmetric, thus the white squares. The posterior probability is represented by the nuances of red towards blue, with red being high probability and blue being low (probability close to 0). The three black contours correspond to 25%, 50% and 90% Bayesian credible regions.

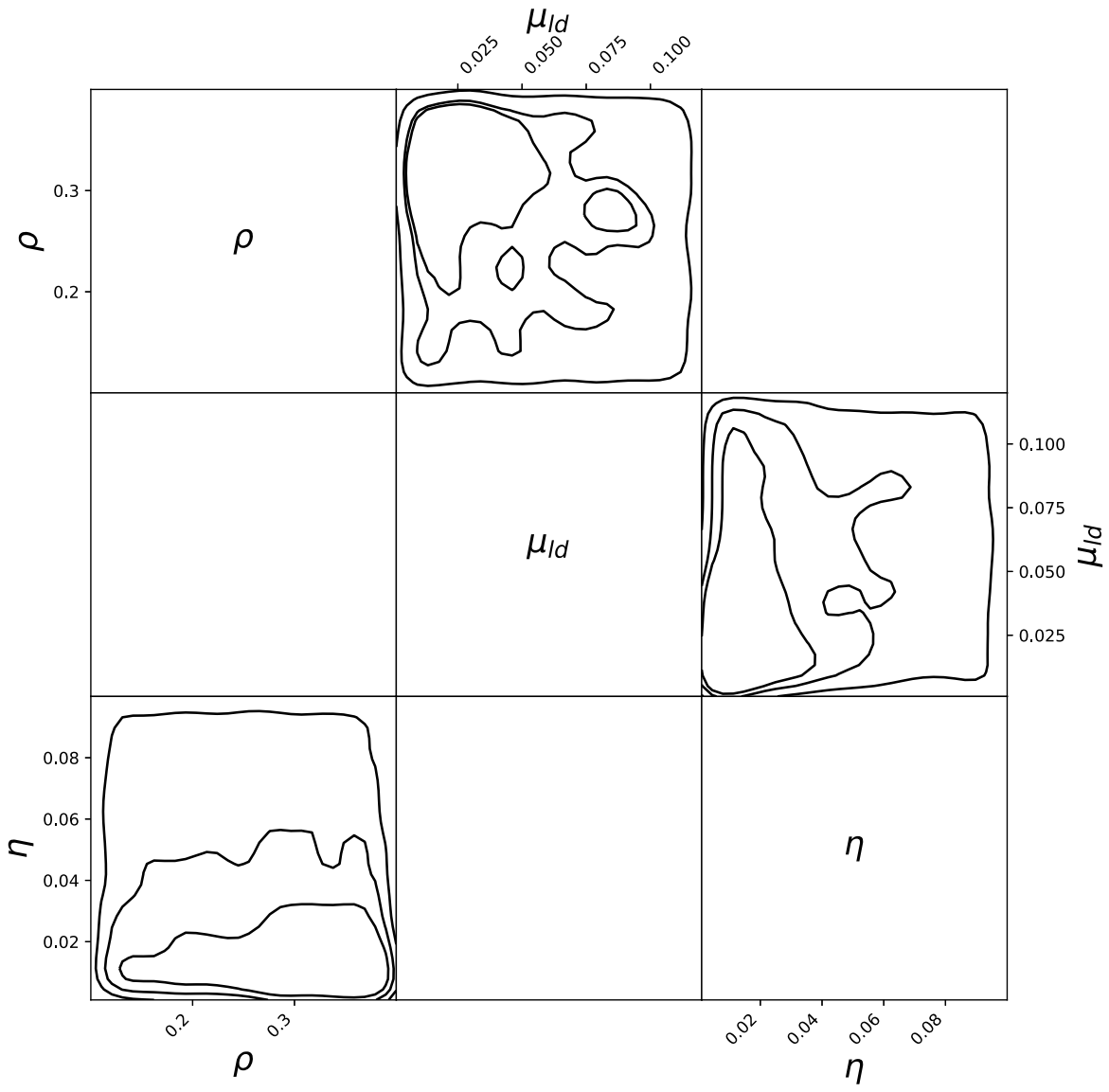

Figure A.7: Estimated posterior probability distribution from Markov Chain Monte Carlo projected over each couple of parameters, for Switzerland. Each square shows 2D projection of the posterior over two parameters. The parameter names are reported at the margins and on the diagonals. Each 2D projection is reported only once once as they are symmetric. The posterior probability is represented by the nuances of red towards blue, with red being high probability and blue being low (probability close to 0). The three black contours correspond to 25%, 50% and 90% Bayesian credible regions.

APPENDIX B

APPENDIX OF MODELLING COVID-19 DYNAMICS AND POTENTIAL FOR HERD IMMUNITY BY VACCINATION IN AUSTRIA, LUXEMBOURG AND SWEDEN

In this Appendix we illustrate the model, the considered data from Luxembourg, Austria and Sweden, a computational approach to estimate herd immunity and the procedures to provide an estimate of the parameters and their uncertainties.

Mathematical model

In this study, we developed a mathematical model of the transmission of COVID-19 within a population, building upon the standard SEIR model [217]. Our extension of the SEIR model is described by Fig. 5.1 in the main text. The total population N of the modelled country at time t is divided into 16 compartments. First, we introduce a separation between detected and undetected cases; in fact, a non-negligible fraction of infected people is usually not detected [218], e.g. for lack of testing or because asymptomatic. Next, we include compartments to model the progression of the disease to more severe states, requiring hospitalisation, intensive care (ICU) or leading to death. Finally, we include compartments for recovered people. The model variables are summarized in Tab. B.1 and represent the number of individuals in different stages, normalized

by the total population of the considered country.

Susceptible (S) and exposed (E) compartments are in common with the standard SEIR model. An exposed person might be detected (via a PCR test), thus entering the "infectious and detected" (II) compartment, and subsequently the "quarantined" (Q) compartment, from where the person cannot infect others any further. At this point, a person might (or not) become "hospitalized" (H), and then either simply "require longer hospitalization" (Hl) or require "intensive care treatment" (ICU). If the health improves, the individual can return to "regular hospital treatment after ICU" ($AICU$). At any of these hospitalization stages, the person can "die in hospitals or ICUs" ($D_{I,hos}$), or "recover from hospital or ICUs" (R_{II}). People who are either recovered or dead are the equivalent of the removed compartment of a standard SEIR model, and thus do not get reinfected a second time in the model. Most detected people are not hospitalized, so they recover at home (NI), or alternatively they can die at home ($D_{I,hom}$). Finally, the fraction of people who got infected but do not get detected are represented by the infectious and undetected compartment (A). Being unaware of their state, they can continue to spread the infection without constraints. These people spend some time recovering outside hospitals (N_{II}), and eventually they end up either recovered undetected (R_A), or dead undetected (D_A). The total number of undetected cases in Fig. 5.2 of the main text is obtained as the sum of the variables $A + NII + D_A + R_A$. We assume conservation of the total population N (people can die, thus entering the dedicated compartments, but there is no removal of individuals from the system, and we neglect birth), such that for each country:

$$1 = S+E+I+Q+H+H_l+ICU+AICU+NI+D_{I,hos}+D_{I,hom}+R_I+A+NII+D_A+R_A \ , \tag{B.1}$$

where the variables have been normalized by N to represent the fraction of the total population being in the corresponding state. The dynamics of our model is described by the following system of ordinary differential equations:

$$\frac{dS}{dt} = -\rho\beta(A + II)S \ , \tag{B.2a}$$
$$\frac{dE}{dt} = \rho\beta S(A + II) - \alpha E \ , \tag{B.2b}$$
$$\frac{dI}{dt} = \alpha p_1 E - \tau_1 I \ , \tag{B.2c}$$
$$\frac{dQ}{dt} = \tau_1 I - Q\tau_2 p_2 - (1 - p_2)\tau_2 Q \ , \tag{B.2d}$$
$$\frac{dH}{dt} = p_2\tau_2 Q - p_3 H\tau_3 - (1 - p_3)H\tau_3 \ , \tag{B.2e}$$
$$\frac{dHl}{dt} = p_3 H\tau_3 - Hl\tau_5(1 - p_5) - \tau_5 p_5 Hl \ , \tag{B.2f}$$
$$\frac{dICU}{dt} = (1 - p_3)H\tau_3 - p_4\tau_4 ICU - (1 - p_4)ICU\tau_4 \ , \tag{B.2g}$$
$$\frac{dAICU}{dt} = \tau_4 p_4 ICU - p_6 AICU\tau_6 - AICU(1 - p_6)\tau_6 \ , \tag{B.2h}$$
$$\frac{dR_I}{dt} = p_6\tau_6 AICU + p_5\tau_5 Hl \ , \tag{B.2i}$$
$$\frac{dR_{I1}}{dt} = p_7\tau_7 NI \ , \tag{B.2j}$$
$$\frac{dNI}{dt} = (1 - p_2)\tau_2 Q - \tau_7(1 - p_7)NI - p_7\tau_7 NI \ , \tag{B.2k}$$
$$\frac{dD_{I,hom}}{dt} = (1 - p_7)\tau_7 NI \ , \tag{B.2l}$$
$$\frac{dD_{I,hos}}{dt} = (1 - p_6)\tau_{6,d} AICU + (1 - p_5)\tau_5 Hl + \tau_4(1 - p_4)ICU \ , \tag{B.2m}$$
$$\frac{dA}{dt} = (1 - p_1)\alpha E - \tau_8 A \ , \tag{B.2n}$$
$$\frac{dNII}{dt} = \tau_8 A - \tau_9(1 - p_9)NII - p_9\tau_9 NII \ , \tag{B.2o}$$
$$\frac{dD_A}{dt} = \tau_9(1 - p_9)NII \ , \tag{B.2p}$$
$$\frac{R_A}{dt} = \tau_9 p_9 NII \ . \tag{B.2q}$$

We initialise every simulation with the initial conditions detailed in Tab. B.1. For any simulation in this work (except those involving vaccination, see B) to numerically solve the set of ordinary differential equations we employ the python (version 3.6.1) solver *odeint* from the package *scipy* (version 1.5.2), which uses the *LSODA* method for numerical integration.

Variable	**Representing fraction of people**	**Value at $t = 0$ days**
$S(t)$	Susceptible	$1 - 1/N$
$E(t)$	Exposed	$1/N$
$I(t)$	Infectious (Detected)	0
$Q(t)$	Quarantined	0
$H(t)$	Hospitalized	0
$Hl(t)$	Hospitalized - Longer	0
$ICU(t)$	in ICU	0
$AICU(t)$	Hospitalized after ICU	0
$NI(t)$	Recovering at Home (Detected)	0
$D_{I,hos}(t)$	Dead in hospitals (Detected)	0
$D_{I,hom}(t)$	Dead at home (Detected)	0
$R_I(t)$	Recovered (Detected)	0
$A(t)$	Infectious (Undetected)	0
$NII(t)$	Recovering at Home (Undetected)	0
$D_A(t)$	Dead at home (Undetected)	0
$R_A(t)$	Recovered (Undetected)	0

Table B.1: The 16 variables represent the fraction of population of a country being in each of the compartments. The initial conditions are the standard ones usually employed for SEIR-like models, with all the population susceptible except one person already exposed to the virus. They are the same for every simulation and country, except for the country's population being $N = 623180$ individuals for Luxembourg, $N = 8901064$ for Austria and $N = 10230000$ for Sweden.

Model parameters

The parameters of the model and their interpretation are detailed in Tab. B.2. The parameters can be divided in three categories, based on what type of physical quantity they describe: rates, probabilities and social interaction.

When individuals can move from one compartment to one of two different compartments, the probability p_i controls which fraction of people will go to one compartment, the remaining fraction $1-p_i$ going to the other. Their value is bounded between 0 and 1. The parameters p_i are indexed with $i = 1, \ldots, 9$.

The parameters α, β and τ_i represent rates. The parameters τ_i are indexed with $i = 1, \ldots, 9$.

Parameter	Description	Units
ρ_n	social interaction $(n = 0, 1, \ldots, \mathcal{N})$	$adim.$
β	average contact rate	$days^{-1}$
α	(mean incubation period)$^{-1}$	$days^{-1}$
τ_1	(mean time in I)$^{-1}$	$days^{-1}$
τ_2	(mean time in Q)$^{-1}$	$days^{-1}$
τ_3	(mean time in H)$^{-1}$	$days^{-1}$
τ_4	(mean time in ICU)$^{-1}$	$days^{-1}$
τ_5	(mean time in Hl)$^{-1}$	$days^{-1}$
τ_6	(mean time in $AICU$)$^{-1}$	$days^{-1}$
τ_7	(mean time in NI)$^{-1}$	$days^{-1}$
τ_8	(mean time in A)$^{-1}$	$days^{-1}$
τ_9	(mean time in NII)$^{-1}$	$days^{-1}$
p_1	probability of $E \to I$	$adim.$
p_2	probability of $Q \to H$	$adim.$
p_3	probability of $H \to H_l$	$adim.$
p_4	probability of $ICU \to AICU$	$adim.$
p_5	probability of $Hl \to R_{II}$	$adim.$
p_6	probability of $AICU \to R_{II}$	$adim.$
p_7	probability of $N_I \to R_{II}$	$adim.$
p_9	probability of $NII \to R_A$	$adim.$

Table B.2: The parameters of the model with their description and unit of measure. For each country and wave, the following assumptions have been made: $\tau_8 = (1/\tau_1 + 1/\tau_2)^{-1}$, $p_9 = p_7$, $\tau_9 = \tau_7$. This is motivated by the fact that these parameters are relative to the undetected branch, and thus cannot be inferred from data. Thus, we assumed that undetected cases would evolve with the same parameter values as detected cases not entering hospitals/ICUs. $\mathcal{N}$ represents the number of times that the social interaction parameter changes: $\mathcal{N} = 13$ for Luxembourg and Sweden and $\mathcal{N} = 16$ for Austria. The values of the manual fit of all the rates and probabilities for each country and wave are summarized in Tab. B.6. The values and dates of change for the social interaction parameter ρ_n are reported in Tab. B.3 for Luxembourg, in Tab. B.4 for Austria and in Tab. B.5 for Sweden.

Each rate represents the inverse of the average time that takes for an individual to move from one compartment to the next. Of particular relevance are the rates α and β, which have the same meaning as the corresponding parameters of a standard SEIR model: α represents the inverse of the mean incubation period of the disease, and β represents the average contact rate.

The average contact rate β is then multiplied by the additional parameter ρ, in order to model any

measure or change in people's behaviour that can lead to a change (decrease or increase) in the average contact rate. Thus, β is a constant and it represents the "natural" average contact rate, while $\rho(t)\beta$ represents an effective average contact rate which considers the measures or social behaviours in place. We assume $\rho_0 = 1$ for any country, before any measure was implemented at the beginning of the pandemic in February 2020. Afterwards, we assume $\rho = \rho(t)$ to be a piece-wise constant function of time, where each value is indicated by ρ_n, with $n = 0, \ldots, 13$ for Luxembourg and Sweden and $n = 0, \ldots, 16$ for Austria. We assume that changes in ρ occur whenever a major new measure is implemented or lifted by the authorities of a country, or in case of a major happening (e.g. schools starting in September in Luxembourg). The dates employed for every country, and which measures where taken/lifted on that date, are summarized in Tab. B.3 for Luxembourg, Tab. B.4 for Austria and Tab. B.5 for Sweden.

Analytical derivation of the effective reproduction number $R_{eff}(t)$

To obtain $R_{eff}(t)$ from the current model we used the next generation matrix method [226, 339, 342]. From the next generation matrix, we find its eigenvalues R_0 and 0. In our case, R_0 is given by:

$$R_0 = \beta \left[\frac{(1-p_1)}{\tau_8} + \frac{p_1}{\tau_1} \right] . \tag{B.3}$$

From R_0, we can deduce $R_{eff}(t)$, given by

$$R_{eff}(t) = \beta \rho(t) \left[\frac{(1-p_1)}{\tau_8} + \frac{p_1}{\tau_1} \right] \frac{S(t)}{N} . \tag{B.4}$$

By substituting the values of the parameters for each country and scenario, we obtain the $R_{eff}(t)$ curves depicted in Fig. 5.3 of the main text, panels **B**, **D**, **F**.

Incorporating vaccination in the model

To include vaccination, we add one additional compartment $V(t)$ representing the fraction of vaccinated population. We assume that a fixed number of people will be vaccinated every day.

Thus, the equation for the number of people vaccinated reads:

$$\frac{dV}{dt} = \tau_{vac} \ , \tag{B.5}$$

with τ_{vac} being the parameter representing how many people will be vaccinated per day. Correspondingly, the equation for the susceptible compartment becomes:

$$\frac{dS}{dt} = -\rho\beta(A + II)S - \tau_{vac} \ , \tag{B.6}$$

since we assume that only people who did not already naturally develop antibodies by being infected will be vaccinated.

In order to simulate three potential vaccination strategies, i.e. 3 vaccines rollout speeds, at which countries might manage to perform vaccination, we fix the parameter τ_{vac} to three values that, if all the population would still be susceptible, would lead to vaccinating all the population of a country within respectively 6 months, 1 year and 1.5 years. These are typical timescales potentially envisaged by different countries. Thus, we consider the three values $\tau_{vac} = 1/\left(365/2\right)$ $days^{-1}$, $\tau_{vac} = 1/365$ $days^{-1}$ and $\tau_{vac} = 1/\left(1.5 \cdot 365\right)$ $days^{-1}$ (recall that model variables are normalized by the total country population N, so they sum up to 1). These three values of τ_{vac} correspond, respectively, to perform approximately 3415, 1707 and 1138 full vaccinations/day in Luxembourg, 48773, 24386 and 16258 full vaccinations/day in Austria and 56055, 28027 and 18685 full vaccinations/day in Sweden. Luxembourg numbers are an order of magnitude smaller than those for Austria and Sweden, proportionally to their total populations. It is in fact reasonable that vaccination capability would scale with country population (for European countries with comparable standards of living), i.e. that the more populated a country, the higher its capacity to perform vaccinations. Thus e.g. performing 56055 full vaccinations/day in Sweden might be as challenging as performing 3415 full vaccinations/day in Luxembourg.

When numerically integrating the system of ordinary differential equations from Eqs. B.2 with the addition of vaccination (Eq. B.5 and Eq. B.6), we consider an additional constraint to prevent the variable $S\left(t\right)$ to decrease below 0, which would happen otherwise due to Eq. B.6. Interrupting the *odeint* routine when the condition $S = 0$ is met is not possible; hence, in all the simulations

involving vaccination, we instead perform numerical integration by means of the forward Euler method with $\tau_{vac} = 0$ if $S \leq 0$. We used an integration time-step $dt = 0.01\ days$ and verified beforehand that further decreasing it would not lead to any significant change in the integration result, while significantly increasing computation time.

Herd immunity

Sec. 5.3.5 of the main text described how to analytically derive the fraction of susceptibles p_c who needs to be fully immune in order to reach herd immunity; we complement that analysis with numerical inspection of the model. Herd immunity by definition occurs when the pandemic is not spreading anymore within a population, without the need of any measure. Hence, p_c is given by 1 minus the fraction of S that yields the maximum of infectious I, when no measure is in place (after the maximum, the epidemic curve decreases on its own with no need of measures). This is a typical approach to numerically estimate the herd immunity threshold p_c in SEIR-like models. Hence, we simulate the time evolution of the baseline model and we plot the results on the phase plane I vs S, obtaining the curve $I(S)$. We then identify the value S_c of S such that the curve $I(S)$ reaches its maximum. S_c is the fraction of susceptible when the number of I naturally starts to decrease, corresponding by definition to $R_{\mathit{eff}}(t) < 1$, i.e. herd immunity. The phase planes are show in Appendix Fig. B.1, panel **A** for Luxembourg, **B** for Austria and **C** for Sweden. To fully investigate the complexity of the model, we consider both the baseline model (no measures from the beginning, blue curve) and the next-to-baseline case (all measures lifted after the last available data point, red curve).

For both blue and red curves, the maxima occur at around 0.27 for Luxembourg and for Austria and 0.24 for Sweden. Since $p_c = 1 - S_c$, we obtain that the computationally estimated values of the herd immunity threshold are 73%, 73% and 76%, respectively. We compare them with the analytic values from the formula $p_c = 1 - 1/R_0$, i.e. 70%, 68% and 75% (*cf.* Sec. 5.3.5): the values are extremely close, with small differences of 3%, 5% and 1%. The threshold values estimated computationally are higher than their counterpart for all countries, possibly due to the additional complexities of our model w.r.t. a standard SEIR model. We thus employ these

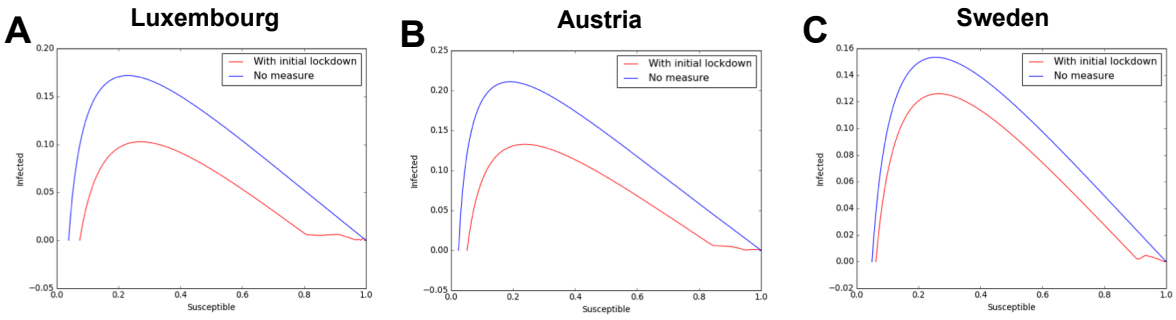

Figure B.1: Phase plane for numerical estimation of the herd immunity threshold. In each panel, the maximum of the curve represents the value of the fraction of susceptible people that would yield herd immunity. Panel **A** for Luxembourg, panel **B** for Austria and panel **C** for Sweden.

computationally obtained ones, both because they account for any additional model complexity and in order to provide a more conservative estimate of when herd immunity might be reached.

Data and analyzed countries

We consider three different countries: Luxembourg, Austria and Sweden. The model structure described above is maintained unchanged across the three countries. For consistency, we change the value of the total country population N and the parameter values so that the model fits the data of the corresponding country. We use data of total detected cases, hospitalized people, people in ICUs and dead people. We gathered these data from https://www.acaps.org/covid19-government-measures-dataset, a public independent database recognised by the WHO (last accessed on 03/12/2020) as well as from the public repositories listed below. Moreover, for each country we allow the social interaction parameter ρ to change when major changes in measures took place. We list below also the sources of information for the changes in measures.

Luxembourg

For Luxembourg, we obtained the dates at which major changes in policy took place in Luxembourg from https://covid19.public.lu/fr/mesures-sanitaires-en-vigueur.html (last accessed 15/12/2020), and summarize them in Tab. B.3. The time-series data of total cases,

hospitalised people, people in ICU and dead people for Luxembourg are publicly available on 5.2 of the main text, along with their 7-days moving average. The moving average smooths detection and intrinsic noise, and filters out the effects of considerable weekend under-testing, consistently observed and confirmed by the considerably lower number of total tests performed over weekend days. The moving average is centered on the day of interest to not induce shifts of the features (like the peaks) of the time-series.

ρ_n	**Starting Date**	**Measure or change in social activities**	**Manual Calibration**	**Which Wave**
ρ_0	–	No restrictions	1	–
ρ_1	16.03	Lockdown	0.4902	$1st$
ρ_2	23.03	Measures fully effective	0.1984	$1st$
ρ_3	20.04	Opening construction sector	0.1918	$1st$
ρ_4	04.05	Opening high schools	0.2507	$1st$
ρ_5	10.06	Relaxation of measures	0.5298	$2nd$
ρ_6	29.06	End of classes splitting	0.4804	$2nd$
ρ_7	13.07	School holidays	0.3101	$2nd$
ρ_8	31.07	Start holidays	0.2203	$2nd$
ρ_9	12.08	Change mobility (Google mobility data)	0.3457	$2nd$
ρ_{10}	23.08	End holidays of construction sector	0.3351	$2nd$
ρ_{11}	14.09	Opening schools	0.4333	$3rd$
ρ_{12}	01.11	Restrictions, including curfew (11 p.m.)	0.341	$3rd$
ρ_{13}	26.11	Stricter measures, HORESCA closure	0.39	$3rd$

Table B.3: Changes in the piece-wise constant social interaction parameter $\rho(t)$ of the model for Luxembourg.

According to the public data mentioned above, the first positive case was detected in Luxembourg on February 29, 2020. Considering the lag between being susceptible, being exposed and being detected, we initialize the model at its initial conditions reported in Tab. B.1 with time $t = 0$ on February 24. Data about the COVID-19 prevalence in the population were obtained from the Con-Vince study [229].

Each country in this study is modelled as a closed system, which might be a limitation for Luxembourg, due to the small size of the country and the high cross-border mobility. The publicly available data employed for Luxembourg and mentioned in this section only include cases

that are detected and resident in Luxembourg. For considerations about cross-border workers in Luxembourg and interplay with economical features, refer to [206].

Our model was used to regularly monitor the progression of the epidemic in Luxembourg and to produce short- and mid-term projections during the crisis. It aimed to promptly deliver preliminary results and then increasingly more refined results and projections as available data increased over time. Hence, some of our parameters have been updated multiple times throughout the course of the crisis, to incorporate new knowledge. In this manuscript, our model is reporter in its state in December 2020, but it has been, overall, a continuously evolving tool.

Austria

We obtained the dates at which major changes in policy took place in Austria from https://de.wikipedia.org/wiki/COVID-19-Pandemie_in_Österreich (collection of various sources, last accessed on 15/12/2020). Tab. B.4 summarizes dates and associated policies. The time-series data of total cases, hospitalised people, people in ICU and dead people for Austria come from https://covid19-dashboard.ages.at/dashboard_Hosp.html (last accessed on 15/12/2020). They are reported in Fig. 5.2 of the main text, where we also report their 7-days moving average. According to the data mentioned above, the first positive case was detected in Austria on February 26, 2020. Considering the lag between being susceptible, being exposed and being detected, we initialize the model at its initial conditions reported in Tab. B.1 on February 21. Similar starting dates for modelling the epidemic in Austria have been used elsewhere, e.g. February 22 in [235] (see Tab. therein). Data about COVID-19 prevalence were obtained from https://www.sora.at/nc/news-presse/news/news-einzelansicht/news/COVID-19-praevalenz-1006.html (last accessed on 15/12/2020).

Sweden

We obtained the dates at which major changes in policy took place in Sweden from [245] until August and from https://www.krisinformation.se/en/news (last accessed on 15/12/2020) later on, and we summarize them in Tab. B.5. The time-series data of total cases, hospitalised people, people in ICU and dead people for Sweden are available on https://www.folkhalsomyndigheten.

ρ_n	**Starting Date**	**Measure or change in social activites**	**Manual Calibration**	**Which Wave**
ρ_0	–	No restrictions	1	–
ρ_1	16.03	Closure schools/universities, limitations in shops/restaurants	0.52	$1st$
ρ_2	30.03	Wearing masks	0.155	$1st$
ρ_3	14.04	Opening small shops	0.22	$1st$
ρ_4	01.05	Opening malls and hairdressers	0.27	$1st$
ρ_5	15.05	Opening certain school classes	0.31	$1st$
ρ_6	29.05	Opening additional schools	0.33	$2nd$
ρ_7	15.06	Mask obligation in public area, no mask in shops/schools	0.38	$2nd$
ρ_8	11.07	School holidays	0.36	$2nd$
ρ_9	21.07	Mask obligation everywhere	0.32	$2nd$
ρ_{10}	13.08	Increase of infections due to people returning from holidays	0.385	$2nd$
ρ_{11}	14.09	Opening schools	0.415	$2nd$
ρ_{12}	21.09	Extended mask obligation / 10 people invitations	0.405	$2nd$
ρ_{13}	25.09	Curfew (10 p.m.) Salzburg, Voralberg and Tirol	0.395	$2nd$
ρ_{14}	23.10	Private gatherings limited to 6 people inside, 12 outside	0.385	$2nd$
ρ_{15}	03.11	Lockdown	0.27	$2nd$
ρ_{16}	07.12	Relief of lockdown	0.34	$2nd$

Table B.4: Changes in the piece-wise constant social interaction parameter $\rho(t)$ of the model for Austria.

se/smittskydd-beredskap/utbrott/aktuella-utbrott/covid-19/statistik-och-analyser/bekraftade-fall-i-sverige/, https://www.icuregswe.org/en/data--results/covid-19-in-swedish https://c19.se (last accessed on 15/12/2020). They are displayed in Fig. 5.2 in main text, where we also report their 7-days moving average.

Swedish policy has been analysed e.g. in [228, 244, 340]. While the very first case detected was on 31st January, no other case was detected until February 26. It is likely that the first case was isolated and did not infect others, otherwise most likely a second case would have been detected earlier; in addition, the first case was reported from a woman who had traveled to Wuhan and was isolated upon detection. On the other hand, following the second detected case on February 26, 9 more cases were detected in the next 2 days. To account for potential further lag in the uncertain starting time of the epidemic in Sweden, we initialise the model at its initial conditions

reported in Tab. B.1 on February 16. Similar starting dates for modelling the epidemic in Sweden have been used elsewhere, with [235] starting their modelling on February 18 (see Tab. 1 therein).

ρ_n	**Starting Date**	**Measure or change in social activites**	**Manual Calibration**	**Which Wave**
ρ_0	–	No restrictions	1	–
ρ_1	11.03	Gatherings of more than 500 people forbidden	0.52	$1st$
ρ_2	16.03	Home office, school above 17 initiate distance learning	0.3	$1st$
ρ_3	27.03	Gatherings of more than 50 people forbidden	0.25	$1st$
ρ_4	30.03	Visits to the elderly care are banned	0.2	$1st$
ρ_5	02.04	Certain students aged >17 allowed back to classroom	0.277	$1st$
ρ_6	10.06	Starting holidays	0.265	$1st$
ρ_7	13.06	Ease of travel restriction	0.28	$1st$
ρ_8	01.07	Further ease of travel restriction	0.23	$1st$
ρ_9	17.08	Opening of schools for children	0.37	$1st$
ρ_{10}	01.10	Visit ban lifted	0.395	$1st$
ρ_{11}	27.10	Stricter guidelines in Skåne	0.41	$2nd$
ρ_{12}	03.11	Stricter guidelines in Jönköping, Halland, Örebro	0.375	$2nd$
ρ_{13}	16.11	Stricter guidelines in Gävleborg, Västernorrland	0.345	$2nd$

Table B.5: Changes in the piece-wise constant social interaction parameter $\rho(t)$ of the model for Sweden.

To fit Sweden, the model needs time-dependent probabilities of detection and hospitalisation, unlike for Luxembourg or Austria

Extending our model to Sweden is to gain insight on a country which applied different policies than Luxembourg and Austria (which adopted similar policies). To fit Swedish data with the same model structure as the other countries, it was not sufficient to consider a different set of parameter values. Instead, it was necessary to introduce time-dependent probabilities of being detected $p_{1\text{Swe}}(t)$ and of being hospitalized $p_{2\text{Swe}}(t)$, within an epidemic wave.

The parameter p_1 corresponds to the probability of an infected individual being detected. To obtain an estimate of this parameter for Sweden, we considered prevalence data estimated weekly

through antibody test for 8 consecutive weeks between mid April and mid June 2020, obtained from [230, 231] and shown in Fig. B.2 panel **A**. The prevalence went from about 4% to 6%, growing over the course of these two months, likely resulting from more infections. Due to the large error bars, multiple functional forms could be considered a reasonable fit, so we chose the simplest linear fit.

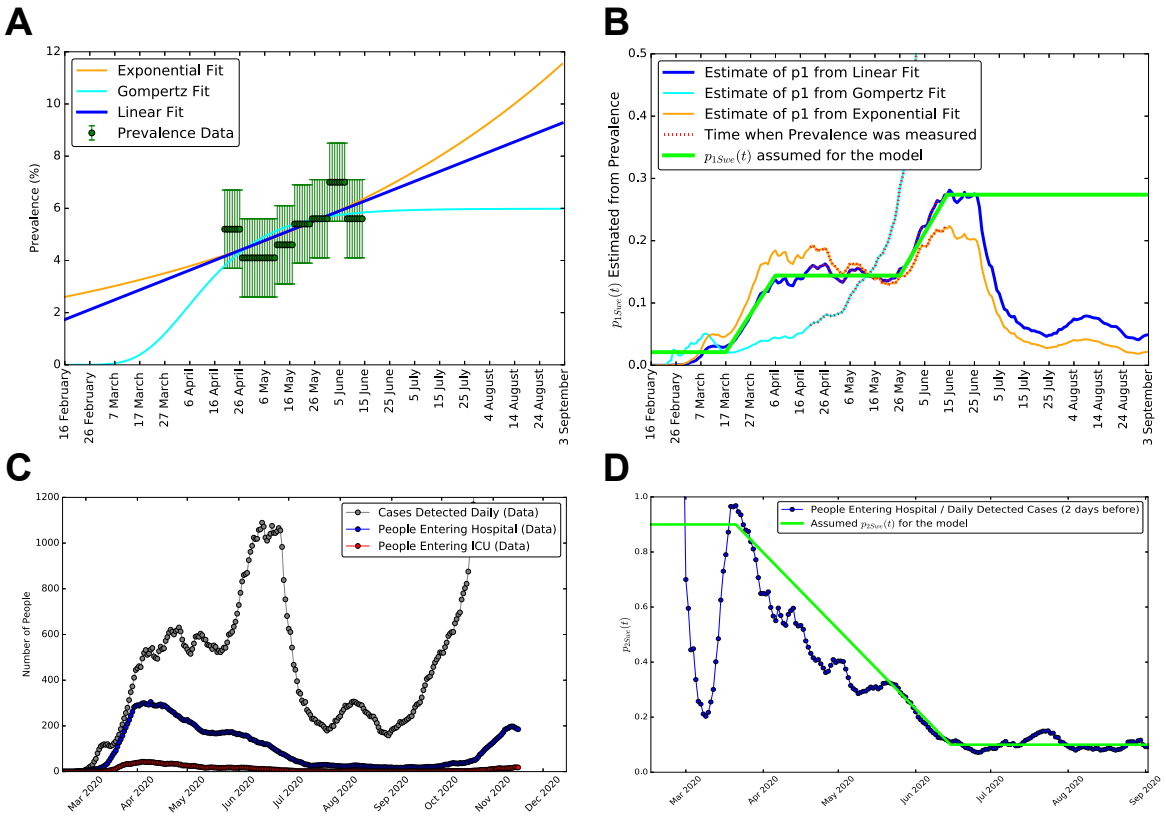

Figure B.2: Derivation of the time-dependent probabilities of detection $p_{1Swe}\,(t)$ and hospitalization $p_{2Swe}\,(t)$, for Sweden. **A**: prevalence data for Sweden from [230, 231], with three alternative fits: a linear, a Gompertz and an exponential (for comparison). **B**: number of detected cases over total cases on time, inferred from prevalence, for the three fits to prevalence of panel **A**. The final functional form for $p_{1Swe}\,(t)$ (the probability of being detected if infected) is in green. **C**: data for daily new detected cases, people entering hospital and people entering ICU (not to be confused with the numbers of people occupying hospitals and ICUs displayed in Fig. 5.2 of the main text). **D**: in blue the ratio of people entering hospitals divided by new daily detected cases two days earlier, which we employ to build the piece-wise linear function (in green). This is assumed for $p_{2Swe}\,(t)$, i.e. the probability of being hospitalized when detected positive.

Prevalence represents the total percentage of the country's population that is estimated to have contracted the virus, including detected and undetected individuals. We obtain an estimate of $p_{1Swe}\,(t)$ as the ratio between the measured detected cases and the total cases estimated from the

prevalence. We do so in Fig. B.2, panel **B**, which reports the number of detected cases divided by the number of total cases inferred based on prevalence, as a function of time, for the three fits to prevalence of panel **A**. In green, we report our final assumption for the functional form for $p_{1Swe}(t)$, i.e. the probability of being detected if infected, which is time-dependent for Sweden. We assumed $p_{1Swe}(t)$ to be piece-wise linear, approximately following the behaviour of the linear fit to prevalence, and saturating after the last available data point (to avoid introducing further assumptions).

Furthermore, we incorporated an additional information: during the early phases of the pandemic in Sweden, the majority of the detected cases were people needing hospitalization. This can be seen from Fig. B.2, panel **C**, which shows data for daily new detected cases, people entering hospital and people entering ICU (not to be confused with the number of people currently occupying hospitals and ICUs). The data of people entering hospital and ICU are publicly available on [332] and https://www.icuregswe.org/en/data--results/COVID-19-in-swedish-intensive-care/. In March and April, the daily number of people entering hospital was more than half of the daily number of detected cases. This ratio is shown in panel **D** (in blue, the ratio of people entering hospitals divided by new daily detected cases two days earlier). This is used to build the piece-wise linear function (in green), which was assumed as a proxy for $P_{2Swe}(t)$, i.e. the probability of being hospitalized when detected positive. This is between approximately 50% and 100% during March and April, as can be seen in both panels **C** and **D**, meaning that, during the early weeks/months of the epidemic, Sweden mostly detected those people that required hospital treatment. This clearly changed in May and June, likely due to the change in testing strategy ordered by the government on May the 3rd [245]. As observed in [244], the peak recorded end of June reflects an extension of the testing strategy to everyone with COVID-19 symptoms and to contact tracing.

Manual calibration of model parameters

We determine the values of the model parameters that provide a good fit to the available data, while having reasonable values w.r.t. the literature. In this section we explain the initial manual calibration, later on we will cross-validate it with Markov Chain Monte Carlo methods in B.

The following methodology was applied similarly for Luxembourg and Austria, and to Sweden, with some differences described in B and B. We recall that most of the parameters have values $\in [0; 1]$ due to their interpretation as rates or probabilities. Rates are in fact defined as the inverse of the average time individuals spend in a compartment; hence, a rate smaller than 1 day^{-1} means an average time in that compartment of 1 day or more, which is a reasonable value given the interpretations of the compartments, e.g. hospital and ICU, where people are very likely staying on average for at least 1 day or more.

The only exception is β, for which we considered values between 0 and 2 (minimum average time of half a day). We initially set α and β following literature values [173, 178]. When possible, we chose for the other parameters a tentative initial value based on domain knowledge. For example, observed average length of stay in hospitals or ICUs [228] are typically several days, leading to correspondingly low initial values of the rates for exiting these compartments. For the remaining parameters, e.g. those concerning non-hospitalized individuals, an initial educated guess was made based on the information available and what seemed reasonable at the time.

Next, we manually tuned the parameter values in order for the simulated model output to fit the available data. It must be stressed that, due to the model structure, individuals can only flow in one direction in the model, i.e. from being initially in the susceptible compartment, to eventually end up in either one of the recovered or dead compartments. Due to this structure, several of the parameters only influence the variables appearing downstream in the flow, not upstream. For instance, while α, β and ρ influence all compartments, the probabilities of being hospitalised or the probability of entering ICU do not influence the total detected cases. Thus, we start the manual fit by fixing those parameters that influence the total detected cases, so that the simulated curve fits the moving average of the available data. Unlike all the others, the parameter ρ changes value every time that a new measure is implemented. Each value is thus fixed in order to improve the model fit to the data of total detected cases (averaged over a week) until the next change, before moving to the next value. Eventually, parameters downstream in the flow of individuals are also changed in order for the model to fit the data of the corresponding boxes. In particular, first parameters impacting total cases, then parameters impacting hospitalisations, than parameters impacting ICU and eventually those impacting death. The procedure was repeated

until a satisfactory fit was achieved. The final values of parameters from our manual fit, for each country and wave of infection, are reported in Tab. B.6.

Parameter	Manual fit Luxembourg			Manual fit Austria		Manual fit Sweden	
	1st wave	**2nd**	**3rd**	**1st wave**	**2nd**	**1st wave**	**2nd**
β	1.287	-	-	1.287	-	1.287	-
α	0.4433	-	-	0.4433	-	0.4433	-
τ_1	0.6808	-	-	0.6808	-	0.6808	-
τ_2	0.5979	-	-	0.5979	-	0.5979	-
τ_3	0.5246	-	-	0.5246	0.5246	0.5246	0.5246
τ_4	0.0513	0.1050	0.106	0.0991	0.0948	0.1875	0.0933
τ_5	0.0617	0.1514	0.1605	0.1047	0.1240	0.2383	0.1247
τ_6	0.0853	0.1514	0.1590	0.1073	0.0856	0.1093	0.0838
τ_7	0.1084	0.1084	-	0.1084	0.1084	0.1084	0.1084
p_1	0.31	0.41	-	0.41245	-	$p_{1Swe}(t)$	0.27389
p_2	0.1534	0.08	0.042	0.162	0.065	$p_{2Swe}(t)$	0.1
p_3	0.7906	0.86	0.78	0.72	0.82	0.72	0.88
p_4	0.7906	0.9048	0.8868	0.6972	0.8345	0.6667	0.8965
p_5	0.8717	0.9814	0.8692	0.8499	0.9275	0.9021	0.9820
p_6	0.9072	0.9816	0.8868	0.8292	0.8946	0.7866	0.9731
p_7	0.9876	0.9979	0.997	0.99	0.992	0.99	0.992

Table B.6: Parameter values for manual calibration of each wave and country. All rates (α, β and each τ) are expressed in $days^{-1}$, the other parameters are dimensionless. The symbol "-" means the parameter is not changed w.r.t. the value to its left in the table. The quantities $p_{1Swe}(t)$ and $p_{2Swe}(t)$ are depicted in Fig. B.2 and their derivation is described in the corresponding section.

We performed this procedure for Luxembourg and for the first wave, which we conventionally assume to end with the minimum of the moving average of new daily cases occurring on June 4. Fitting the cases of the second wave with the parameter set from the first wave lead to a significant over-prediction of the number of people in hospital and ICU for the second wave, with respect to what is observed in the data. Thus, some of the parameter values need to be changed in order for the model to fit the data of the second wave. Similarly for the third wave. For both, we repeat the procedure of manual parameter calibration described above starting from the values of the parameters for the previous wave, and incorporating any further domain knowledge about average length of stay in hospitals and so on that become available in the meantime.

Most parameters were initially tuned for Luxembourg, and then employed for Austria and Sweden with the necessary changes to achieve a reasonably good fit to the data, or where literature was available reporting a country-specific estimate, as it is the case for the probability of being detected p_1, inferred from country-specific prevalence studies as detailed below. While this procedure is repeated for Austria with only changes in parameter values, it is not sufficient to fit Sweden. For Sweden, we further need to derive time-dependent probabilities of detection $p_{1,Swe}(t)$ and of hospitalizations $p_{2,Swe}(t)$, as described in detail in B. These two functions are reported in Fig. B.2.

Similarly to Luxembourg, we assume the 1st wave to end with the minimum of the moving average of new daily cases on June 12 for Austria and on August 31 for Sweden. We further assume the 3rd wave in Luxembourg to start from the re-opening of schools on September the 15th. We do not split Austria or Sweden data in a third wave as only the data for Luxembourg show clearly three waves of infections, see Fig. 5.2 in main text. The final values of parameters from our manual fit, for each country and wave of infection, are reported in Tab. B.6.

A key parameter for each country is the probability of being detected if infected, which has been derived from prevalence studies. For Luxembourg we consider this probability to be $p_1 = 0.31$ in the first wave thanks to the Con-Vince study [229], and we assume it to be $p_1' = 0.4$ for the second and third wave based on internal communication. These numbers correspond to values for total cases over detected cases of respectively $1/0.31$=3.2 and $1/0.4$=2.5, which are close to the value 2.3 reported as an approximated estimate for several countries by [232]. For Austria, $p_1 \approx 0.41$ has been as well derived from prevalence data https://www.sora.at/nc/news-presse/news/news-einzelansicht/news/covid-19-praevalenz-1006.html (last accessed on 15/12/2020). For Sweden, we describe how we obtain $p_{1,Swe}(t)$ and $p_{2,Swe}(t)$ in B. This estimate is also based on the prevalence data from [230, 231] displayed in Fig. B.2, panel **A**. As shown in Fig. B.2, panel **B**, we assume a time-dependent $p_{1Swe}(t)$ which increases from an estimated value of 0.02 in March to an estimated value of 0.27 from June onward.

Bayesian inference for cross-validation of parameters and evaluation of uncertainties

The parameter sets obtained by manual calibration are used in the manuscript to illustrate a number of qualitative and quantitative results. Nevertheless, the next question naturally arising is "how unique is each of these parameter sets, given the available data?". We thus want to investigate to what extent the available data constrain the parameters of the model, and to which extent these parameter values can change, i.e. to quantify the uncertainties in the estimation of these parameters, given the data. A Bayesian framework provides a natural perspective to explore this uncertainty. For this purpose, we apply Bayesian Inference, and in particular Markov Chain Monte Carlo (MCMC) methods to I) quantify the uncertainty (via credible intervals) of the estimates of each parameter given the data, and to II) assess uncertainties on combinations of parameters (credible regions), often better identifiable than the corresponding individual parameters. In order to apply Bayesian inference and MCMC methods, we employ the dedicated python library pymcmcstat [330], version 1.9.0.

Sum of square residuals for the likelihood function

To perform Bayesian inference by MCMC, we need to construct a likelihood function of parameter values given the available data and to provide prior probability distributions for each parameter, which allows us to incorporate our prior knowledge. The vector of parameters, which will be specific for each country and wave, is here indicated as $\overline{\tau}$.

The pymcmcstat package employs for the Likelihood $\mathcal{L}\left(\overline{\tau}|data\right)$ function the sum of square residuals (SSR), such that the minimum of the SSR corresponds to the maximum of the Likelihood. This choice of the likelihood function corresponds to assuming that deviations of data from the model are due to Gaussian errors, which is the simplest assumption to make without additional knowledge of the potential sources of errors.

The SSR for Luxembourg is:

$$\begin{aligned} SSR\left(\overline{\tau}|data\right) = & \sum_{i=T_0}^{T_f}\left[C^{data}\left(t_i\right) - C^{model}\left(t_i,\overline{\tau}\right)\right]^2 + \\ & \sum_{i=T_0}^{T_f}\left[H^{data}\left(t_i\right) - H^{model}\left(t_i,\overline{\tau}\right)\right]^2 + \\ & \sum_{i=T_0}^{T_f}\left[ICU^{data}\left(t_i\right) - ICU^{model}\left(t_i,\overline{\tau}\right)\right]^2 + \\ & \sum_{i=T_0}^{T_f}\left[D_{home}^{data}\left(t_i\right) - D_{home}^{model}\left(t_i,\overline{\tau}\right)\right]^2 + \\ & \sum_{i=T_0}^{T_f}\left[D_{hosp}^{data}\left(t_i\right) - D_{hosp}^{model}\left(t_i,\overline{\tau}\right)\right]^2 \ , \end{aligned} \tag{B.7}$$

where $\overline{\tau}$ is the array of parameters, $t_i = T_0, T_0+1, \ldots, T_f-1, T_f$ indicates the number of days from the beginning of the epidemic (assumed for that country), T_0 and T_f are respectively the first and last day of the wave under investigation (1st wave, 2nd wave or, for Luxembourg, 3rd wave), C is the cumulative total number of detected cases, H is the number of people in hospital, ICU is the number of people in ICU, D_{hosp} and D_{home} are respectively the number of people dead in hospital (including ICU) or outside hospital (D_{home} includes also nursing houses). The same SSR was employed for Austria and Sweden (with the corresponding data and model variables), except that the two compartments for deaths were merged into one compartment due to lack of more fine-grained data.

The quantities in Eq. B.7 derived from the model, omitting the dependencies on time and parameters for ease of notation, in terms of the model variables (Tab. B.1) are given by:

$$C^{model} \doteq R + II + Q + D_{I,hos} + D_{I,hom} + H + Hl + ICU + AIUC + NI \ , \tag{B.8}$$

$$H^{model} \doteq H + Hl + AICU \ , \tag{B.9}$$

$$ICU^{model} \doteq ICU \ , \tag{B.10}$$

$$D_{home}^{model} \doteq D_{I,hom} \ , \tag{B.11}$$

$$D_{hosp}^{model} \doteq D_{I,hos} \ . \tag{B.12}$$

The sum of square residuals Eq. B.7 attributes the same weight to all time-series data. While this choice is the simplest, it is worth noticing that it is not unique and more complex weighting approaches could represent valid choices as well.

Prior probability distributions

For each country and wave, we assume flat prior probability distributions on each parameter over a reasonable parameter space. The reasons in doing so are mainly two. First, flat priors are the simplest choice which does not require any additional knowledge — except the intervals over which these priors should be extended. Second, flat priors are the less informative choice we can make, without introducing bias toward a particular parameter set. This allows to cross-validate the manually calibrated parameter set, as the result only depend on the public time-series data and on a reasonable limitation of the available parameter space by means of the priors.
The social interaction parameter ρ_n ranges from 0 to 1. Each rate parameter ranges from 0 days^{-1} to 1 days^{-1}, except for beta that ranges from 0 days^{-1} to 2 days^{-1}. Each probability parameter is from 0 to 0.5 or 0.5 to 1 depending what the probability represents. We opt for these somewhat reduced parameter space rather than the full interval from 0 to 1 because, without loss of generality (we do not expect probabilities of dying being above 0.5, i.e. 50%, and so on), it is less demanding in terms of time and computational resources needed for the MCMC chains to converge. Similarly, we further restricted the priors between 0 and 0.5 for those rates associated to an average length of stay which is known to be considerably larger than a day, e.g. for the rate of exiting ICU. These flat prior probability distributions are reported for each country and wave as the light gray area in Fig. B.3, where we observe that the posterior probability distributions are indeed narrower than the priors. The posteriors are depicted via their 50% and 90% credible regions, respectively in blue and cyan.

Markov Chain Monte Carlo (MCMC) method

After defining the likelihood function and the priors, we calculated the posterior probability distribution over the parameter space (for each country and wave separately) by means of Markov Chain Monte Carlo (MCMC) methods available via the dedicated python library pymcmcstat.
Among the different Metropolis based sampling techniques, we employ the Delayed Rejection Adaptive Metropolis (DRAM) algorithm. It is a combination of the Delayed-Rejection (DR) algorithm, which delays rejection by sampling from a narrower distribution, and the Adaptive-Metropolis (AM) algorithm, which adapts the covariance matrix of the proposal Gaussian distribution at specified intervals.
To increase the speed of our sampling, we run 8 chains in parallel. Each chain is initialized at random initial conditions extracted from the flat prior distribution for each parameter. The multiple chains will also be useful to assess convergence of the chains (see next section). Each chain is run for 500000 iterations to ensure chain convergence (measured by the method described in the next sections). The first half of each chain is automatically discarded as burn-in (default settings of the package), while the second half is employed to determine the posterior probability distributions.

Thinning of the chains only for visualization

We did not employ the thinning of chains (only considering one sample every several) as it is not usually appropriate when the goal is precision of estimates from an MCMC sample [338]. Nevertheless, thinning can be useful for other reasons, such as memory or time constraints in post-chain processing. It was thus used to generate the figures with estimates of the posteriors, e.g. Fig. B.4. To generate these figures, we thinned the chains keeping only every 100th sample. Rather than thinning, we monitored the convergence of the MCMC estimates by comparing the outputs of multiple independent chains [338]. We thus considered the variation among these independent chains to implement the Gelman-Rubin diagnostic [336, 337].

Ensuring convergence of MCMC chains through Gelman-Rubin diagnostic

By visual inspection of the posterior probability distributions derived by each independent chain (a simple approach also performed in [341]), it seems that all the chains have converged to about the same distribution (with the exception of very few parameters where one or few chains lead to slightly different posteriors). We nevertheless further used a more quantitative approach.
There are many diagnostics available for assessing chain convergence. As suggested by [338], a robust approach is to use the Gelman-Rubin diagnostic [336, 337], which requires several sets of chains for comparison. The Gelman-Rubin approach essentially performs an analysis of the variances within each chain set and between each chain set. The same diagnostic was used for the same purpose in the framework of MCMC convergence in modelling COVID-19 in e.g. [234, 235]. The Gelman-Rubin diagnostics for the full chains returns values of R, the so-called "Potential Scale Reduction Factor (PSRF)", that are extremely close to 1 for most parameters, which indicates that the chains have converged [336, 337].

Results from the MCMC

In order to confirm the viability of the choice of parameter values from the manual calibration, we show in the Results section of the main text that the simulations generated by our model fit the available data for these countries. Additionally, we show in B that the manually calibrated sets are consistent with the Markov Chain Monte Carlo estimates. This, in turn, shows that the available data constrain the parameters only to some extent, leaving considerable uncertainties. When possible, we had informed our manually calibrated parameter set with values obtained from literature or from domain knowledge, e.g. length of stay of patients in ICUs and hospitals. Instead, the MCMC was let free to reproduce the raw time-series data. This induces larger uncertainties and yields some degeneracy between parameters, with combinations (e.g. ratios) of parameters being better constrained by the data than individual parameters (see B).

Manually calibrated parameter sets are compatible with Bayesian inference estimate, which underlines wide uncertainties in parameter values

The parameter sets from the manual calibration of the model discussed in B are summarized in Tab. B.6, Tab. B.3, Tab. B.4 and Tab. B.5 and are employed through the manuscript. Fig. B.3 shows the Bayesian estimates of these parameters given the time series data, obtained by MCMC (credible intervals) and employed to cross-validate them.

Posteriors are indicated by their 50% (blue) and 90% (cyan) credible intervals, and are usually considerably narrower than the assumed flat prior distributions (from B). Nevertheless, this is not the case for some parameters, for which the posteriors are almost flat and as wide as the priors. This means that some parameters are not well identified by the available data and model structure. Fig. B.3 reports the point-estimates from the MCMC, i.e. mean and maximum a posteriori estimate of the posterior of each parameter. For rather symmetric distributions the two values tend to correspond, while they differ for very skewed distributions. Moreover, for almost flat posterior distributions (like e.g. those for most of the parameters τ_i with $i = 4, 5, 6$) the maximum is not very representative of the distribution.

Fig. B.3 shows that, for all countries and waves, the values of the manual fit (green) are mostly very close to either the maximum or the mean a posteriori estimate. It is usually within the 50% credible interval of the posterior, or at least inside the 90% credible interval, with only a couple of exceptions. Thus, our manually calibrated sets of parameters are fully consistent with the Bayesian estimate based on MCMC. However, credible intervals are relatively wide, which indicates that the estimated uncertainties of these parameters, based on the data alone, are rather large. In particular, at a qualitative level, the values of the social interaction parameter ρ_n are in general better constrained than the other parameters, with the probabilities p_i being slightly better constrained than the rates τ_i. These are in general poorly identified, except for α and β which are affected by smaller uncertainties w.r.t. other rates. In turn, the probability p_7 (out of "recovery at home") to be extremely well constrained (to values close to 1) in most of the waves and countries.

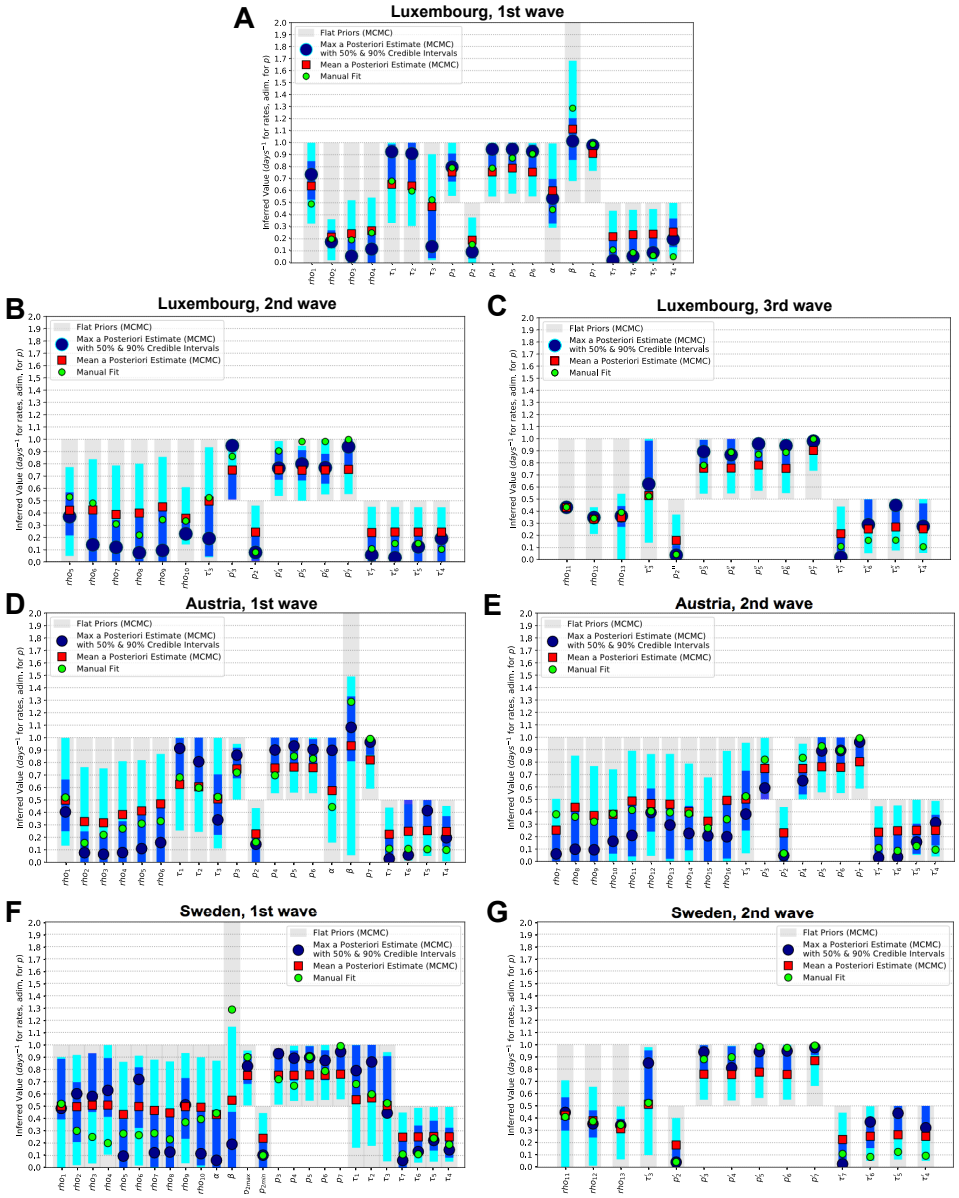

Figure B.3: Posterior probability distributions from MCMC for each parameter, compared with priors and with manual fits, for each country and wave. Luxembourg (**A**: 1st wave, **B**: 2nd wave, **C**: 3rd wave), Austria (**D**: 1st wave, **E**: 2nd wave) and Sweden (**F**: 1st wave, **G**: 2nd wave). For each parameter, prior probability distributions are reported as gray areas, while the posteriors are reported by means of their 50% (blue) and 90% (cyan) credible intervals, with their maxima reported as large blue dots and their means as red squares. The parameter values for the manual fit (Tab. B.6 for probabilities and rates, Tab. B.3, Tab. B.4 and Tab. B.5 for ρ_n) are reported as green small circles.

Quantifying uncertainties on estimate of parameters by MCMC: wide uncertainties, but degeneracy in parameter estimations

The domain of the posterior probability distribution obtained via the MCMC, B, has the same number of dimensions as the number of parameters considered, e.g. 19 for the 1st wave of Luxembourg. When we are interested in one parameter at a time, we project the chains on one dimension (which, if we had an analytic form for the posterior, would be done by integrating over all parameters except the one of interest, thus obtaining the marginal posterior distribution). This is how the 1D posteriors in Fig. B.3 were obtained.

The next question is: are the wide uncertainties affecting some parameters an effect of having projected to a lower dimensional space, or are certain parameters poorly identified? Both types of situations arise, depending on the parameter.

To investigate this, we project the posterior distribution over two parameters at a time, for each couple of parameters in Fig. B.4 for the MCMC run of the 1st Wave of Luxembourg, and in Fig. B.5, B.6, B.7, B.8, B.9 and B.10 for the other waves and countries. While certain parameter pairs are very well constrained, others are not; certain parameter pairs appear to be correlated or anti-correlated. We hence observe a degree of degeneracy between parameters: there is not a unique combination of parameters that allows a good fit of the model to the data, but many of them.

Moreover, certain combinations (e.g. ratios) of parameters are better constrained than the individual parameters. Consider e.g. the parameters α and β, which come from the standard SEIR model.

Their credible intervals are displayed in Fig. B.3. The joint posterior over the two parameters (close to the center of Fig. B.4 for Luxembourg, Fig. B.7 for Austria and Fig. B.9 for Sweden) is narrow and rotated toward the diagonal direction, showing anti-correlation between the estimates of the two parameters. This means that low values of β can only be considered together with high values of α, and the other way around. These patterns occur for other parameters as well, and they are conserved to some extent across countries. So, they are likely specific to the model's structure and parameters rather than to the country. Other interesting patterns are

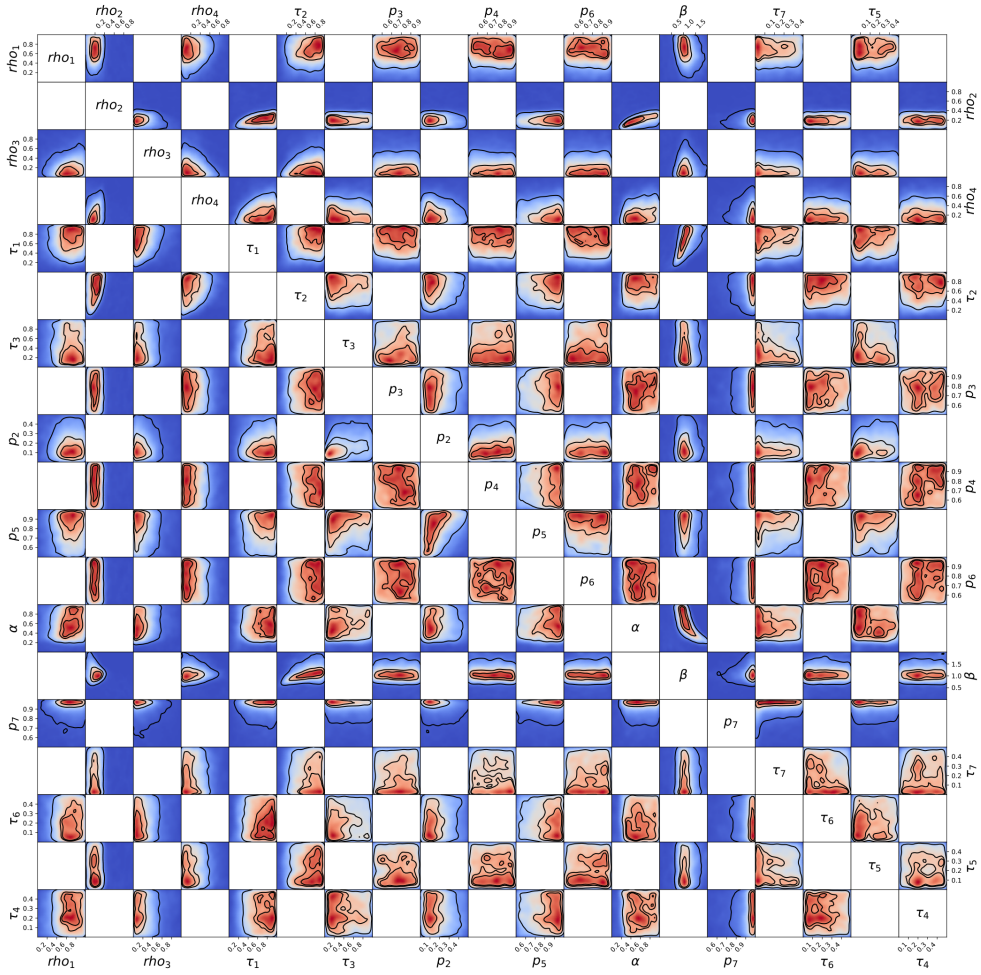

Figure B.4: Posterior probability distribution from MCMC projected over each pair of parameters, for the 1st wave of Luxembourg. On each square, the 2D projections of the posterior probability distribution estimated (*cf.* B) correspond to the 1D projections of Fig. B.3. For visual clarity, the parameters' names and scales are reported only at the margins of the figure and on the diagonal, but they apply to all subplots. As the figure is symmetric along the diagonal, each projection is only reported once (hence the white squares). The heatmap colors represent posterior probability values: red equals high and blue low probability. Dark blue represents a probability close to 0. The three black contours reported in each panel represent 25%, 50% and 90% Bayesian credible regions. Correlations, anti-correlations and more complex degeneracy between parameter pairs are visible.

visible, e.g. anti-correlation between each ρ_n and the subsequent in time in the 2nd and 3rd waves of Luxembourg, the 2nd wave of Sweden and to some extent in the 1st and 2nd waves

of Austria. This can easily be understood in terms of the model: lowering the social interaction one time-period and increasing it the next, or doing the converse, can equally lead to the same good agreement with data. While certain couples of parameters seem to be well constrained, other parameters have projected posteriors that are still close to flat, resulting in squares that are predominantly red in Fig. B.4. This effect is weaker for certain waves and countries (3rd wave of Luxembourg and the 2nd wave of Sweden), but stronger for others (1st wave of Sweden, where parameters seem to be very poorly identified). This could be related to the dimension of the domain of the posterior (the higher the number of parameters, the less constrained), as the 3rd wave of Luxembourg and the 2nd wave of Sweden both have indeed “only" 14 parameters each, while the 1st wave of Sweden has 26 of them.

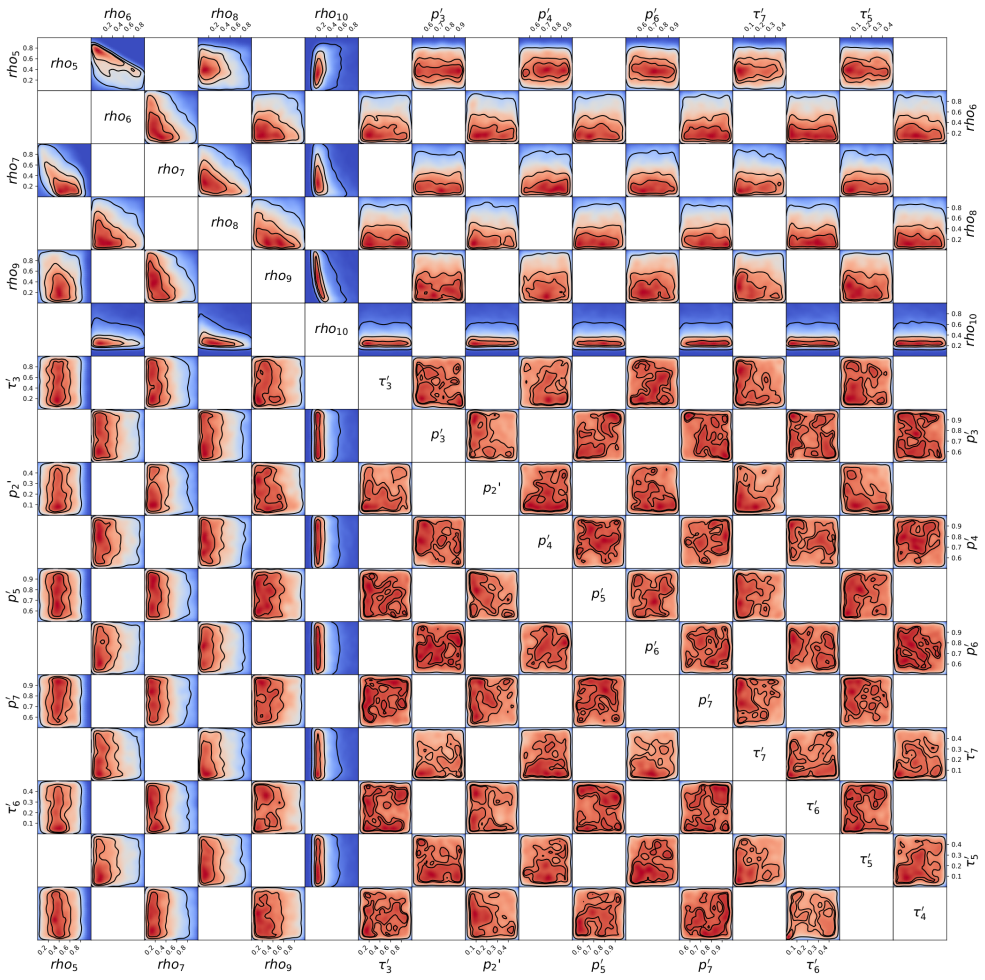

Figure B.5: Posterior probability distribution from MCMC projected over each couple of parameters, for the 2nd wave of Luxembourg. This figure is constructed in the same way described in the caption of Fig. B.4

.

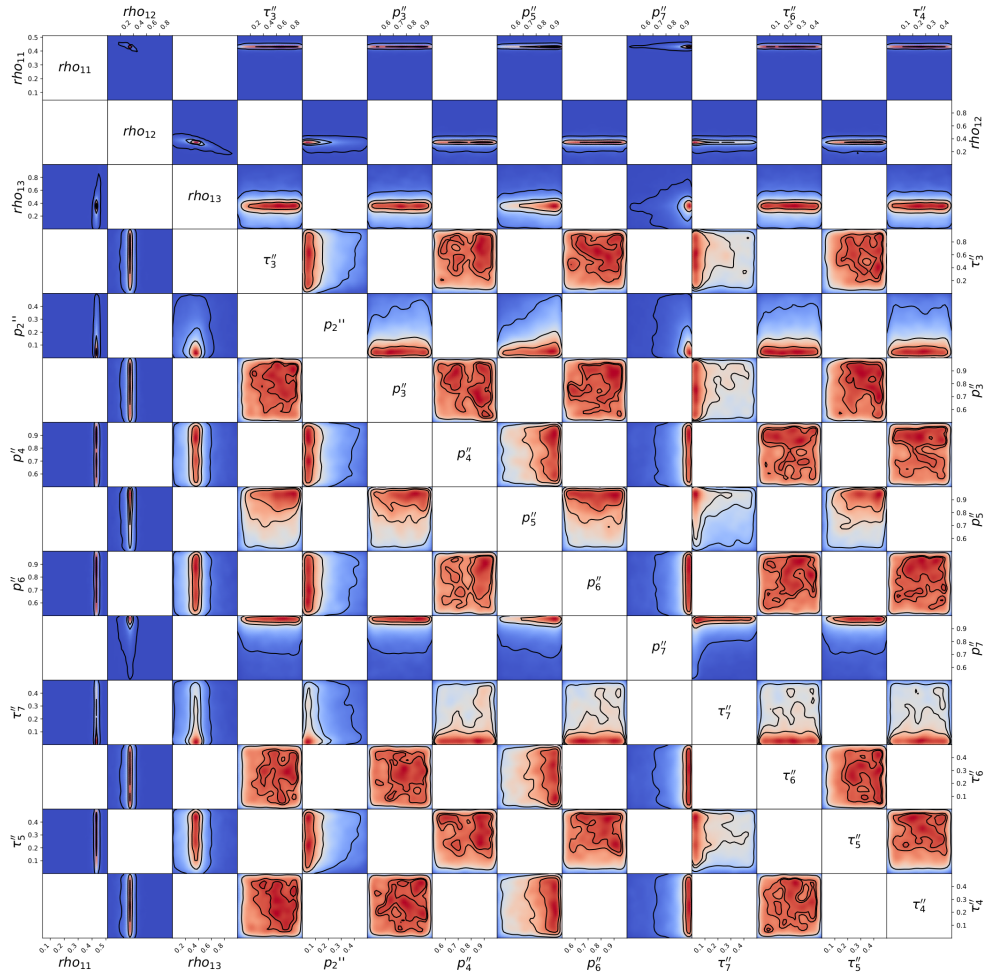

Figure B.6: Posterior probability distribution from MCMC projected over each couple of parameters, for the 3rd wave of Luxembourg. This figure is constructed in the same way described in the caption of Fig. B.4

.

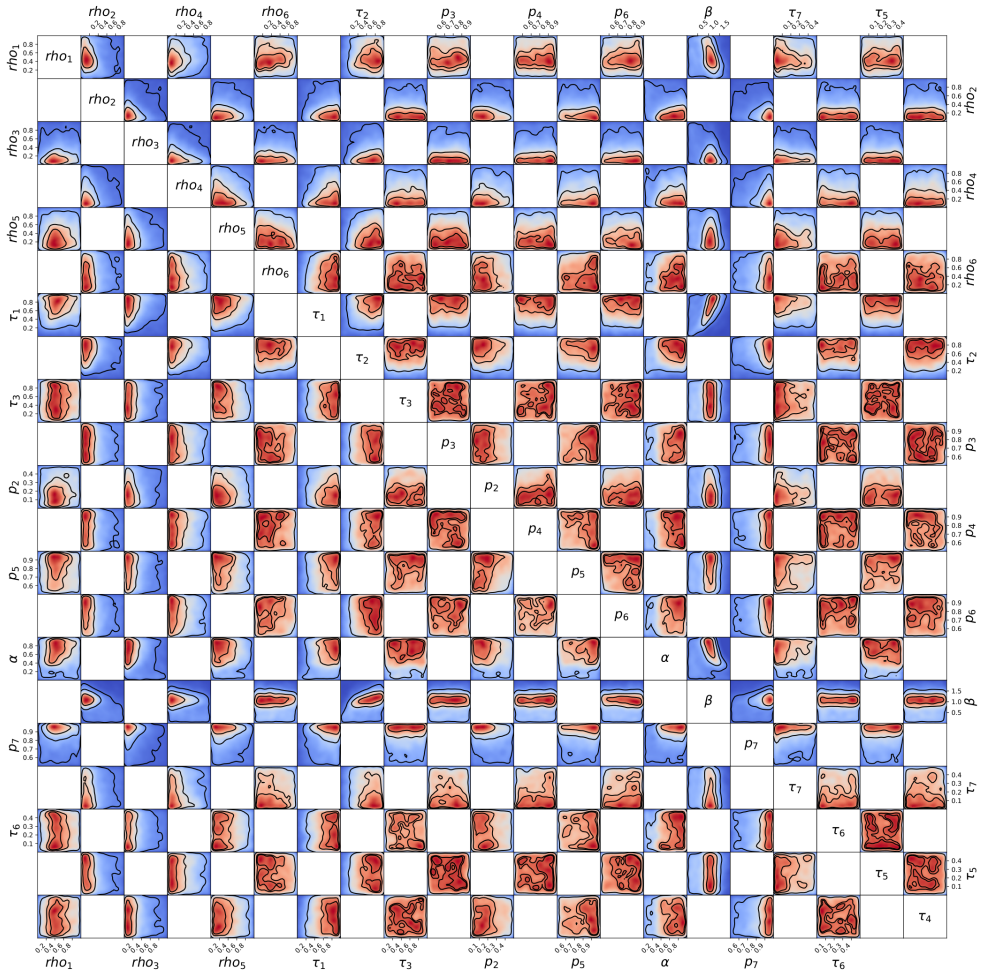

Figure B.7: Posterior probability distribution from MCMC projected over each couple of parameters, for the 1st wave of Austria. This figure is constructed in the same way described in the caption of Fig. B.4

.

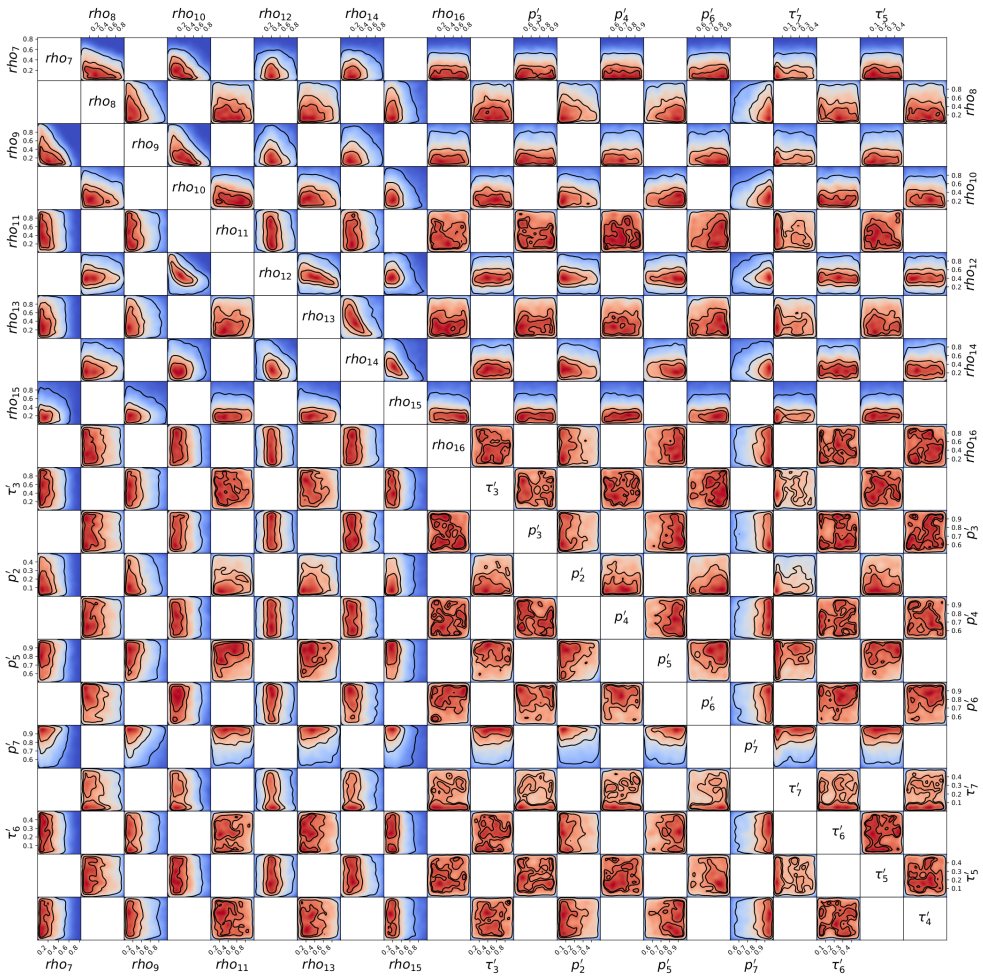

Figure B.8: Posterior probability distribution from MCMC projected over each couple of parameters, for the 2nd wave of Austria. This figure is constructed in the same way described in the caption of Fig. B.4

.

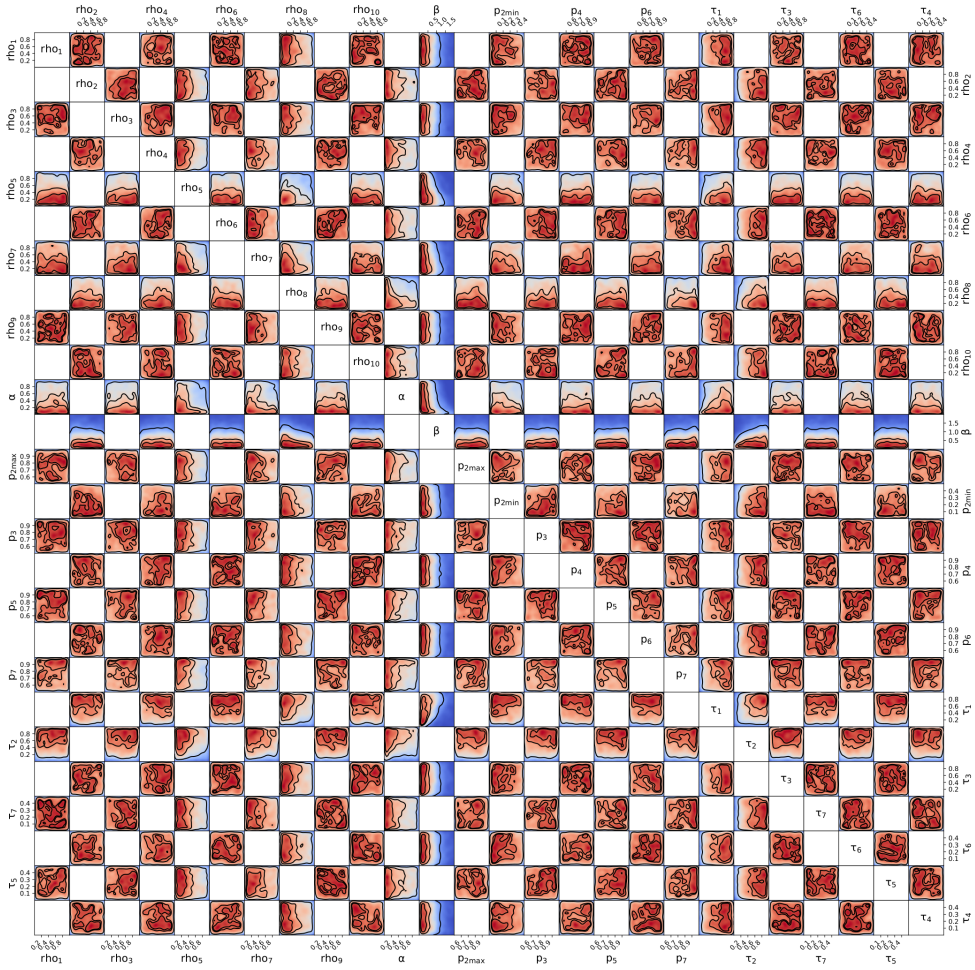

Figure B.9: Posterior probability distribution from MCMC projected over each couple of parameters, for the 1st wave of Sweden. This figure is constructed in the same way described in the caption of Fig. B.4

.

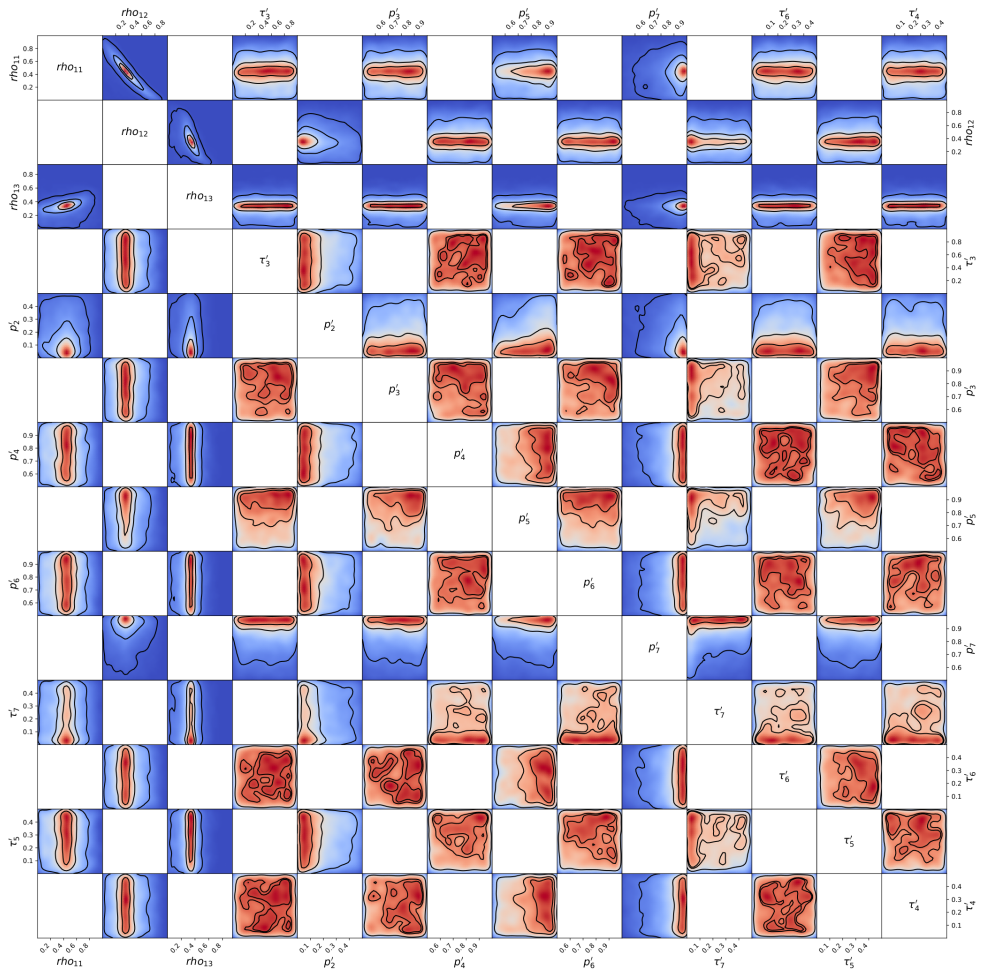

Figure B.10: Posterior probability distribution from MCMC projected over each couple of parameters, for the 2nd wave of Sweden. This figure is constructed in the same way described in the caption of Fig. B.4

.

APPENDIX C

APPENDIX OF COVID-19 CRISIS MANAGEMENT IN LUXEMBOURG: INSIGHTS FROM AN EPIDEMIONOMIC APPROACH

Architecture of the epidemiological block

In line with the time structure of our economic block, our epidemiological block formalizes the dynamics of the stocks of susceptible ($L^S_{i,t}$), infected ($L^I_{i,t}$) and recovered ($L^R_{i,t}$) workers in industry i over periods of one week ($t = 1, \cdots, T$). Traditional SIR models have a daily interpretation ($\tau = 1, \cdots, $) and assume a closed system implying constant population ($L_i = L^S_{i,\tau} + L^I_{i,\tau} + L^R_{i,\tau} \forall \tau$) and no contamination by outsiders. Starting from a standard SIR model, this Appendix discusses the steps that lead to our weekly epidemiological model with dynamic recovery rates, inter-industry linkages and contamination by outsiders.

Dynamic vs probabilistic recovery rates

Discretization of the standard daily SIR system gives:

$$\begin{cases} L^S_{i,\tau+1} = L^S_{i,\tau} - \beta_{i,\tau} L^S_{i,\tau} \frac{L^I_{i,\tau}}{L_i} = L^S_{i,\tau}(1 - \beta_{i,\tau} \frac{L^I_{i,\tau}}{L_i}) \\ L^I_{i,\tau+1} = L^I_{i,\tau}(1-\gamma_{i,\tau}) + \beta_{i,\tau} L^S_{i,\tau} \frac{L^I_{i,\tau}}{L_i} = L^I_{i,\tau}(1 - \gamma_{i,\tau} + \beta_{i,t} \frac{L^S_{i,\tau}}{L_i}) \\ L^R_{\tau+1} = L^R_{\tau} + \gamma_{i,\tau} L^I_{\tau} \end{cases}$$

where τ is the daily time index, $\beta_{i,\tau}$ and $\gamma_{i,\tau}$ are interpreted as the daily transmission and recovery rates in industry i at time τ. The daily transmission rate, $\beta_{i,\tau}$ can be influenced by industry-specific characteristics (physical proximity, number of contacts, exposure to disease) and by public health policies (physical distancing, hygiene and prevention measures, etc.). Hence, it must be treated as an endogenous and time-varying rate.

As for the recovery rate, it is usually perceived as a biological and disease-specific parameter that is linked to the average duration of infectious period. In the case of COVID-19, the length of the contagion period is about 10 days, implying that the average daily recovery rate is usually expressed as one over ten days ($\gamma_{i,\tau}$= 0.1 $\forall i, \tau$). This value is relevant in two particular situations:

- In a deterministic case where contagious people recover after 10 days, $\gamma = 0.1$ is relevant if the total stock of infected people at time τ is uniformly distributed over the 10 infected daily cohorts (whose sizes are given by $\beta_{i,\tau-k} L^S_{i,\tau k} \frac{L^I_{i,\tau-k}}{L_i} \forall k = 0, \cdots, 9$).[1]
- In a probabilistic setting, $\gamma = 0.1$ is relevant if each infected individual has a constant daily probability to recover regardless of when she became infectious.

Apart from these situations, the number of healings varies along the life cycle of the disease. In the (arguably most relevant) deterministic case where the length of the contagion period is assumed to be exactly equal to 10 days, the number of healings at day τ is equal to the number

[1] This is illustrated in Fig. C.3 where each pair of vertical bars represents a cohort of infected people. Each bar spreads over 10 contagion days. The plain-color area is meant to represent the asymptomatic period (i.e., 2/10 days for symptomatic cases and 10/10 days for asymptomatic cases). The stock of infected people at day τ (or at day $\tau+7$) is surrounded by the thick-border box in gray (or on black). On average, infected people at time τ will remain contagious during 4.5 days after day τ (0 day for cohort $\tau - 9$, 1 day for cohort $\tau - 8, \cdots, and 9 days for cohort \tau$).

of people who became contagious at day $\tau - 9$. This number is given by $\beta_{i,t-9}\frac{L^S_{i,\tau-9}L^I_{i,\tau-9}}{L_i}$ this setting, system C must be rewritten as:

$$\begin{cases} L^S_{i,\tau+1} = L^S_{i,\tau} - \beta_{i,t}\frac{L^S_{i,\tau}L^I_{i,\tau}}{L_i} \\ L^I_{i,\tau+1} = L^I_{i,\tau} + \beta_{i,t}\frac{L^S_{i,\tau}L^I_{i,\tau}}{L_i} - \beta_{i,t-9}\frac{L^S_{i,\tau-9}L^I_{i,\tau-9}}{L_i}) \\ L^R_{\tau+1} = L^R_{i,\tau} + \beta_{i,t-9}\frac{L^S_{i,\tau-9}L^I_{i,\tau-9}}{L_i} \end{cases}$$

A numerical example allows to illustrate the implication of approximating system C using system C. Consider a closed system with 1,000 people starting at time 1 with 999 susceptible and 1 infected individuals (and $L^I_{i,\tau} = 0 \forall \tau < 1$). The initial transmission rate is equal to 0.2 and people fully recover after 10 days. This implies that without prevention measures, there would be 226 susceptible, 2 infected and 772 recovered individuals after 365 days. However, at day 22 (beginning of fourth week), the transmission rate falls to 0.15 due to an exogenous intervention. This implies that there will be 440 susceptible, 2 infected and 558 recovered individuals after 365 days. We introduce this change in $\beta_{i,t}$ to examine whether it can be accurately identified by the system. The continuous curve in Fig. (C.1a) shows the evolution of the stocks of susceptible, infected and recovered individuals over the first 14 weeks.

Fig. (C.1b) shows the evolution of the ratio of daily healings to the stock of contagious individuals, the true measure of $\gamma_{i,\tau}$. These curves start from 0 at the beginning of the epidemic (days 1 to 9), as the very first infected individual needs 10 days to recover. Then, it becomes positive but smaller than 0.1 (denoted by γ_0 henceforth and represented in dashed gray) at the beginning of the epidemic (until day 31). This is because earlier infected cohorts are smaller in size than the most recent ones. The shock in the transmission rate on day 22 translates into a decrease in the recovery rate 10 days later. Then $\gamma_{i,\tau}$ increases again and at the end of the epidemic, it is larger than γ_0. This is because earlier infected cohorts are greater in size than the most recent ones.

The fact that the true fraction $\gamma_{i,\tau}$ varies over the life cycle of the epidemic has important implications for the estimation of the SIR model. Many SIR models are used to identify the dynamics of transmission rates ($\beta_{i,\tau}$) that fit the dynamics of the share of infected people ($L^I_{i,\tau}$) assuming a constant level for (say $\gamma_0 = 0.1$), and then use projections of $\beta_{i,\tau}$ to predict the future

share of infected people. By imposing a constant γ_0 which is greater than the actual recovery rate at the beginning of the epidemic, the calibrated level of $\beta_{0,\tau}$ is greater than its actual value. The opposite pattern ($\beta_{0,\tau} < \beta_{i,\tau}$) emerges after the peak of the infection curve.

Fig.(C.1c) illustrates the biases ($\beta_{0,\tau}$ $\beta_{i,\tau}$) implied by the hypothesis of a constant γ_0. The true value of β is represented by the continuous black curve. First, deviations from the true value are large. If one uses $\beta_{0,\tau}$ to forecast the number of infected people, projections errors might be important. Second, $\beta_{0,\tau}$ exhibits more gradual changes that are not compatible with the one-shot decrease in the true $\beta_{i,\tau}$. Third, a constant γ_0 leads to an overestimation of the change in transmission rates between the initial and final phases of the epidemic. Fourth, although the identification of $\beta_{0,\tau}$ is such that the model replicates the trajectory of L_τ^I , another implication of misestimating $\beta_{i,\tau}$ and $\gamma_{i,\tau}$ is that the model wrongly predicts the long-run levels of $L_{i,\tau}^S$ (by -10.2%) and $L_{i,\tau}^R$ (by +7.8%). This is illustrated in Figure A.1a, where the true trajectory of these variables (continuous curves) is compared with predicted values (dashed curves). It is worth noticing that smoothing $\beta_{i,\tau}$ does not attenuate the biases. In contrast, calibrating system C allows to retrieve the true parameters. This is the reason why we opt for a dynamic (rather than for a probabilistic) recovery process.

From a daily to a weekly structure

Starting from the daily system with a dynamic recovery process, the evolution of the stocks of susceptible, infected and recovered across weeks is governed by:

$$\begin{cases} L_{i,\tau+7}^S = L_{i,\tau}^S - \sum_{k=0}^{6} \beta_{i,\tau+k} \frac{L_{i,\tau+k}^S L_{i,\tau+k}^I}{L_i} \\ L_{i,\tau+7}^I = L_{i,\tau}^I + \sum_{k=0}^{6} \beta_{i,\tau+k} \frac{L_{i,\tau+k}^S L_{i,\tau+k}^I}{L_i} - \sum_{k=0}^{6} \beta_{i,\tau+k-9} \frac{L_{i,\tau+k}^S L_{i,\tau+k-9}^I}{L_i}) \\ L_{\tau+7}^R = L_{i,\tau}^R + \beta_{i,\tau+k-9} \frac{L_{i,\tau+k-9}^S L_{i,\tau+k-9}^I}{L_i} \end{cases}$$

Changing time notations such that t now represents weeks (and not days) and starting from the same day ($t = \tau$), our weekly system can be expressed in its reduced form as:

$$\begin{cases} L^S_{i,t+1} = L^S_{i,t} - b_{i,t}\frac{L^S_{i,t}L^I_{i,t}}{L_i} \\ L^I_{i,t+1} = L^I_{i,t} + b_{i,t}\frac{L^S_{i,t}L^I_{i,t}}{L_i} - G^R_{i,t} \\ L^R_{i,t+1} = L^R_{i,t} + G^R_{i,t} \end{cases}$$

where $b_{i,t} = \sum_{k=0}^{6} \beta_{i,\tau+k}\frac{L^S_{i,\tau+k}L^I_{i,\tau+k}}{L^S_{i,t}L^I_{i,t}}$ is interpreted as the weekly transmission rate and $G^R_{i,t} = \sum_{k=0}^{6} \beta_{i,\tau+k-9}\frac{L^S_{i,\tau+k-9}L^I_{i,\tau+k-9}}{L_i}$ is the weekly flow of recovered.

As approximation, we assume a uniform distribution of new infections within a week. This does not imply that the total stock of infected people, $L^I_{i,\tau+k}$, is uniformly distributed over the 10 infected cohorts at time t, an assumption that would allow to use a constant recovery rate (see previous section). This means that $L^I_{i,\tau+k}$ increases by the same number at each day of the week or, equivalently, that the slope of the infection curve is constant within a week. It writes as:

$$\beta_{i,\tau+k}\frac{L^S_{i,\tau+k}L^I_{i,\tau+k}}{L_i} \approx \beta_{i,\tau}\frac{L^S_{i,\tau}L^I_{i,\tau}}{L_i}\forall k = 0,\cdots 6 \forall k = 0,\cdots 6 \forall k = 0,\cdots 6.$$

This assumption implies that (i) the weekly flow of new contagion is seven times larger than the daily flow, (ii) that the weekly transmission rate is seven times larger than the daily transmission rate, $b_{i,t} = 7 * \beta_{i,\tau}$, and (iii) that the weekly flow of recovered can be approximated by

$$G^R_{i,t} = \frac{2}{7}b_{i,t-2}\frac{L^S_{i,t-2}L^I_{i,t-2}}{L_i} + \frac{5}{7}b_{i,t-1}\frac{L^S_{i,t-1}L^I_{i,t-1}}{L_i}$$

This is illustrated in Fig. C.3. The stock of contagious people at the beginning of time $t+1$ (box surrounded by the thick black border) is equal to the stock of contagious people at the beginning of time $t+1$ (box surrounded by the thick gray border, including cohorts colored in red and in green), minus the recovered (cohorts colored in green), plus the weekly flow of new infections (cohorts colored in yellow). The weekly flow of recovered comprises two of the seven cohorts that were infected during week $t2$ (i.e., the first term in Eq.C) as well as five of the seven cohorts that

were infected during week $t1$ (i.e., the second term in Eq.C). The recovery rate in week t can be expressed as $g_{i,t} = G^R_{i,t}/L^I_{i,t}$. Is this assumption of a constant slope of the within-week infection curve more satisfactory than the assumption of a constant γ_0 in the probabilistic model? The answer is definitely affirmative. Starting from the numerical example of the previous section and gathering data on the number of infected people at the beginning of each week, we recursively compute the weekly flow of new infections, the weekly flow of recovered (equal to lagged infection flows as defined in Eq.C), and identify the parameters $b_{i,t}$ and $g_{i,t}$ that perfectly fit the infection curve. We then simulate the evolution of the number of susceptible and recovered. Fig. (C.2a) shows that the simulated numbers (thin curves with diamonds) almost perfectly correspond to the true numbers (solid thick curves). As for the identification of $b_{i,t}$ and $g_{i,t}$, their evolution is depicted in Fig. (C.2b). The $g_{i,t}$ curve resembles that of the daily model (after some rescaling). The $b_{i,t}$ curve shows a big drop between week 3 and week 4, in line with the transmission shock. As $b_{i,t}$ is an average of seven days, this shock is smoothed over a few periods. Fitting this curve with two parameters, one pre-shock level and one post-shock level, would give a very good fit.

Adding contamination by outsiders

Another feature of our model is that susceptible individuals in industry i can be contaminated by infected people outside the labor market (in family or in social life). Virus transmission is now a weighted sum the transmission rates on the job (with weight $\kappa_{i,t}$) and outside the labor market (with weight $1-\kappa_{i,t}$). Hence, system C becomes:

$$\begin{cases} L^S_{i,t+1} = L^S_{i,t} - \kappa_{i,t} b_{i,t} L^S_{i,t} \frac{L^S_{i,t} L^I_{i,t}}{L_i} - (1-\kappa_{i,t}) b_{0,t} L^S_{i,t} p_t \\ L^I_{i,t+1} = L^I_{i,t} + \kappa_{i,t} b_{i,t} \frac{L^S_{i,t} L^I_{i,t}}{L_i} + (1-\kappa_{i,t}) b_{0,t} L^S_{i,t} p_t \\ L^R_{i,t+1} = L^R_{i,t} + G^R_{i,t} \end{cases}$$

where $\kappa_{i,t}$ denotes the time spent on the labor market by workers from industry i at time t, $b_{0,t}$ is the weekly transmission rate outside the labor market, and p_t is the proportion of infected people

(a) Dynamics of SIR stocks over the first 14 weeks

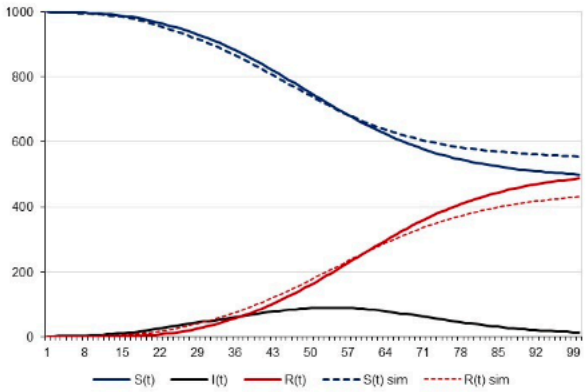

(b) Estimation of the daily fraction of recovered ($\gamma_{i,\tau}$)

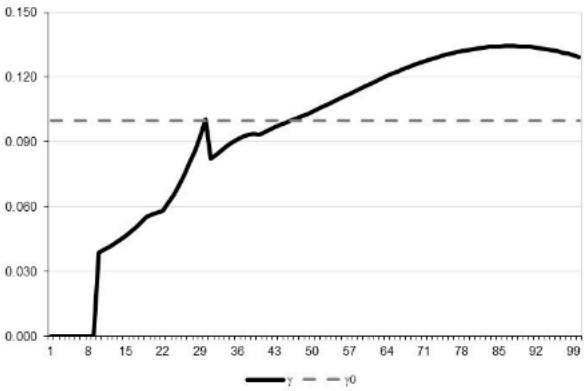

(c) Estimation of the daily transmission rate ($\beta_{i,\tau}$)

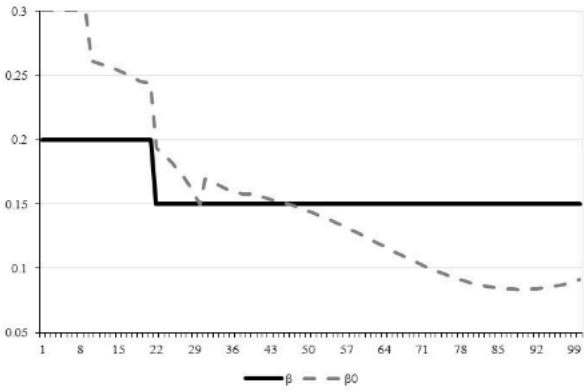

Figure C.1: Daily model with lags vs constant recovery rate

(a) Dynamics of SIR stocks over the first 14 weeks

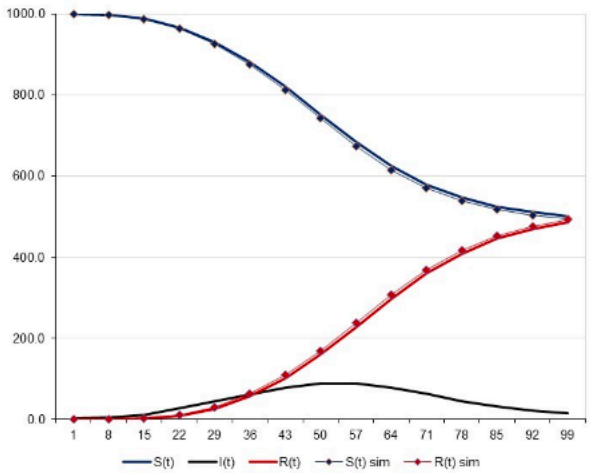

(b) Estimation of the weekly transmission rate ($b_{i,t}$)

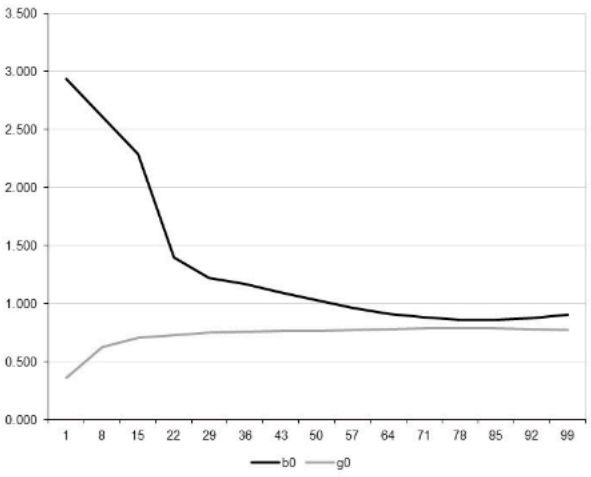

Figure C.2: Weekly model with dynamic recovery process

in the total population. The weekly flows of recovered within group i must be rewritten as:

$$G^R_{i,t} = \frac{2}{7}[\kappa_{i,t-2} b_{i,t-2} \frac{L^S_{i,t-2} L^I_{i,t-2}}{L_i} + (1-\kappa_{i,t-2}) b_{0,t-2} L^S_{i,t-2} p_{t-2}] + \frac{5}{7}[\kappa_{i,t-1} b_{i,t-1} \frac{L^S_{i,t-1} L^I_{i,t-1}}{L_i} + (1-\kappa_{i,t-1}) b_{0,t-1} L^S_{i,t-}$$

If p_t always remains positive, the only steady state of this economy involves $L^R_i = L_i$. However, p_t is linked to the average proportion of infected across all groups and might converge to zero. This implies that this extended SIR model has similar properties as the standard one.

Endogenizing virus transmission

The link between the economic and epidemiological blocks of the model operates through $\chi_{i,t}$. Weighted transmission rates are influenced by economic conditions, by industry-specific characteristics, and by public health measures. For a given proportion of susceptible and infected workers in industry i, on-the-job virus transmission depends on the share of daily interactions/contacts experienced on the labor market (1), on the average number of contacts per person per unit of time (2), and on the probability that infected people can have contacts with susceptible subjects (3). We express it as:

$$\kappa_t b_{i,t} = \underbrace{\epsilon e_{i,t}}_{(1)} \underbrace{\bar{b}_i \rho_{i,t}}_{(2)} \underbrace{[(1-\theta)\mu^v_{i,t} + \theta \mu^a_{i,t}]}_{(3)}$$

where $\epsilon e_{i,t}$ the interaction time spent on the job (product of the average fraction of time spent on the labor market by the fraction of time spent in daily social interactions on the job); this is meant to represent effect (1). As for effect (2), it is the product of $\bar{b}_i$, an industry-specific parameter that reflects working conditions in normal times (physical proximity and exposure to disease), by $\rho_{i,t}$. the latter is a variable capturing prevention and physical distancing measures implemented in the industry. Effect (3) is expressed as $[(1-\theta)\mu^v_{i,t} + \theta\mu^a_{i,t}]$, which captures the probability that a contagious worker goes to work at time t.

If $\rho_{i,t}$ depends on the density of workers at the workplace (proxied by $e_{i,t}$), changes in em- ployment rates influence transmission rates through the extensive margin changes in time spent on the job and the intensive margin physical distancing on the job. A potential specification is $\rho_{i,t} = \bar{\rho}_t e^x_{i,t}$ where x is the elasticity of physical distancing to the presence of workers at the workplace. If

$x = 0$, a lockdown-driven decrease in $\rho_{i,t}$ is permanent; if $x > 0$, part of that decrease is lost when workers get back to their workplace.

Similarly, transmission rates outside the labor market can be expressed as:

$$(1 - \kappa_t)b_{0,t} = \underbrace{(1 - \epsilon e_{i,t})}_{(1)} \underbrace{\bar{b_0}\rho_{0,t}}_{(2)}$$

where $1\epsilon e_{i,t}$,t is the interaction time spent outside the labor market (one minus interaction time spent on the job),$\bar{b_0}$ is a region-specific parameter that reflects living conditions, $\rho_{0,t}$ is a variable capturing prevention and physical distancing measures implemented outside the labor market.

Timing of the epidemiological process

To approximate the parameters governing the effectiveness of testing policies, we count the number of working days supplied by all infected cohorts during the first six days of week t (i.e. from day τ to$\tau + 6$) ignoring the relative size of the different cohorts. Fig. C.3 shows that 15 cohorts can supply labor during week t. Each cohort is represented by a vertical bar whose length corresponds to 10 infectious days. Members of the green, red and yellow cohorts can supply a maximum of 27, 18 and 15 days, respectively. This means a maximum of 60 working days. We assume new infected people are asymptomatic during at least 2 days, represented in light green, red or yellow. Then, symptomatic people show symptoms during 8 additional days, represented in dashed color. Asymptomatic people never show symptoms.

If *no testing is done* during week t, we can count the share of working days (excluding $\tau + 7$) that symptomatic workers from cohort t 1 spend on the labor market without symptoms: this gives 0 days for the green cohorts, 3 days for the red ones, and 9 days for the yellow ones. This represents a total of 12 days out of 60. Hence, $\mu^v_{i,t} = 0.20$. As for asymptomatic people, $\mu^v_{i,t} = 0.25$

If a *weekly test* is performed (say on Monday 8AM) and results are known immediately (Or equivalently, the test can be performed on Sunday at 8PM and results are known on Monday morning), the only workers supplying working days are those of the yellow cohorts, with 9 days for the symptomatic and 15 for the asymptomatic. We thus have $\mu^v_{it} = 0.15$ and $\mu^v_{it} = 0.25$.

Finally, in case a daily test is done at 8AM with immediate results, we have $\mu_{it}^v = \mu_{it}^a = 0$.

Validation of our calibrated transmission rates

Heterogeneity in transmission rates across industries is supposed to reflect differences in exposure to risk. To validate our calibration strategy, we correlate our blab with an index $b_{i,t}^{lab}$ of exposure to risk. We use data on the need of physical proximity to operate ($ER_{1,i}$) and on workers exposure to diseases ($ER_{2,i}$). Occupation-specific proximity indices can be computed using the ONet database,[2] and aggregated by industry using the occupational shares in employment. Disease exposure indices can also be computed using the industry shares of workers heavily occupied in medical occupations and health services reported in the same ONet database. To construct an index of exposition to risks for each industry i (ER_i), we standardize each risk factor $ER_{k,i}$ so that the maximal value equals 100, and combine them using a risk technology that gives greater weights to larger values:

$$ER_i = [\frac{\sum_k ER_{k,i}^{1+\xi}}{K}]^{\frac{1}{1+\xi}}$$

where $\xi \geq 0$ is a parameter penalizing large values (if $\xi = 0$, ER_i is the arithmetic mean of $ER_{k,i}$), K is the number of risk indicators (only 2 in our case).

Results are depicted in the last column of Table B.1 for $\xi = 4$. The minimal exposition to risk is obtained for Agriculture, forestry and Fishing, whereas the maximal level is obtained in the Health and social work sector, followed by Accommodation and Food, and Education. Then, Fig. C.4 shows the correlation between the basic reproduction numbers and the exposure to risk across industries.

Cost of the lockdown by sector

Fig. C.5 describes the health and economic implications of the lockdown measures for each industry. Aggregate effects are presented in the core of the text (see Figure 4).

[2] See http://www.onetcenter.org/

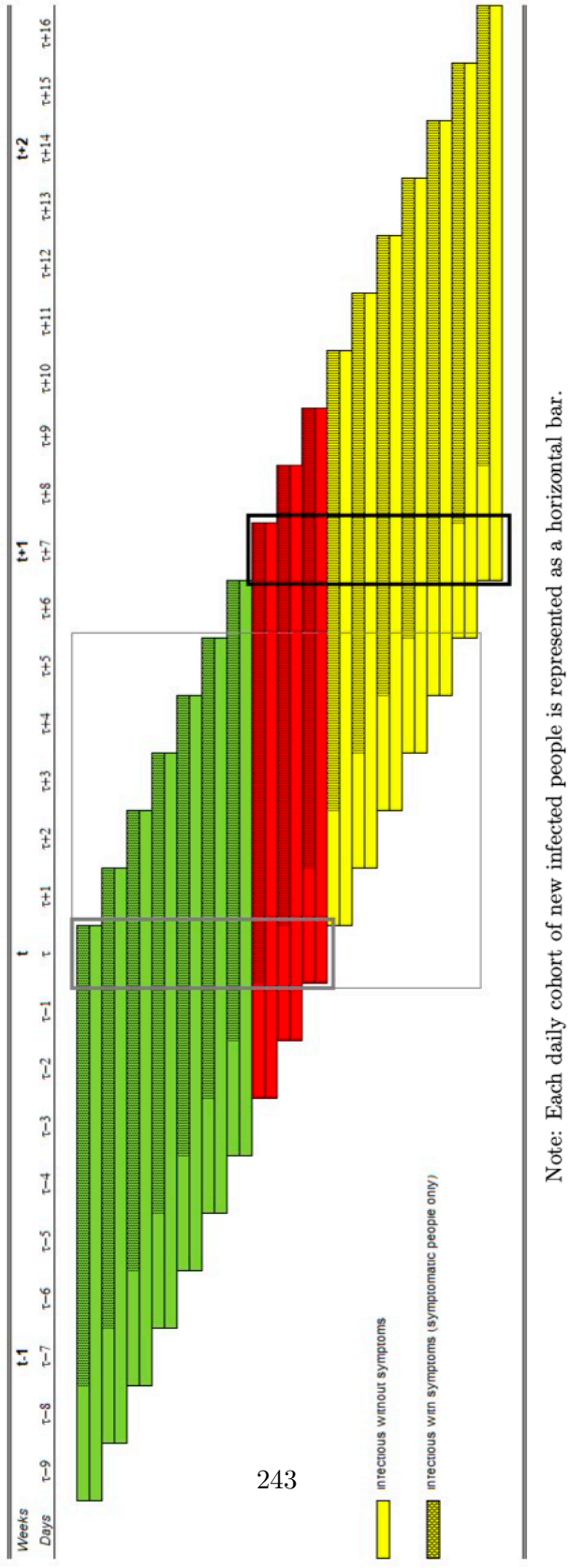

Figure C.3: Adjustment of epidemiological parameters to the weekly time structure

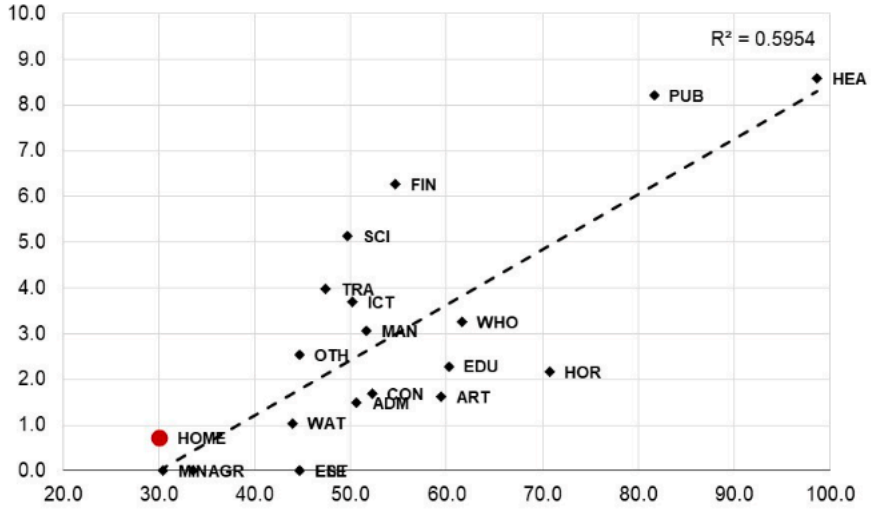

Note: Authors' computations. On the vertical axis, $b_{i,1}$ is our proxy for the basic transmission rates by industry at the early stage of the Covid-19 crisis.

Figure C.4: Correlation between basic transmission rates and indices of exposure to risk

Reopening construction sites and schools

The first restarting stage, which started on April 20th, mainly involved the reopening of construction sites. In addition, schools have partly reopened since May 4. The reopening started with graduating classes in the secondary education, practical exercise classes and internships at University and for the Advanced Technician Certificates (BTS). In a second stage starting on May 11, secondary schools have been reopen. In the third stage starting on May 25, primary schools have been reopen and public childcare services have been organized. Teachers (considered as teleworkers during the lockdown) gradually get back to their work- place and have interactions with pupils. Public teachers represent around 22.2% of public administration; 58.6% percent of public teachers work in the secondary education and 41.4% percent in primary schools [3]. In the first stage, only a fraction of secondary school teachers return to work (5.2% of teaching staff in private education, representing 1.2% of public ad- ministration). In the second stage, the remaining secondary teachers return to school which translates in an additional return of 36.2% of

[3] The distribution between primary and secondary classes is assumed to also hold in the private education sector, for which we do not have this detailed information.

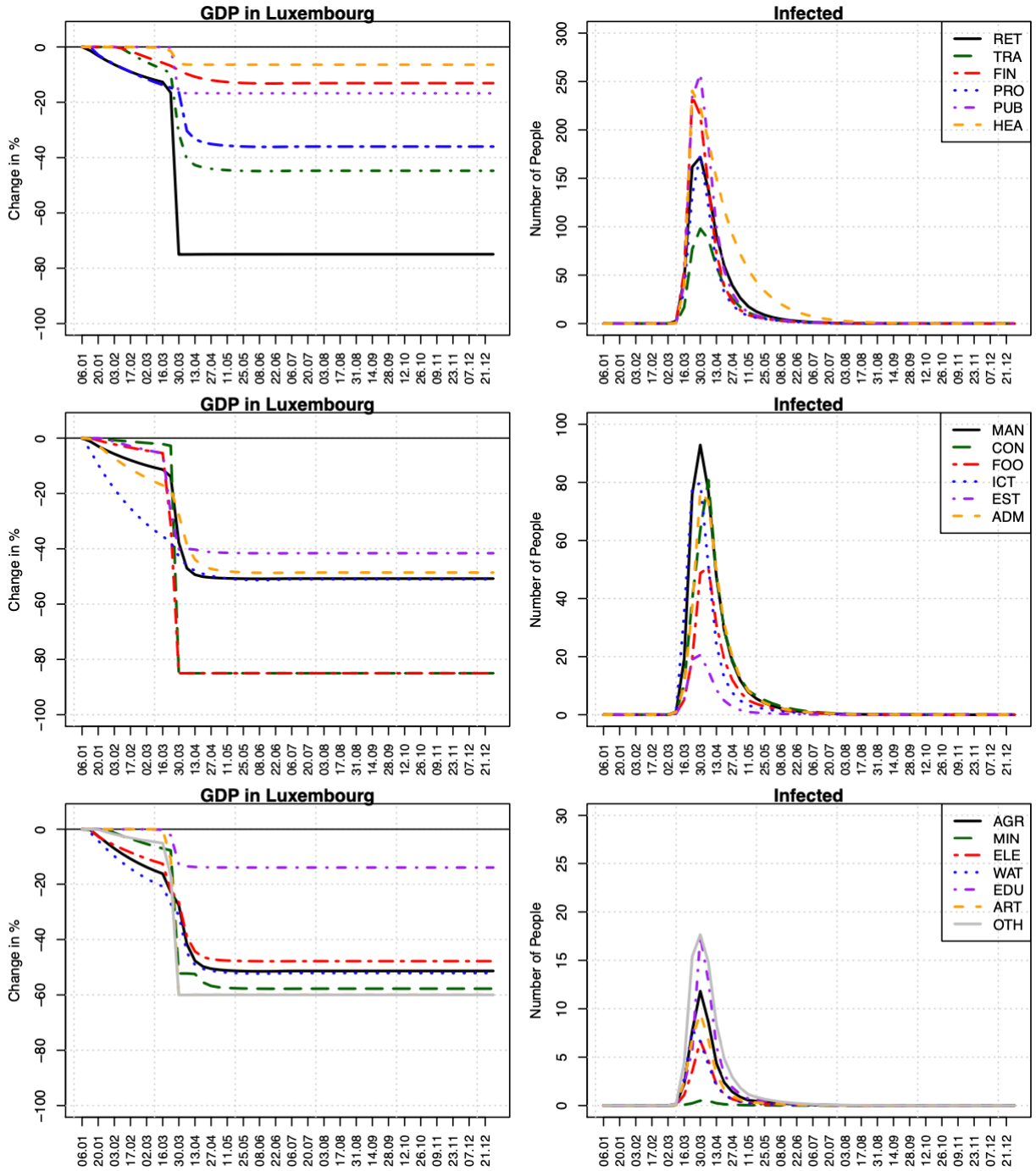

Note: Authors' computations. Permanent lockdown and permanent disruption of the global economy.

Figure C.5: Economic and public health effects of a permanent lockdown by sector

Table C.1: Macroeconomic shocks by industry (as of April 1st, 2020)

	Proximity	ProxMax	Exp disease	ExpMax	Index
Agric., forestry, fishing	30.6	0.430	4.9	0.181	0.395
Mining, quarrying	45.7	0.642	1.6	0.0593	0.591
Manufactured products	52	0.730	1.2	0.0444	0.672
Electricity, gas, steam	50.9	0.715	1.3	0.048	0.658
Water, sewerage, waste	44.2	0.621	13.7	0.507	0.579
Construction	60.6	0.851	1	0.037	0.783
Wholesale, retail, repair	62	0.871	3.1	0.115	0.801
Transport, storage	47.2	0.663	4.2	0.156	0.610
Accommodation, food	71.2	1.000	2.6	0.096	0.920
Information, comm.	50.5	0.709	0.3	0.011	0.653
Financial, insurance	50.4	0.708	1.0	0.037	0.651
Real estate	46.1	0.647	0.3	0.011	0.596
Prof, scient, techn	45.3	0.636	2.2	0.082	0.585
Adminis, support	47	0.660	7.1	0.263	0.607
Public administration	54.1	0.760	10.8	0.4	0.699
Education	67	0.941	27	1.000	0.980
Health, social work	0.084	1.000	0.019	0.134	-0.200
-0.079					
Arts, entertainment	61	0.857	3.6	0.133	0.788
Other services	57.9	0.813	13.6	0.504	0.749
Serv. HH as employers	41	0.576	12.4	0.459	0.536

Source: Authors computations based on O'Net data on physical proximity between workers and exposure to diseases by profession, and SILC data on occupational shares by industry.

private education workers and 8% of public administration workers. In the third stage, 58.6% of primary private education workers and 13% of private education workers return to teach in class. We simulate the effects of these shocks under alternative reproduction and testing scenarios. To be consistent, we combine the reopening of construction sites and schools with the inter- mediate (half-recovery) trade scenario described in Section 2.3. Hence, we jointly capture the effect of the first restarting stage and the partial recovery of exports. Results are presented in Fig. C.6 assuming that nothing else happens until the end of the year. The economic effects of these shocks are strongly robust to the public health policy. The weekly costs of the lockdown gradually decrease from 27% to 23% when construction sites are reopened. Reopening schools mostly impacts the economy through its effect on parental leave. Parental leave has been broadly lifted with the final stage of school reopening on May 25, remaining available to parents in a few exceptional

cases only. We therefore assume that only 10% of workers that benefit from parental leave are remaining in this status after May 25. Gradual economic gains due to the partial recovery in exports and decrease in parental leave are ob- served. By the end of the year, the weekly output loss lies in the vicinity of 12% (i.e., 15 percentage points smaller than during the full lockdown). Turning to the epidemiological consequences of these shocks, the top-right panel of Fig. C.6 compares the results obtained under the three intensive-margin scenarios (x equal to 0, 0.2 and 0.4) and in the absence of on-the-job PCR testing. In the least pessimistic scenarios (dashed dark and light gray curves corresponding to $x = 0$ and $x = 0.2$), restarting the construction industry and reopening schools has no effect on the aggregate infection curve. In the pessimistic scenario (solid black curve corresponding to $x = 0.4$), a rebound in the infection curve is observed, with a new peak at 1,600 detected active COVID-19 cases during the third week of December. Note that the rebound is negligible until the end of May but then, the infection curve exhibits a strong rebound. Hence, in the absence of massive testing, epidemiological results are sensitive to the size of the intensive margin effect of employment. However, mitigation policies can be used to avoid a relapse. On the bottom-right panel of Fig. C.6, we focus on the pessimistic scenario and consider two testing strategies, which consists of testing workers on a weekly or monthly basis. Testing workers on a monthly basis suffices to avoid the rebound.

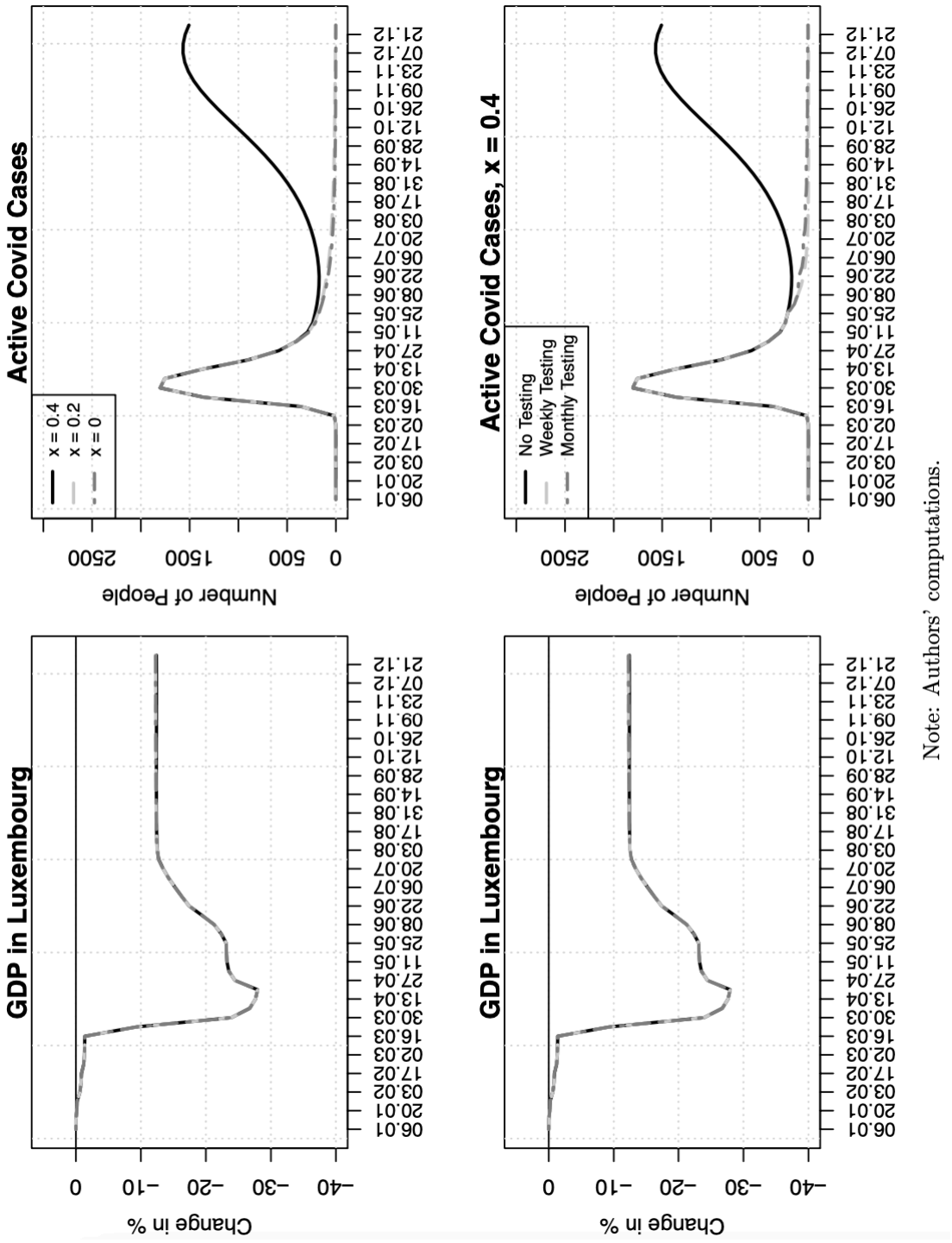

Figure C.6: Economic and public health effects of reopening construction sites by April 20

APPENDIX D

APPENDIX OF PERFORMANCE OF EARLY WARNING SIGNALS FOR DISEASE RE-EMERGENCE: A CASE STUDY ON COVID-19 DATA AGAINST EPIDEMIC OUTBREAKS

Mathematical models and assumptions

As described in the Main Text, early warning signals (EWS) are measures that rest upon modelling assumptions. To clarify the most relevant assumptions, which are tested in the present study, we recall how EWS are theoretically derived.

When consistent with a mean-field approximation, the dynamics of COVID-19 infectiousness is well described by SIR-like models [142, 431]. To illustrate how early warning signals can be subsequently derived, we here recall the process described in [438]. SIR models describe disease processes in homogeneous populations of susceptible individuals (X), which can get infectious (Y) and eventually removed (Z) by death or recovery. In the deterministic SIR, transitions among states are governed by the infection rate β and the removal rate γ, which lumps recovery and death rate. Empirical values for COVID-19 can be traced in the abundant literature, e.g. [178]. In addition, systems are often open with influx rate μ' and outflux rate μ'' of people. However, as many travelling restrictions[1] were in place during the year 2020, we can assume that such fluxes

[1] Refer to the ACAPS website (https://bit.ly/3nFFqUS) for a dataset of government measures.

are small and balanced: $\mu' = \mu'' = \mu$. Along with that, we model an influx rate of new cases η that can trigger subsequent disease outbreaks. Finally, intervention measures introduce a probability p that some susceptible individuals are isolated and protected, either physically (e.g. through non-pharmaceutical interventions limiting social interaction or through changes in people's behaviour) or by vaccination [325]. The model reads:

$$\begin{aligned} \dot{X} &= \mu(1-p) - \beta XY - (\eta+\mu)X \\ \dot{Y} &= \beta XY + \eta X - (\gamma+\mu)Y \\ \dot{Z} &= \mu p + \gamma Y - \mu Z\,. \end{aligned} \tag{D.1}$$

It is assumed that the population size N is constant, that is $X + Y + Z = 1$ since variables are normalized. In this case, the control parameter R is given by [438]:

$$R = \frac{\beta}{\gamma+\mu}(1-p) \tag{D.2}$$

and reaches its critical value 1 for $p^* = 1 - (\gamma+\mu)/\beta$, at which the dynamics undergo a transcritical bifurcation on the (Y, p) bifurcation diagram [438]. We remark that we consider here an example from literature: R might change in time after being driven by other evolving parameters such as one that tunes the contact rate β [431]. Without protection and extra fluxes, the basic reproduction number for COVID-19 was estimated at the beginning of the pandemic in the range $2 < R < 4$ (*cf., e.g.,* [329]).

If $p(t)$ changes slowly over time, we can mathematically express the SIR model D.1 approaching the transition as a slow-fast system:

$$\begin{cases} \text{Eq. } D.1 \\ \dot{p} = \epsilon f(X, Y, p) \end{cases} \tag{D.3}$$

where $0 < \epsilon \ll 1$ and f is a function that describes its change. A limit case is $\epsilon \to 0$. This condition is necessary to interpret the dynamical shift as a slow crossing through a bifurcation point, and to compute its associated summary statistics [469]. Often [435, 438], the function f is assumed to be a constant $f = \tilde{p}$. This way, the protection probability is, at first approximation,

a linear function of time:

$$p = p_0 + \tilde{p}t\,, \tag{D.4}$$

and R as well, following Eq. D.2. If $\tilde{p} > 0$, then R gets reduced and, if it was above 1, the bifurcation is crossed from above towards elimination. If $\tilde{p} < 0$, R increases and, if it was below 1, the bifurcation is crossed from below, towards a new emergence. Only the second case can be investigated with COVID-19 data, as most countries implemented suppression measures very rapidly [467] and thus Eq. D.3 is usually not satisfied in the first case.

When the transition is approached from below, and if there are few cases, stochastic fluctuations are not negligible. Hence, we need to consider the transitions described by a stochastic master equation. Reducing the stochastic master equation to Eq. D.3 and a Fokker-Plank equation for the fluctuations was already performed in [438, 471]. Hence, we briefly recall them to illustrate the assumptions underlying the behavior of early warning signals prior to the transition.
First, note that system D.1, along with condition $\dot{N} = 0$, can be reduced to its first two equations. Hence, we just need to consider the transitions in and out X and Y. Second, for each small time step dt, the quasi-steady state p is constant.
Transitions in and out states are described as random jump processes. Such states are (X, Y), $(X-1, Y)$, $(X, Y+1)$ and so on. Using $\alpha = (X, Y)$ to describe the "basic" state, $\bar{\alpha}$ is any other state and $P(X, Y, t) = \mathrm{Prob}(X(t), Y(t) = (x, y))$ is the probability that the state vector is equal to some pair of non negative integer numbers (x, y). Finally, $T_i(\alpha, \bar{\alpha})$ is the transition probability between states, and is a function of transition rates. The subscript i denotes all possible jumps in and out of the states. Examples of $T_i(\alpha, \bar{\alpha})$ are found in [132, 438], depending on the system of interest. Consequently, the master equation for the stochastic process is:

$$\frac{dP(\alpha, t)}{dt} = \sum_{\alpha \neq \bar{\alpha}} T_i(\alpha|\bar{\alpha})P(\bar{\alpha}, t) - \sum_{\alpha \neq \bar{\alpha}} T_i(\bar{\alpha}|\alpha)P(\alpha, t) \tag{D.5}$$

In general, Eq. D.5 is nonlinear. To have analytical results about its average behavior and the fluctuations around it, the van Kampen expansion can be used [445] to approximate the discrete

random variables with continuous random variables. This depends on having large N, which holds in our case when we consider the population of medium to big countries. To leading order, the expansion of Eq. D.5 is equivalent to Eq. D.3. To quantify the fluctuations at next-to-leading order, the obtained Fokker-Plank equation is equivalent to the following system of stochastic differential equations [471]:

$$\begin{aligned} \frac{d\sigma}{dt} &= b_{11}\sigma(t) + b_{12}\zeta(t) + \Gamma_1(t) \\ \frac{d\zeta}{dt} &= b_{21}\sigma(t) + b_{22}\zeta(t) + \Gamma_2(t) \end{aligned} \tag{D.6}$$

where Γ_j are white noise processes and the elements of the matrix $B = \{b_{kl}\}$ are functions of transition rates. Eq. D.6 connects the stochastic description of the epidemic with SIR-like models like Eq. D.1 would with a noise term.

Eq. D.6 can be analysed by its Fourier transform. By considering the fluctuations around the infectious state, we can derive the power spectrum and, through integration, the variance, the autocorrelation and other statistical moments. Their specific values depend on the eigenvalues of matrix B and of the covariance matrices of Γ_j. The evolution of variance and autocorrelation next to the transition, as obtained in [438], is shown in Fig. D.1 for a slow and a fast approach to $R(t) = 1$. The trend of these summary statistical indicators on the fluctuations, prior to the transition, constitutes the set of signals that could detect the transition itself; for instance, the increase in variance, often measured in terms of Kendall's τ. The Kendall's τ score is a non-parametric measure of ranks correlation, which is usually used to identify increasing trends [134, 454]. Such increasing trends are known in the literature as early warning signals (EWS) [453].

Finally, let us recall the general theory of EWS on bifurcations. Any system approaching a transcritical bifurcation is, in its vicinity, topologically equivalent to a transcritical normal form [468, 470]. This is a minimal model that retains the systems' behavior and resilience properties in the vicinity of a bifurcation. Models can be transformed to a normal form after an appropriate change of variables [124]. The normal form associated to a transcritical bifurcation has the form:

$$\dot{\theta} = q\theta - \theta^2 \tag{D.7}$$

where q is the bifurcation parameter and θ the variable of interest (Y from eq. D.1, in this specific case). This form represents a system whose extinction state and positive steady state coalesce and exchange stability when q reaches its critical value. If there are statistical fluctuations ξ, we can write their evolution as a linearization around the equilibrium $\tilde{\theta}$, thus resulting in a Langevin equation [457, 469]:

$$d\xi = -\frac{\partial f}{\partial \theta}[]\tilde{\theta}\xi + \sqrt{\sigma^2 g^2(\tilde{\theta})}dW \tag{D.8}$$

where dW is a Wiener process, σ^2 models the noise level and g is the diffusion coefficient of the associated Fokker-Planck equation. With a linear $|\partial f/\partial\theta|_{\tilde{\theta}}| = k$, Eq. D.8 is an OrnsteinUhlenbeck process with known statistical moments [448]. Hence, we can complement the theoretical results described above with those from the theory of statistical indicators of normal forms, e.g. [447, 457, 469]. Important remarks are that: a) multiplicative noise can modify the indicators trend, e.g. by making it decrease; b) EWS are expected to work best in the vicinity of the transition; c) there can be bifurcation delays associated to out-of-equilibrium phenomena, i.e. changes of the system state (and of its indicators) that lag behind the bifurcation of the limit case.

Data collection and curation

Among all the countries that registered a re-emergence of COVID-19 epidemic between April and September 2020, we first selected those for which meaningful prevalence data could be directly obtained from official sources or reconstructed with Eq. 2 from Main Text. Examples of discarded data series are reported in Fig. D.2. We recall the underlying hypothesis of this study: that dynamical early warning signals are expected to work when the investigated system can be described by a proper dynamical model. Hence, we did not consider time series for which active cases do not display the typical SEIR-like behavior like that described in [25, 335,

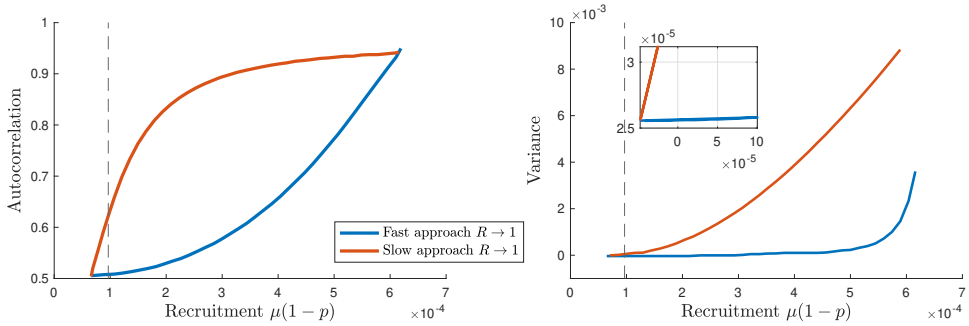

Figure D.1: Theoretical EWS for epidemic re-emergence. Left: the lag-1 autocorrelation increases before the transition if the approach of R to 1 is slow (slow-fast assumption satisfied, red); otherwise it increases after the transition (bifurcation delay, blue). Right: the variance increases before the transition (dashed grey line) if the approach of R to 1 is slow (slow-fast assumption satisfied, red; the inset magnifies the effect). Otherwise, it increases after the transition (bifurcation delay, blue). The plots are derived from the analytical results of [438] and reproduce its Fig. 9, d—e. On the x-axis: values for the recruitment rate $[d^{-1}]$ of new infectious that could trigger a re-emergence.

431, 433] (mostly due to data management and reporting), or for which recovered cases are reported with different frequencies, resulting in sawtooth curves for active cases. In the later case, the detrended fluctuations would be associated to reporting standards and would not be representative of dynamical fluctuations associated to EWS. Other selecting criteria to increase the quality of the dataset are discussed in "Materials and Methods" of the Main Text.

Information about the specific restrictions in place was not directly used as we concentrated on their lumped effect captured by $R(t)$. Nonetheless, it is possible to verify on the ACAPS database[2] [160] that all considered countries issued a lockdown of varying intensity and additional measures, to push $R(t)$ below 1 after the first wave.

Curves of active cases for all countries considered in Main Text, their smoothing and the associated $R(t)$ are displayed in Fig. D.3. The smoothed curves serve as basis for the detrending, the analysis of the noise distribution of each country and the subsequent investigation of early warning signals, as explained in Main Text. Specific information about population, surface and testing strategy of the considered countries is also reported in Tab. D.1.

[2]ACAPS is an independent, non-profit information provider helping humanitarian actors to respond more effectively to disasters. The ACAPS analysis team has aggregated and classified interventions from different sources (media, governments and international organizations), for all countries and in time.

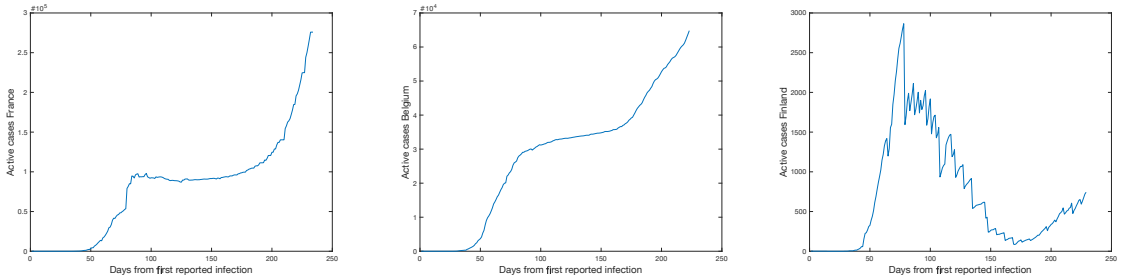

Figure D.2: Examples of discarded time series, following some of the criteria explained in "Material and Methods" of Main Text. Among others, France and Belgium had active cases curves that differ from the typical bell-shaped SEIR-like behavior. This is related to reporting of recovered and dead patients. On the other hand, Finland is an example of sawtooth evolution, due to recovered cases being reported with different frequencies than daily cases. Data from [161].

Country	Population	Area $[km^2]$	Avg. daily tests/1000 inh.	Share positive tests
State of Victoria (AUT)	6.681	227.444	1.8	<0.1%
Austria	8.917	83,879	0.6	[0.1; 0.6]%
Denmark	5.831	42,933	2.0	[0.1; 1]%
Israel	9.217	22,145	1.9	[0.3; 2]%
Japan	125.8	377,975	0.1	[1; 3.9]%
Korea, South	51.78	100,210	0.15	[0.3; 0.7]%
Luxembourg	0.632	2,586	10	[0.1; 0.4]%
Nepal	29.14	147,516	0.2	[0.3; 4.7]%
Singapore	5.686	728.6	5.1	[1.7; 3.7]%
Veneto (ITA)	4.906	18,345	0.7	[0.4; 2.7]%

Table D.1: Additional information about the selected countries: population (in millions inhabitants), area (in km^2), average number of daily tests per 1000 inhabitants, performed during the considered period (March - August 2020) and share of positive tests (in the same considered period, in percentage range from min to max values). The last two indicators derive from [163], to which we refer for the full time evolution. As mentioned in the main text, Luxembourg stands out for its higher number of tests performed per inhabitant.

Estimating $\mathrm{R(t)}$ with Bayesian inference using MCMC

Following standard methodologies [135, 413], we reconstruct the day-by-day evolution of the reproduction number $R(t)$ by fitting a Poisson transmission model with Markov Chain Monte Carlo (MCMC) methods.

When modelling "arrivals" of discrete-state stochastic processes (*cf.* section S1), Poisson processes are widely employed. For instance, they effectively modeled the transmission of Ebola [418] and

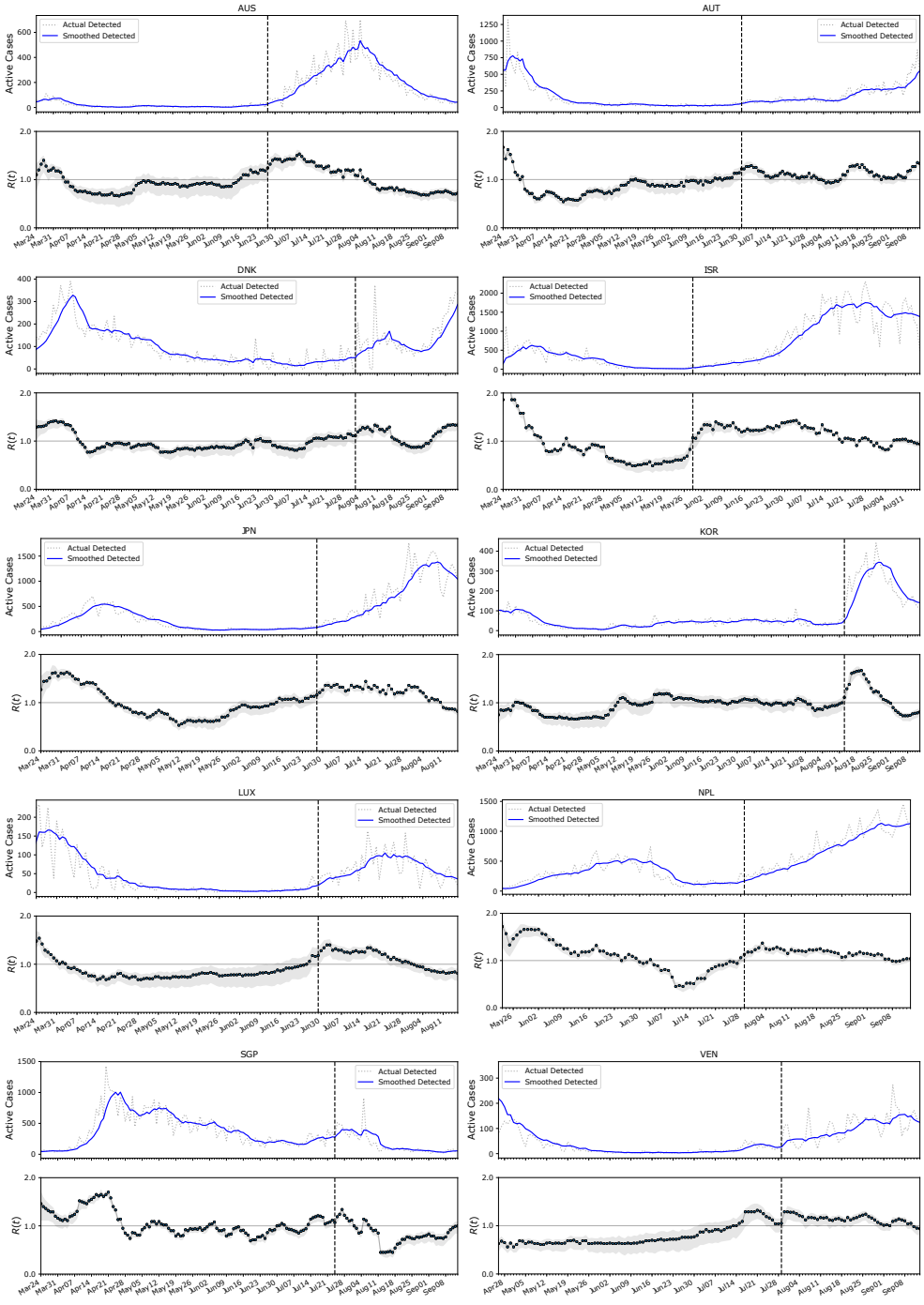

Figure D.3: Curves of active cases for the considered countries, along with their associated $R(t)$ (median values and 50% credible intervals). The vertical dashed line identifies the day marked for the transition an reported in Table 1 of Main Text.

Influenza [417]. Given an average rate of λ new cases per day, the probability of seeing k new cases is distributed according to the Poisson distribution:

$$p(k|\lambda) = \frac{\lambda^k e^{-\lambda}}{k!}. \tag{D.9}$$

In turn, λ depends on R as [416]:

$$\lambda = k_{t-1} e^{\gamma(R-1)} \tag{D.10}$$

for all time points. γ is the reciprocal of the serial interval, which is around 4 days for COVID-19 [419, 420]. To account for such uncertainty, we treat γ as a random sample from a Gaussian distribution centered in 4 days with an assumed standard deviation of 0.2. Hence, the probability of observing a time series $x = \{x_t\}$ for each t between t_0 and T discretised by a small step δ is given by:

$$p(x|R) = \prod_{t=t_0}^{T-\delta} p(k_{t+\delta}|\lambda_t) \tag{D.11}$$

Before t_0, no case was reported. Following Bayes' rule, the posterior distribution of R, for each time point, is given by (up to a normalization constant):

$$p(R|x) \propto p(x|R)q(R), \tag{D.12}$$

where $q(R)$ is a prior distribution. For each time point after $t_0 + 1$, the prior equals the preceding posterior. We follow the implementation of [414] to generate thousands of MCMC samples with the Metropolis Hastings algorithm, starting with a Gaussian prior $\mathcal{N}(R, \sigma)$. We assumed $\sigma = 0.15$. From the posterior distribution, we also estimated the probability that $R(t)$ is greater than 1, which was in turn used to define the "ground truth" date of regime transition for the epidemic trend (see also "Materials and Methods" of Main Text for further discussion). Fig. D.3 shows the results of the Bayesian $R(t)$ estimation (median values and 50% credible intervals) for the considered countries.

Determining the rate of approach for $\mathbf{R(t) \to 1}$

As explained in the Main Text, we are interested in evaluating how rapidly the transition point is approached, for each country. To do so, the simplest linear trend

$$y = a + b \cdot x, \tag{D.13}$$

corresponding to Eq. 13 in Main Text, is assumed and fitted to $R(t)$ time series, obtained as described above and reported in Fig. D.3. The estimated regression coefficient is informative about the rate of approach of $R(t) \to 1$.

The fitting was performed with *scipy.optimize* routine, considering as uncertainty the 50% credible interval from the distribution of $R(t)$. The goodness of fit was evaluated with the reduced χ^2 score. Results are displayed in Fig. D.4. The $\chi^2_{\text{red}} < 1$ guarantees the goodness of the linear fit, which allows to extrapolate the regression coefficient as a measure of the rate of $R(t) \to 1$. The values of $b \pm \sigma_b$ are then reported in Fig. 1c of Main Text.

Evolution of indicators for all countries

In this section, we show and discuss the evolution of the considered early warning indicators for all countries, including those that are not shown in Fig. 3 of Main Text.

Let us first consider EWS obtained from Gaussian filter detrending. In Fig. D.5 we observe the evolution of the indicators, either globally (D.5a) or locally, just prior to the bifurcation (D.5b for the variance, the most robust one as discussed in Main Text). We can observe the patterns discussed in the Main Text, associated to the different countries belonging to the test set $\mathcal{Y}$ or not ($\mathcal{N}$). Within $\mathcal{Y}$, the variance increases prior to the transition and gives very few spurious signals before, whereas other indicators can be more misleading when the transition still did not happen. Overall, predicted trends of EWS prior to the bifurcation are associated to satisfied theoretical assumptions such as gradual approach of $R(t) \to 1$ and white noise (*cf.* Fig. 1 in Main Text and discussion thereafter). Not satisfying these requirements might disrupt the expected increasing trend and results in misleading signals, see in Fig. D.5 the countries listed in $\mathcal{N}$. Hence, if a

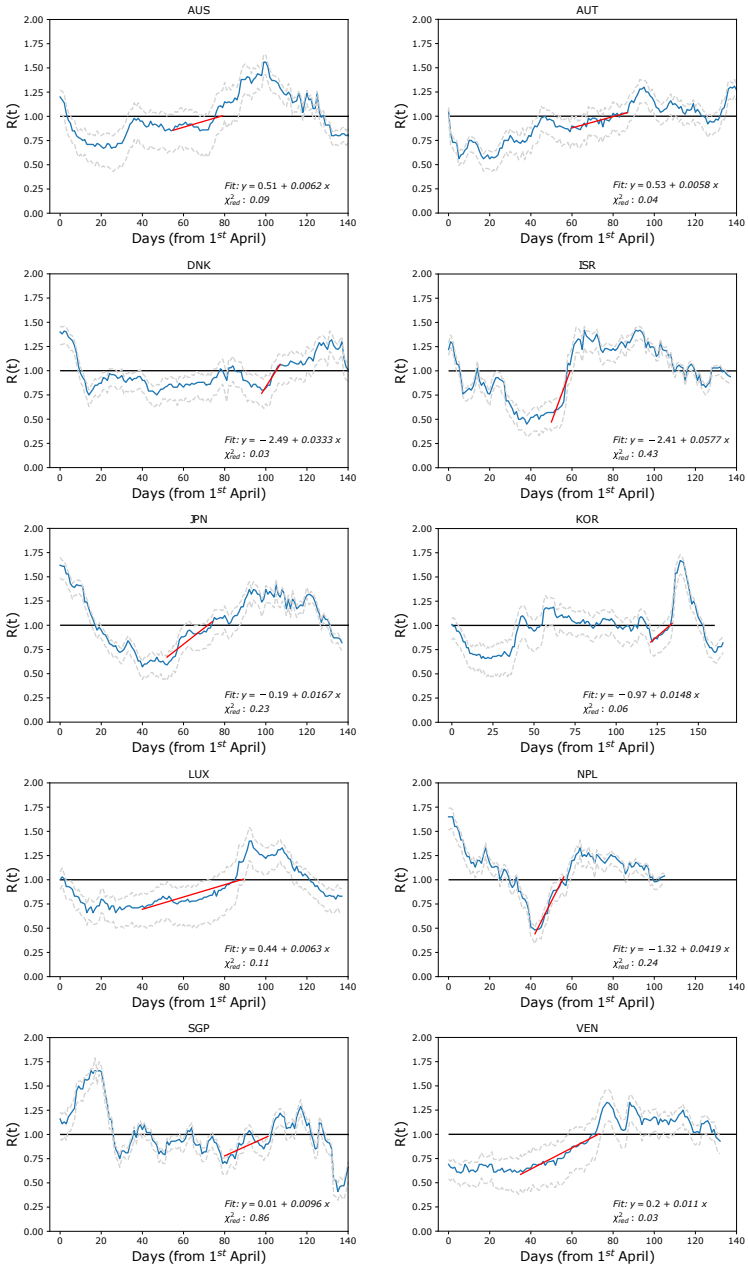

Figure D.4: Estimate of transition rate to R critical value. Fitting $R(t)$ evolution (blue line; dashed lines are $\pm 50\%$ CI) with a linear trend prior to the transition estimates the rate of approach to the threshold value 1. The fit begins around the minimum of $R(t)$ (excluding small fluctuations) until when the median value crosses 1 (horizontal line). The best fit curve is in red. $\chi^2_{\text{red}} < 1$ guarantees that a good fit is achieved for the simple linear function Eq. D.13. The regression coefficient b is a proxy for the rate of approach to 1. Its associated uncertainty is not reported here but is shown in Fig. 1 of Main Text.

system is not known or there is difficulty in determining the type of data, incorrect conclusions could be drawn when interpreting the time series trend. Fig. 4 and Table 2 of Main Text quantify the performance of EWS for all countries.

ARIMA detrending and corresponding global EWS

As explained in the Main Text, on top of moving average smoothing and Gaussian kernel filtering, we tested the ARIMA detrending method. ARIMA (Auto Regressive Integrated Moving Average) is an automatic method to identify the leading trends of a time series [430], depending on three terms (p, q, d) that need to be adjusted for each data set. Initially, the d term is identified by checking for stationarity in the data. Then, the other terms are automatically identified with the python function *pmdarima* for ARIMA estimation. Table D.2 summarises the selected ARIMA as well as their residuals mean and standard deviation, for each country.

Country	ARIMA parameters	Residuals mean	Residuals std
State of Victoria (Australia)	(0,2,1)	-2.51	197.9
Austria	(1,2,0)	2.58	121.5
Denmark	(0,2,1)	3.17	86.97
Israel	(3,2,2)	34.21	823.5
Japan	(1,2,2)	-0.279	349.12
Korea, South	(3,1,3)	6.462	141.14
Luxembourg	(2,1,3)	0.340	30.90
Nepal	(1,2,0)	0.248	241.66
Singapore	(1,2,0)	-0.070	152.47
Veneto (Italy)	(0,2,1)	0.133	70.048

Table D.2: ARIMA model parameter combinations over prevalence data, residuals mean and standard deviation, for each country.

Further investigation on AUC values

Table 2 of Main Text reports AUC values close to 0 for variance and CV for the $\mathcal{N}$ test set, in particular after ARIMA detrending. This would correspond to good detection performance for

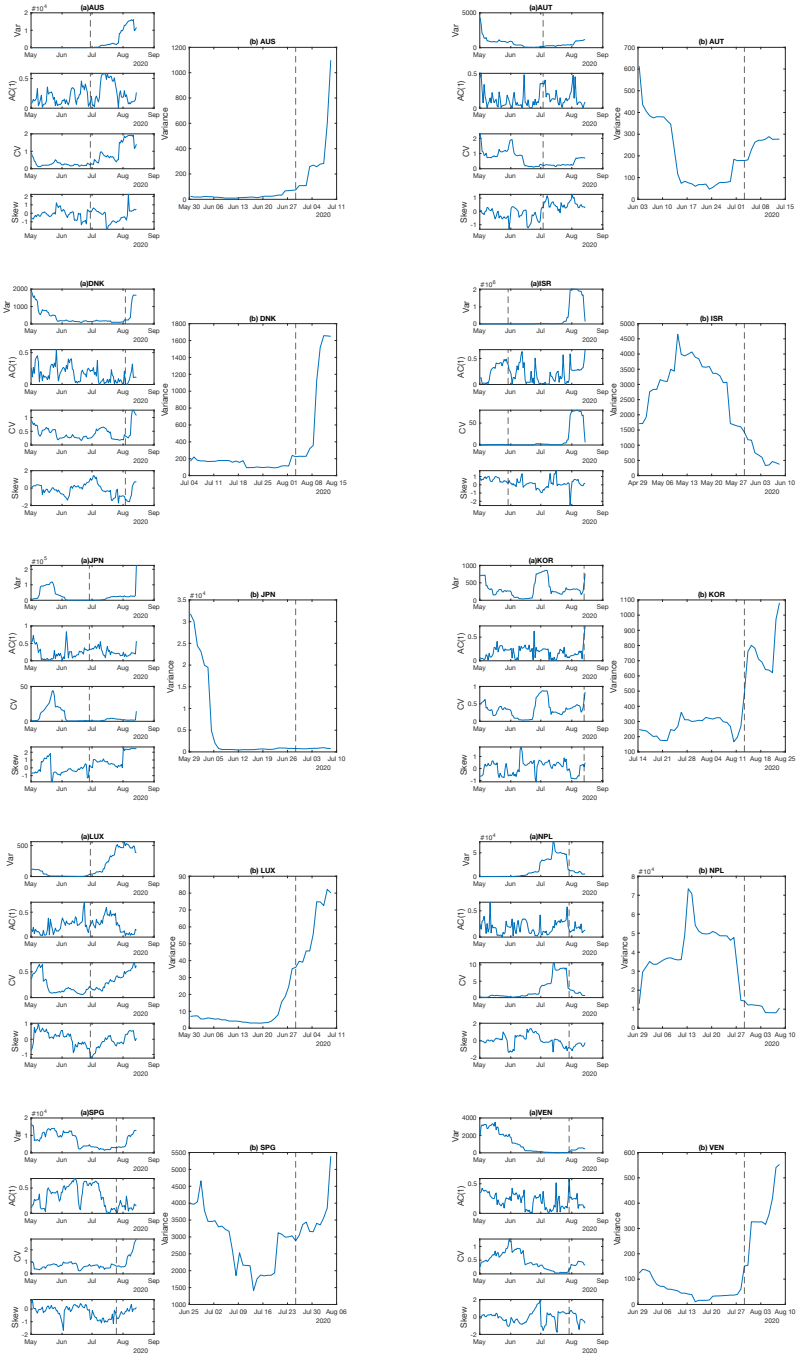

Figure D.5: Evolution of the considered indicators for all countries. Figs (a) report their global evolution, from the end of the first wave to the second. Figs (b) focus on the behavior of the variance close to the transition (local behavior). As discussed in the Main Text, we report the values of indicators after a moving window of size 14 days, associated to the rightmost data point to avoid "looking into the future". The vertical dashed line marks the transition point.

decreasing trends of such indicators, which would contradict the theoretical results. We have carried out a further investigation to address this oddity. In Fig. D.6 we an observe that a decreasing variance is indeed observed close to the transition of $\mathcal{N}$ countries. Zooming out, we nonetheless observe that this corresponds to one of the following situations: a continuation of a decreasing trend after the first wave or fluctuations is a rather stable trend, eventually followed by a delayed increase after the transition. We hypothesise that these features are again associated with the rapid re-emergence and the noise distribution. On the one hand, the indicator had little time to settle to stable trends and then increase again; on the other hand, there could be some bifurcation delay playing a role. Hence, we suggest that this is a spurious effect. These observations calls for caution when interpreting the AUC values related to decreasing trends and reminds of the importance to compare the results with theoretical predictions.

Analysis on incidence data

As mentioned in the main text, we complement the analysis on prevalence data with that on incidence data (daily new cases). The latter avoids potential bias induced by the estimation of recovered patients, but might be more sensitive to systematic fluctuations associated with testing routines. Hence, the two analysis can be regarded as representative of real-world monitoring capacities.

The analysis is performed in the same way as the one described in main text; the indicators and methodologies are also consistent. Therefore, we refer to the main text (Methods and figures corresponding to the ones presented here) for methodological explanations.

In accordance with preliminary studies that investigated incidence data for re-emergence of infectious diseases [132, 436], the results here obtained are similar to what observed for prevalence data. However, there is a number of differences worth stressing. In the remaining of this section, we will highlight both similarities and differences.

To begin with, the distribution of fluctuations around the average trend is different than what observed in Fig. 1 of the main text. In the case of incidence data, the deviation from Gaussian

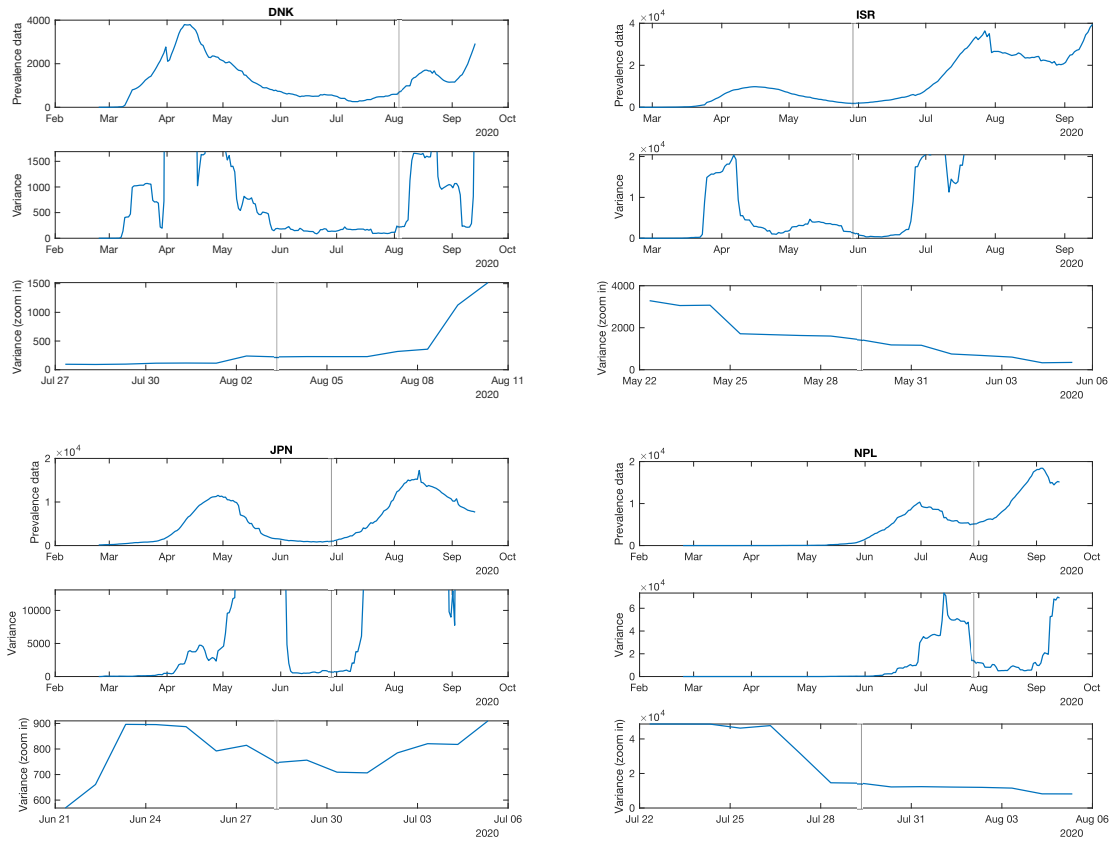

Figure D.6: Investigation of variance for countries in $\mathcal{N}$. For each country, the top panel reports the prevalence data, the middle one is for the full time series of variance, while the bottom one zooms in the vicinity of the transition. Note that ISR and JPN were zoomed to better see the variance trends; when it's not visible anymore, the variance reached higher values that those encompassed in the y-axis scale.

noise distribution is more pronounced (see Fig. D.7b), which reflects the larger fluctuations usually associated with testing protocols like reduced weekend testing (an example is shown in Fig. D.7a). Interpreting the subsequent results as consequences linked to the noise distribution is therefore more challenging. In addition, we observe (Fig. D.7b) that Japan and South Korea have different skewness and excess of kurtosis than what reported in Fig.1 of main text. Therefore, as the rate of approach to $R(t) = 1$ is conserved (Fig. D.7c), we follow the initial criterion of placing one country in the test set $\mathcal{Y}$ and one in $\mathcal{N}$, but we swap them: Japan is placed in $\mathcal{Y}$ and South Korea in $\mathcal{N}$. We do this for consistency with the previous analysis, but we also verified that the following results are little sensitive to this choice.

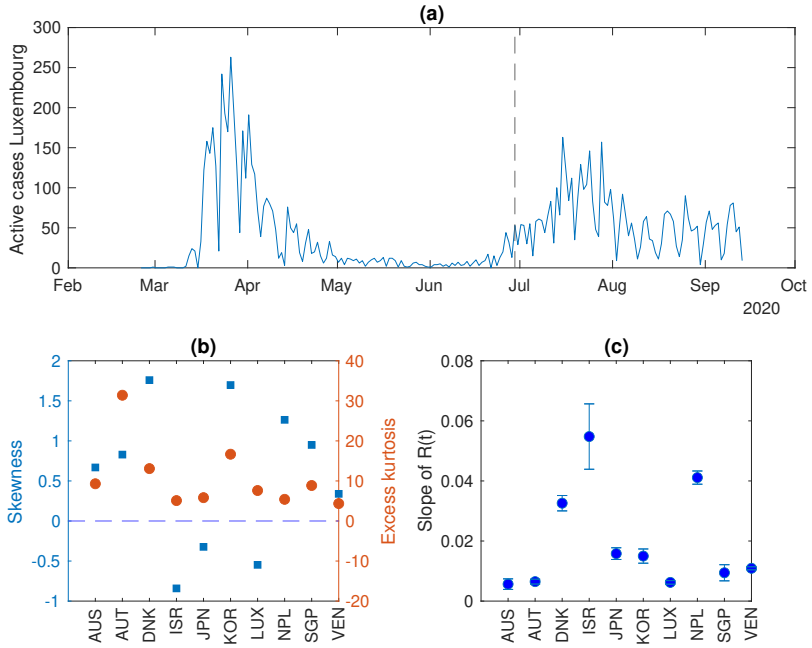

Figure D.7: Analysis of the dynamical characteristics of the countries included in the data set, for incidence data. a) An example of an epidemiological curve of daily new cases from Luxembourg. The dashed line indicates the transition, measured by $R > 1$. b) Measures of the distribution of data fluctuations. Skewness μ indicates the symmetry of the distribution, whereas excess of kurtosis $\gamma - 3$ indicates the relevance of its peak with respect to the tails. Large deviations from $\mu = 0$ (dashed line) and $\gamma = 3$ are associated with non-normal distributions. c) The regression coefficient of $R(t)$ and its associated uncertainty.

Next, we verify that the detrending methods provide consistent results to those already observed in the main text. Moving average and Gaussian filtering are similar to one another (Fig. D.8); in this case, the ARIMA is notably better correlated with the other two methods, possibly due to the short-term fluctuations being mostly driven by systematic testing routines (compare the smoother trend in Fig. 1a with the weekly oscillating pattern in S7a) that are smoothed by all filtering procedures. In addition, the local behavior of the variance shows an increasing trend, as expected from preliminary theoretical studies (Fig. D.9); differently from the case with prevalence data, both the eyeball visualization and the Kendall's τ are very similar between ARIMA and Gaussian filtering results. We recall that we first perform this study on Luxembourg, as the Large Scale Testing scheme [396] in place suggests that it is the mostly controlled setting.

The qualitative global behavior of statistical indicators for EWS is also similar to what observed

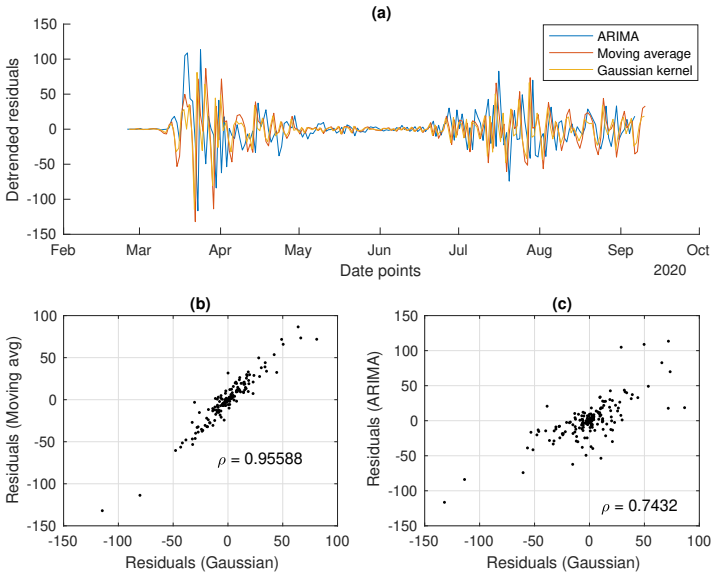

Figure D.8: [Analysis of the residuals from the detrending methods (one case study from Luxembourg shown). a) The detrended fluctuations time series. b) Correlation between residuals obtained from Gaussian or moving average filtering. c) Correlation between residuals obtained from Gaussian or ARIMA filtering.

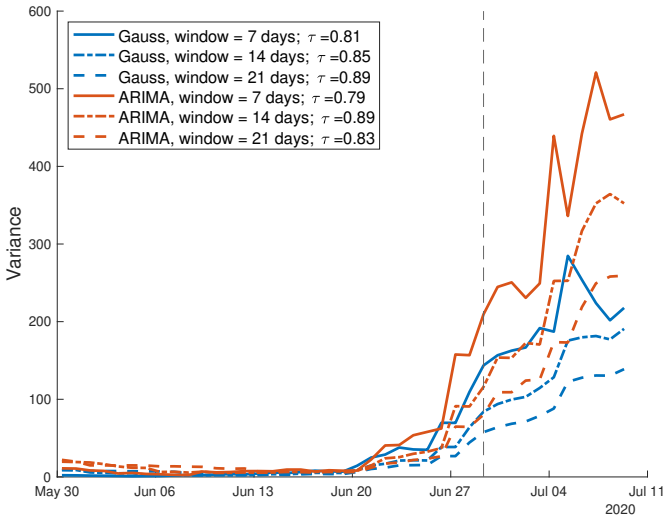

Figure D.9: Analysis of the variance in the Luxembourg setting. Its increase is evident prior to the transition (dashed vertical line). τ, which quantifies the overall increasing trend, is little sensitive to the sliding window size, as displayed by the three curves and by τ values reported in the text. The variance is computed over the residuals from Gaussian filtering and ARIMA detrending. The increasing trend during the considered time window is quantified by the associated τ values.

in the case of prevalence data (Fig. D.11). For the same countries used in Fig. 4 of main text, we observe an increase of the variance prior to the transition and potentially spurious fluctuations of the AC(1) and CV, likely associated to moving window effects and fluctuations of the raw data. In contrast, the skewness seems to follow a more pronounced increasing trend. Likewise for the main text, these eyeball observations are subsequently quantified with ROC and AUC analysis.

From the quantitative analysis about sensitivity and specificity of the indicators in detecting the transition, we observe overall similar results to those reported in the main text: the AC(1) and CV are worse than a random classifier even for countries in $\mathcal{Y}$, whereas the variance provides more robust results (Fig. D.10 and Table D.3). However, we observe a number of interesting differences over both ARIMA and Gaussian filtering results. To begin with, variance and CV on the $\mathcal{N}$ set are less associated with decreasing trends close to the transition but are closer to the performance of random classifiers. This might suggest that, as discussed in the main text, the result on prevalence data was likely spurious and related to the decreasing of the first wave. As daily new cases do not have a time delay due to recovered cases, such effect is indeed less marked. The second, more striking difference regards the skewness. As shown in Fig. D.10, and quantified in Table D.3, the skewness is particularly good in detecting the transition to disease emergence on the test set $\mathcal{Y}$. This observation differs from what anticipated in [132] but is more in line to what was suggested in [473]. Since there are only few studies connecting observed EWS to noise distribution (like the one observed in Fig. D.7), we cannot make a conclusive interpretation of this fact. Nonetheless, we speculate that the detection performance might be linked to the sensitivity of the skewness to the noise distribution (as already introduced in [473]): potentially, the correct combination of fluctuations and approach to the $R(t) = 1$ might have yielded the observed result. Here, we limit ourselves to reporting the observation, demanding further analytical and computational studies to investigate the issue. In any case, the skewnees is again no better than a random classifier on the $\mathcal{N}$ set.

Overall, this complementing analysis on incidence data provides additional insights and questions, to be further compared with theoretical studies. Nonetheless, it contributes in stressing one of the main points of the main study: as the considered indicators rely on a number of assumptions, we are justified in using them when such assumption are satisfied, which is not always the case

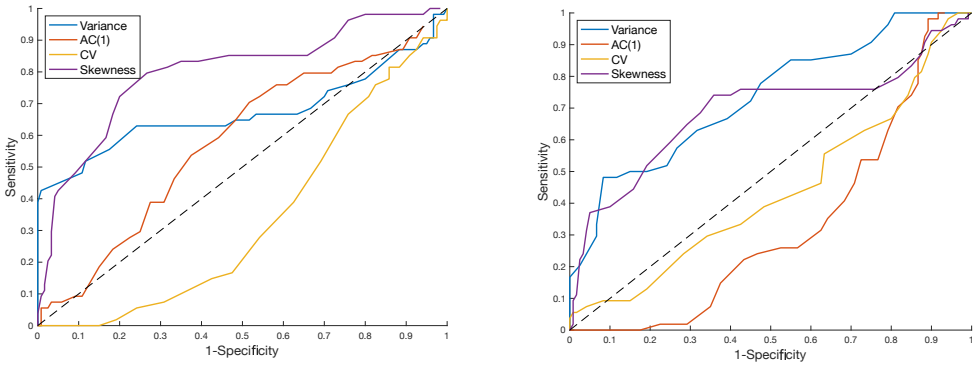

Figure D.10: ROC curves for each considered indicator, with sensitivity and specificity calculated on each timepoint for all countries in $\mathcal{Y}$. Each point corresponds to a test value for τ, to define if the detection if positive. The diagonal line corresponds to the ROC of a random classifier. Curves above it imply better performance. Left: Computed on Gaussian filtered data. Right: Computed on ARIMA detrended data.

	Gaussian det.		ARIMA det.	
Indicator	over $\mathcal{Y}$	over $\mathcal{N}$	over $\mathcal{Y}$	over $\mathcal{N}$
Variance	0.6718	0.4681	0.7334	0.2561
AC(1)	0.5234	0.3132	0.2624	0.6021
CV	0.3370	0.2019	0.4380	0.1813
Skewness	0.7826	0.5005	0.6805	0.4991

Table D.3: AUC scores for different indicators, over $\mathcal{Y}$ and $\mathcal{N}$ datasets, after Gaussian or ARIMA detrending methods.

in real-world settings. Otherwise, the EWS sensitivity to such assumptions might yield spurious signals and hinder our capability to extend them in uncertain contexts.

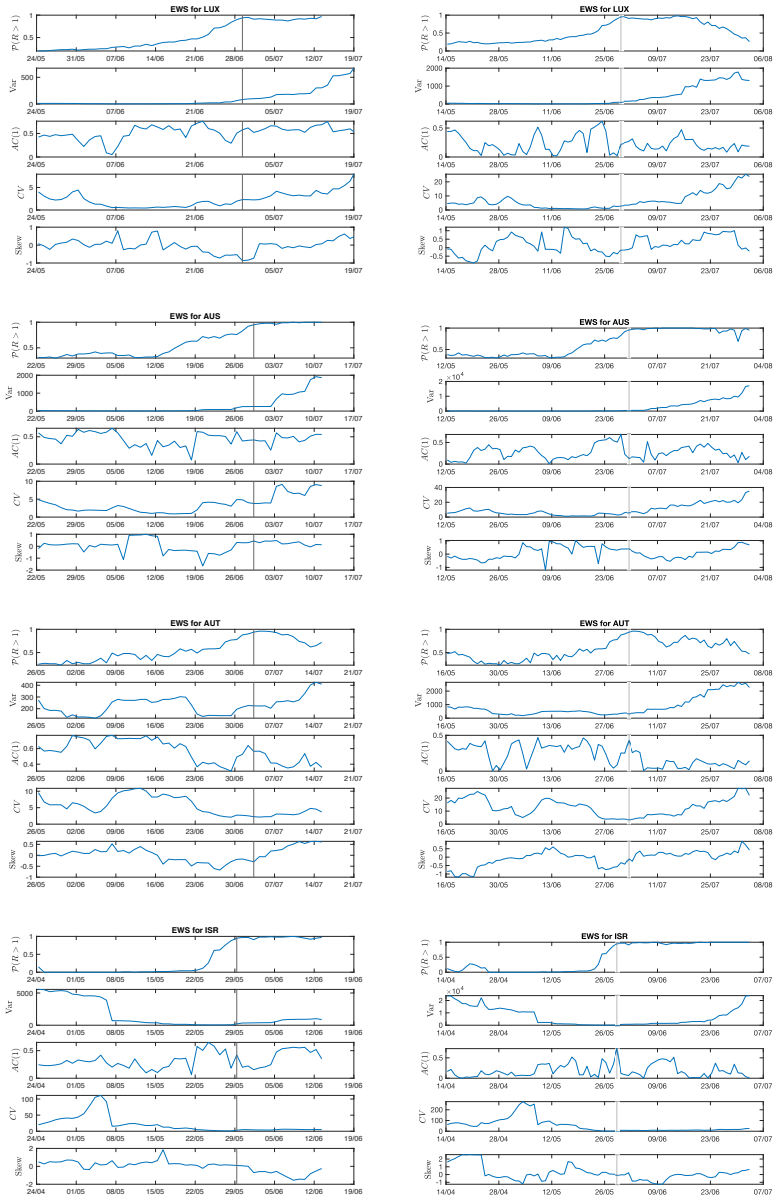

Figure D.11: Evolution of EWS far from the transition point. Four example countries are shown: Luxembourg and Austria, with controlled features; State of Victoria (Australia), with small deviations from controlled features; and Israel that does not satisfy theoretical conditions. Considered EWS are the most common ones (variance, lag-1 autocorrelation, coefficient of variation, skewness). In addition, to mark the approach to the transition, $\mathcal{P}(R(t) > 1)$ from the Bayesian estimation (see main text) is displayed. The vertical line reports the transition date. Left column: detrending method employed: Gaussian filtering. Right column: detrending method employed: ARIMA.

Country	ARIMA parameters	Residuals mean	Residuals std
State of Victoria (Australia)	(2,1,0)	0.39	52.82
Austria	(1,1,4)	5.43	93.63
Denmark	(3,1,0)	3.17	46.87
Israel	(0,1,1)	0.41	349.6
Japan	(7,1,5)	3.58	110.0
Korea, South	(0,1,1)	0.501	58.96
Luxembourg	(2,1,5)	0.319	25.92
Nepal	(0,1,1)	-0.099	91.999
Singapore	(1,1,1)	0.46	121.61
Veneto (Italy)	(5,1,3)	1.25	50.66

Table D.4: ARIMA model parameter combinations over incidence data, residuals mean and standard deviation, for each country.

APPENDIX E

APPENDIX OF LARGE-SCALE TESTING IN LUXEMBOURG

The social interaction $\rho(t)$ takes into account for non-pharmaceutical interventions. $\rho(t) = 1$ corresponds to the social interaction before the pandemic. The changes of $\rho(t)$ and the reason of NPI are given by the table:

Date	Non-pharmaceutical interventions	Social interaction parameter
18.03.2020	-Full lockdown	ρ_1
25.03.2020	-Measures are getting visible	ρ_2
20.04.2020	-reopening of construction sector -reopening of diy and gardening shops -wedding and funeral are possible (max. 20 participants) -prohibition to wear masks in public transport and activities that accommodate the public -prolongation of the duration of the restriction to travel	ρ_3

28.04.2020	-access to sports activities allowed for athletes -possibility for activities of medical practice	
11.05.2020	-opening of all shops (except HORECA) -possibility to meet 20 people outside -possibility to invite 6 people at home -generalization of wearing masks for all activities if 2 meter distance can not be respected	ρ_4
30.05.2020	-Start of school holidays	ρ_5
07.06.2020	-End of school holidays	ρ_6
15.06.2020	-reopening of the borders for people coming from third countries	
24.06.2020	- Prohibition for meetings with more 20 people - Obligation to wear a mask in public transport and during activities which accommodate the public - Opening of indoor games - Authorisation of sports activities except physical contacts - Lifting of the measures in HORESCA	ρ_7
16.07.2020	- Start of school holidays	ρ_8
24.07.2020	- Restriction to accommodate 10 people at home - Fine in case of non respect of quarantine	
31.07.2020	-Start of congé collectif	ρ_9
23.08.2020	-End of congé collectif	ρ_{10}

14.09.2020	- End of school holidays	ρ_{11}
23.09.2020	- Reduction of isolation from 14 to 10 days - Testing date after contact is moved from 5th to 6th day after contact with an infected person	
29.10.2020	- Curfew from 11 pm to 6 am - Restriction to accommodate 4 people at home - Prohibition of sports activities with more than 4 people - Closing-time for restaurants and bars at 11 pm - Gathering of 10 to 100 just possible with masks and seating - Prohibition of gatherings with more than 100 persons	ρ_{12}
25.11.2020	- Limitation to accommodate 2 people at home coming from the same household - Closure of bars, restaurants, sports complexes, cinema and culture locations	ρ_{13}
15.12.2020	- Prohibition of consumption inside of shopping centers - Continuation of the rules of 25.11.2020	
19.12.2020	- Start of school holidays	ρ_{14}
24.12.2020	- Curfew at 9 pm - Closure of non-essential shops - Prohibition to drink alcohol in public spaces - Continuation of closure of bars, restaurants and sports complexes - Maximum 2 people for leisure and sports activities	ρ_{15}

03.01.2021	- End of school holidays	
09.01.2021	- Curfew at 11 pm - Opening of non-essential shops (one client per 10 m2) - Prohibition to drink alcohol in public - Closure of bars, restaurants and sports complexes - Ability to do sports with one additional person without any restrictions - Sports activities with 10 people are allowed with 2 meters distance - Reopening of sport complexes - Revival of cultural activities	ρ_{16}
13.02.2021	- Start of school holidays	ρ_{17}
21.02.2021	- End of school holidays	ρ_{18}
12.03.2021	- Continuation of wearing masks during school activities - Pupils in secondary school education do home schooling	ρ_{19}
02.04.2021	- Opening of terraces under strict rules: schedule (6 am-6pm), 2 people on one table, wearing masks for staff and clients in the case of not being seated	ρ_{20}
03.04.2021	- Start of school holidays	
18.04.2021	- End of school holidays	ρ_{21}
23.04.2021	- Limitation of 10 people during sports activities is removed - Sports activities with larger groups up to 100 are allowed with 2 meters distance - 10 people can play music together with 2 meters distance	ρ_{22}

14.05.2021	- Curfew at 12 pm - Restriction to accommodate 4 people at home - Table with 4 people in HORECA is allowed - For consumption inside of a restaurant or bar a negative test is needed - Gatherings with 150 people are allowed - Gatherings above 150 to 1000 people are allowed with a sanitary protocol	ρ_{23}
22.05.2021	- Start of school holidays	ρ_{24}
30.05.2021	- End of school holidays	ρ_{25}
22.06.2021	- National day effect	ρ_{26}
15.07.2021	- Adaption of COVID check regime - Adaptation of sanitary rules for school activities - Modification of gathering rules	
16.07.2021	- Start of school holidays	ρ_{27}
30.07.2021	-Start of congé collectif	ρ_{28}
22.08.2021	-End of congé collectif	ρ_{29}
14.09.2021	- End of school holidays	

Table E.1: Social interaction parameter ρ

The social interaction is a piece-wise function which changes in the case that a new NPI is in place. The plot of the social interaction is shown in Fig.E.1.

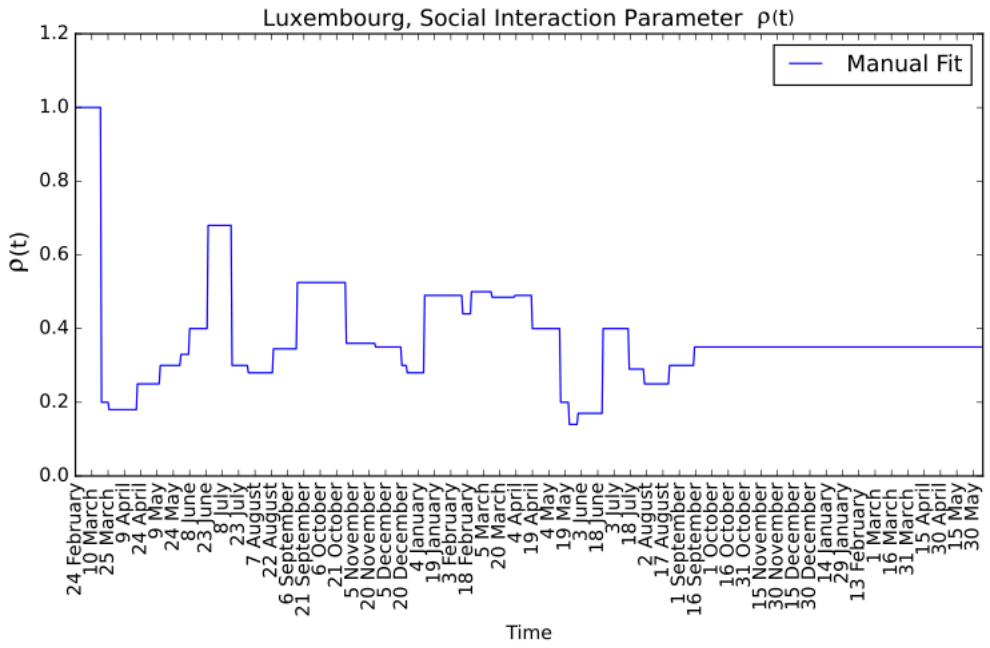

Figure E.1: Social interaction

BIBLIOGRAPHY

1. Sandford, A. & Euronews. *Coronavirus: Half of humanity now on lockdown as 90 countries call for confinement* https://www.euronews.com/2020/04/02/coronavirus-in-europe-spain-s-death-toll-hits-10-000-after-record-950-new-deaths-in-24-hou. (accessed: 19.05.2022).
2. Luxembourg, R. *COVID-19 Task Force* https://www.researchluxembourg.org/en/covid-19-task-force/. (accessed: 05.05.2022).
3. Gostic, K. M. *et al.* Practical considerations for measuring the effective reproductive number, Rt. *PLOS Computational Biology* **16,** 1–21. https://doi.org/10.1371/journal.pcbi.1008409 (Dec. 2020).
4. Luxembourg, R. *Large-scale testing* https://www.researchluxembourg.org/en/covid-19-task-force/projects/large-scale-testing/. (accessed: 9.04.2022).
5. Wilmes, P. *et al.* SARS-CoV-2 transmission risk from asymptomatic carriers: Results from a mass screening programme in Luxembourg. *The Lancet Regional Health - Europe* **4,** 100056 (May 2021).
6. BIOSYL. *What is systems biology?* http://www.biosyl.org/about-biosyl/what-is-systems-biology. (accessed: 30.05.2022).

7. Klipp, E., Liebermeister, W., Wierling, C., Kowald, A. & Herwig, R. *Systems Biology : A Textbook* ISBN: 9783527675661. http://ebookcentral.proquest.com/lib/unilu-ebooks/detail.action?docID=4498648 (John Wiley and Sons, Incorporated, Berlin, GERMANY, 2014).

8. For Complexity, W. I. & Innovation. *What are complex systems?* https://uwaterloo.ca/complexity-innovation/about/what-are-complex-systems. (accessed: 30.05.2022).

9. Sayama, H. *Complex Systems in a Nutshell* https://math.libretexts.org/Bookshelves/Scientific_Computing_Simulations_and_Modeling/Book%3A_Introduction_to_the_Modeling_and_Analysis_of_Complex_Systems_(Sayama)/01%3A_Introduction_to_Modeling_and_Analysis/1.01%3A_Complex_Systems_in_a_Nutshell. (accessed: 31.05.2022).

10. Sayama, H. *2.3: Modeling Complex Systems* https://math.libretexts.org/Bookshelves/Scientific_Computing_Simulations_and_Modeling/Book%3A_Introduction_to_the_Modeling_and_Analysis_of_Complex_Systems_(Sayama)/02%3A_Fundamentals_of_Modeling/2.03%3A_Modeling_Complex_Systems. (accessed: 30.05.2022).

11. Weber, M. *Experimental Modeling in Biology: In Vivo Representation and Stand-Ins as Modeling Strategies* https://www.journals.uchicago.edu/doi/abs/10.1086/678257?journalCode=phos. (accessed: 27.05.2022).

12. Silk, D., Kirk, P. D. W., Barnes, C. P., Toni, T. & Stumpf, M. P. H. Model Selection in Systems Biology Depends on Experimental Design. *PLOS Computational Biology* **10,** 1–14. https://doi.org/10.1371/journal.pcbi.1003650 (June 2014).

13. Of Auckland, U. *Mathematical modelling* https://www.auckland.ac.nz/en/liggins/about-the-institute/facilities-and-expertise/mathematical-modelling.html. (accessed: 27.05.2022).

14. Hunter, J. K. *Introduction to dynamical systems* 2011. https://www.math.ucdavis.edu/~hunter/m207a/ch1.pdf. (accessed: 6.06.2022).

15. Martcheva, M. *An Introduction to Mathematical Epidemiology* 1st. ISBN: 1489976116 (Springer Publishing Company, Incorporated, 2015).

16. Bradley, L. & Bradley, L. *Smallpox inoculation: an eighteenth century mathematical controversy* (University of Nottingham, Department of Adult Education, 1971).

17. Bernoulli, D. *Essai d'une nouvelle analyse de la mortalité causée par la petite vérole, et des avantages de l'inoculation pour la prévenir* 1–45 (Mém. de l'Acad. Roy. des Sciences de l'Année 1760, 1766).

18. Kermack, W. O. & McKendrick, A. G. A contribution to the mathematical theory of epidemics. *Proceedings of the royal society of london. Series A, Containing papers of a mathematical and physical character* **115,** 700–721 (1927).

19. Lunelli, A., Pugliese, A. & Rizzo, C. Epidemic patch models applied to pandemic influenza: Contact matrix, stochasticity, robustness of predictions. *Mathematical Biosciences* **220,** 24–33. ISSN: 0025-5564. https://www.sciencedirect.com/science/article/pii/S0025556409000637 (2009).

20. Gupta, S., Lal, V., Jain, R. & Gupta, O. Modeling of H1N1 Outbreak in Rajasthan: Methods and Approaches. *Indian journal of community medicine : official publication of Indian Association of Preventive and Social Medicine* **36,** 36–8 (Feb. 2011).

21. Funk, S. *et al.* Assessing the performance of real-time epidemic forecasts: A case study of Ebola in the Western Area region of Sierra Leone, 2014-15. *PLOS Computational Biology* **15,** 1–17. https://doi.org/10.1371/journal.pcbi.1006785 (Feb. 2019).

22. Kozyreff, G. Hospitalization dynamics during the first COVID-19 pandemic wave: SIR modelling compared to Belgium, France, Italy, Switzerland and New York City data. *Infectious Disease Modelling* **6,** 398–404. ISSN: 2468-0427. https://www.sciencedirect.com/science/article/pii/S2468042721000099 (2021).

23. He, S., Peng, Y. & Sun, K. SEIR modeling of the COVID-19 and its dynamics. *Nonlinear Dynamics* **101** (Aug. 2020).

24. Sjoedin, H. *et al.* COVID-19 healthcare demand and mortality in Sweden in response to non-pharmaceutical mitigation and suppression scenarios. *International Journal of Epidemiology.* dyaa121. ISSN: 0300-5771. eprint: https://academic.oup.com/ije/advance-article-

pdf/doi/10.1093/ije/dyaa121/33775089/dyaa121.pdf. https://doi.org/10.1093/ije/dyaa121 (Sept. 2020).

25. Reno, C. *et al.* Forecasting COVID-19-Associated Hospitalizations under Different Levels of Social Distancing in Lombardy and Emilia-Romagna, Northern Italy: Results from an Extended SEIR Compartmental Model. *J. Clin. Med.* **9,** 1492 (5 2020).

26. Dings, C. *et al. CoSim Online COVID-19 Simulator* Accessed: 2022-06-05. https://shiny.covid-simulator.com/covidsim/.

27. Dehning, J. *et al.* Inferring change points in the spread of COVID-19 reveals the effectiveness of interventions. *Science* **369,** eabb9789. eprint: https://www.science.org/doi/pdf/10.1126/science.abb9789. https://www.science.org/doi/abs/10.1126/science.abb9789 (2020).

28. Davies, N. *et al.* Effects of non-pharmaceutical interventions on COVID-19 cases, deaths, and demand for hospital services in the UK: a modelling study. *The Lancet Public Health* **5** (June 2020).

29. Kerr, C. C. *et al.* Covasim: An agent-based model of COVID-19 dynamics and interventions. *PLOS Computational Biology* **17,** 1–32. https://doi.org/10.1371/journal.pcbi.1009149 (July 2021).

30. Meyers, R. A. *Systems biology* ISBN: 3-527-32607-3 (Wiley-Blackwell, Weinheim, 2012).

31. eng. in *Systems Biology Definitions and Perspectives* (2005). ISBN: 9783540314530.

32. Westerhoff, H. V. & Palsson, B. O. The evolution of molecular biology into systems biology. *Nature Biotechnology* **22,** 1249–1252. https://doi.org/10.1038/nbt1020 (2004).

33. Gatherer, D. So what do we really mean when we say that systems biology is holistic? *BMC systems biology* **4,** 22 (Mar. 2010).

34. Kitano, H. Systems Biology: A Brief Overview. *Science* **295,** 1662–1664. ISSN: 0036-8075. eprint: https://science.sciencemag.org/content/295/5560/1662.full.pdf. https://science.sciencemag.org/content/295/5560/1662 (2002).

35. ISB. *What is Systems Biology* https://isbscience.org/about/what-is-systems-biology/. (accessed: 04.10.2021).

36. Bruggeman, F., Hornberg, J., Boogerd, F. & Westerhoff, H. English. in *Plant Systems Biology* (eds Baginsky, S. & Fernie, A.) 97, 1–19 (Experientia Supplementum, 2007). https://doi.org/10.1007/978-3-7643-7439-6_1DOI.

37. Shahzad, K. & Loor, J. J. Application of Top-Down and Bottom-up Systems Approaches in Ruminant Physiology and Metabolism. *Current genomics* **13,** 379–394. https://pubmed.ncbi.nlm.nih.gov/23372424 (Aug. 2012).

38. Bruggeman, F. & Westerhoff, H. The Nature of Systems Biology. *Trends in microbiology* **15,** 45–50 (Feb. 2007).

39. NESCI. *ABOUT NECSI, Advancing analytics and its application to the challenges of society* https://necsi.edu/about. (accessed: 07.10.2021).

40. Jones, R. C. Adapting to Uncertainty: Complexity Science and COVID-19. https://www.niskanencenter.org/adapting-to-uncertainty-complexity-science-and-covid-19/ (June 2020).

41. Aderem, A. Systems biology: its practice and challenges. **121,** 511–513 (May 2005).

42. Britannica. *Complexity and emergent properties* https://www.britannica.com/science/systems-biology#ref1218077. (accessed: 19.04.2022).

43. Lorenz, D., Jeng, A. & Deem, M. The Emergence of Modularity in Biological Systems. *Physics of life reviews* **8,** 129–60 (Feb. 2011).

44. Wernli, D. *et al.* A Complexity Lens on the COVID-19 Pandemic. *International Journal of Health Policy and Management,* -. ISSN: 2322-5939. eprint: https://www.ijhpm.com/article_4054_8118e2add4abc2045532e9a6384f4704.pdf. https://www.ijhpm.com/article_4054.html (2021).

45. Duan, L. *et al.* The SARS-CoV-2 Spike Glycoprotein Biosynthesis, Structure, Function, and Antigenicity: Implications for the Design of Spike-Based Vaccine Immunogens. *Frontiers in Immunology* **11** (Oct. 2020).

46. Britannica, T. E. o. E. *Coronavirus* https://www.britannica.com/science/coronavirus-virus-group. (accessed: 23.03.2022).

47. Chen, Y., Liu, Q. & Guo, D. Emerging coronaviruses: Genome structure, replication, and pathogenesis. *Journal of Medical Virology* **92** (Aug. 2020).

48. Rahbari, R., Moradi, N. & Abdi, M. rRT-PCR for SARS-CoV-2: Analytical considerations. *Clinica Chimica Acta* **516,** 1–7. ISSN: 0009-8981. https://www.sciencedirect.com/science/article/pii/S0009898121000206 (2021).

49. For Disease Control, C. & (CDC), P. *Human Coronavirus Types* https://www.cdc.gov/coronavirus/types.html. (accessed: 24.05.2022).

50. Of Cleveland Clinic, C. *Coronaviruses Have Been Around For Centuries: What Differentiates COVID-19? What to know about transmission, who is at risk and how to protect your patients* https://consultqd.clevelandclinic.org/coronaviruses-have-been-around-for-centuries-what-differentiates-2019-ncov/. (accessed: 24.05.2022).

51. For Disease Control, C. & (CDC), P. *Information about Middle East Respiratory Syndrome (MERS)* https://www.cdc.gov/coronavirus/mers/downloads/factsheet-mers_en.pdf. (accessed: 24.05.2022).

52. For Disease Control, C. & (CDC), P. *Severe Acute Respiratory Syndrome* https://www.cdc.gov/sars/about/fs-SARS.pdf. (accessed: 19.05.2022).

53. Institut, R. K. *SARS-CoV-2: Virologische Basisdaten sowie Virusvarianten* https://www.rki.de/DE/Content/InfAZ/N/Neuartiges_Coronavirus/Virologische_Basisdaten.html. (accessed: 11.02.2022).

54. For Systems Science, C. & at Johns Hopkins University, E. *COVID-19 Dashboard* https://coronavirus.jhu.edu/map.html. (accessed: 24.05.2022).

55. Organization, W. H. *Coronavirus disease* https://www.who.int/health-topics/coronavirus#tab=tab_3. (accessed: 25.01.2022).

56. Organization, W. H. *Tracking SARS-CoV-2 variants* https://www.who.int/en/activities/tracking-SARS-CoV-2-variants/. (accessed: 16.03.2022).

57. 2020, W. H. O. *Modes of transmission of virus causing COVID-19: implications for IPC precaution recommendations* https://www.who.int/news-room/commentaries/detail/modes-of-transmission-of-virus-causing-covid-19-implications-for-ipc-precaution-recommendations. (accessed: 23.03.2022).

58. Organization, W. H. *Coronavirus disease (COVID-19): How is it transmitted?* https://www.who.int/news-room/questions-and-answers/item/coronavirus-disease-covid-19-how-is-it-transmitted. (accessed: 24.03.2022).

59. For Disease Control, C. & Prevention. *How COVID-19 Spreads* https://www.cdc.gov/coronavirus/2019-ncov/prevent-getting-sick/how-covid-spreads.html. (accessed: 24.03.2022).

60. For Disease Control, C. & Prevention. *How can I reduce my risk of getting COVID-19?* https://www.who.int/news-room/questions-and-answers/item/coronavirus-disease-covid-19-how-is-it-transmitted. (accessed: 24.03.2022).

61. Reviews article collection, A. *Societal impact of the COVID-19 pandemic* https://www.annualreviews.org/page/covid-society. (accessed: 20.04.2022).

62. Of Economic, T. U. D. & DESA), S. A. (*Everyone Included: Social Impact of COVID-19* https://www.un.org/development/desa/dspd/everyone-included-covid-19.html. (accessed: 20.04.2022).

63. Sohn, E. *As long COVID cases grow, clues emerge about who is most at risk* https://www.nationalgeographic.com/science/article/who-is-most-at-risk-for-long-covid-new-clues-emerge. (accessed: 20.04.2022).

64. Habibzadeh, P., Mohammad Mofatteh, M. S., Ghavami, S. & Faghihi, M. A. Molecular diagnostic assays for COVID-19: an overview. *Critical reviews in clinical laboratory sciences* **58,** 385–398 (2021).

65. Mo, Y., Wan, R. & Zhang, Q. Application of Reverse Transcription-PCR and Real-Time PCR in Nanotoxicity Research. *Methods in molecular biology (Clifton, N.J.)* **926,** 99–112 (Sept. 2012).

66. Institute, N. H. G. R. *Understanding COVID-19 PCR Testing* https://www.genome.gov/about-genomics/fact-sheets/Understanding-COVID-19-PCR-Testing. (accessed: 24.03.2022).

67. Jawerth, N. *How is the COVID-19 virus detected using real time RTPCR?* https://www.iaea.org/bulletin/how-is-the-covid-19-virus-detected-using-real-time-rt-pcr. (accessed: 24.03.2022).

68. For Disease Control, C. & Prevention. *Antigen Testing Guidelines* https://www.cdc.gov/coronavirus/2019-ncov/lab/resources/antigen-tests-guidelines.html. (accessed: 24.05.2022).

69. Scholz, N. *Coronavirus testing Contributing to efforts to stem the second wave* https://www.europarl.europa.eu/RegData/etudes/BRIE/2020/659389/EPRS_BRI(2020)659389_EN.pdf. (accessed: 24.05.2022).

70. Guglielmi, G. Fast coronavirus tests: what they can and can't do. *Nature* **585** (Sept. 2020).

71. For Disease Prevention, E. C. & Control. *Non-pharmaceutical interventions against COVID-19* https://www.ecdc.europa.eu/en/covid-19/prevention-and-control/non-pharmaceutical-interventions. (accessed: 11.05.2022).

72. Morens, D. M., Folkers, G. K. & Fauci, A. S. The Concept of Classical Herd Immunity May Not Apply to COVID-19. *The Journal of Infectious Diseases*. jiac109. ISSN: 0022-1899. eprint: https://academic.oup.com/jid/advance-article-pdf/doi/10.1093/infdis/jiac109/43471679/jiac109.pdf. https://doi.org/10.1093/infdis/jiac109 (Mar. 2022).

73. Oé, J. *Luxemburg bekommt fürs Erste rund 9.700 Impfdosen von Pfizer geliefert* https://www.tageblatt.lu/headlines/luxemburg-bekommt-fuers-erste-rund-9700-impfdosen-von-pfizer-geliefert/. (accessed: 27.05.2022).

74. National de santé, L. *First UK variant B1.1.7 detected in Luxembourg* https://lns.lu/first-uk-variant-b1-1-7-detected-in-luxembourg/. (accessed: 27.05.2022).

75. National de santé, L. *Semaine 18 respiratory viruses in Luxembourg (REVILUX)* https://lns.lu/grippe/semaine-18/. (accessed: 27.05.2022).

76. National de santé, L. *Semaine 32 respiratory viruses in Luxembourg (REVILUX) Weekly report (09 15 August 2021)* https://lns.lu/grippe/semaine-32/. (accessed: 27.05.2022).

77. National de santé, L. *Respiratory Viruses in Luxembourg (ReViLux) Weekly report (17 23 January 2022)* https://lns.lu/wp-content/uploads/2022/02/revilux_2022_week03.pdf. (accessed: 27.05.2022).

78. National de santé, L. *Respiratory Viruses in Luxembourg (ReViLux) Weekly report (3 9 January 2022)* https://lns.lu/wp-content/uploads/2022/01/revilux_2022_week01.pdf. (accessed: 27.05.2022).

79. MARTIN, S. L. *Le variant Omicron BA.2 est majoritaire au Luxembourg* https://www.wort.lu/fr/luxembourg/le-variant-omicron-ba-2-est-majoritaire-au-luxembourg-623451a8de135b92361877ee. (accessed: 27.05.2022).

80. Dictionary, C. *Model* https://www.collinsdictionary.com/dictionary/english/model. (accessed: 11.10.2021).

81. Britannica, T. E. o. E. *Scientific-modeling* https://www.britannica.com/science/scientific-modeling. (accessed: 6.06.2022).

82. Gunawardena, J. in, 19–47 (Apr. 2010). ISBN: 9780470556757.

83. portfolio, N. *Biological models* https://www.nature.com/subjects/biological-models. (accessed: 6.06.2022).

84. Marion, G. *An Introduction to Mathematical Modelling* Mhttps://people.maths.bris.ac.uk/~madjl/course_text.pdf. (accessed: 6.06.2022).

85. Dangelmayr, G. & Kirby, M. *MATHEMATICAL MODELING A Comprehensive Introduction* https://www.math.colostate.edu/~gerhard/MATH331/331book.pdf. (accessed: 6.06.2022).

86. Antti Solonen Heikki Haario, M. L. *Statistical Analysis in Modeling* http://www2.compute.dtu.dk/~pcha/UQ/sam_lecture_notes.pdf.

87. Ellner, S. P. & Guckenheimer, J. in *Dynamic Models in Biology* 1–30 (Princeton University Press, 2011). https://doi.org/10.1515/9781400840960-004.

88. Stan, G.-B. *Modelling in Biology* version 9.0. Sept. 2021. https://gstan.bg-research.cc.ic.ac.uk/2010_Course_MiB_article.pdf.

89. Brauer, F. Mathematical epidemiology is not an oxymoron. *BMC Public Health* **9.** https://doi.org/10.1186/1471-2458-9-S1-S2 (2009).

90. Kaiser, G. & Stender, P. in *Teaching mathematical modelling: Connecting to research and practice* 277–293 (Springer, 2013).

91. Li, H. Systems biology approaches to epidemiological studies of complex diseases. *Wiley Interdisciplinary Reviews: Systems Biology and Medcine* **6,** 677–686 (May 2013).

92. For Disease Control, C. & Prevention. *Section 1:Definition of Epidemiology* https://www.cdc.gov/csels/dsepd/ss1978/lesson1/section1.html. (accessed: 21.01.2022).

93. Hethcote, H. W. in *Mathematical Understanding of Infectious Disease Dynamics* 1–61 (). eprint: https://www.worldscientific.com/doi/pdf/10.1142/9789812834836_0001. https://www.worldscientific.com/doi/abs/10.1142/9789812834836_0001.

94. For Disease Control, C. & (CDC), P. *Section 10: Chain of Infection* https://www.cdc.gov/csels/dsepd/ss1978/lesson1/section10.html. (accessed: 24.05.2022).

95. Organization, W. H. *Zoonoses* https://www.who.int/news-room/fact-sheets/detail/zoonoses. (accessed: 27.05.2022).

96. Of Health, B. M. *The Difference Between Droplet and Airborne Transmission* http://www.cda-adc.ca/_files/about/covid-19/The%20Difference%20Between%20Droplet%20and%20Airborne%20Transmission.pdf. (accessed: 27.05.2022).

97. For Disease Control, C. & Prevention. *Section 11: Epidemic Disease Occurrence* https://www.cdc.gov/csels/dsepd/ss1978/lesson1/section11.html. (accessed: 25.05.2022).

98. Of Public Health, C. M. S. *Epidemic, Endemic, Pandemic: What are the Differences?* https://www.publichealth.columbia.edu/public-health-now/news/epidemic-endemic-pandemic-what-are-differences. (accessed: 2.06.2022).

99. *Mathematical Epidemiology* eng. ISBN: 9783540789116 (2008).

100. Blackwood, J. & Childs, L. An introduction to compartmental modeling for the budding infectious disease modeler. *Letters in Biomathematics* **5,** 195–221. https://lettersinbiomath.journals.publicknowledgeproject.org/index.php/lib/article/view/81 (Dec. 2018).

101. Delamater, P. L., Street, E. J., Leslie, T. F., Yang, Y. T. & Jacobsen, K. H. Complexity of the Basic Reproduction Number (R0). *Emerging Infectious Diseases* **25,** 45–50 (Feb. 2019).

102. Anderson, R. M. & May, R. M. Directly Transmitted Infections Diseases: Control by Vaccination. *Science* **215,** 1053–1060. https://www.science.org/doi/abs/10.1126/science.7063839 (1982).

103. Cintrón-Arias, A., Castillo-Chávez, C., Bettencourt, L. M. A., Lloyd, A. L. & Banks, H. T. The estimation of the effective reproductive number from disease outbreak data. *Mathematical Biosciences and Engineering* **6,** 261–282 (2009).

104. Valderrama-Bahamóndez, G. & Fröhlich, H. MCMC Techniques for Parameter Estimation of ODE Based Models in Systems Biology. *Frontiers in Applied Mathematics and Statistics* **5** (Nov. 2019).

105. Miles, P. R. pymcmcstat: A python package for bayesian inference using delayed rejection adaptive metropolis. *Journal of Open Source Software* **4,** 1417 (2019).

106. Marquardt, D. W. An Algorithm for Least-Squares Estimation of Nonlinear Parameters. *Journal of the Society for Industrial and Applied Mathematics* **11,** 431–441. ISSN: 03684245. http://www.jstor.org/stable/2098941 (2022) (1963).

107. Gavin, H. P. *The Levenberg-Marquardt method for nonlinear least squares curve-fitting problems c l'* in (2013).

108. Van Ravenzwaaij D Cassey P, B. S. A simple introduction to Markov Chain Monte-Carlo sampling. *Psychonomic Bull Review* **25,** 143–154. https://doi.org/10.1371/journal.pcbi.1008409 (Feb. 2018).

109. Miles, P. & Smith, R. *Parameter Estimation Using the Python Package pymcmcstat* in (Jan. 2019), 93–100.

110. Speagle, J. S. A Conceptual Introduction to Markov Chain Monte Carlo Methods. *arXiv: Other Statistics* (2019).

111. Haario, H., Saksman, E. & Tamminen, J. An Adaptive Metropolis Algorithm. *Bernoulli* **7,** 223–242. ISSN: 13507265. http://www.jstor.org/stable/3318737 (2001).

112. Ballnus, B. *et al.* Comprehensive benchmarking of Markov chain Monte Carlo methods for dynamical systems. *BMC Systems Biology* **11.** https://doi.org/10.1186/s12918-017-0433-1 (2017).

113. Haario, H., Laine, M., Mira, A. & Saksman, E. DRAM: efficient adaptive MCMC. *Statistics and computing* **16,** 339–354 (2006).

114. Mira, A. On Metropolis-Hastings algorithms with delayed rejection. *Metron* **59** (Apr. 2001).

115. Brooks, S. & Roberts, G. Assessing Convergence of Markov Chain Monte Carlo Algorithms. **8.** https://www2.stat.duke.edu/~scs/Courses/Stat376/Papers/ConvergeDiagnostics/brooks97assessing.pdf (Aug. 1997).

116. Haugh, M. *MCMC and Bayesian Modeling* http://www.columbia.edu/~mh2078/MachineLearningORFE/MCMC_Bayes.pdf. (accessed: 11.04.2022).

117. Roy, V. Convergence Diagnostics for Markov Chain Monte Carlo. *Annual Review of Statistics and Its Application* **7,** 387–412. eprint: https://doi.org/10.1146/annurev-statistics-031219-041300. https://doi.org/10.1146/annurev-statistics-031219-041300 (2020).

118. Sahlin, K. *Estimating convergence of Markov chain Monte Carlo simulations* https://www2.math.su.se/matstat/reports/master/2011/rep2/report.pdf.

119. Scheffer, M. *et al.* Early-warning signals for critical transitions. *Nature* **461,** 53–59 (2009).

120. Kuehn, C. A mathematical framework for critical transitions: normal forms, variance and applications. *Journal of Nonlinear Science* **23,** 457–510 (2013).

121. Kuehn, C. A mathematical framework for critical transitions: Bifurcations, fastslow systems and stochastic dynamics. *Physica D: Nonlinear Phenomena* **240,** 1020–1035. ISSN: 0167-2789. https://www.sciencedirect.com/science/article/pii/S0167278911000443 (2011).

122. Southall, E., Brett, T. S., Tildesley, M. J. & Dyson, L. Early warning signals of infectious disease transitions: a review. *Journal of The Royal Society Interface* **18,** 20210555. eprint: https://royalsocietypublishing.org/doi/pdf/10.1098/rsif.2021.0555. https://royalsocietypublishing.org/doi/abs/10.1098/rsif.2021.0555 (2021).

123. Bury, T. M., Bauch, C. T. & Anand, M. Detecting and distinguishing tipping points using spectral early warning signals. *Journal of The Royal Society Interface* **17,** 20200482. eprint: https://royalsocietypublishing.org/doi/pdf/10.1098/rsif.2020.0482. https://royalsocietypublishing.org/doi/abs/10.1098/rsif.2020.0482 (2020).

124. Strogatz, S. H. *Nonlinear dynamics and chaos with student solutions manual: With applications to physics, biology, chemistry, and engineering* (CRC press, 2018).

125. George, S., Kachhara, S. & Ambika, G. *Early warning signals for critical transitions in complex systems* July 2021.

126. Wieczorek, S., Ashwin, P., Luke, C. M. & Cox, P. M. Excitability in ramped systems: the compost-bomb instability. *Proceedings of the Royal Society A: Mathematical, Physical and Engineering Sciences* **467,** 1243–1269. eprint: https://royalsocietypublishing.org/doi/pdf/10.1098/rspa.2010.0485. https://royalsocietypublishing.org/doi/abs/10.1098/rspa.2010.0485 (2011).

127. Of Standards, N. I. & Technology. *Measures of Skewness and Kurtosis* https://www.itl.nist.gov/div898/handbook/eda/section3/eda35b.htm. (accessed: 20.04.2022).

128. Of Science, P. E. C. *Autocorrelation and Time Series Methods* https://online.stat.psu.edu/stat462/node/188/. (accessed: 23.03.2022).

129. Hyndman, R. J. & Athanasopoulos, G. *Forecasting: Principles and Practice* https://otexts.com/fpp2/moving-averages.html. (accessed: 27.04.2022).

130. Hayes, A. *Autoregressive Integrated Moving Average (ARIMA)* https://www.investopedia.com/terms/a/autoregressive-integrated-moving-average-arima.asp. (accessed: 8.06.2022).

131. Kotu, V. & Deshpande, B. in *Data Science (Second Edition)* (eds Kotu, V. & Deshpande, B.) Second Edition, 395–445 (Morgan Kaufmann, 2019). ISBN: 978-0-12-814761-0. https://www.sciencedirect.com/science/article/pii/B9780128147610000125.

132. Southall, E., Tildesley, M. & Dyson, L. Prospects for detecting early warning signals in discrete event sequence data: Application to epidemiological incidence data. *PLoS Comput Biol* **16,** e1007836 (2020).

133. Cross, M. E. & Plunkett, E. V. E. in *Physics, Pharmacology and Physiology for Anaesthetists: Key Concepts for the FRCA* 2nd ed., 369–369 (Cambridge University Press, 2014).

134. Boettiger, C. & Hastings, A. Early warning signals and the prosecutor's fallacy. *Proceedings of the Royal Society B: Biological Sciences* **279,** 4734–4739 (2012).

135. Brett, T. *et al.* Detecting critical slowing down in high-dimensional epidemiological systems. *PLoS Comp. Biol.* **16,** e1007679 (2020).

136. Fawcett, T. An introduction to ROC analysis. *Pattern recognition letters* **27,** 861–874 (2006).

137. Boettiger, C. & Hastings, A. Quantifying limits to detection of early warning for critical transitions. *Journal of The Royal Society Interface* **9,** 2527–2539. eprint: https://royalsocietypublishing.org/doi/pdf/10.1098/rsif.2012.0125. https://royalsocietypublishing.org/doi/abs/10.1098/rsif.2012.0125 (2012).

138. Proverbio, D., Kemp, F., Magni, S. & Gonçalves, J. Performance of early warning signals for disease re-emergence: A case study on COVID-19 data. *PLOS Computational Biology* **18,** 1–22. https://doi.org/10.1371/journal.pcbi.1009958 (Mar. 2022).

139. Ng, Y. *et al.* Evaluation of the effectiveness of surveillance and containment measures for the first 100 patients with COVID-19 in Singapore–January 2–February 29, 2020 (2020).

140. Currie, C. S. *et al.* How simulation modelling can help reduce the impact of COVID-19. *J. Simul.* **14,** 83–97 (2020).

141. Kucharski, A. J. *et al.* Effectiveness of isolation, testing, contact tracing and physical distancing on reducing transmission of SARS-CoV-2 in different settings. *medRxiv* (2020).

142. Anderson, R. M. & May, R. M. Population biology of infectious diseases: Part I. *Nature* **280,** 361–367 (1979).

143. Legrand, J., Grais, R. F., Boelle, P.-Y., Valleron, A.-J. & Flahault, A. Understanding the dynamics of Ebola epidemics. *Epidemiology and Infection* **135,** 610–621 (2007).

144. Lai, S. *et al.* Effect of non-pharmaceutical interventions to contain COVID-19 in China. *Nature* **585,** 410–413 (2020).

145. de-Camino-Beck, T. A modified SEIR Model with Confinement and Lockdown of COVID-19 for Costa Rica. *medRxiv* (2020).

146. Anand, N., Sabarinath, A., Geetha, S. & Somanath, S. Predicting the Spread of COVID-19 Using SIR Model Augmented to Incorporate Quarantine and Testing. *Transactions of the Indian National Academy of Engineering* **5,** 141–148 (2020).

147. WHO. Tracking Public Health and Social Measures - a global dataset. *https://www.who.int/emergencies/d coronavirus-2019/phsm* (2020).

148. Anderson, R. M., Heesterbeek, H., Klinkenberg, D. & Hollingsworth, T. D. How will country-based mitigation measures influence the course of the COVID-19 epidemic? *The Lancet* **395,** 931–934 (2020).

149. Mancastroppa, M., Burioni, R., Colizza, V. & Vezzani, A. Active and inactive quarantine in epidemic spreading on adaptive activity-driven networks. *Physical Review E* **102,** 020301 (2020).

150. Alrashed, S., Min-Allah, N., Saxena, A., Ali, I. & Mehmood, R. Impact of lockdowns on the spread of COVID-19 in Saudi Arabia. *Informatics in Medicine Unlocked* **20,** 100420 (2020).

151. Yan, P. & Liu, S. SEIR epidemic model with delay. *The ANZIAM Journal* **48,** 119–134 (2006).

152. Gatto, M. *et al.* Spread and dynamics of the COVID-19 epidemic in Italy: Effects of emergency containment measures. *Proceedings of the National Academy of Sciences* **117,** 10484–10491 (2020).

153. Arino, J. *et al.* A multi-species epidemic model with spatial dynamics. *Mathematical Medicine and Biology* **22,** 129–142 (2005).

154. Giordano, G. *et al.* Modelling the COVID-19 epidemic and implementation of population-wide interventions in Italy. *Nature Medicine,* 1–6 (2020).

155. Syafruddin, S. & Noorani, M. SEIR model for transmission of dengue fever in Selangor Malaysia. *IJMPS* **9,** 380–389 (2012).

156. Fraser, C. *et al.* Pandemic potential of a strain of influenza A (H1N1): early findings. *Science* **324,** 1557–1561 (2009).

157. Althaus, C. L. Estimating the reproduction number of Ebola virus (EBOV) during the 2014 outbreak in West Africa. *PLoS Currents* **6** (2014).

158. World Health Organization and others. Coronavirus disease 2019 (COVID-19): situation report, 88 (2020).

159. Hale, T., Petherick, A., Phillips, T. & Webster, S. Variation in government responses to COVID-19. *Blavatnik school of government working paper* **31** (2020).

160. ACAPS. COVID-19 Government measures dataset. *https://www.acaps.org/covid19-government-measures-dataset* (2020).

161. Dong, E., Du, H. & Gardner, L. An interactive web-based dashboard to track COVID-19 in real time. *The Lancet infectious diseases* **20,** 533–534 (2020).

162. Dipartimento della Protezione Civile - Emergenza Coronavirus. Dati COVID-19 Italia. *https://github.com/pcm-dpc/COVID-19/tree/master/dati-regioni* (Accessed 14 Jun 2020).

163. Max Roser Hannah Ritchie, E. O.-O. & Hasell, J. Coronavirus Pandemic (COVID-19). *Our World in Data.* https://ourworldindata.org/coronavirus (2020).

164. Lee, K.-B., Han, S. & Jeong, Y. COVID-19, flattening the curve, and Benfords law. *Physica A: Statistical Mechanics and its Applications* **559,** 125090 (2020).

165. Kennedy, A. P. & Yam, S. C. P. On the authenticity of COVID-19 case figures. *PloS one* **15,** e0243123 (2020).

166. Google. COVID-19 Community Mobility Reports. *https://www.google.com/covid19/mobility/* (Accessed 14 Jun 2020).

167. Ferguson, N. M. *et al.* Impact of non-pharmaceutical interventions (NPIs) to reduce COVID-19 mortality and healthcare demand. *Imperial College, London. DOI: https://doi. org/10.25561/77482* (2020).

168. Alvarez, F. E., Argente, D. & Lippi, F. *A simple planning problem for COVID-19 lockdown* tech. rep. (National Bureau of Economic Research, 2020).

169. Altig, D. *et al.* Economic uncertainty before and during the COVID-19 pandemic. *Journal of Public Economics* **191,** 104274 (2020).

170. Atkeson, A. *What will be the economic impact of COVID-19 in the us? rough estimates of disease scenarios* tech. rep. (National Bureau of Economic Research, 2020).

171. Lau, H. *et al.* The positive impact of lockdown in Wuhan on containing the COVID-19 outbreak in China. *Journal of travel medicine* **27,** taaa037 (2020).

172. Feng, Z. Final and peak epidemic sizes for SEIR models with quarantine and isolation. *Mathematical Biosciences and Engineering* **4,** 675 (2007).

173. Liu, Y., Gayle, A. A., Wilder-Smith, A. & Rocklöv, J. The reproductive number of COVID-19 is higher compared to SARS coronavirus. *Journal of Travel Medicine* (2020).

174. Wearing, H. J., Rohani, P. & Keeling, M. J. Appropriate models for the management of infectious diseases. *PLoS medicine* **2** (2005).

175. Li, M. Y., Graef, J. R., Wang, L. & Karsai, J. Global dynamics of a SEIR model with varying total population size. *Mathematical biosciences* **160,** 191–213 (1999).

176. Heffernan, J. M., Smith, R. J. & Wahl, L. M. Perspectives on the basic reproductive ratio. *Journal of the Royal Society Interface* **2,** 281–293 (2005).

177. Kucharski, A., Russell, T., Diamond, C. & Liu, Y. Analysis and projections of transmission dynamics of nCoV in Wuhan. *CMMID repository* **2** (2020).

178. Wu, J. T., Leung, K. & Leung, G. M. Nowcasting and forecasting the potential domestic and international spread of the 2019-nCoV outbreak originating in Wuhan, China: a modelling study. *The Lancet* **395,** 689–697 (2020).

179. Taylor, J. An Introduction to Error Analysis - University Science Books. *Mill Valley, California* (1997).

180. Liu, X. *et al.* Modelling the situation of COVID-19 and effects of different containment strategies in China with dynamic differential equations and parameters estimation. *Available at SSRN 3551359* (2020).

181. Kretzschmar, M. E. *et al.* Impact of delays on effectiveness of contact tracing strategies for COVID-19: a modelling study. *The Lancet Public Health* **5,** e452–e459 (2020).

182. Corman, V. M. *et al.* Detection of 2019 novel coronavirus (2019-nCoV) by real-time RT-PCR. *Eurosurveillance* **25,** 2000045 (2020).

183. Hanel, R. & Thurner, S. Boosting test-efficiency by pooled testing strategies for SARS-CoV-2. *arXiv preprint arXiv:2003.09944* (2020).

184. Deutsche Gesellschaft für Epidemiologie. Stellungnahme der Deutschen Gesellschaft für Epidemiologie (DGEpi) zur Verbreitung des neuen Coronavirus (SARS-CoV-2). *www.dgepi.de* (2020).

185. Moodley, K., Obasa, A. & London, L. Isolation and quarantine in South Africa during COVID-19: Draconian measures or proportional response? *SAMJ: South African Medical Journal* **110,** 1–2 (2020).

186. Liu, Y., Eggo, R. M. & Kucharski, A. J. Secondary attack rate and superspreading events for SARS-CoV-2. *The Lancet* **395,** e47 (2020).

187. Vinceti, M. *et al.* Lockdown timing and efficacy in controlling COVID-19 using mobile phone tracking. *EClinicalMedicine,* 100457 (2020).

188. Newville, M., Stensitzki, T., Allen, D. B. & Ingargiola, A. *LMFIT: Non-Linear Least-Square Minimization and Curve-Fitting for Python* version 0.8.0. Sept. 2014. https://doi.org/10.5281/zenodo.11813.

189. Roda, W. C., Varughese, M. B., Han, D. & Li, M. Y. Why is it difficult to accurately predict the COVID-19 epidemic? *Infectious Disease Modelling* **5,** 271–281. ISSN: 2468-0427. http://www.sciencedirect.com/science/article/pii/S2468042720300075 (2020).

190. Stutt, R. O., Retkute, R., Bradley, M., Gilligan, C. A. & Colvin, J. A modelling framework to assess the likely effectiveness of facemasks in combination with lock-downin managing the COVID-19 pandemic. *Proceedings of the Royal Society A* **476,** 20200376 (2020).

191. Okell, L. C. *et al.* Have deaths from COVID-19 in Europe plateaued due to herd immunity? *The Lancet* (2020).

192. López, L. & Rodó, X. The end of social confinement and COVID-19 re-emergence risk. *Nature Human Behaviour* **4,** 746–755 (2020).

193. Postnikov, E. B. Estimation of COVID-19 dynamics on a back-of-envelope: Does the simplest SIR model provide quantitative parameters and predictions? *Chaos, Solitons and Fractals* **135,** 109841 (2020).

194. Comunian, A., Gaburro, R. & Giudici, M. Inversion of a SIR-based model: a critical analysis about the application to COVID-19 epidemic. *Physica D: Nonlinear Phenomena* **413,** 132674 (2020).

195. Cowling, B. J. *et al.* Impact assessment of non-pharmaceutical interventions against coronavirus disease 2019 and influenza in Hong Kong: an observational study. *The Lancet Public Health* (2020).

196. Peak, C. M. *et al.* Individual quarantine versus active monitoring of contacts for the mitigation of COVID-19: a modelling study. *The Lancet Infectious Diseases* (2020).

197. Kissler, S. M., Tedijanto, C., Goldstein, E., Grad, Y. H. & Lipsitch, M. Projecting the transmission dynamics of SARS-CoV-2 through the postpandemic period. *Science* **368,** 860–868 (2020).

198. Mohanty, S., Satapathy, A., Naidu, M. *et al.* Severe acute respiratory syndrome coronavirus-2 (SARS-CoV-2) and coronavirus disease 19 (COVID-19) - anatomic pathology perspective on current knowledge. *Diagn. Pathol.* **15 (1):103** (2020).

199. Emery, J. *et al.* The contribution of asymptomatic SARS-CoV-2 infections to transmission on the Diamond Princess cruise ship. *eLife* **9** (Aug. 2020).

200. Cazelles, B. *et al.* A mechanistic and data-driven reconstruction of the time-varying reproduction number: Application to the COVID-19 epidemic. *medRxiv.* https://www.medrxiv.org/content/early/2021/05/13/2021.02.04.21251167 (2021).

201. Gatto, M. *et al.* Spread and dynamics of the COVID-19 epidemic in Italy: Effects of emergency containment measures. *Proc. Natl. Acad. Sci. USA* **117,** 10484–10491. ISSN: 0027-8424 (2020).

202. Gevertz, J. L., Greene, J. M., Sanchez-Tapia, C. H. & Sontag, E. D. A novel COVID-19 epidemiological model with explicit susceptible and asymptomatic isolation compartments reveals unexpected consequences of timing social distancing. *J. Theor. Biol.* **510,** 110539. ISSN: 0022-5193 (2021).

203. Proverbio, D. *et al.* Dynamical SPQEIR model assesses the effectiveness of non-pharmaceutical interventions against COVID-19 epidemic outbreaks. *PLOS ONE* **16,** 1–21. https://doi.org/10.1371/journal.pone.0252019 (May 2021).

204. Yang, W., Shaff, J. & Shaman, J. Effectiveness of non-pharmaceutical interventions to contain COVID-19: a case study of the 2020 spring pandemic wave in New York City. *J. Roy. Soc. Interface* **18,** 20200822 (Feb. 2021).

205. Parino, F., Zino, L., Porfiri, M. & Rizzo, A. Modelling and predicting the effect of social distancing and travel restrictions on COVID-19 spreading. *J. Ro. Soc. Interface* **18,** 20200875 (Feb. 2021).

206. Burzynski, M. *et al.* COVID-19 Crisis Management in Luxembourg: Insights from an Epidemionomic Approach. *Luxembourg Institute of Socio-Economic Research (LISER) Working Paper Series* **2020-08,** Available at SSRN (June 2020).

207. Rashid, H., Khandaker, G. & Booy, R. Vaccination and herd immunity: What more do we know? *Curr. Opin. Infect. Dis.* **25,** 243–9 (June 2012).

208. Fontanet, A. & Cauchemez, S. COVID-19 herd immunity: where are we? *Nat. Rev. Immunol.* **20** (Sept. 2020).

209. Poland, G. A., Ovsyannikova, I. G. & Kennedy, R. B. SARS-CoV-2 immunity: review and applications to phase 3 vaccine candidates. *Lancet* **396,** 1595–1606 (10262 2020).

210. Brett, T. S. & Rohani, P. Transmission dynamics reveal the impracticality of COVID-19 herd immunity strategies. *Proc. Natl. Acad. Sci. USA* **117,** 25897–25903. ISSN: 0027-8424 (2020).

211. Nokes, D. & Anderson, R. The use of mathematical models in epidemiological study of infectious diseases and in the design of mass immunization programmes. *Epidemiol. Infect.* **101,** 1–20 (Sept. 1988).

212. Anderson, R. M., Vegvari, C., Truscott, J. & Collyer, B. S. Challenges in creating herd immunity to SARS-CoV-2 infection by mass vaccination. *The Lancet* **396,** 1614–1616 (2020).

213. Deng, J., Tang, S. & Shu, H. Joint impacts of media, vaccination and treatment on an epidemic Filippov model with application to COVID-19. *J. Theor. Biol.,* 110698. ISSN: 0022-5193 (2021).

214. Saad-Roy, C., Levin, S., Metcalf, C. J. & Grenfell, B. Trajectory of individual immunity and vaccination required for SARS-CoV-2 community immunity: a conceptual investigation. *J. Roy. Soc. Interface* **18,** 20200683 (Feb. 2021).

215. Good, M. F. & Hawkes, M. T. The Interaction of Natural and Vaccine-Induced Immunity with Social Distancing Predicts the Evolution of the COVID-19 Pandemic. *mBio* **11** (ed Sher, A.) (2020).

216. Moore, S., Hill, E., Dyson, L., Tildesley, M. & Keeling, M. Modelling optimal vaccination strategy for SARS-CoV-2 in the UK. *PLOS Computational Biology* **17,** e1008849. https://doi.org/10.1371/journal.pcbi.1008849 (May 2021).

217. Kermack, W. O., McKendrick, A. G. & Walker, G. T. A contribution to the mathematical theory of epidemics. *Proc. Roy. Soc. A-Math. Phy.* **115,** 700–721 (1927).

218. Li, R. *et al.* Substantial undocumented infection facilitates the rapid dissemination of novel coronavirus (SARS-CoV-2). *Science* **368,** 489–493. ISSN: 0036-8075 (2020).

219. Tracy, M., CerdAą, M. & Keyes, K. M. Agent-Based Modeling in Public Health: Current Applications and Future Directions. *Annu. Rev. Publ. Health* **39.** PMID: 29328870, 77–94 (2018).

220. Thompson, J. & Wattam, S. Estimating the impact of interventions against COVID-19: from lockdown to vaccination. *medRxiv*. https://www.medrxiv.org/content/early/2021/03/26/2021.03.21.21254049 (2021).

221. Shattock, A. J. *et al.* Impact of vaccination and non-pharmaceutical interventions on SARS-CoV-2 dynamics in Switzerland. *medRxiv*. https://www.medrxiv.org/content/early/2021/04/20/2021.04.14.21255503 (2021).

222. Chang, S., Harding, N., Zachreson, C., Cliff, O. & Prokopenko, M. Modelling transmission and control of the COVID-19 pandemic in Australia. *Nat. Commun.* **11** (Nov. 2020).

223. Althouse, B. *et al.* Superspreading events in the transmission dynamics of SARS-CoV-2: Opportunities for interventions and control. *PLOS Biol.* **18,** e3000897 (Nov. 2020).

224. Hethcote, H. W. in *Mathematical Understanding of Infectious Disease Dynamics* 91–128 (). https://www.worldscientific.com/doi/abs/10.1142/9789812834836_0003.

225. Cao, H. & Zhou, Y. The discrete age-structured SEIT model with application to tuberculosis transmission in China. *Mathematical and Computer Modelling* **55,** 385–395. ISSN: 0895-7177. https://www.sciencedirect.com/science/article/pii/S0895717711004973 (2012).

226. Diekmann, O., Heesterbeek, J. A. P. & Roberts, M. G. The construction of next-generation matrices for compartmental epidemic models. *J. Roy. Soc. Interface* **7,** 873–885 (2010).

227. Britton, T., Ball, F. & Trapman, P. A mathematical model reveals the influence of population heterogeneity on herd immunity to SARS-CoV-2. *Science* **369,** 846–849. ISSN: 0036-8075 (2020).

228. Rees, E. *et al.* COVID-19 length of hospital stay: A systematic review and data synthesis. *BMC Med.* **18,** 270 (Sept. 2020).

229. Snoeck, C. J. *et al.* Prevalence of SARS-CoV-2 infection in the Luxembourgish population: the CON-VINCE study. *medRxiv*. eprint: https://www.medrxiv.org/content/early/2020/05/18/2020.05.11.20092916.full.pdf. https://www.medrxiv.org/content/early/2020/05/18/2020.05.11.20092916 (2020).

230. Folkhalsomyndigheten. *Påvisning av antikroppar efter genomgången covid-19 i blodprov från öppenvården (Delrapport 1)* 2020. %7Bhttps://www.folkhalsomyndigheten.se/contentassets/9c5893f84bd049e691562b9eeb0ca280/pavisning-antikroppar-genomgangen-covid-19-blodprov-oppenvarden-delrapport-1.pdf%7D.

231. Folkhalsomyndigheten. *Påvisning av antikroppar efter genomgången covid-19 hos blodgivare (Delrapport 2)* 2020. %7Bhttps://www.folkhalsomyndigheten.se/contentassets/376f9021a4c84da08de18ac597284f0c/pavisning-antikroppar-genomgangen-covid-19-blodgivare-delrapport-2.pdf%7D.

232. Böhning, D., Rocchetti, I., Maruotti, A. & Holling, H. Estimating the undetected infections in the Covid-19 outbreak by harnessing capture-recapture methods. *Int. J. Infect. Dis.* **97,** 197–201. ISSN: 1201-9712 (2020).

233. Castro, M., Ares, S., Cuesta, J. A. & Manrubia, S. The turning point and end of an expanding epidemic cannot be precisely forecast. *Proc. Natl. Acad. Sci.* **117,** 26190–26196. ISSN: 0027-8424 (2020).

234. Dehning, J. *et al.* Inferring change points in the spread of COVID-19 reveals the effectiveness of interventions. *Science* **369.** ISSN: 0036-8075 (2020).

235. Bryant P, E. A. Estimating the impact of mobility patterns on COVID-19 infection rates in 11 European countries. *PeerJ* (2020).

236. Bicher, M. *et al.* Model Based Estimation of the SARS-CoV-2 Immunization Level in Austria and Consequences for Herd Immunity Effects. *medRxiv.* https://www.medrxiv.org/content/early/2021/03/12/2021.03.10.21253251 (2021).

237. Locatelli, I., Traechsel, B. & Rousson, V. Estimating the basic reproduction number for COVID-19 in Western Europe. *PLoS ONE.* https://doi.org/10.1371/journal.pone.0248731 (Mar. 2021).

238. Ke, R., Romero-Severson, E., Sanche, S. & Hengartner, N. Estimating the reproductive number R0 of SARS-CoV-2 in the United States and eight European countries and implications for vaccination. *Journal of Theoretical Biology* **517,** 110621. ISSN: 0022-5193.

https://www.sciencedirect.com/science/article/pii/S0022519321000436 (2021).

239. Yuan, J., Li, M., Lv, G. & Lu, Z. K. Monitoring transmissibility and mortality of COVID-19 in Europe. *International Journal of Infectious Diseases* **95,** 311–315. ISSN: 1201-9712. https://www.sciencedirect.com/science/article/pii/S120197122030182X (2020).

240. Buss, L. F. *et al.* Three-quarters attack rate of SARS-CoV-2 in the Brazilian Amazon during a largely unmitigated epidemic. *Science* **371,** 288–292. ISSN: 0036-8075 (2021).

241. De la Sen, M. & Alonso-Quesada, S. Vaccination strategies based on feedback control techniques for a general SEIR-epidemic model. *Appl. Math. Comput.* **218,** 3888–3904. ISSN: 0096-3003 (2011).

242. Sabino, E. *et al.* Resurgence of COVID-19 in Manaus, Brazil, despite high seroprevalence. *The Lancet* (Jan. 2021).

243. Vrugt, M. t., Bickmann, J. & Wittkowski, R. Effects of social distancing and isolation on epidemic spreading modeled via dynamical density functional theory. *Nature Communications* **11** (Nov. 2020).

244. Kavaliunas, A., Ocaya, P., Mumper, J., Lindfeldt, I. & Kyhlstedt, M. Swedish policy analysis for Covid-19. *Health Policy Techn.* **9.** The COVID-19 pandemic: Global health policy and technology responses in the making, 598–612. ISSN: 2211-8837 (2020).

245. Ludvigsson, J. F. The first eight months of Sweden COVID-19 strategy and the key actions and actors that were involved. *Acta Paediatr.* **109,** 2459–2471 (2020).

246. Ragonnet, R. *et al.* Optimising social mixing strategies achieving COVID-19 herd immunity while minimising mortality in six European countries. *medRxiv* (2020).

247. Jahn, B. *et al.* Targeted COVID-19 Vaccination (TAV-COVID) Considering Limited Vaccination Capacities - An Agent-Based Modeling Evaluation. *Vaccines* **9.** ISSN: 2076-393X. https://www.mdpi.com/2076-393X/9/5/434 (2021).

248. Bubar, K. M. *et al.* Model-informed COVID-19 vaccine prioritization strategies by age and serostatus. *medRxiv* (2021).

249. MacIntyre, C. R., Costantino, V. & Trent, M. Modelling of COVID-19 vaccination strategies and herd immunity, in scenarios of limited and full vaccine supply in NSW, Australia. *medRxiv* (2020).

250. Edridge, A. W. D. *et al.* Seasonal coronavirus protective immunity is short-lasting. *Nature Medicine* **26,** 1691–1693. https://doi.org/10.1038/s41591-020-1083-1 (2020).

251. Simmonds, P., Williams, S. & Harvala, H. Understanding the outcomes of COVID-19–does the current model of an acute respiratory infection really fit? *J. Gen. Virol.,* 001545 (2020).

252. Tillett, R. L. *et al.* Genomic evidence for reinfection with SARS-CoV-2: a case study. *Lancet Infec. Dis.* **21,** 52–58 (2021).

253. Polack, F. P. *et al.* Safety and Efficacy of the BNT162b2 mRNA Covid-19 Vaccine. *New Engl. J. Med.* **383,** 2603–2615 (2020).

254. Baden, L. R. *et al.* Efficacy and Safety of the mRNA-1273 SARS-CoV-2 Vaccine. *New Engl. J. Med.* **384,** 403–416 (2021).

255. Kennedy, D. & Read, A. Monitor for COVID-19 vaccine resistance evolution during clinical trials. *PLOS Biol.* **18,** e3001000 (Nov. 2020).

256. Starr, T. N. *et al.* Prospective mapping of viral mutations that escape antibodies used to treat COVID-19. *Science* **371,** 850–854. ISSN: 0036-8075 (2021).

257. Kissler, S., Fauver, J. R., Mack, C., Tai, C. G. & Breban, M. I. e. a. *Densely sampled viral trajectories suggest longer duration of acute infection with B.1.1.7 variant relative to non-B.1.1.7 SARS-CoV-2.* 2021.

258. Baldwin, R. & Weder di Mauro, B. Economics in the Time of COVID-19. *VoxEU.org Book, CEPR* (2020).

259. Barro, R., Ursua, J. & Weng, J. Coronavirus meets the Great Influenza Pandemic. *VoxEU* **March** (2020).

260. Gourinchas, P. Flattening the Pandemic and Recession Curves. *VoxEU* **March** (2020).

261. Correia, S., Luck, S. & Verner, E. Pandemics Depress the Economy, Public Health Interventions Do Not: Evidence from the 1918 Flu. *Manuscript available online at https://ssrn.com/abstract=3561560* (2020).

262. OECD. Evaluating the initial impact of Covid-19 containment measures on economic activity. *Note is produced by the OECD Economics Department* **March** (2020).

263. *RECOV*id. Economic effects of Covid-19 in Luxembourg – First *RECOV*id working note with preliminary estimates. *Research Luxembourg, Covid-19 Task Force* **April** (2020).

264. Greenstone, M. & Nigam, V. Does social distancing matter? *Covid Economics Vetted and Real-Time Papers* **7,** 1–22 (2020).

265. Barbieri, T., Basso, G. & Scicchitano, S. Italian workers at risk during the Covid-19 epidemic. *INAPP WP* **46** (2020).

266. Dingel, J. & Neiman, B. How many jobs can be done at home? *Journal of Public Economics* **189** (2020).

267. Koren, M. & Peto, R. Business disruptions from social distancing matter. *Covid Economics Vetted and Real-Time Papers* **2,** 13–31 (2020).

268. Alvarez, F., Argente, D. & Lippi, F. A simple planning problem for Covid-19 lockdown. *NBER Working Papers* **26981** (2020).

269. Atkeson, A. What will be the economic impact of Covid-19 in the US? Rough estimates of disease scenarios. *Staff Report, Fed Reserve Bank of Minneapolis* **595** (2020).

270. Berger, D., Herkenhoff, K. & Mongey, S. An SEIR Infectious Disease Model with Testing and Conditional Quarantine. *NBER Working Papers* **26901** (2020).

271. Jones, C., Philippon, T. & V., V. Optimal mitigation policies in a pandemic: social distancing and working from home. *NBER Working Paper* **26984** (2020).

272. Eichenbaum, M., Rebelo, S. & Trabandt, M. The macroeconomics of epidemics. *NBER Working Papers* **26882** (2020).

273. Fadinger, H. & Schymik, J. The costs and benefits of home office during the Covid-19 pandemic: Evidence from infections and an input-output model for Germany. *Covid Economics Vetted and Real-Time Papers* **9,** 107–134 (2020).

274. Barrot, J., Grassi, B. & Sauvagnat, J. Sectoral effects of social distancing. *Covid Economics Vetted and Real-Time Papers* **3,** 85–102 (2020).

275. Burzynski, M. *et al.* COVID-19 Crisis Management in Luxembourg: Insights from an Epidemionomic Approach. *LISER Working Paper series* **2020-08** (2020).

276. Heneghan, C., Brassey, J. & Jefferson, T. COVID-19: What proportion are asymptomatic? *Online publication available at: https://www.cebm.net/covid-19/covid-19-what-proportion-are-asymptomatic/* (2020).

277. Fontanet, A. *et al.* Cluster of COVID-19 in Northern France: a Retrospective Closed Cohort Study. *medRxiv* (2020).

278. Ferretti, F. *et al.* Quantifying SARS-CoV-2 transmission suggests epidemic control with digital contact tracing. *Science* **368** (2020).

279. Oxford-Economics. Global Scenarios Service: Q2 2020 – After the pandemic. *Oxford Economics Ltd: London* (2020).

280. Ashwin, P., Wieczorek, S., Vitolo, R. & Cox, P. Tipping points in open systems: bifurcation, noise-induced and rate-dependent examples in the climate system. *Philosophical Transactions of the Royal Society A: Mathematical, Physical and Engineering Sciences* **370,** 1166–1184. eprint: https://royalsocietypublishing.org/doi/pdf/10.1098/rsta.2011.0306. https://royalsocietypublishing.org/doi/abs/10.1098/rsta.2011.0306 (2012).

281. Chung, M. T., Mastalerz, P. M. H., Morrow, M. A. K., Venkatesan, M. P. A. & Parker, M. P. A. *Long COVID: Long-Term Effects of COVID-19* https://www.hopkinsmedicine.org/health/conditions-and-diseases/coronavirus/covid-long-haulers-long-term-effects-of-covid19. (accessed: 14.06.2022).

282. Dr Charles Benoy Carlo Diederich, P. F. & Staub, D. T. *Que faire en cas d'affection post-COVID-19 ou COVID long?* https://covid19.public.lu/fr/blog/quotidien/long-covid.html. (accessed: 14.06.2022).

283. BBC. *Long Covid: What is it and what are the symptoms?* https://www.bbc.com/news/health-57833394. (accessed: 14.06.2022).

284. National de santé, L. *UK variant causes 75% of new infections in Luxembourg* https://lns.lu/en/rtl-today-uk-variant-causes-75-of-new-infections-in-luxembourg-2/. (accessed: 27.05.2022).

285. Arons, M. M. *et al.* Presymptomatic SARS-CoV-2 infections and transmission in a skilled nursing facility. *New England journal of medicine* **382,** 2081–2090 (2020).

286. Sharma, M. *et al.* Understanding the effectiveness of government interventions against the resurgence of COVID-19 in Europe. *Nature Communications* **12** (Oct. 2021).

287. Contreras, S. *et al.* The challenges of containing SARS-CoV-2 via test-trace-and-isolate. *Nature Communications* **12** (Jan. 2021).

288. Nasreen, S. *et al.* Effectiveness of COVID-19 vaccines against symptomatic SARS-CoV-2 infection and severe outcomes with variants of concern in Ontario. *Nature Microbiology* **7,** 1–7 (Mar. 2022).

289. Islam, S., Islam, T. & Islam, M. New Coronavirus Variants are Creating More Challenges to Global Healthcare System: A Brief Report on the Current Knowledge. *Clinical Pathology* **15,** 1–7 (Feb. 2022).

290. Gandhi, M., Yokoe, D. S. & Havlir, D. V. *Asymptomatic transmission, the Achilles heel of current strategies to control Covid-19* 2020.

291. Of Disease Control, C. & Prevention. *SARS-CoV-2 Variant Classifications and Definitions* https://www.cdc.gov/coronavirus/2019-ncov/variants/variant-classifications.html. (accessed: 06.06.2022).

292. Dolton, P. THE STATISTICAL CHALLENGES OF MODELLING COVID-19. *National Institute Economic Review* **257,** 46–82 (2021).

293. Panovska-Griffiths, J., Kerr, C., Waites, W. & Stuart, R. in *Data Science: Theory and Applications* (eds Srinivasa Rao, A. S. & Rao, C.) 291–326 (Elsevier, 2021). https://www.sciencedirect.com/science/article/pii/S016971612030050X.

294. Irwin, M. & Wang, Z. in *The International Encyclopedia of Communication Research Methods* 1–12 (John Wiley and Sons, Ltd, 2017). ISBN: 9781118901731. eprint: https://onlinelibrary.wiley.com/doi/pdf/10.1002/9781118901731.iecrm0074. https://onlinelibrary.wiley.com/doi/abs/10.1002/9781118901731.iecrm0074.

295. PTC. *Dynamic modeling overview* https://support.ptc.com/help/modeler/r9.1/en/index.html#page/Integrity_Modeler/rtsme/dynamic_modeling_overview.html. (accessed: 30.05.2022).

296. Du Grand-Duché de Luxembourg, L. G. *COVID-19-Impfung Mat Solidaritéit zeréck an dNormalitéit* https://bletz.lu/wp-content/uploads/2021/05/10193_DISA_Cov19_Vaxx_Toutesboites_2021-03_v7.pdf. (accessed: 27.05.2022).

297. Gouvernment, L. *COVID-19-Impfung für Kinder im Alter von 5 bis 11 Jahren: jetzt in drei Impfzentren möglich* https://gouvernement.lu/de/actualites/toutes_actualites/communiques/2021/12-decembre/23-vaccination-enfants.html. (accessed: 27.05.2022).

298. (WHO), W. H. O. *Middle East respiratory syndrome coronavirus (MERS-CoV)* https://www.who.int/health-topics/middle-east-respiratory-syndrome-coronavirus-mers#tab=tab_1. (accessed: 24.05.2022).

299. Van Ravenzwaaij, D., Cassey, P. & Brown, S. A simple introduction to Markov Chain MonteCarlo sampling. *Psychon Bull Rev* **25,** 143–154 (2018).

300. Robert, C. P., Elvira, V., Tawn, N. & Wu, C. Accelerating MCMC algorithms. *WIREs Computational Statistics* **10,** e1435. eprint: https://wires.onlinelibrary.wiley.com/doi/pdf/10.1002/wics.1435. https://wires.onlinelibrary.wiley.com/doi/abs/10.1002/wics.1435 (2018).

301. Scerri, K. *MCMC Methods for data modeling* https://www.sheffield.ac.uk/polopoly_fs/1.60510!/file/MCMC.pdf. (accessed: 28.03.2022).

302. Organization, W. H. *WHO Coronavirus (COVID-19) Dashboard* https://covid19.who.int. (accessed: 25.01.2022).

303. Ideker, T. *et al.* Integrated Genomic and Proteomic Analyses of a Systematically Perturbed Metabolic Network. *Science* **292,** 929–934. eprint: https://www.science.org/doi/pdf/10.1126/science.292.5518.929. https://www.science.org/doi/abs/10.1126/science.292.5518.929 (2001).

304. Ihmels, J. H. & Bergmann, S. Challenges and prospects in the analysis of large-scale gene expression data. *Briefings in Bioinformatics* **5,** 313–327. ISSN: 1467-5463. eprint: https://academic.oup.com/bib/article-pdf/5/4/313/738665/313.pdf. https://doi.org/10.1093/bib/5.4.313 (Dec. 2004).

305. Daran-Lapujade, P. *et al.* Role of Transcriptional Regulation in Controlling Fluxes in Central Carbon Metabolism of Saccharomyces cerevisiae: A CHEMOSTAT CULTURE STUDY*. *Journal of Biological Chemistry* **279,** 9125–9138. ISSN: 0021-9258. https://www.sciencedirect.com/science/article/pii/S0021925817478203 (2004).

306. Spellman, P. T. *et al.* Comprehensive Identification of Cell Cycleregulated Genes of the Yeast Saccharomyces cerevisiae by Microarray Hybridization. *Molecular Biology of the Cell* **9.** PMID: 9843569, 3273–3297. eprint: https://doi.org/10.1091/mbc.9.12.3273. https://doi.org/10.1091/mbc.9.12.3273 (1998).

307. Eisen, M. B., Spellman, P. T., Brown, P. O. & Botstein, D. Cluster analysis and display of genome-wide expression patterns. *Proceedings of the National Academy of Sciences* **95,** 14863–14868. ISSN: 0027-8424. eprint: https://www.pnas.org/content/95/25/14863.full.pdf. https://www.pnas.org/content/95/25/14863 (1998).

308. Haefner, J. W. *The Modeling Process* 17–31. ISBN: 978-0-387-25012-0. https://doi.org/10.1007/0-387-25012-3_2 (Springer US, Boston, MA, 2005).

309. Kitano, H. *Foundations of Systems Biology* ISBN: 9780262277204. https://doi.org/10.7551/mitpress/3087.001.0001 (The MIT Press, Oct. 2001).

310. FJ Bruggeman, H. W. The nature of systems biology. **15,** 45–50 (Jan. 2007).

311. Spall, J. Estimation via Markov chain Monte Carlo. *IEEE Control Systems Magazine* **23,** 34–45 (2003).

312. Kirschner, M. The meaning of systems biology. **121,** 503–504 (May 2005).

313. Palsson, B. Ø. in *Systems Biology: Constraint-based Reconstruction and Analysis* 1–14 (Cambridge University Press, 2015).

314. Proverbio, D. *et al.* Model-based assessment of COVID-19 epidemic dynamics by wastewater analysis. *Science of The Total Environment* **827,** 154235. ISSN: 0048-9697. https://www.sciencedirect.com/science/article/pii/S0048969722013274 (2022).

315. Bucher, M. *LIH-Immunologe / Warum es in Luxemburg immer mehr Corona-Reinfektionen gibt und was das zu bedeuten hat* https://www.tageblatt.lu/headlines/warum-es-in-luxemburg-immer-mehr-corona-reinfektionen-gibt-und-was-das-zu-bedeuten-hat/. (accessed: 17.04.2022).

316. Bénassy-Quéré, A. *et al.* Covid-19: Europe needs a catastrophe relief plan. *VoxEU* **March** (2020).

317. Dewatripont, M., Goldman, M., Eric Muraille, E. & Platteau, J. Rapidly identifying workers who are immune to Covid-19 and virus-free is a priority for restarting the economy. *VoxEU* **March** (2020).

318. Jarvis, C. *et al.* Quantifying the impact of physical distance measures on the transmission of COVID-19 in the UK. *CMMID Repository* **forthcoming** (2020).

319. Milton, D., MP., F., BJ., C., ML., G. & JJ., M. Influenza virus aerosols in human exhaled breath: particle size, culturability, and effect of surgical masks. *PLoS Pathogens* **9** (2013).

320. Oberg, T. & Brosseau, L. Surgical mask filter and fit performance. *American Journal of Infection Contro* **36,** 276–282 (2008).

321. Rabbie, T. & Curtis, V. Handwashing and risk of respiratory infections: a quantitative systematic review. *Tropical Medicine and International Health* **11,** 258–267 (2006).

322. STATEC. La situation économique au Luxembourg – Evolution récente et perspectives. *Note de conjoncture* **Mai** (2020).

323. Robert Koch-Institut, Universität Bonn, Esri Initiative zum Corona Impact 2020. Robert Koch-Institut: COVID-19-Dashboard. https://experience.arcgis.com/experience/478220a4c454480e823b17327b2bf1d4 (Accessed 14 Jun 2020).

324. Maharaj, S. & Kleczkowski, A. Controlling epidemic spread by social distancing: Do it well or not at all. *BMC Public Health* **12,** 679 (2012).

325. Peng, L., Yang, W., Zhang, D., Zhuge, C. & Hong, L. Epidemic analysis of COVID-19 in China by dynamical modeling. *arXiv preprint arXiv:2002.06563* (2020).

326. Hellewell, J. *et al.* Feasibility of controlling COVID-19 outbreaks by isolation of cases and contacts. *The Lancet Global Health* (2020).

327. Ferguson, N. M. *et al.* Strategies for mitigating an influenza pandemic. *Nature* **442,** 448–452 (2006).

328. Iyer, A. S. *et al.* Persistence and decay of human antibody responses to the receptor binding domain of SARS-CoV-2 spike protein in COVID-19 patients. *Science Immunology* **5.** https://immunology.sciencemag.org/content/5/52/eabe0367 (2020).

329. Liu, Y., Gayle, A. A., Wilder-Smith, A. & Rocklöv, J. The reproductive number of COVID-19 is higher compared to SARS coronavirus. *Journal of Travel Medicine* **27** (Feb. 2020).

330. Miles, P. R. pymcmcstat: a Python package for Bayesian Inference Using Delayed Rejection Adaptive Metropolis. *J. Open Source Softw.* **4,** 1417 (2019).

331. Li, R. *et al.* Global COVID-19 pandemic demands joint interventions for the suppression of future waves. *Proc. Natl. Acad. Sci. USA* **117,** 26151–26157. ISSN: 0027-8424 (2020).

332. Socialstyrelsen. *Utvecklingen över tid, nyinskrivningar, avlidna och smittade på särskilt boende* 2020. https://www.socialstyrelsen.se/statistik-och-data/statistik/statistik-om-covid-19/sammanfattande-statistik-over-tid/.

333. Hethcote, H. W. The Mathematics of Infectious Diseases. *SIAM Rev.* **42,** 599–653 (2000).

334. Balabdaoui, F. & Mohr, D. Age-stratified discrete compartment model of the COVID-19 epidemic with application to Switzerland. *Sci. Rep.* **10,** 21306 (2020).

335. Reiner, R. C. *et al.* Modeling COVID-19 scenarios for the United States. *Nat. Med.* **27,** 94–105 (2020).

336. Gelman, A. & Rubin, D. B. Inference from Iterative Simulation Using Multiple Sequences. *Statist. Sci.* **7,** 457–472 (Nov. 1992).

337. Brooks, S. & Gelman, A. General Methods for Monitoring Convergence of Iterative Simulations. *J. Comput. Graphi. Stat.* **7,** 434–455 (Dec. 1998).

338. Link, W. A. & Eaton, M. J. On thinning of chains in MCMC. *Methods Ecol. Evol.* **3,** 112–115 (2012).

339. Blackwood, J. C. & Childs, L. M. An introduction to compartmental modeling for the budding infectious disease modeler. *Letters in Biomathematics* **5,** 195–221. ISSN: 23737867 (Dec. 2018).

340. Larsson, E. *et al.* Characteristics and outcomes of patients with COVID19 admitted to ICU in a tertiary hospital in Stockholm, Sweden. *Acta Anaesth. Scand.* (Sept. 2020).

341. Mbuvha R, M. T. Bayesian inference of COVID-19 spreading rates in South Africa. *PLoS ONE* **15,** e0237126 (8 2020).

342. Van den Driessche P. Reproduction numbers of infectious disease models. *Infect. Dis. Model.* **29;2,** 288–303 (3 2017).

343. Giordano, G. *et al.* Modelling the COVID-19 epidemic and implementation of population-wide interventions in Italy. *Nat. Med.* **26,** 855–860 (6 2020).

344. Rivera-Rodriguez, C. & Urdinola, B. P. Predicting Hospital Demand During the COVID-19 Outbreak in BogotÃą, Colombia. *Front. Pub. Heal.* **8,** 710. ISSN: 2296-2565. https://www.frontiersin.org/article/10.3389/fpubh.2020.582706 (2020).

345. Jinhong Zhang Jianwen Jia, X. S. Analysis of an SEIR Epidemic Model with Saturated Incidence and Saturated Treatment Function. *Sci. World J.* (2014).

346. Long, Q.-X. *et al.* Clinical and immunological assessment of asymptomatic SARS-CoV-2 infections. *Nat. Med.* **26,** 1200–1204 (2020).

347. Robbiani, D. *et al.* Convergent antibody responses to SARS-CoV-2 in convalescent individuals. *Nature* **584(7821),** 437–442 (Aug. 2020).

348. Davis, M. & Leo, S. BlackLitterman in continuous time: the case for filtering. *Quant. Financ. Lett.* **1,** 30–35 (2013).

349. Gillespie, D. The chemical Langevin equation. *J. Chem. Phys.* **113,** 297–306 (2000).

350. Kalman, R. A new approach to linear filtering and prediction problems. *J. Basic Eng.* **82,** 35–45 (1960).

351. Cluzel, N. *et al.* A nationwide indicator to smooth and normalize heterogeneous SARS-CoV-2 RNA data in wastewater. *Environment International* **158,** 106998 (2022).

352. Kemp, F. *et al.* Modelling COVID-19 dynamics and potential for herd immunity by vaccination in Austria, Luxembourg and Sweden. *J. Theo. Biol.,* 110874. ISSN: 0022-5193 (2021).

353. Petropoulos, F. & Makridakis, S. Forecasting the novel coronavirus COVID-19. *PloS one* **15,** e0231236 (2020).

354. Harvey, A. C. *Forecasting, structural time series models and the Kalman filter* (Cambridge university press, 1990).

355. Marchesseau, S. *et al.* Personalization of a cardiac electromechanical model using reduced order unscented Kalman filtering from regional volumes. *Med. Im. An.* **17,** 816–829 (2013).

356. B. Nagy Stovner, T.A. Johansen, T.I. Fossen & I. Schjølberg. Attitude estimation by multiplicative exogenous Kalman filter. *Automatica* **95,** 347–355 (2018).

357. D. Proverbio *et al.* Dynamical SPQEIR model assesses the effectiveness of non-pharmaceutical interventions against COVID-19 epidemic outbreaks. *PLOS ONE* **16,** 1–21 (May 2021).

358. Snoeck, C. J. *et al.* Prevalence of SARS-CoV-2 infection in the Luxembourgish population the CON-VINCE study. *medRxiv,* 2020.05.11.20092916 (2020).

359. Bandala, E. R. *et al.* Impacts of COVID-19 pandemic on the wastewater pathway into surface water: A review. *Science of the Total Environment,* 145586 (2021).

360. Lahrich, S. *et al.* Review on the contamination of wastewater by COVID-19 virus: Impact and treatment. *Science of The Total Environment* **751,** 142325 (2021).

361. Sala-Comorera, L. *et al.* Decay of infectious SARS-CoV-2 and surrogates in aquatic environments. *Water Res.,* 117090 (2021).

362. Fernandez-Cassi, X. *et al.* Wastewater monitoring outperforms case numbers as a tool to track COVID-19 incidence dynamics when test positivity rates are high. *Water research* **200,** 117252 (2021).

363. He, S., Peng, Y. & Sun, K. SEIR modeling of the COVID-19 and its dynamics. *Nonlinear dynamics* **101,** 1667–1680 (2020).

364. Cássaro, F. A. & Pires, L. F. Can we predict the occurrence of COVID-19 cases? Considerations using a simple model of growth. *Sci. Tot. Env.* **728,** 138834 (2020).

365. Gundy, P. M., Gerba, C. P. & Pepper, I. L. Survival of coronaviruses in water and wastewater. *Food Environ. Virol.* **1,** 10–14 (2009).

366. Kapo, K. E., Paschka, M., Vamshi, R., Sebasky, M. & McDonough, K. Estimation of US sewer residence time distributions for national-scale risk assessment of down-the-drain chemicals. *Sci. Total Environ.* **603,** 445–452 (2017).

367. Néant, N. *et al.* Modeling SARS-CoV-2 viral kinetics and association with mortality in hospitalized patients from the French COVID cohort. *Proc. Natl. Acad. Sci. USA* **118** (2021).

368. Wölfel, R. *et al.* Virological assessment of hospitalized patients with COVID-2019. *Nature* **581,** 465–469 (2020).

369. Saguti, F. *et al.* Surveillance of wastewater revealed peaks of SARS-CoV-2 preceding those of hospitalized patients with COVID-19. *Water Res.* **189,** 116620 (2021).

370. Zhu, Y. *et al.* Early warning of COVID-19 via wastewater-based epidemiology: potential and bottlenecks. *Sci. Total Environ.,* 145124 (2021).

371. Kollepara, P. K., Siegenfeld, A. F. & Bar-Yam, Y. Modeling complex systems: A case study of compartmental models in epidemiology. *arXiv,* arXiv:2110.02947 (2021).

372. Huisman, J. S. *et al.* Wastewater-based estimation of the effective reproductive number of SARS-CoV-2. *medRxiv,* 2021.04.29.21255961 (2021).

373. Santosh, K. COVID-19 prediction models and unexploited data. *Journal of medical systems* **44,** 1–4 (2020).

374. Goldberg, Y. *et al.* Waning immunity after the BNT162b2 vaccine in Israel. *New England Journal of Medicine* **385,** e85 (2021).

375. Ahmed, W. *et al.* Wastewater surveillance demonstrates high predictive value for COVID-19 infection on board repatriation flights to Australia. *Environ. Int.,* 106938 (2021).

376. Reeves, K. *et al.* High-resolution within-sewer SARS-CoV-2 surveillance facilitates informed intervention. *Water Res.* **204,** 117613. ISSN: 0043-1354 (2021).

377. Quilliam, R. S. *et al.* COVID-19: The environmental implications of shedding SARS-CoV-2 in human faeces. *Environ. Int.* **140,** 105790 (2020).

378. Tiwari, S. B. *et al.* Surveillance of Wastewater for Early Epidemic Prediction (SWEEP): Environmental and health security perspectives in the post COVID-19 Anthropocene. *Environ. Res.* **195,** 110831 (2021).

379. Hasan, S. W. *et al.* Detection and quantification of SARS-CoV-2 RNA in wastewater and treated effluents: Surveillance of COVID-19 epidemic in the United Arab Emirates. *Sci. Total Environ.* **764,** 142929 (2021).

380. Miura, F., Kitajima, M. & Omori, R. Duration of SARS-CoV-2 viral shedding in faeces as a parameter for wastewater-based epidemiology: Re-analysis of patient data using a shedding dynamics model. *Sci. Total Environ.* **769,** 144549 (2021).

381. Or, I. B. *et al.* Regressing SARS-CoV-2 sewage measurements onto COVID-19 burden in the population: a proof-of-concept for quantitative environmental surveillance. *MedRxiv* (2020).

382. Wurtzer, S. *et al.* Evaluation of lockdown effect on SARS-CoV-2 dynamics through viral genome quantification in waste water, Greater Paris, France, 5 March to 23 April 2020. *Eurosurveillance* **25,** 2000776 (2020).

383. Randazzo, W., Cuevas-Ferrando, E., Sanjuán, R., Domingo-Calap, P. & Sánchez, G. Metropolitan wastewater analysis for COVID-19 epidemiological surveillance. *Int. J. Hyg. Envir. Heal.* **230,** 113621 (2020).

384. Daughton, C. G. Wastewater surveillance for population-wide COVID-19: the present and future. *Sci. Total Environ.* **736,** 139631 (2020).

385. Farkas, K., Hillary, L. S., Malham, S. K., McDonald, J. E. & Jones, D. L. Wastewater and public health: the potential of wastewater surveillance for monitoring COVID-19. *Curr. Opin. Envir. Sci. Heal.* **17,** 14–20 (2020).

386. Kumar, M., Joshi, M., Patel, A. K. & Joshi, C. G. Unravelling the early warning capability of wastewater surveillance for COVID-19: A temporal study on SARS-CoV-2 RNA detection and need for the escalation. *Environ. Res.* **196,** 110946 (2021).

387. Nemudryi, A. *et al.* Temporal detection and phylogenetic assessment of SARS-CoV-2 in municipal wastewater. *Cell Rep. Med.* **1,** 100098 (2020).

388. Peccia, J. *et al.* Measurement of SARS-CoV-2 RNA in wastewater tracks community infection dynamics. *Nat. Biotechnol.* **38,** 1164–1167 (2020).

389. Kumar, M. *et al.* First proof of the capability of wastewater surveillance for COVID-19 in India through detection of genetic material of SARS-CoV-2. *Sci. Total Environ.* **746,** 141326 (2020).

390. Larsen, D. A. & Wigginton, K. R. Tracking COVID-19 with wastewater. *Nat. Biotechnol.* **38,** 1151–1153 (2020).

391. Li, X. *et al.* Data-driven estimation of COVID-19 community prevalence through wastewater-based epidemiology. *Sci. Total Environ.,* 147947 (2021).

392. Weidhaas, J. *et al.* Correlation of SARS-CoV-2 RNA in wastewater with COVID-19 disease burden in sewersheds. *Sci. Total Environ.* **775,** 145790 (2021).

393. Cao, Y. & Francis, R. On forecasting the community-level COVID-19 cases from the concentration of SARS-CoV-2 in wastewater. *Sci. Total Environ.* **786,** 147451 (2021).

394. Naughton, C. C. *et al.* Show us the data: Global COVID-19 wastewater monitoring efforts, equity, and gaps. *medRxiv,* 2021.03.14.21253564 (2021).

395. Bibby, K., Bivins, A., Wu, Z. & North, D. Making Waves: Plausible Lead Time for Wastewater Based Epidemiology as an Early Warning System for COVID-19. *Water Research,* 117438 (2021).

396. Wilmes, P. *et al.* SARS-CoV-2 transmission risk from asymptomatic carriers: results from a mass screening programme in Luxembourg. *Lancet Reg. Heal.-Europe* **4,** 100056 (2021).

397. Vallejo, J. A. *et al.* Modeling the number of people infected with SARS-COV-2 from wastewater viral load in Northwest Spain. *Science of The Total Environment,* 152334 (2021).

398. McMahan, C. S. *et al.* COVID-19 wastewater epidemiology: a model to estimate infected populations. *The Lancet Planetary Health* **5,** e874–e881 (2021).

399. Pollán, M. *et al.* Prevalence of SARS-CoV-2 in Spain (ENE-COVID): a nationwide, population-based seroepidemiological study. *The Lancet* **396,** 535–544 (2020).

400. Ghaffarzadegan, N. & Rahmandad, H. Simulation-based estimation of the early spread of COVID-19 in Iran: actual versus confirmed cases. *System Dynamics Review* **36,** 101–129 (2020).

401. D'Aoust, P. M. *et al.* Catching a resurgence: Increase in SARS-CoV-2 viral RNA identified in wastewater 48 h before COVID-19 clinical tests and 96 h before hospitalizations. *Sci. Total Environ.* **770,** 145319 (2021).

402. Slot, E. *et al.* Low SARS-CoV-2 seroprevalence in blood donors in the early COVID-19 epidemic in the Netherlands. *Nat. Commun.* **11,** 1–7 (2020).

403. Lopez, C. A. *et al.* Disparities in SARS-CoV-2 seroprevalence among individuals presenting for care in central North Carolina over a six-month period. *medRxiv* (2021).

404. Byambasuren, O. *et al.* Comparison of seroprevalence of SARS-CoV-2 infections with cumulative and imputed COVID-19 cases: systematic review. *PloS one* **16,** e0248946 (2021).

405. CDC, U. *National Wastewater Surveillance System (NWSS)* 2021. https://bit.ly/3zkaQFY.

406. EU Science Hub. *Coronavirus: Commission adopts a common approach to track COVID-19 through wastewater monitoring* 17/03/2021. https://bit.ly/3itvWLp.

407. Saeed, S. *et al.* SARS-CoV-2 seroprevalence among blood donors after the first COVID-19 wave in Canada. *Transfusion* **61,** 862–872. eprint: https://onlinelibrary.wiley.com/doi/pdf/10.1111/trf.16296. https://onlinelibrary.wiley.com/doi/abs/10.1111/trf.16296 (2021).

408. Poljak, M. *et al.* Seroprevalence of SARS-CoV-2 in Slovenia: results of two rounds of a nationwide population study on a probability-based sample, challenges and lessons learned. *Clinical Microbiology and Infection* **27** (Apr. 2021).

409. Courbariaux, M. *et al.* A flexible smoother adapted to censored data with outliers and its application to SARS-CoV-2 monitoring in wastewater. *Frontiers in Applied Mathematics and Statistics* **8** (2022).

410. Thompson, J. M. T. & Sieber, J. Predicting climate tipping as a noisy bifurcation: a review. *International Journal of Bifurcation and Chaos* **21,** 399–423 (2011).

411. Ditlevsen, P. D. & Johnsen, S. J. Tipping points: Early warning and wishful thinking. *Geophysical Research Letters* **37** (2010).

412. Hillmer, S. C. & Tiao, G. C. An ARIMA-model-based approach to seasonal adjustment. *Journal of the American Statistical Association* **77,** 63–70 (1982).

413. Abbott, S. *et al.* Temporal variation in transmission during the COVID-19 outbreak [version 1; peer review: awaiting peer review]. *Wellcome Open Res* **5** (2020).

414. Systrom, K., Vladek, T. & Krieger, M. *Rt.live* https://github.com/rtcovidlive/covid-model. 2020.

415. luxembourgeois, G. *Coronavirus - grapiques* https://covid19.public.lu/fr/graph.html. last accessed.

416. Bettencourt, L. M. & Ribeiro, R. M. Real time bayesian estimation of the epidemic potential of emerging infectious diseases. *PloS one* **3,** e2185 (2008).

417. Liu, Q.-H. *et al.* Measurability of the epidemic reproduction number in data-driven contact networks. *Proceedings of the National Academy of Sciences* **115,** 12680–12685 (2018).

418. Ajelli, M. *et al.* Spatiotemporal dynamics of the Ebola epidemic in Guinea and implications for vaccination and disease elimination: a computational modeling analysis. *BMC medicine* **14,** 1–10 (2016).

419. Du, Z. *et al.* Serial interval of COVID-19 among publicly reported confirmed cases. *Emerging infectious diseases* **26,** 1341 (2020).

420. Park, M., Cook, A. R., Lim, J. T., Sun, Y. & Dickens, B. L. A systematic review of COVID-19 epidemiology based on current evidence. *Journal of clinical medicine* **9,** 967 (2020).

421. Harris, M. J., Hay, S. I. & Drake, J. M. Early warning signals of malaria resurgence in Kericho, Kenya. *Biology letters* **16,** 20190713 (2020).

422. Southall, E., Brett, T. S., Tildesley, M. J. & Dyson, L. Early warning signals of infectious disease transitions: a review. *Journal of the Royal Society Interface* **18,** 20210555 (2021).

423. Liu, R. *et al.* Predicting local COVID-19 outbreaks and infectious disease epidemics based on landscape network entropy. *Science Bulletin* (2021).

424. Brett, T. S. & Rohani, P. Dynamical footprints enable detection of disease emergence. *PLoS biology* **18,** e3000697 (2020).

425. Dablander, F., Heesterbeek, H., Borsboom, D. & Drake, J. M. Overlapping Time Scales Obscure Early Warning Signals of the Second COVID-19 Wave. *Proceedings of the Royal Society B* **289,** 20211809 (2022).

426. OBrien, D. A. & Clements, C. F. Early warning signals predict emergence of COVID-19 waves. *medRxiv* (2021).

427. Phillips, B., Anand, M. & Bauch, C. T. Spatial early warning signals of social and epidemiological tipping points in a coupled behaviour-disease network. *Scientific reports* **10,** 1–12 (2020).

428. Brett, T. S., Drake, J. M. & Rohani, P. Anticipating the emergence of infectious diseases. *Journal of The Royal Society Interface* **14,** 20170115 (2017).

429. Lyngse, F. P. *et al.* SARS-CoV-2 Omicron VOC Transmission in Danish Households. *medRxiv.* eprint: https://www.medrxiv.org/content/early/2021/12/27/2021.12.27.21268278.full.pdf. https://www.medrxiv.org/content/early/2021/12/27/2021.12.27.21268278 (2021).

430. Benvenuto, D., Giovanetti, M., Vassallo, L., Angeletti, S. & Ciccozzi, M. Application of the ARIMA model on the COVID-2019 epidemic dataset. *Data in brief* **29,** 105340 (2020).

431. Proverbio, D. *et al.* Dynamical SPQEIR model assesses the effectiveness of non-pharmaceutical interventions against COVID-19 epidemic outbreaks. *PloS one* **16,** e0252019 (2021).

432. Levin, E. G. *et al.* Waning Immune Humoral Response to BNT162b2 Covid-19 Vaccine over 6 Months. *New England Journal of Medicine* **385,** e84. eprint: https://doi.org/10.1056/NEJMoa2114583. https://doi.org/10.1056/NEJMoa2114583 (2021).

433. Kemp, F. *et al.* Modelling COVID-19 dynamics and potential for herd immunity by vaccination in Austria, Luxembourg and Sweden. *Journal of Theoretical Biology,* 110874. ISSN: 0022-5193 (2021).

434. Davies, N. G. *et al.* Estimated transmissibility and severity of novel SARS-CoV-2 Variant of Concern 202012/01 in England. *MedRxiv,* 2020–12 (2021).

435. Ashwin, P., Wieczorek, S., Vitolo, R. & Cox, P. Tipping points in open systems: bifurcation, noise-induced and rate-dependent examples in the climate system. *Philosophical Transactions of the Royal Society A: Mathematical, Physical and Engineering Sciences* **370,** 1166–1184 (2012).

436. ODea, E. B. & Drake, J. M. Disentangling reporting and disease transmission. *Theoretical Ecology* **12,** 89–98 (2019).

437. Wu, J. T. *et al.* Nowcasting epidemics of novel pathogens: lessons from COVID-19. *Nature Medicine* **27,** 388–395 (2021).

438. ORegan, S. M. & Drake, J. M. Theory of early warning signals of disease emergenceand leading indicators of elimination. *Theoretical Ecology* **6,** 333–357 (2013).

439. Miller, P. B., ODea, E. B., Rohani, P. & Drake, J. M. Forecasting infectious disease emergence subject to seasonal forcing. *Theoretical Biology and Medical Modelling* **14,** 1–14 (2017).

440. Dessavre, A. G., Southall, E., Tildesley, M. J. & Dyson, L. The problem of detrending when analysing potential indicators of disease elimination. *Journal of theoretical biology* **481,** 183–193 (2019).

441. Dakos, V. *et al.* Methods for detecting early warnings of critical transitions in time series illustrated using simulated ecological data. *PloS one* **7,** e41010 (2012).

442. Dakos, V., Van Nes, E. H., d'Odorico, P. & Scheffer, M. Robustness of variance and autocorrelation as indicators of critical slowing down. *Ecology* **93,** 264–271 (2012).

443. Scheffer, M. & Carpenter, S. R. Catastrophic regime shifts in ecosystems: linking theory to observation. *Trends in ecology and evolution* **18,** 648–656 (2003).

444. Clements, C. F., Drake, J. M., Griffiths, J. I. & Ozgul, A. Factors influencing the detectability of early warning signals of population collapse. *The American Naturalist* **186,** 50–58 (2015).

445. Van Kampen, N. G. *Stochastic processes in physics and chemistry* (Elsevier, 1992).

446. Horstmeyer, L., Kuehn, C. & Thurner, S. Network topology near criticality in adaptive epidemics. *Physical Review E* **98,** 042313 (2018).

447. ORegan, S. M. & Burton, D. L. How stochasticity influences leading indicators of critical transitions. *Bulletin of mathematical biology* **80,** 1630–1654 (2018).

448. Allen, L. J. in *Mathematical epidemiology* 81–130 (Springer, 2008).

449. Xu, S. & Li, Y. Beware of the second wave of COVID-19. *The Lancet* **395,** 1321–1322 (2020).

450. Cacciapaglia, G., Cot, C. & Sannino, F. Second wave COVID-19 pandemics in Europe: a temporal playbook. *Scientific reports* **10,** 1–8 (2020).

451. Hsiang, S. *et al.* The effect of large-scale anti-contagion policies on the COVID-19 pandemic. *Nature* **584,** 262–267 (2020).

452. Brett, T. S. *et al.* Anticipating epidemic transitions with imperfect data. *PLoS computational biology* **14,** e1006204 (2018).

453. Scheffer, M. *et al.* Anticipating critical transitions. *science* **338,** 344–348 (2012).

454. Dakos, V. *et al.* Slowing down as an early warning signal for abrupt climate change. *Proceedings of the National Academy of Sciences* **105,** 14308–14312 (2008).

455. Adam, D. A guide to Rthe pandemic's misunderstood metric. *Nature* **583,** 346–348 (2020).

456. Delamater, P. L., Street, E. J., Leslie, T. F., Yang, Y. T. & Jacobsen, K. H. Complexity of the basic reproduction number (R0). *Emerging infectious diseases* **25,** 1 (2019).

457. Kuehn, C. A mathematical framework for critical transitions: Bifurcations, fast–slow systems and stochastic dynamics. *Physica D: Nonlinear Phenomena* **240,** 1020–1035 (2011).

458. Ricon-Becker, I., Tarrasch, R., Blinder, P. & Ben-Eliyahu, S. A seven-day cycle in COVID-19 infection, hospitalization, and mortality rates: Do weekend social interactions kill susceptible people? *medRxiv* **10.1101/2020.05.03.20089508** (2020).

459. Biggs, R., Carpenter, S. R. & Brock, W. A. Turning back from the brink: detecting an impending regime shift in time to avert it. *Proceedings of the National academy of Sciences* **106,** 826–831 (2009).

460. Rivieccio, B. A. *et al.* Heterogeneity of COVID-19 outbreak in Italy. *Acta Bio Medica: Atenei Parmensis* **91,** 31 (2020).

461. Nishiura, H., Linton, N. M. & Akhmetzhanov, A. R. Serial interval of novel coronavirus (COVID-19) infections. *International Journal of Infectious Diseases* **93,** 284–286. ISSN: 1201-9712 (2020).

462. Dai, L., Vorselen, D., Korolev, K. S. & Gore, J. Generic indicators for loss of resilience before a tipping point leading to population collapse. *Science* **336,** 1175–1177 (2012).

463. Liu, Y., Gayle, A. A., Wilder-Smith, A. & Rocklöv, J. The reproductive number of COVID-19 is higher compared to SARS coronavirus. *Journal of Travel Medicine* **27** (Feb. 2020).

464. Pedersen, S. F., Ho, Y.-C. *et al.* SARS-CoV-2: a storm is raging. *The Journal of clinical investigation* **130** (2020).

465. Bauchner, H., Golub, R. M. & Zylke, J. Editorial concernpossible reporting of the same patients with COVID-19 in different reports. *Jama* **323,** 1256–1256 (2020).

466. Lenton, T., Livina, V., Dakos, V., Van Nes, E. & Scheffer, M. Early warning of climate tipping points from critical slowing down: comparing methods to improve robustness. *Philosophical Transactions of the Royal Society A: Mathematical, Physical and Engineering Sciences* **370,** 1185–1204 (2012).

467. Flaxman, S. *et al.* Estimating the effects of non-pharmaceutical interventions on COVID-19 in Europe. *Nature* **584,** 257–261 (2020).

468. Kuznetsov, Y. A. *Elements of applied bifurcation theory* (Springer Science and Business Media, 2013).

469. Berglund, N. & Gentz, B. *Noise-induced phenomena in slow-fast dynamical systems: a sample-paths approach* (Springer Science and Business Media, 2006).

470. Lee, J. *Introduction to topological manifolds* (Springer Science and Business Media, 2010).

471. Alonso, D., McKane, A. J. & Pascual, M. Stochastic amplification in epidemics. *Journal of the Royal Society Interface* **4,** 575–582 (2007).

472. Diamond, J., Robinson, J. A. *et al. Natural experiments of history* (Harvard University Press, 2010).

473. Guttal, V. & Jayaprakash, C. Changing skewness: an early warning signal of regime shifts in ecosystems. *Ecology letters* **11,** 450–460 (2008).

474. Kendall, M. G. A new measure of rank correlation. *Biometrika* **30,** 81–93 (1938).